Surfactants and Chromophoric Dissolved Organic Matter (CDOM) in the Atlantic Ocean surface microlayer and the corresponding underlying waters

BITA SABBAGHZADEH

SUBMITTED TO THE UNIVERSITY OF NEWCASTLE UPON TYNE IN PARTIAL FULFILEMENT OF THE REQUIREMENTS FOR THE DEGREE OF DOCTOR OF PHILOSOPHY

School of Natural and Environmental Sciences

March 2018

Abstract

The sea surface microlayer (SML; depth < 400 µm) is a physically and biogeochemically distinct interface covering the entire ocean surface. Biologically-derived surfactants are ubiquitous in the SML, where they limit air-sea gas exchange and the formation of marine boundary layer aerosols that impact atmospheric chemistry and climate.

Total surfactant activity (SA) and chromophoric dissolved organic matter (CDOM) were measured in the SML, in depth profiles (≤ 100 m) and semi-continuously in sub-surface water (SSW: 7 m non-toxic seawater supply) on Atlantic Meridional Transect (AMT) cruises 24 (2014) and 25 (2015), from 50°N to 50°S. On-board estimates of the gas transfer velocity (k_w) of CH_4 (custom gas exchange tank) were related to SA distributions in the SML to evaluate surfactant control of air-sea gas exchange.

SML and SSW SA (mg L^{-1} eq. T-X-100) was always higher in the Northern Hemisphere than in the Southern Hemisphere (0.10 - 1.76 in the Northern Hemisphere; 0.08 - 0.63 in the Southern Hemisphere).

A constant enrichment of SA in the SML was observed at all wind speeds encountered. SA enrichment factors (EF = SA_{SML}/SA_{SSW}) ranged between 0.95 – 4.25 in the Atlantic Ocean, higher in the Northern Hemisphere than in the Southern Hemisphere. EF >1 up to the maximum mean wind speed recorded (~13 m s^{-1}) challenges the idea that high latitude wind speeds > 12 m s^{-1} preclude high EFs and implies that the SML is self-sustaining concerning SA.

CDOM absorption coefficient (a_{300}) in general was higher in the Northern Hemisphere (range 0.10 - 1.52 m^{-1}) than in the Southern Hemisphere (range 0.17 - 0.82 m^{-1}). CDOM spectral slope ($S_{275-295}$) showed an inverse correlation with CDOM (a_{300}) and was significantly lower (t-test, $p < 0.001$) in the SML than in the SSW (SML; 0.033 ± 0.005 nm^{-1}, SSW; 0.038 ± 0.007 nm^{-1}) suggesting in-situ CDOM production in the SML and more refractory CDOM in the SSW.

CH_4 k_{660} (k_w for CO_2 in seawater at 20°C) derived from the gas exchange tank (6.9 - 9.8 cm h^{-1}) gave film factors ($R_{660}´$; sample k_w / surfactant-free MilliQ k_w) that strongly correlated with SML SA ($r^2 = 0.63$, $p = 0.001$, n = 13). Corresponding $R_{660}´$ suppressions ~ 25% imply a strong control of Atlantic Ocean gas exchange by surfactant.

Dedication

To the heros of my life; my dad, my mum, Dr Leila, Mohammad Javad and my lovely Lida.

Acknowledgements

This long journey could not have ended happily and gratefully without some people's support whom I would like to mention here.

I would like first to thank my supervisors, Professor Rob Upstill-Goddard, Professor Phil Nightingale and Dr. Rachael Beal for their friendship and uninterrupted support. I cannot express how much I have enjoyed working with them and would love to continue to do so in the future.

I would also like to thank all members of the Oceans and Climate Research Group; Guenther, John, Ryan and Philippa for such being good friends and colleagues. I would particularly like to thank Guenther for his help with discussion on CDOM data.

I would like to send my gratitude to all the crew of the R.R.S. *James Clark Ross*, particularly Simon for making me the gimbal table, Ken for helping with the Garrett Screen, Colin for his delicious bread and pastry and Rich for taking pretty photos.

Long hours of work on board were not possible without the support of a bunch of fantastic people, dear PSO Tim, pretty and smiley Arwen, Robyn with her nice dark and salty chocolates, Caroline with her wonderful support, Liza with her fancy sea salt in sauna, Michelle with a big heart and lovely Laura.

I would like to thank David McGeeney from the school of Mathematics for his advice on statistics. I would also like to thank British Oceanography Data Centre; Rob Thomas and Arvin Bargery in particular for providing ancillary data. I thank Dr Grant Forster from University of East Anglia for his assistance on creating T-S diagram and Dr Matthew Salter from Stockholm University for his advice on surfactant measurement.

This work was supported by the UK Natural Environment Research Council (NERC: Grant# NE/K00252X/1) and is a component of RAGNARoCC (Radiatively active gases from the North Atlantic Region and Climate Change), which contributes to NERC's Greenhouse Gas Emission and Feedbacks program (http://www.nerc.ac.uk/research/funded/programmes/greenhouse/).

Abbreviations, Acronyms and Units

%	percentage
°C	degree in Celsius
°N	north
°S	south
µg L^{-1}	microgram per litre
µL	microlitres = 1 x 10^{-6} litres
µm	micrometre
µM	micromolar = 1 x 10^{-6} mols
µmolL^{-1}	micromole per litre
a_{275}	absorption coefficient at 275 nm
a_{295}	absorption coefficient at 295 nm
a_{300}	absorption coefficient at 300 nm
a_{350}	absorption coefficient at 350 nm
a_{400}	absorption coefficient at 400 nm
a_{440}	absorption coefficient at 440 nm
AC	Azores current
Ag/AgCl	silver/silver chloride
AMT	Atlantic meridional transect
Ar	arsenic
ASUW	Atlantic Subarctic Upper Water
AUs	absorbance unit
a_{λ}	absorption coefficient at λ nm
BC	Brazil current
BenC	Benguela current
BODC	British oceanography data centre
C	carbon
Ca	calcium
CC	Canary current
CC_i	capacitive current
Cd	cadmium
CDOM	chromophoric dissolved organic matter
cells ml^{-1}	cells per millilitre
CH_4	methane
cm h^{-1}	centimetre per hour
cm^2	cubic centimetre
cm^3	cubic centimetre
CO_2	carbon dioxide
Cr	chromium
CSEC	central south equatorial current
CTD	conductivity, temperature and density
Cu	copper
CZCS	coastal zone colour scanner
Da	dalton
DCM	deep chlorophyll maximum
DOC	dissolved organic carbon
DOM	dissolved organic matter

DON	dissolved organic nitrogen
DOP	dissolved organic phosphorous
DS	drop size
E	east
EF	enrichment factor
ENACW	eastern north Atlantic central water
ETRA	eastern tropical Atlantic
F	flux
FC	Falklands current
Fe	iron
FKLD	southwest Atlantic continental shelf (Falkland Islands)
GC	Guinea current
H	hydrogen
h	hour
HCHs	hexachlorocyclohexane
HCl	hydrochloric acid
HDPE	high-density polyethylene
He	helium
HMDE	hanging mercury drop electrode
HWU	Heriot Watt university
Hz	hertz
K	potassium
KCl	potassium chloride
kg L^{-1}	kilogram per litre
Km	kilometre
km	kilometre
L	litre
LCW	liquid core waveguide
LN	natural logarithm
LPU	Liverpool university
m s^{-1}	meter per second
m	metre
m^{-1}	per meter
mg C m^{-2} mth^{-1}	milligram carbon per cubic meter per month
mg C m^{-3} d^{-1}	milligram carbon per cubic meter per day
mg L^{-1}	milligram per litre
mg m^{-3}	milligram per cubic meter
Mg	magnesium
ml min^{-1}	millilitre per minute
ml/cm^2	millilitre per square centimetre
ml/dip	millilitre per dip
MLD	mixed layer depth
mm	millimetre
MODIS	moderate resolution imaging spectroradiometer
mol L^{-1}	mol per litre
MW	molecular weight
N	nitrogen
n	sample number
N_2O	nitrous oxide
Na	sodium

NaCl	sodium chloride
NACW	north Atlantic central water
NADR	north Atlantic drift region
NAG	northern Atlantic subtropical gyre
NAST (E)	north Atlantic sub-tropical (Eastern)
NAST (W)	north Atlantic sub-tropical (Western)
NATR	north Atlantic tropical
NBC	north Benguela current
NEC	north equatorial current
NECC	north equatorial counter current
ng L^{-1}	nomogram per litre
NH_3	ammonia
NH_4^+	ammonium
Ni	nickel
nm	nanometre
nM	nanomolar = 1 x 10^{-9} mols
NO_2^-	nitrite
NO_3^-	nitrate
O_2	oxygen
P	phosphorous
p	probability
PAHs	polycyclic aromatic hydrocarbon
Pb	lead
PC	Portugal current
PCBs	polychlorinated biphenyls
PCP	pentachlorophenol
PML	Plymouth marine laboratory
PO_4^{3-}	phosphate
RAGNARoCC	radiatively active gases from the north Atlantic region and climate change
ref	reference
RI	refractive index
RRS	Royal research ship
S	salinity
S	sulphur
SA	surfactant activity
SAC	south Atlantic current
SACW	south Atlantic subarctic central water
SAG	southern Atlantic subtropical gyre
SAR	synthetic aperture radar
SASW	sub-Antarctic surface waters
SATL	south Atlantic gyral
S_c	Schmidt number
SEC	south equatorial current
SF_6	sulphur hexafluoride
SiO_4^{2-}	silicate
SML	sea surface microlayer
Sr	strontium
SSTC	south sub-tropical convergence
SSW	sub-surface water
TDC	total dissolved carbohydrates

TEP	transparent exopolymer particles
TOC	total organic carbon
Tp	total phosphorous
T-S	temperature-salinity
t-test	student's T-test
V	voltage
W	west
WNACW	western north Atlantic central water
WPI	world precision instruments
WTRA	western tropical Atlantic
Zn	zinc
λ	wavelength
σ_t	The density of a seawater sample determined from its *in situ* temperature and salinity

Table of Contents

List of Figures

List of Tables

Chapter 1. General Introduction

1.1 Sea Surface MicroLayer (SML)

The sea surface microlayer (SML) is the boundary between the surface ocean and the atmosphere with strong gradients in physical and biogeochemical characteristics due to reduced mixing with the underlying water (Hardy, 1982; Williams *et al.*, 1986; Liss *et al.*, 2005; Cunliffe *et al.*, 2013). It is ubiquitous in the oceans and covers ~70% of the Earth's surface (Liss *et al.*, 2005).

The SML contains a heterogeneous mixture of organic compounds including high-molecular-weight (HMW) polysaccharides (extracellular phytoplankton products) (Sieburth *et al.*, 1976; Plavšić and Ćosović, 2000; Gogou and Repeta, 2010), lipids (Gašparović *et al.*, 1998; Gogou and Repeta, 2010), proteins and amino acids (Gašparović *et al.*, 1997; Kuznetsova *et al.*, 2004; Gogou and Repeta, 2010) and humic substances (Hunter and Liss, 1981; Barger and Means, 1985; Williams *et al.*, 1986; Frew and Nelson, 1992) with surface active properties and different degrees of solubility.

Flagellates and virus-like particles (Joux *et al.*, 2006), archaea (Cunliffe and Murrell, 2010), bacteria (Bezdek and Carlucci, 1972; Cunliffe and Murrell, 2010), zooplankton (Passow and Alldredge, 1999; Kujawinski *et al.*, 2002) and protists (Kujawinski *et al.*, 2002) are also abundant in the SML, as are zooplankton grazing products (Kujawinski *et al.*, 2002; Cunliffe and Murrell, 2010), bacterially produced refractory material (Jiao *et al.*, 2010) and anthropogenic pollutants (Wurl and Obbard, 2004).

The SML retains its integrity even at high surface turbulence (Wurl *et al.*, 2011b; Sabbaghzadeh *et al.*, 2017) and recovers within seconds following physical disturbance. Cunliffe *et al*. (2013) conducted tank experiments that showed reformation of the SML and its components within seconds following physical disruption.

When the concentration of surface active compounds (surfactants) exceeds some threshold value (i.e. more than two or three times higher than concentrations in the corresponding underlying waters), the SML becomes visibly distinguishable from the surrounding waters (Romano, 1996). This monomolecular surface film of ~ 2 – 3 nm thickness is usually referred to as a ‘‘visible slick’’ and frequently as a surface nano layer (SNL). It has a similar composition

to the SML and persists under low to moderate wind speed conditions (Williams *et al.*, 1986; Hühnerfuss, 2006; Cunliffe *et al.*, 2013) (Figure 1.1).

Figure 1.1. Visible slicks on the sea surface. Photograph adapted from Engel *et al.* (2017).

Visible slicks can be identified as dark (grey) areas (Figure 1.1). For example, synthetic aperture radar (SAR) detects visible oil spills based on physical characteristics such as film thickness and its effect on damping sea surface roughness. It has been shown that nearly 75% of the sea surface may be covered by visible slicks at wind speeds between 2 and 3 m s^{-1} (Romano, 1996; Gade *et al.*, 2006). Liss (1983) previously established that visible slicks do not persist beyond light winds.

As well as visible slicks, there is a ubiquitous, dynamic, "invisible" SML with a typical thickness between 150 µm and 400 µm (Liss *et al.*, 2005; Cunliffe *et al.*, 2013). It is this component that persists at high surface turbulence, routinely being detectable at wind speeds higher than the global oceanic average of 6.6 m s^{-1} (Archer and Jacobson, 2005) and even up to ~12 m s^{-1} (Wurl *et al.*, 2011b; Sabbaghzadeh *et al.*, 2017). This invisible SML is studied further during this thesis with respect to its persistence at high wind speeds, its broad chemical composition, selected chemical enrichment factors relative to the underlying water and its control on gas transfer velocity (k_w) in the open ocean.

The SML is also defined operationally by its thickness as determined using various samplers (Cunliffe *et al.*, 2013; Cunliffe and Wurl, 2014). Zuev *et al*. (2001) described the SML as varying from ~ 30 µm to 300 µm. Later, Zhang *et al*. (2003) described the SML as a "layer of sudden change" in physiochemical properties with a thickness of 50 ± 10 µm.

The SML is enriched or depleted in a range of organic and inorganic components, controlled by several mechanisms (Figure 1.2).

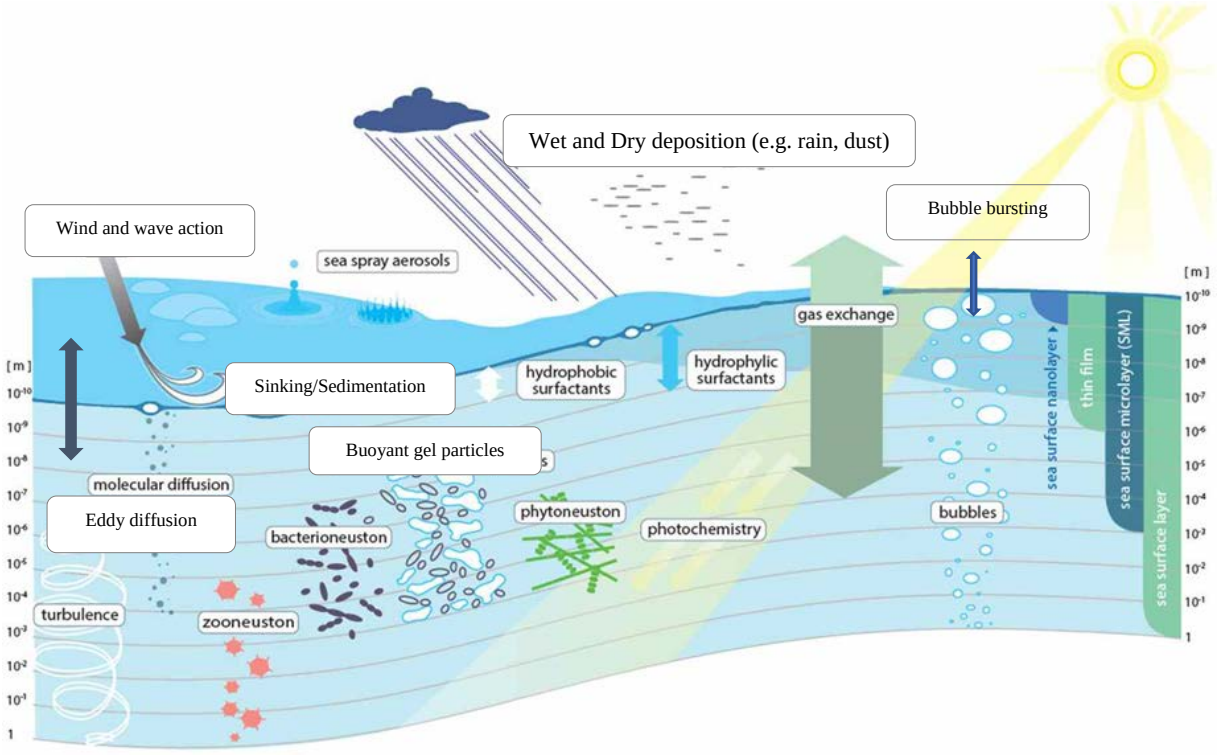

Figure 1.2. The dynamics of organic and inorganic compounds in sea surface microlayer (SML). Adapted from Hunter (1980) and Engel *et al.* (2017).

Materials are transported from deep waters to the SML mainly by bubble scavenging and turbulence, driven by wind and wave action (Žutić *et al.*, 1981; Hunter, 1997; Gašparović *et al.*, 1998; Stefan and Szeri, 1999; Wurl *et al.*, 2011b; Cunliffe *et al.*, 2013). The SML materials are dispersed in the presence of breaking waves at high wind speeds. However, these materials are reabsorbed at the surface of the rising bubbles generated by the same breaking waves and released back to the SML or to the atmosphere as aerosols via bubble bursting (Hunter, 1975; Gao *et al.*, 2012; Cunliffe *et al.*, 2013; Sabbaghzadeh *et al.*, 2017). The foamy patches frequently observed after breaking waves are a consequence of surfactant scavenging by bubbles rising towards the SML (Wurl *et al.*, 2011b).

Bubbles increase the surface area available for surfactants to be accumulated. Tseng *et al.* (1992) studied the transfer of surfactants from seawater to the atmosphere by bursting bubbles and concluded that small bubbles are more effective in transporting surfactants to the air-sea interface. Based on a dimensional analysis of bubbles they proposed that the amount of surfactants scavenged by bubbles rising to the surface is proportional to the number of bubbles and the average bubble surface area (Tseng *et al.*, 1992).

Other mechanisms including upwelling, convection, direct deposition from the atmosphere (MacIntyre, 1974; Hunter, 1975; Dragcevic and Pravdic, 1981; Hardy, 1982), molecular diffusion, the formation of Transparent Exopolymer Particles (TEP), zooplankton grazing, bacterial degradation, UV irradiation (photochemical reactions), sea spray formation and sedimentation mediates enrichment and depletion of compounds in the SML (Cullen *et al.*, 1989; Azetsu-Scott and Passow, 2004; Wurl *et al.*, 2009; Russell *et al.*, 2010) (Figure 1.2).

The SML controls the exchange rates of heat, gas and momentum between the oceans and the atmosphere. Thus, the SML influences the biogeochemical cycling of compounds in the short term and global climate regulation in the long term (Cunliffe *et al.*, 2013).

1.1.1 *Historical perspective: The development of early models of the SML*

Several conceptual models have been proposed to help describe the SML structure based on its biological and chemical characteristics.

The very first concept of the SML introduced the ‘neuston’; a layer containing small organisms at the sea surface (Naumann, 1917). Later research led to the identification of three categories of organisms in the SML: bacteria (bacterioneuston), phytoplankton (phytoneuston) and zooplankton (zooneuston). For all, their abundance in the SML is higher than in underlying water, as a result of, for example, diurnal vertical migration and positive photo taxis (Hardy, 1971; Marumo *et al.*, 1971; Hardy, 1973; Kjelleberg and Håkansson, 1976; Wandschneider, 1979).

The classical description of surfactant characteristics in the SML was the “wet dry” model (Hardy, 1982). This model defines two different surfactant layers: an uppermost defined as “dry surfactant”, containing lipids and fatty acids and accounting for the bulk of total surfactant, and a lower, “wet surfactant” layer consisting of proteins and polysaccharides (Hardy, 1982).

Later, Sieburth (1983) proposed another layered model to characterize the SML as a more complicated structure based on its components. In this model an extra layer of neuston (Naumann, 1917) containing bacterioneuston, phytoneuston and zooneuston underlies the two layers defined by Hardy (1982). It was also hypothesized that carbohydrates were the main

component of marine surfactants, with smaller contributions from proteins and lipids (Sieburth, 1983).

This model has recently been further revised (Cunliffe and Murrell, 2009), supported by the characterization of enriched microgel particles in the SML (Wurl and Holmes, 2008; Cunliffe *et al.*, 2013). In this "hydrated gelatinous matrix model" the SML is enriched in polysaccharides in the form of Transparent Exopolymer Particles (TEP) which assist the formation and stability of the SML, plausibly by forming metal ion bridges and hydrogen bonds (Berman and Passow, 2007; Wurl and Holmes, 2008; Cunliffe and Murrell, 2009; Cunliffe *et al.*, 2009b; Frka *et al.*, 2009) (Figure 1.3).

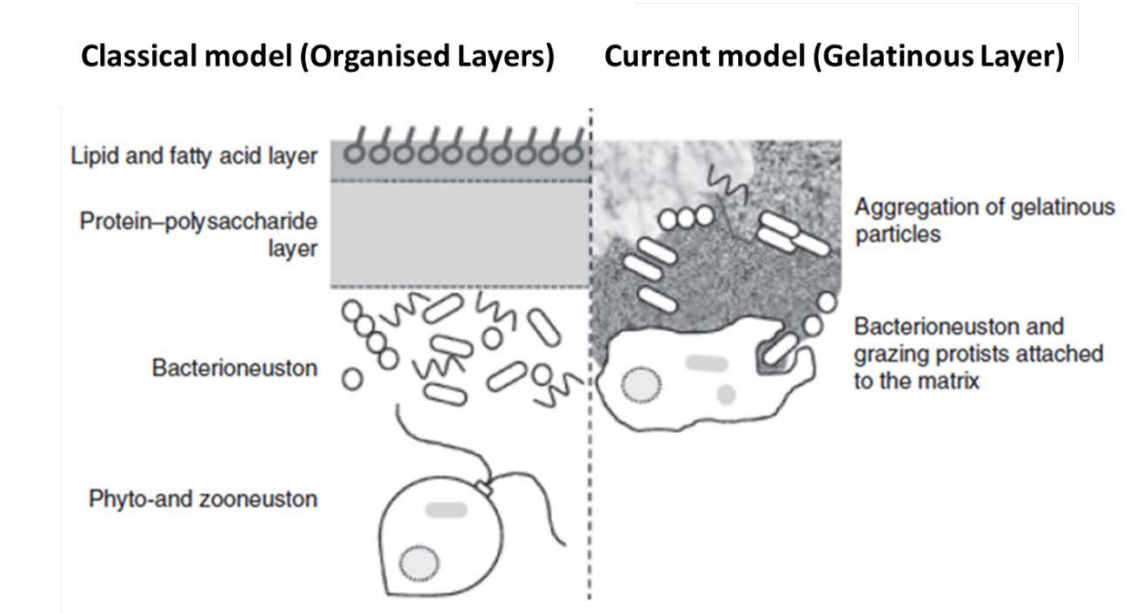

Figure 1.3. Schematic of SML structure from Cunliffe *et al*. (2011), as adapted from the ideas of Sieburth (1983), Maki (1993) and Hardy (1982)

1.1.2 *SML sampling techniques*

Renewed interest in studying the SML has focused attention on the various available samplers, which collect samples of varying thickness and composition. The most commonly used methods for SML sampling include the mesh screen (Garrett, 1965), rotating drum, membrane filters and glass plate (Harvey, 1972; Hatcher and Parker, 1974).

Other methods, including the floating tray, freezing probe and polyvinyl chloride (PVC) film (Hamilton and Clifton, 1979) have been much less frequently used and are now out of favour for sampling the SML. For example, floating trays were used to collect thicker samples

especially suitable for diverse downstream analyses. However, such samples might not be suitable for determination of chemical and biological compound enrichments in the SML due to dilution by subsurface waters (Hatcher and Parker, 1974). Thus, floating trays are now deemed impractical for SML sampling.

One common sampler in use is the glass plate (Figure 1.4), first described by Harvey and Burzell (1972). It is one of the most efficient techniques but collects relatively "thin" samples (i.e. 20 – 150 µm) compared to other commonly used samplers such as the Garrett screen (~150 – 400 µm; see below) (Harvey and Burzell, 1972; Cunliffe *et al.*, 2009a; Cunliffe and Wurl, 2014).

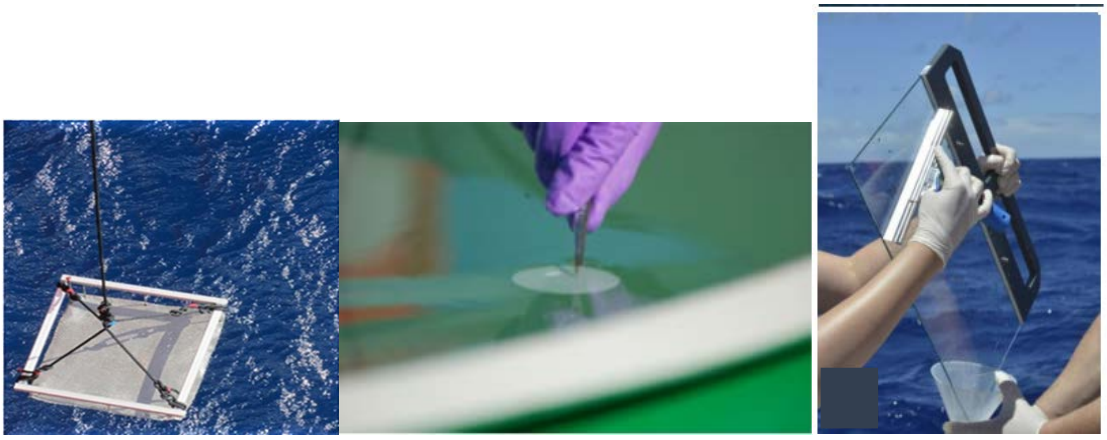

Figure 1.4. Some typical SML samplers: Garrett screen (left), membrane filter (middle) and glass plate (right). Adapted from Cunliffe and Wurl (2014).

Samples collected with the glass plate are suitable for biological composition studies and for determining chemical and microbial enrichment in the SML (Hatcher and Parker, 1974; Cunliffe and Wurl, 2014). Glass plates are also hydrophobic, which means that dissolved organic matter components of low hydrophilic nature such as amino acids and lipids can be collected efficiently (Momzikoff *et al.*, 2004). Frka *et al*. (2009) suggested that the glass plate is particularly appropriate for less productive oligotrophic oceanic regions since it collects a relatively thin SML.

However, it is impractical to use glass plate samplers on a large vessel as the glass plate needs to be deployed by hand and because it is impossible to reach the water surface. In addition, sample volumes are relatively small (~ 22 ml min^{-1}), which limits the number of subsequent analyses, especially in multidisciplinary studies and for biological products with high degradation rates. The sampling needs to be short enough in duration to prevent sample degradation prior to biological analyses (Guitart *et al.*, 2004; Cunliffe and Wurl, 2014).

Another important issue in the use of glass plates is that plate withdraw rates are both user-specific and vary with weather conditions such as wind speed that influence the SML thickness collected (Cunliffe and Wurl, 2014). Therefore, it is recommended that glass plates are used only at low wind speeds (i.e. below 5 m s^{-1}) (Guitart *et al.*, 2004).

Single use membrane filters are the most efficient means of collecting small volume samples (sampling depth ~ 6 – 42 µm) that are exclusively SML, i.e. with minimal dilution by underlying water (Franklin *et al.*, 2005; Cunliffe and Murrell, 2009; Cunliffe and Wurl, 2014) (Figure 1.4).

The two most common filter membranes in use are polycarbonate (sampling depth 35 – 42 µm) (Franklin *et al.*, 2005) and polytetrafluoroethylene (PTFE) (sampling depth ~ 6 µm) (Cunliffe *et al.*, 2009a). These are the most appropriate for molecular analyses of bacterial communities, bacterioneuston studies and microbiological research (Franklin *et al.*, 2005; Cunliffe *et al.*, 2009a; Cunliffe and Wurl, 2014). The filters are deployed by floating them directly on the surface waters and then collecting the filters using forceps (Figure 1.4).

However, such small sample volumes may limit the number of analyses in multidisciplinary biological studies (Hamilton *et al.*, 2014). Their use is also limited to conditions of negligible waves and light winds, and like glass plates their use is not practical on large vessels (Cunliffe *et al.*, 2009a; Cunliffe and Wurl, 2014).

The mesh screen (Garrett screen) sampler, first described by Garrett (1965), collects a relatively large sample volume, sampling a depth ~150 – 400 µm, and is therefore of most use for multiple subsequent analyses (Garrett, 1965; Carlson, 1982; Cunliffe *et al.*, 2009a).

The Garrett screen can be used to routinely collect ~ 2.5 litres hr^{-1} (Schneider-Zapp *et al.*, 2014), which is more than can be collected with a glass plate, especially at relatively high sea states (Momzikoff *et al.*, 2004). The SML sample thickness collected with a Garrett Screen is also more consistent than that collected with a glass plate (Carlson, 1982; Cunliffe and Wurl, 2014). The Garrett screen is one of the most suitable samplers for multidisciplinary biological studies and is also beneficial for some specific components like amino acids with high degradation rates (Kuznetsova and Lee, 2001). Consequently, Garrett screens have been widely used in recent years for successfully determining the spatial and temporal variability of a range of the

SML components (Frka *et al.*, 2009; Salter *et al.*, 2011; Cunliffe and Wurl, 2014; Pereira *et al.*, 2016).

The Garrett screen has been shown to be especially suitable for characterizing suspended organic matter (Momzikoff *et al.*, 2004), large phytoplankton cells such as diatoms and heterotrophic nanofelagellates, viruses and bacteria, and chlorophyll (Agogué *et al.*, 2004).

However, it has been suggested that the large sample volumes collected with a Garrett screen could be diluted by a factor of six to eight with underlying water (Yang *et al.*, 2001), which may compromise its ability to accurately define SML composition. This potential for "contamination" with bulk seawater is the major drawback of using the Garrett screen.

Taking account of the advantages and disadvantages of the several SML samplers available, and in order to maintain consistency with previous research to enable data comparison, the Garrett screen was selected for exclusive use during the work described in this thesis. Additionally, the Garrett screen is the best and most practical sampler for deployment from a large vessel. In a previous study at Newcastle University the Garrett screen and glass plate samplers were compared for collecting SML surfactants in the River Tyne estuary. The two samplers had a statistically similar performance as determined by subsequent surfactant measurements (t-test; $p = 0.15$, n = 16) (Salter, 2010).

1.1.3 *SML composition*

Defining the chemical composition of the SML remains a controversial subject due to the lack of a single standardized sampling method and subsequent analytical procedures (Frka *et al.*, 2009). Even so, the SML appears to be a complex matrix of polymeric molecules with a wide range in solubility, surface active properties, molecular weights and sources (Mazurek *et al.*, 2008). These properties reflect the origin of these individual components in deep water, in the terrestrial domain and their deposition from the atmosphere (Wurl *et al.*, 2009; Cunliffe *et al.*, 2013).

The chemical matrix of the SML includes various organic and inorganic compounds. For example, total (including dissolved and particulate) organic carbon, nitrogen and phosphorous, dissolved ammonia and nitrate, metals (Barker and Zeitlin, 1972) including copper, iron and

zinc, heavy metals (Hardy *et al.*, 1990) and marine pollutants of both natural and anthropogenic origin (Cunliffe *et al.*, 2013) are enriched in the SML (Goering and Menzel, 1965; Williams, 1967; Barker and Zeitlin, 1972; Williams *et al.*, 1986) (Table 1.1).

Table 1.1. Global distribution of organic and inorganic compounds, metals and heavy metals concentrations in surface microlayer (SML) and their enrichment factors

Compound	SML concentration (Mean ± SD) , range	EF (Mean ± SD.) , range	Reference
DOC	0.44*	-	Goering and Menzel (1969)
DOC	1.82 - 18.10mgL^{-1}	Up to 1.33 (coastal waters)	Carlson (1983)
DOC	1.20 - 3.73mgL^{-1}	1-96 - 2080	Carlson (1983)
DOC	161.2 ± 98 µmolL^{-1}	1.44^{+}	Reinthaler *et al*. (2008)
DOC	143.1 ± 25.3 µmolL^{-1}	1.83^{+}	Reinthaler *et al*. (2008)
PO_4^{3-}	0.08*	-	Goering and Menzel (1969)
PO_4^{3-}	0.09 ± 0.11 µmolL^{-1}	1.5^{+}	Reinthaler *et al*. (2008)
PO_4^{3-}	0.04 ± 0.02µmolL^{-1}	4.0^{+}	Reinthaler *et al*. (2008)
NH_3	0.311*	-	Goering and Menzel (1969)
NH_3	11.1 ± 2.62, 8.2 - 14.4[1]	20.67 ± 12.64, 5 - 36^{+}	Willias (1967)
NH_4	1.76 ± 1.13 µmolL^{-1}	8.0^{+}	Reinthaler *et al*. (2008)
NH_4	2.30 ± 1.05 µmolL^{-1}	10.45^{+}	Reinthaler *et al*. (2008)
NO_2^{-}	0.0084*	-	Goering and Menzel (1969)
NO_2^{-}	0.28 ± 0.37, 0 - 1[1]	1.25 ± 1.06, 0.5 - 2^{+}	Williams (1967)
NO_2^{-}	0.02 ± 0.01 µmolL^{-1}	2.0^{+}	Reinthaler *et al*. (2008)
NO_2^{-}	0.02 ± 0.01 µmolL^{-2}	2.0^{+}	Reinthaler *et al*. (2008)
NO_3^{-}	4.5 ± 3.4µgL^{-1}	10.97^{+}	Barker and Zeitlin (1972)
NO_3^{-}	2 ± 1.86, 0.2 - 6.3[1]	4.81 ± 3.92, 1.23 - 12^{+}	Willias (1967)
NO_3^{-}	0.09 ± 0.11 µmolL^{-1}	1.8^{+}	Reinthaler *et al*. (2008)
NO_3^{-}	0.39 ± 0.14 µmolL^{-1}	13^{+}	Reinthaler *et al*. (2008)
SiO_4^{2-}	0.723*	-	Goering and Menzel (1969)
DON	24.21 ± 12.35, 8.7 - 39.2[1]	2.78 ± 1.35, 1.38 - 4.89^{+}	Willias (1967)
DON	18.3 ± 7.9 µmolL^{-1}	3.32^{+}	Reinthaler *et al*. (2008)
DON	18.7 ± 6.0 µmolL^{-1}	3.89^{+}	Reinthaler *et al*. (2008)
DOP	0.24 ± 0.05 µmolL^{-1}	1.2^{+}	Reinthaler *et al*. (2008)
TOC	18.4 ± 16.5mgL^{-1}	10.2^{+}	Barker and Zeitlin (1972)
Tp	0.40 ± 0.23µgL^{-1}	4.0^{+}	Barker and Zeitlin (1972)
Na	10950 ± 120 ppm	1.03^{+}	Barker and Zeitlin (1972)
K	408 ± 11ppm	1.07^{+}	Barker and Zeitlin (1972)
Ca	442 ± 16ppm	1.08^{+}	Barker and Zeitlin (1972)

Dissolved organic carbon (DOC), dissolved organic nitrogen (DON), dissolved organic phosphorous (DOP), total organic carbon (TOC), total phosphorous (Tp), phosphate (PO_4^{3-}), ammonia (NH_3), ammonium (NH_4), nitrite (NO_2^{-}), nitrate (NO_3^{-}), sodium (Na), potassium (k), calcium (Ca),magnesium (Mg), copper (Cu),lead (Pb), zinc (Zn), arsenic (Ar), chromium (Cr), nickel (Ni), strontium (Sr), cadmium (Cd) and iron (Fe). * display mean difference between SML and 1m depth. ** shows the range of the concentration in SML or the range of enrichment factor of the compound. + represents the data with sub-surface water < 1m. [1] shows SML average concentration (µmolL^{-1}) and its range.

Table 1.1. (Continued) Global distribution of organic compounds, inorganic compounds, metals and heavy metal concentrations in surface microlayer (SML) and their enrichment factors

Compound	SML concentration (Mean ± SD) , range	EF (Mean ± SD.) , range	Reference
Mg	1311 ± 8ppm	1.01+	Barker and Zeitlin (1972)
Sr	8.68 ± 0.49ppm	18.86+	Barker and Zeitlin (1972)
Fe	56.8 ± 8ppb	4.20+	Barker and Zeitlin (1972)
Zn	39.7 ± 13.7ppb	2.83+	Barker and Zeitlin (1972)
Zn	0.17 - 0.55 (Dissolved)μgL^{-1}**	<5 - <50 (Dissolved)**	Pattenden et al. (1981)
Zn	18.90 - 58.90 (Total)μgL^{-1}**	2.6 (Total)**	Hardy et al. (1990)
Zn	0.20 - 5.80 (Dissolved)μgL^{-1}**	2.0 (Dissolved)	Brügmann et al. (1992)
Zn	10.20 - 20.50 (Total)μgL^{-1}**	1.1 - 4.7 (Total)**	Hardy and Cleary (1992)
Zn	5.42 - 15.37 (Total)μgL^{-1}**	1.6 - 3 (Total)	Cuong et al. (2008)
Cd	0.11 - 0.20 (Total)μgL^{-1}**	0.4 (Total)**	Hardy et al. (1990)
Cd	0.02 - 0.08 (Total)μgL^{-1}**	1.1 - 1.6 (Total)**	Hong and Lin (1990)
Cd	0.001 - 0.10 (Dissolved)μgL^{-1}**	1.5 (Dissolved)	Brügmann et al. (1992)
Cd	0.20 - 18.40 (Total)μgL^{-1}**	1.6 - 2.7 (Total)**	Hardy and Cleary (1992)
Cd	4.8μgL^{-1} (Total)	55 (Total)	Migon and Nicholas (1998)
Cd	0.02 - 0.08 (Total)μgL^{-1}**	0.7- 2.6 (Total)	Cuong et al. (2008)
Cu	11.5 ± 3.7ppb	15.2+	Barker and Zeitlin (1972)
Cu	4.20 - 16.20 (Total)μgL^{-1}**	8.0 (Total)**	Hardy et al. (1990)
Cu	0.60 - 2.30 (Total)μgL^{-1}**	1.0 - 2.61 (Total)**	Hong and Lin (1990)
Cu	<0.001 - 2.20 (Dissolved)μgL^{-1}**	1.5 (Dissolved)	Brügmann et al. (1992)
Cu	1.40 - 4.70 (Total)μgL^{-1}**	1.9 - 8.7 (Total)**	Hardy and Cleary (1992)
Cu	0.06μgL^{-1} (particulate)	1.6 (Total)	Grotti et al. (2001)
Cu	1.25 - 5.72 (Total)μgL^{-1}**	1.7 - 5.0 (Total)	Cuong et al. (2008)
Cr	0.65 - 2.72 (Total)μgL^{-1}**	1.4 - 2.8 (Total)	Cuong et al. (2008)
Pb	0.29 - 1.00 (Dissolved)μgL^{-1}**	140 - 410 (Dissoved)**	Pattenden et al. (1981)
Pb	4.90 - 24.20 (Total)μgL^{-1}**	43 (Total)**	Hardy et al. (1990)
Pb	<0.001 - 0.40 (Dissolved)μgL^{-1}**	2.2 (Dissolved)	Brügmann et al. (1992)
Pb	0.77 - 2.07 (Total)μgL^{-1}**	1.9 - 6.1 (Total)**	Hardy and Cleary (1992)
Pb	1.2 - 6.5μgL^{-1} (Total)**	19 (Total)	Migon and Nicholas (1998)
Pb	0.11 - 0.51 (Total)μgL^{-1}**	1.9 - 3.4 (Total)	Cuong et al. (2008)
As	0.34 - 1.19 μgL^{-1} (Dissolved)**	0.9 - 1.1 (Dissolved)	Cuong et al. (2008)
Ni	0.46 - 2.10 (Total)μgL^{-1}**	0.9 - 2.2 (Total)	Cuong et al. (2008)

Dissolved organic carbon (DOC), dissolved organic nitrogen (DON), dissolved organic phosphorous (DOP), total organic carbon (TOC), total phosphorous (Tp), phosphate (PO_4^{3-}), ammonia (NH_3), ammonium (NH_4), nitrite (NO_2^-), nitrate (NO_3^-), sodium (Na), potassium (k), calcium (Ca),magnesium (Mg), copper (Cu),lead (Pb), zinc (Zn), arsenic (Ar), chromium (Cr), nickel (Ni), strontium (Sr), cadmium (Cd) and iron (Fe). * display mean difference between SML and 1m depth. ** shows the range of the concentration in SML or the range of enrichment factor of the compound. + represents the data with sub-surface water < 1m. [1] shows SML average concentration ($\mu molL^{-1}$) and its range.

For total dissolved organic compounds, SML enrichment factors of up to 10^3 have been recorded relative to underlying water (Liss *et al.*, 2005). For some individual components, enrichments may be smaller but still important. For example, Frew *et al*. (1990) found that extracellular production of dissolved carbohydrates during the stationary phase [1] of phytoplankton growth led to their enrichment in the SML by up to 47% (Frew *et al.*, 1990).

One recent comprehensive study of SML chemical composition was conducted by Gade *et al*. (2006) who investigated surface film elasticity in the Southern California Bight and U.S. Middle Atlantic Bight. The SML was sampled in eutrophic coastal and oligotrophic waters, representing various enrichments of surfactants including lipids, biopolymers, synthetic polymers and humic materials. The relative proportions of these compounds within the SML was shown to influence SML elasticity (Gade *et al.*, 2006).

The enrichments of some important classes of compounds in the SML, along with some details of their sources and cycling, is reviewed below.

1.1.3.1 Marine pollution

The SML is a source and/or sink for a range of marine pollutants deriving from terrestrial sources, transported via rivers, and atmospheric deposition (Cincinelli *et al.*, 2001; Wurl and Obbard, 2004; Guitart *et al.*, 2007; Cunliffe *et al.*, 2013) (Table 1.2).

[1] The growth dynamics of phytoplankton is characterized by four phases according to cell density, including a lag or induction phase in which little increase in cell density occurs. The next stage is the exponential phase in which cell density increases over the time. In the stationary phase the cell density is relatively constant and in the final, death phase, it decreases rapidly.

Table 1.2. Marine pollutants in SML. SML concentrations (ngL^{-1}) and enrichment factor (EF) of pesticide (DDTs), hexachlorocyclohexane (HCHs), polychlorinated biphenyls (PCBs), polycyclic aromatic hydrocarbon (PAHs) and n-alkanes in marine environments

Region	Year	Compound	SML Concentration (ngL^{-1})	EF	Reference
Biscayne Bay, Florida Straits	1968	DDT residues	80–12710	80–12710	Seba and Corcoran (1969)
Narragansett Bay, Rhode Island	1972	PCBs	450–4200	9–62	Duce *et al*. (1972)
North Central Pacific	1972	DDT residues	<0.02–15.4	<15	Williams and Robertson (1973)
		PCBs	5.2–50	0.9–3	
Swedish West Coast	1972	DDT residues	39×10^6		Larsson *et al*. (1974)
		PCBs	33×10^6		
Sargasso Sea	1973	DDT residues	<0.05 - 0.7	0.8–4	Bidleman and Olney (1974)
		PCBs	<3.8 - 19.3	2.7–20	
Western Baltic Sea	1974	DDT residues	0.1 - 3.4		Stadler and Ziebarth (1976)
		PCBs	1.1 - 5.9		
Western Mediterranian Sea (coastal area)	1976	n-alkanes	15×10^3 - 1214×10^3	6.3 - 169.1	Marty and Saliot (1976)
English Channel (coastal area)	1976	n-alkanes	17710 - 97990	161 - 350	Marty and Saliot (1976)
Western Baltic Sea	1976 - 1978	DDT	<0.05		Gaul and Ziebarth (1980)
		HCHs	<0.02 - 19.0	0.6 - 3.0	
		PCBs	29.9 - 235.2	12–21	
Mediterranean Sea	1977	DDT residues	39.9		Mikhaylov (1979)
Rijeka Bay, Adriatic Sea, Croatia	1977 - 1981	*p,p´*-DDT	<1–12.5	1–39	Picer and Picer (1992)
		PCBs	1–597	2.2 - 59	
Blanca Bay, Argentina	*1980 - 1981*	*o,p´-DDT*	<3.6–100.7	0.1–21.3	Sericano and Pucci (1984)
		ß-HCH	14.3–219.5	0.5–23.1	
Mediterranean Sea, Monaco	1981 - 1982	PCBs	3.2 - 35.9	15 - 49	Burns *et al*. (1985)
Baltic Sea and north-east Atlantic	1980 - 1984	DDT	0.22 - 17.9	<0.1 - 44	Mohnke *et al*. (1986)
		HCHs	0.06 - 11.9	<0.1 - 8	
Los Angeles, California	1986	DDTs	47 - 179		Cross *et al*. (1987)
		PCBs	8141 - 30708		
Northern Adriatic Sea		n-alkanes	97 - 1073	2.8 - 3.12	Marty *et* al. (1988)
Atlantic Ocean and Gulf of Mexico	1989	HCHs	0.15 - 1.75	0.8 - 1.4	Chernyak *et al*. (1995)
Barents Sea	1992	*p,p´*-DDT	<0.0006		Chernyak *et al*. (1995)
		HCHs	0.11 - 0.51	0.7 - 1.8	
		PCBs	<0.001		
Alexandria, Egypt	1997	DDT	0.1 - 14	1.9 - 3.2	Abd-Allah (1999)
		PCBs	36.6 - 412.2	1.9 - 2.9	
Tyrrhenian Sea (Coastal area near Leghorn)	2001	n-alkanes	$213 - 3674 \times 10^3$	1.5 - 350	Cincinelli *et al*. (2001)
North-west of Mediterranean Sea	2007	PAHs	730	4.26	Guitart *et al*. (2007)

Many of the marine pollutants previously studied are no longer in use and more recent research is tending to focus on microplastics in the SML, both in situ (Collington *et al.*, 2012) and more recently in artificial SMLs in the laboratory (Guo *et al.*, 2016).

The concentrations of pollutants in the SML is often elevated near to the source of the pollution. For example, the typical concentration range for total seawater hydrocarbons is 1 to 50 µg L^{-1} but this rises to mg L^{-1} levels in the SML close to pollution sources such as oil discharge or terrestrial runoff (Saliot, 1981).

One of the most abundant classes of anthropogenic pollutants in the marine environment, distributed in the water column, sediments, atmosphere and the SML are phthalate esters, which may be very harmful to biota both in the SML and in water column (Giam *et al.*, 1978; Murray *et al.*, 1981b; Turner and Rawling, 2000).

Some other hydrophobic marine pollutants such as polychlorinated biphenyls (PCBs), pesticide DDT and pentachlorophenol (PCP) have a strong tendency to accumulate in the SML, although their concentrations are typically less than 10 ng L^{-1} even close to the source of pollution. Even so, these concentrations are still toxic to SML organisms (Murray *et al.*, 1981a; Murray *et al.*, 1981b; Duinker and Boon, 1986).

1.1.3.2 Dissolved Organic Matter (DOM)

In aquatic environments, organic matter exists in dissolved, colloidal and particulate forms (Mopper *et al.*, 1996; Patel-Sorrentino *et al.*, 2002). Dissolved organic matter (DOM) is the dominant organic carbon reservoir in the oceans (~ 97% of total organic carbon) (Hansell, 2013; Kowalczuk *et al.*, 2013). Figure 1.5 represents DOM in the SML. Surfactants are an important DOM fraction so the study of total DOM or selected DOM fractions such as chromophoric dissolved organic matter (CDOM) can provide insights into surfactant both in the SML and in SSW, which may have differing DOM and surfactant compositions and behaviour.

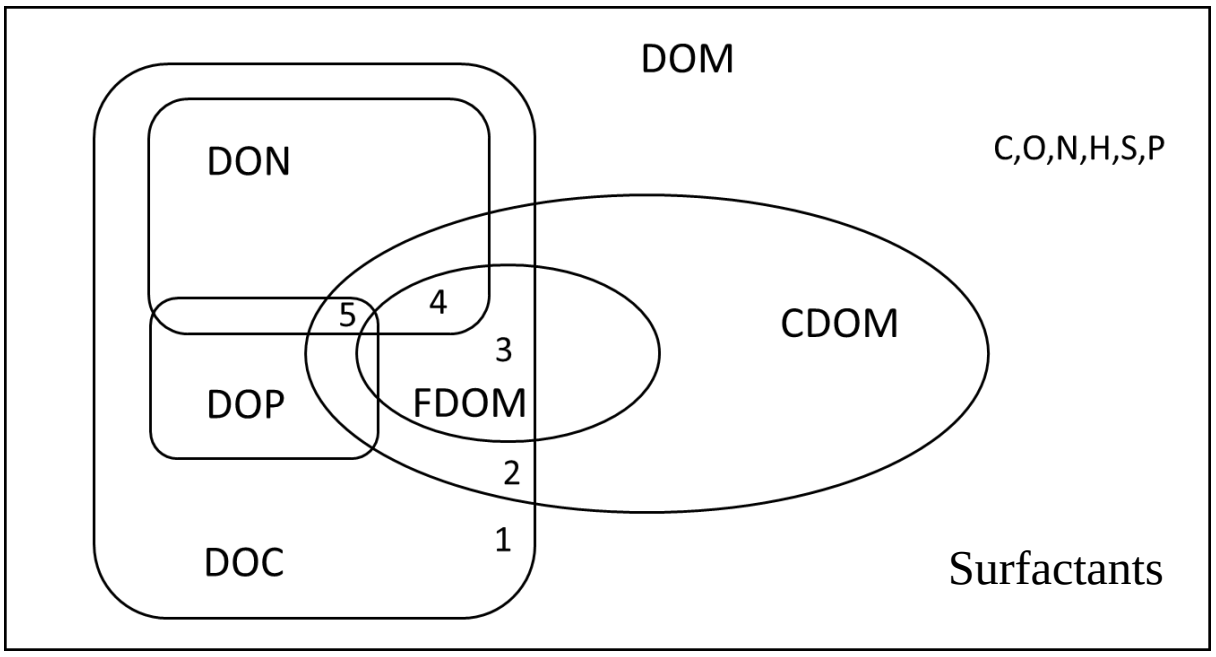

Figure 1.5. Schematic of Dissolved organic matter (DOM) pools adapted from Hansell and Carlson (2014).The numbered boxes and circles represent different subsets of compounds of DOM including dissolved organic nitrogen (DON), dissolved organic phosphorous (DOP), dissolved organic carbon (DOC), fluorescent dissolved organic matter (FDOM) and chromophoric dissolved organic matter (CDOM). DOM is primarily composed of carbon (C), oxygen (O), nitrogen (N), hydrogen (H) phosphorous (P) and sulphur (S).

DOM is primarily composed of carbon, oxygen, nitrogen, hydrogen, sulphur and phosphorous. A variable fraction of DOM, chromophoric dissolved organic matter (CDOM), is light absorbing which has led to the use of absorbance spectrophotometry to estimate the total concentration of marine DOM and broadly characterize its composition (Korshin *et al.*, 1997). A part of CDOM can fluoresce if excited by light of particular wavelengths (fluorescent dissolved organic matter: FDOM) (Hansell and Carlson, 2014). Varieties of DOM including dissolved organic nitrogen (DON), dissolved organic phosphorous (DOP) and dissolved organic carbon (DOC) also have a light absorbing fraction which can fluoresce (Figure 1.5).

DOM is a heterogeneous mixture of different molecular weight organic compounds such as carbohydrates, fatty acids, amino acids, their polymers and various complexes, e.g. with trace metals (Kowalczuk *et al.*, 2013; Hansell and Carlson, 2014). Even so, more than 85% of oceanic DOM has yet to be characterized due to its chemical complexity (Benner, 2002).

The primary sources of DOM in the marine environment are autochthonous (i.e. formed in situ) and allochtonous (i.e. originating outside the system). The relative contributions of each to total DOM are dependent upon specific location and environmental conditions (Kowalczuk *et al.*, 2013). Autochthonous DOM dominates in the open ocean and comprises of material deriving

from phytoplankton, bacteria and their degradation products and material arising via photochemical activity. Allochtonous DOM is more abundant in coastal waters due to their proximity to terrestrial source areas (Nagata, 2000; Carlson, 2002; Hudson *et al.*, 2007; Kowalczuk *et al.*, 2013; Hansell and Carlson, 2014).

Kowalczuk *et al*. (2013) studied the composition of DOM in the Atlantic Ocean using Fluorescence Excitation Emission Matrix spectroscopy along with Parallel Factor Analysis (PARAFAC) modelling. They suggested that DOM composition varies in relation to dominant water masses. The analyses revealed six different DOM components including two-humic like compounds with a terrestrial origin and microbial production, one marine humic-like component and three protein-like components (Kowalczuk *et al.*, 2013).

The dynamics of humic-type materials are maintained by microbial production and recycling in deep waters below the base of the mixed layer in the vast region of the Atlantic Ocean and removal in the mixed layer in subtropical and tropical regions due to their susceptibility to high solar radiation (Stedmon and Markager, 2005; Omori *et al.*, 2010; Kowalczuk *et al.*, 2013).

Protein-like components with similar optical characteristics to tyrosine, tryptophan and phenylalanine were found to be dominant in the mixed layer of oligotrophic gyres, suggestive of in-situ biological DOM production, and were low on the coastal western European continental shelf.

The ratio of the intensity of protein-like components to corresponding humic-like components is also indicative of the modification of DOM composition (Kowalczuk *et al.*, 2013).

1.1.3.2.1 Chromophoric Dissolved Organic Matter (CDOM)

As mentioned briefly above, chromophoric dissolved organic matter (CDOM) is an optically active fraction of the seawater DOM pool (filtrate < 0.2 µm) (see Figure 1.5) and the major contributor to the attenuation of solar irradiation in seawater. CDOM absorbs light in the UV range (100 – 400 nm; responsible for ~ 90% of UV attenuation) (Johannessen *et al.*, 2003; Smyth, 2011; Zepp *et al.*, 2011) and in the visible range (400 – 700 nm), (Bricaud *et al.*, 1981; Siegel and Michaels, 1996; Blough and Del Vecchio, 2002; Siegel *et al.*, 2002; Coble, 2007; Hansell and Carlson, 2014). CDOM can be a substantial fraction (up to 90%) of the total DOM pool in natural waters (Thurman, 1985). CDOM also reduces the availability of photosynthetically active radiation (PAR), particularly important in the surface layers of the

euphotic zone (Ferrari *et al.*, 1996; Nelson and Siegel, 2013) and modifies the light available for ocean color remote sensing (Smith *et al.*, 1992; Siegel *et al.*, 2002; Twardowski *et al.*, 2004; Siegel *et al.*, 2005b).

In the open ocean away from coastal influence, CDOM is mainly produced in-situ (Bricaud *et al.*, 1981), such as by direct excretion by zooplankton and cyanobacteria (Steinberg *et al.*, 2004), sloppy feeding by zooplankton and leaching from zooplankton faecal pellets (Siegel and Michaels, 1996; Nelson *et al.*, 1998; Nelson and Siegel, 2002; Nelson *et al.*, 2004), and as a by-product of the microbial degradation of DOC (Nelson *et al.*, 1998). In coastal waters, additional sources are terrestrially derived material of varying reactivity (Meyers-Schulte and Hedges, 1986; Nelson *et al.*, 1998). Some plant degradation products such as lignin and tannins are also introduced as primary sources of CDOM in rivers and estuaries (Coble, 2007; Stubbins *et al.*, 2010).

Considering the various origins of CDOM in the marine environment prompts the idea that CDOM production is a depth-related process that thus varies throughout the water column. While CDOM dynamics in surface waters is facilitated by high solar radiation (i.e. photochemical production and destruction), microbial activity is thought to be responsible for considerable CDOM production in deep waters with low light availability (Siegel *et al.*, 1995; Nelson *et al.*, 1998). This is supported by the observed similarity between profiles of CDOM and heterotrophic bacterial abundance below 50 m in the Sargasso Sea (Carlson *et al.*, 1996). Laboratory experiments with Sargasso Sea water also showed bacteria consume DOM and produce CDOM simultaneously in dark cultures (Nelson *et al.*, 1998).

Research has also been carried out to investigate CDOM production in the Atlantic and Pacific Oceans. For example, Yamashita and Tanoue (2008) and Yamashita *et al*. (2010) suggested CDOM production in the Pacific Ocean by in-situ oxidation of organic matter. This agreed with the conclusions of Swan *et al*. (2009) and Nelson *et al.* (2010) that CDOM production in the oceans is facilitated by in-situ oxidation of particulate organic matter, a conclusion reached via relationships between CDOM absorbance at 325 nm (a_{325}) and apparent oxygen utilization (AOU). On the other hand, Murphy *et al*. (2008) suggested that terrestrial deposition of humic-like materials might make a significant contribution to CDOM production across the Atlantic and Pacific Oceans close to the continental shelves. Andrew *et al*. (2013) also suggested that CDOM optical changes in the Equatorial Atlantic Ocean are indicative of chemical or microbial modification of humic-like materials with terrestrial sources.

Table 1.3 summarizes the ranges of average CDOM absorbance (m^{-1}) in various aquatic environments with different trophic levels.

Table 1.3. CDOM absorption coefficient (m^{-1}) in a range of wavelengths in the various aquatic environments. The mean, standard deviation and the range of CDOM are displayed. Adopted from Tilstone et al. (2012)

		CDOM (m^{-1})		
Region	**Wavelength (nm)**	**Mean ± SD**	**Range (m^{-1})**	**Reference**
Equatorial Atlantic Ocean	355	0.155 ± 0.190	0.057 - 0.943m^{-1}	Andrew *et al*. (2013)
Arabian Sea	375	0.112	0.051 - 0.071	DelCastillo and Coble (2000)
North Sea	443	-	0.04 - 0.30	Babin *et al*. (2003)
North Sea	442	-	0.066 - 0.21	Warnock *et al*. (1999)
English Channel	442	0.30 ± 0.07	0.007 - 0.65	Vantrepotte *et al*. (2007)
NW UK Coast	440	0.378	0.089 - 1.57	Bowers *et al*. (2000)
UK Coast	442	0.031	0.004 - 0.48	Foden *et al*. (2008)
Irish Sea	442	0.376 ± 0.039	0.009 - 0.957	Tilstone *et al*. (2005)
Baltic Sea	440	-	0.015 - 1.7	Darecki *et al*. (2003)
Skagerrak	442	0.56 ± 0.16	0.03 - 1.08	Stedmon *et al*. (2000)
Skagerrak	442	0.62	0.2 - 2.0	Sørensen *et al*. (2007)
Skagerrak	442	0.74 ± 0.16	-	Højerslev and Aas (2001)
Baltic Sea	442	0.37 ± 0.19	0.1 - 1.44	Kowalczuk *et al*. (2006)
Belgium Coast	442	-	0.20 - 1.31	Astoreca *et al*. (2009)
North Sea	442	0.348 ± 0.013	0.020 - 2.164	Tilstone *et al*. (2012)
North Sea	412	-	0.022 - 0.327	Brown (1977)
Baltic proper	412	-	0.136 - 0.284	Brown (1977)
Baltic riverine	412	-	2.49	Brown (1977)
Bermuda	412	-	~ 0.1 - 0.4	Nelson *et al*. (1998)
Gulf of Paria	412	-	1.25 - 4.59	Blough *et al*. (1993)

Table 1.3. (continued) CDOM absorption coefficient (m^{-1}) in a range of wavelengths in the various aquatic environments. The mean, standard deviation and the range of CDOM are displayed. Adopted from Tilstone et al. (2012)

		CDOM (m^{-1})		
Region	**Wavelength (nm)**	**Mean ± SD**	**Range (m^{-1})**	**Reference**
S. Florida/Gulf of Mexico	412	-	0.01 - 6.32	Green and Blough (1994)
Amazon River Estuary	412	-	0.03 - 1.33	Green and Blough (1994)
Coastal Mid-Atlantic Bight	412	-	0.14 0.71	Vodacek *et al*. (1997)
Offshore Mid-Atlantic Bight	412	-	0.009 - 0.14	Vodacek *et al*. (1997)
Gulf of Paria	412	-	0.09 - 1.34	DelCastillo *et al*. (1999)
Coastal NewZealand	412	-	0.023 - 0.165	Davies-Colley (1992)
Danish fjords and coastal waters	412	-	0.14 - 3.46	Stedmon *et al*. (2000)
Greenland Sea	412	-	0.04 - 0.70	Stedmon and Markager (2001)
Mauritanian upwelling	412	-	0.03 - 0.12	Bricaud *et al*. (1981)
Gulf of Guinea	412	-	0.04 - 0.17	Bricaud *et al*. (1981)
Villefrance Bay	412	-	0.09 - 0.24	Bricaud *et al*. (1981)
Var River	412	-	0.21	Bricaud *et al*. (1981)
Baltic Sea	412	-	2.18	Bricaud *et al*. (1981)
Gulf of Fos-sur-Mer	412	-	0.12 - 0.82	Bricaud *et al*. (1981)
Globally representative	412	-	~0.003 - 10.0	Schwarz *et al*. (2002)
Gulf of Mexico	412	-	0.002 - 0.074	Carder *et al*. (1989)
Baltic proper	412	-	0.782	Kalle (1966)
North Sea	412	-	0.251	Kalle (1966)
North Atlantic	412	-	0.038	Kalle (1966)
Gulf of California	412	-	~0.095	Maske *et al*. (1998)
Jiazhou Bay (China)	305	5.99mgL^{-1}	-	Ren *et al*. (2010)

CDOM vertical distributions (excluding the SML) typically show a surface-minimum and subsurface-maximum, with subsurface CDOM production during the summertime. CDOM production in the summertime is also balanced by CDOM photooxidation (photobleaching) due to high solar radiation, water stratification and a shallower mixed layer depth (Siegel *et al.*, 1995; Siegel and Michaels, 1996; Nelson *et al.*, 1998). However, the magnitude of this pattern is location-dependent and varies with environmental conditions.

In the wintertime, CDOM is suggested to distribute more homogenously throughout the water column because of deepening of the mixed layer resulting from a well-mixed water column (Hansell and Carlson, 2014).

There are several reports on CDOM dynamics in the marine environment. For example, Siegel and Michaels (1996) proposed the vertical CDOM distribution in the Atlantic Ocean to be controlled by CDOM production around the Deep Chlorophyll Maximum (DCM) depth and upward transport via diffusion and by biological transport through the diurnal migration of plankton, with its removal mostly by photooxidation in summer. In-situ CDOM microbial production (using DOM as the substrate), CDOM removal by photodegradation (mainly in surface waters) and microbial consumption were also proposed to contribute to CDOM dynamics in the Sargasso Sea (Nelson *et al.*, 1998).

Photodegradation as the major removal pathway of CDOM in mostly surface waters including the SML. Photodegradation causes CDOM to lose its absorption capacity and become modified to optically inactive DOM following prolonged light exposure (photobleaching or photodegradation). Photodegradation also facilitates the formation of lower molecular weight organic matter with more absorption at shorter wavelengths from higher molecular weight CDOM components with higher longer wavelengths absorption (Siegel *et al.*, 1995; Nelson *et al.*, 1998; Del Castillo and Coble, 2000; Stedmon and Markager, 2001; Twardowski and Donaghay, 2002; Nelson *et al.*, 2004; Helms *et al.*, 2008; Kowalczuk *et al.*, 2013; Galgani and Engel, 2016). It was shown that 96% of allochthonous and almost 100% of autochthonous CDOM removal occurring in the oligotrophic gyres of the South Pacific Ocean is due to photobleaching (Swan *et al.*, 2009). On the other hand, photochemical breakdown may increase the biological availability of carbon and ease bacterial carbon uptake from refractory materials (Mopper, 1989), thereby increasing heterotrophic respiration and CO_2 exchange with the atmosphere (Blough and Del Vecchio, 2002; Loiselle *et al.*, 2012; Nelson and Siegel, 2013).

By contrast there is no published information specifically on the degradation rates of surfactants in the SML or in SSW.

CDOM minima were observed in near surface waters of the Mid Atlantic Bight (MAB) during summer, with CDOM turnover times of between 1 and 3 months (Siegel and Michaels, 1996; Nelson *et al.*, 1998; Boss *et al.*, 2001). A reduction in the CDOM/DOC ratio due to CDOM photochemical degradation was also reported in the Western North Atlantic (Vodacek *et al.*, 1997; Del Vecchio and Blough, 2004). Therefore, the size of the marine CDOM pool reflects a balance between its biological sources and photooxidation removal (DeGrandpre *et al.*, 1996; Siegel and Michaels, 1996; Hansell and Carlson, 2014).

Galgani and Engel (2016) proposed a model to describe CDOM dynamics based on CDOM absorption and fluorescence in the ocean and particularly in the SML of the upwelling region off the coast of Peru.

According to this model, in-situ biological CDOM produced in underlying water is scavenged to the SML by upwelled waters, resulting in CDOM accumulation in the SML (Galgani and Engel, 2016). Also, there is some contribution from in-situ microbial fresh[2] CDOM production in the surface waters (Galgani and Engel, 2016). The accumulation of CDOM in the SML is balanced by microbial and photochemical degradation.

1.1.3.2.2 Fluorescent Dissolved Organic Matter (FDOM)

Fluorescent dissolved organic matter (FDOM; see Figure 1.5) is a CDOM fraction that is excited by light in the UV-blue region of the spectrum (i.e. excitation step) and releases the absorbed energy as fluorescence (i.e. emission step) (Lakowicz, 1999; Coble, 2007). The wavelength at which the fluorescence occurs depends upon FDOM composition. For example, two major FDOM components including humic and fulvic-like materials[3] are blue fluorescent whereas proteins are UV fluorescent (Mopper and Schultz, 1993; Coble, 1996; Baker, 2001; Chen *et al.*, 2003; Stedmon *et al.*, 2003; Baker and Spencer, 2004).

[2] According to Kitidis *et al*. (2006) fresh and old CDOM refers to history of CDOM, while fresh materials are recently produced, the old CDOM has a history of exposure to light and/or bacterial degradation.

[3] Detailed compositions of the CDOM and FDOM pools are poorly characterized. Therefore, their broad compositional characteristics are often described based on similarity to known compound groups such as humic and fulvic acids, hence the terms “humic-like” and fulvic-like.

Fluorescence Excitation-Emission Matrices (EEM) are valuable for characterizing DOM based on excitation/emission intensity maxima that identify different types of fluorophores, which are characteristic of classes of compounds that absorb and release the energy (Coble *et al.*, 1990; Green, 1992; Coble, 1996). CDOM in oceanic samples tends to have a fluorescence maximum at shorter wavelengths (UV region) than CDOM of terrestrial origin (Coble, 1996; Stedmon *et al.*, 2003).

The characterization of FDOM in Horsens fjord, Denmark, revealed five different fluorescent DOM fractions, including four allochtonous fluorophores of terrestrial origin and one autochthonous fluorophore from marine production (Stedmon *et al.*, 2003). In natural freshwaters, FDOM characterization also revealed that humic type materials released by the breakdown of organic matter in water and soil are dominant (Hudson *et al.*, 2007).

Kowalczuk *et al.* (2013) identified six distinct DOM components in the Atlantic Ocean in the SML and throughout the water column to 300 m depth based on fluorescence spectroscopy and PARAFAC. Of these components two were “humic-like”, associated with microbial remineralization and DOM production by marine phytoplankton (Kowalczuk *et al.*, 2013). The two common humic substances in marine environments are humic and fulvic acids with different chemical and optical properties (Harvey *et al.*, 1983; Carder *et al.*, 1989). Three “protein-like” components had fluorescent spectral characteristics similar to tryptophan and tyrosine (Kowalczuk *et al.*, 2013).

1.1.3.3 Surface active compounds (Surfactants)

Surface active compounds or surfactants are a subgroup of the DOM pool with surface active properties. They are amphiphilic molecules consisting of a hydrophilic (polar) head (such as polysaccharides) and a hydrophobic (non-polar) tail (such as lipids) within the same molecule. As a result of this structure, surfactants partition preferentially at the interface between fluid phases with different degrees of polarity and hydrogen bonding, such as water boundaries with the atmosphere, bubbles, particles and sediments (Lang and Wullbrandt, 1999; Gade *et al.*, 2006; Hühnerfuss, 2006) (Figure 1.6).

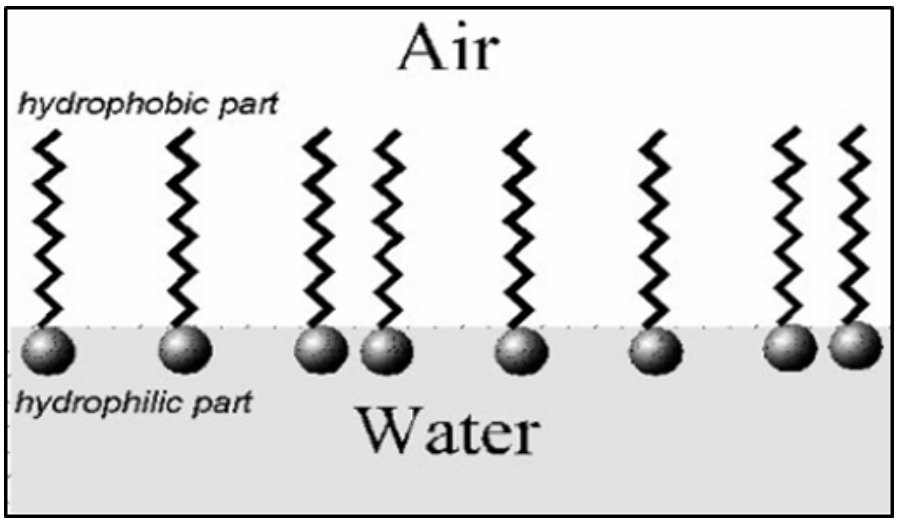

Figure 1.6. Schematic of surfactant arrangements at the air-water interface. The hydrophobic tail is directed into the air while the hydrophilic head is in the water phase. Adapted from Hühnerfuss (2006).

The tail structures of different surfactants are similar, containing hydrocarbon chains; however, the polar head could have different characteristics. Non-ionic surfactants for example have neutral groups whereas ionic surfactants carry an electrical charge in the head part of the molecule. Surfactants with positive charge are known as cationic such as bromide compounds whereas anionic surfactants like phosphate esters have a negatively charged polar head. Typical surfactants are relatively insoluble and the degree of their surface active properties depends on their solubility (Tsai and Yue, 1995).

Pollard *et al.* (2006) reported that anionic surfactants have especially high solubility, being soluble in all solvents tested, whereas cationic surfactants had limited solubility in most solvents.

For a gas/liquid binary system, changes in the concentration of a dissolved component (e.g. a surfactant) in contact with the gas-liquid interface are related to changes in the surface tension (γ), which is influenced by the surface excess of the dissolved component in question, and which results in a corresponding change in surface energy. This is described by the Gibbs adsorption equation. The accumulation or depletion of a dissolved component towards the interface (i.e. adsorption) thus influences γ. A large amount of energy is required to increase the surface area when γ is high. Surfactants with a high tendency towards interfacial accumulation as compared to SSW, exert a large positive surface excess, which reduces the surface tension and surface potential due to a lowering of the Gibbs free surface energy G:

$\gamma = (dG/dA)_{T,P}$ (equation: 1.1.3.3.1).

By comparison, sodium chloride has a negative surface excess (high concentrations in SSW), which would tend to increase the surface tension and surface potential. The resistance of the interface to changes in the surface area (A) is known as viscoelasticity:

$\varepsilon' = -d\pi / d \ln A$ (equation: 1.1.3.3.2)

where π is the surface tension (Barger and Means, 1985; Frew and Nelson, 1992).

In surface films with high elasticity and no viscosity $\varepsilon' = \varepsilon_0$, the Gibbs or equilibrium elasticity. In the presence of surfactants, the Gibbs elasticities have demonstrated ε_0 values in the range 2-40 m Nm^{-1}, sufficient for wave damping (Barger and Means, 1985; Frew and Nelson, 1992). The latter authors confirmed how the compositional difference alters the physical properties of surface films. They showed how the π – A isotherm differs between slicks and non-slick microlayers. A slick microlayer at the same surface pressure as a non-slick microlayer has a consistently higher elastic modulus than a non-slick microlayer (Bock *et al.*, 1999).

Surfactant enrichment in the SML (see section 1.1), as well as altering its physiochemical properties, influences its optical properties and mass and energy transfer between the atmosphere and ocean (MacIntyre, 1974; Hunter, 1977; Frew, 2005; Liss *et al.*, 2005).

Importantly from the standpoint of this thesis, surfactants suppress the air-sea transfer velocity (k_w) of CO_2 and of other climate-active gases (Liss *et al.*, 2005; Nightingale, 2009; Salter *et al.*, 2011; Pereira *et al.*, 2016).

According to the classical model of the SML (see Figure 1.3), organic compounds accumulated at the air-sea interface are characterized as either dry or wet surfactants (Gladyshev, 2002). Dry surfactants such as hydrophobic lipids (Hunter and Liss, 1981; Ćosović, 2005; Frka *et al.*, 2009) form the top layer and enable the further accumulation of less surface active compounds (i.e. “wet surfactants”) such as polysaccharides, proteins and humic-type materials in the SML (Gladyshev, 2002; Frka *et al.*, 2009).

There are several reports of surfactant enrichment in the SML relative to underlying waters in the oceans, based on indirect evaluations, e.g. satellite-derived, or field measurements of primary productivity as a proxy for biological-derived surfactant distributions. For example,

Ćosović and Vojvidić (1982) reported surfactant enrichment in the SML by a factor of ≤ 2.5 in samples from the Adriatic Sea. Gašparović (2012) also recorded SML surfactant enrichment factors of between 1.03 and 1.10 in the Northern Adriatic Sea and Gašparović *et al.* (2007) reported surfactant enrichment factors in the range 1.2 to 2.8 in a Norwegian fjord.

Wurl *et al*. (2011) reported surfactant enrichment factors of between 0.5 and 5.9 in the SML of various marine environments, extrapolated from relationships between surfactants and primary productivity. Salter (2010) found surfactant enrichment factors between 1.2 and 20 in the SML of North Sea coastal samples and Pereira *et al*. (2016) found surfactant enrichments ranging from ~1.0 to 1.9 during 20 km offshore transects in the North Sea. Thus, a wide range of surfactant enrichment factors have been observed (between 1 and 20) clearly dependent on location and probably also time of year.

1.1.3.3.1 Lipids

Lipids are a surfactant sub-group derived from phytoplankton exudates and primary production (Parrish *et al.*, 2005). Total lipid concentration in plankton was reported to account for 3.4 ± 1.7% of dry weight, with a maximum of 6.3 ± 2.5% observed during a phytoplankton bloom in Newfoundland, Canada (Parrish *et al.*, 2005). Also, 16 different chemical structures of marine lipids were identified in dissolved and particulate forms at microgram per litre levels (Parrish, 1988). The main compounds included hydrocarbons, esters, triglycerides, fatty acids, sterols, glycolipids and phospholipids (Parrish, 1988).

In early research, low solubility lipid molecules containing hydrophobic moieties were identified as being associated with the SML (Norkrans, 1980; Hardy, 1982). However, there is some disagreement over lipid abundances in the SML. Garrett (1967) showed that lipids are a major component of the SML in both slick and non-slick conditions, however, Hunter and Liss (1981) reported a smaller lipid contribution to dissolved organic matter (DOM) collected from the SML compared to other organic compounds. They also assumed that high lipid concentrations reported in some SML coastal areas may result from terrestrial input or oil pollution (Hunter and Liss, 1981). Frka *et al*. (2009) proposed that lipids contribute to early stage formation and stabilisation of the SML.

One of the earliest studies of fatty acids specifically, found the highest total concentration in the Mediterranean Sea to be 11.6 µg L^{-1} but there was no correlation with chlorophyll a

concentration. It was suggested that fatty acids are released after the zooplankton bloom as a result of excretion and degradation processes (Goutx and Saliot, 1980).

While the major sources of fatty acids in the oceans are from natural sources such as phytoplankton, anthropogenic sources can also result in high concentrations of fatty acids in rivers, particularly in urban areas (Parrish, 1988). For example, total fatty acid concentrations up to 1 mg L^{-1} were observed in some Japanese coastal areas with a higher contribution of particulate than dissolved fatty acids (Matsumoto, 1981). Hydrocarbons as a pollution indicator in seawaters also account for 20% of total dissolved inorganic lipids in the marine environment (Barbier *et al.*, 1973; Kolattukudy, 1976).

The distribution of dissolved and especially particulate SML lipids show seasonal and spatial variability controlled by biological productivity and water temperature (Gašparović *et al.*, 1998; Parrish *et al.*, 2005; Penezić *et al.*, 2010). For example, Gašparović *et al*. (1998) found that total lipid concentrations were much lower in spring than in summer due to lower biological productivity in the cold waters in the northern Adriatic Sea during spring.

1.1.3.3.2 Carbohydrates

Carbohydrates including monosaccharides and polysaccharides are released by marine phytoplankton such as dinoflagellates and diatoms as intra or extracellular products forming gelatinous compounds. Carbohydrates are also derived as by-products of bacterial decomposition and accumulate in the SML (Myklestad, 1974; Haug and Myklestad, 1976; Sakugawa and Handa, 1985a; Sakugawa and Handa, 1985b; Alldredge *et al.*, 1993).

Early research by Sieburth (1983) considered carbohydrates to be an important component during SML formation and defined the SML as a "*highly hydrated loose gel of tangled macromolecules and colloids*" (see section 1.1.1). This early hypothesis was confirmed later during several field experiments, carbohydrates being reported to contribute to SML formation in the form of microgels (Wurl and Holmes, 2008; Cunliffe and Murrell, 2009; Cunliffe *et al.*, 2009b; Wurl *et al.*, 2009; Wurl *et al.*, 2011b; Gao *et al.*, 2012; Cunliffe *et al.*, 2013).

An alternative explanation of the gelatinous nature of the SML is the excretion of extracellular exopolymer gel particles by bacterioneuston which accumulate in the SML as a defensive mechanism against high solar radiation (Elasri and Miller, 1999; Ortega-Retuerta *et al.*, 2009).

Samples collected from a Sargasso Sea surface slick during a *Trichodesmium* bloom were associated with elevated amylolytic (conversion of starch to sugar) bacterial activity. Lower proteolytic (conversion of protein to sugar) and lipolytic (conversion of lipids to sugar) activities were also found (Sieburth and Conover, 1965). Therefore, it was suggested that carbohydrates must be a larger component of the SML than lipids (Sieburth, 1983). This is supported by recent research showing that marine DOM contains 40% carbohydrates compared to only a 5 – 25% contribution from lipids (Leenheer and Croué, 2003; Carpenter and Nightingale, 2015).

Benner *et al*. (1992) suggested that high molecular weight polysaccharides (> 1000 Daltons molecular weight) are dominant in the surface waters (~50%) supporting heterotrophic activity compared to the deeper waters (~25%). It was also reported higher concentrations of carbohydrates in the surface waters compared to both the oxygen minimum zone and deeper waters in the North Pacific Ocean (Benner and Pakulski, 1992).

There are several reports of carbohydrate contributions to marine organic matter pool outside the SML. Sakugawa and Handa (1985a) proposed that carbohydrates account for only 10 – 20% of DOM in the marine environment. Burney *et al*. (1979) reported that macromolecule sugars may contribute up to nearly 70% of total dissolved carbohydrate in the North Atlantic Ocean. Wheeler (1976) also found that polysaccharides are a major portion of dissolved carbohydrates in seawater off the Georgia coast. These high molecular weight compounds were the most abundant dissolved carbohydrates in surface seawater of Mikawa Bay, Japan (Sakugawa and Handa, 1985b).

Hetero-polysaccharide compounds were also collected from Mikawa Bay, Japan during a dinoflagellate (*Procentrum minimum*) bloom, suggesting the aggregation of phytoplankton-produced carbohydrates via extracellular release or cell lysis (Sakugawa and Handa, 1985a).

1.1.3.3.3 Transparent Exopolymer Particles (TEP)

Transparent Exopolymer Particles (TEP) are operationally defined as particles containing surface-active acidic carbohydrates (Mopper *et al.*, 1995), that form in the water column from abiotic coagulation of DOM precursors (Wei-Chun *et al.*, 1998). They accumulate in the SML via their surface active properties and contribute to its gelatinous structure (Alldredge *et al.*, 1993; Passow, 2002b; Engel, 2004; Wurl and Holmes, 2008; Cunliffe and Murrell, 2009; Wurl *et al.*, 2011a).

TEPs facilitate the transfer of dissolved carbon to the particulate form known as marine snow (Verdugo *et al.*, 2004) by coagulation/aggregation in the water column, and assist subsequent vertical transport of carbon and associated nutrients to the deep ocean (Alldredge and Gotschalk, 1988; Azam and Long, 2001). Therefore TEPs are an important component of the marine carbon and nutrient cycles (Passow *et al.*, 2001; Verdugo *et al.*, 2004; Cunliffe *et al.*, 2011).

There are several sources of TEPs in the oceans; these derive from micro - and macro - organism exudates including those of phytoplankton, bacterioplankton, some macroalgae species, oysters, mussels, scallops and sea snails (Passow, 2002a; McKee *et al.*, 2005; Heinonen *et al.*, 2007).

Smith *et al*. (1995) discussed the production of TEPs in the SML via two different mechanisms. It was suggested that TEPs may be a by-product released by phytoplankton as a defensive mechanism against bacteria or be directly-released by bacteria involved in phytoplankton cell hydrolysis.

Enrichment of TEPs in the SML relative to corresponding sub-surface waters was reported in oceanic samples previously, with enrichment factors relative to the underlying water ranging from 1.7 to 4.8 in the North Pacific, offshore of Hawaii and in the Arctic Ocean (Wurl *et al.*, 2011a).

Cunliffe *et al*. (2009) found TEPs enrichment in the SML ranging between 2.3 and 2.9 during a mesocosm phytoplankton bloom experiment using Norwegian fjord waters.

TEPs demonstrate seasonal variations, with high concentrations during phytoplankton blooms in aquatic environments (Passow, 2002b). It was highlighted that the TEP maxima may occur at the end of a phytoplankton bloom and coincide with higher rates of polysaccharide exudation by nutrient limited phytoplankton (Corzo *et al.*, 2000; Engel *et al.*, 2002; Wurl *et al.*, 2011a).

Wurl *et al*. (2011) also described TEP dynamics via in-situ biological production in the euphotic zone and accumulation in the SML due to their surface-active properties. TEPs then grow within the SML through further aggregation and finally sink to deep waters via grazing or degradation processes or are ejected to the atmosphere via air bubbles bursting at the air-sea interface (Wurl *et al.*, 2011a).

TEPs are recycled within the water column through grazing and degradation processes, by zooplankton and other microorganisms and as a food source for bacteria. Hence, their concentrations decrease with depth due to this bacterial consumption (Mari and Kiørboe, 1996; Engel, 2004; Berman and Holenberg, 2005; Wurl *et al.*, 2011a).

1.1.3.3.4 Proteins

Proteins constitute between 25% and 50% of dissolved organic matter in aquatic environments (Leenheer and Croué, 2003; Carpenter and Nightingale, 2015). However, later research showed that extracellular phytoplankton derived proteins are also enriched in the SML but their accumulation is less efficient than for other components such as carbohydrates due to bacterial utilization of amino acids (Kuznetsova and Lee, 2001; Matrai *et al.*, 2008; Cunliffe *et al.*, 2013).

Early research reported proteins (e.g. glycoprotein) as the most abundant component in the SML (Williams *et al.*, 1986). Later research found that proteins constitute between 25% and 50% of dissolved organic matter in aquatic environments (Leenheer and Croué, 2003; Carpenter and Nightingale, 2015).

Microbial uptake of organic matter is facilitated by enzymatic hydrolysis of protein compounds and other biopolymers in many aquatic environments (Kuznetsova and Lee, 2001). Hydrolysis of accumulated protein via bacterial remineralization in the SML resulted in a lower concentration of amino acids than in underlying water in Stony Book Harbour, New York (Kuznetsova and Lee, 2001). However later studies in the Atlantic Ocean and Mediterranean Sea showed that bacterial growth efficiencies in the SML were low indicating limited bacterial remineralization of proteins in the SML (Reinthaler *et al.*, 2008).

Kuznetsova *et al*. (2004) also reported an inverse correlation between protein enrichment in the SML and primary productivity, with higher SML protein enrichments observed in oligotrophic open ocean waters than in eutrophic coastal waters. This implies that more rapid protein removal occurs in the oligotrophic SML than in the eutrophic SML (Kuznetsova *et al.*, 2004).

1.1.3.3.5 Humic-like materials

The enrichment of humic materials in the SML results from the biological and chemical degradation of terrestrial and aquatic plant material (Stedmon *et al.*, 2003). The major aquatic humic components are humic acids, which have relatively low solubility in very acidic waters, fulvic acids with solubility independent of pH and insoluble humins (Aiken *et al.*, 1985).

The SML enrichment of marine humic-like compounds consisting of 'fresh' marine humic materials associated with biological activity and salinity gradients was reported in a variety of freshwater and marine environments previously (Coble, 1996; Parlanti *et al.*, 2000). Humic materials with terrestrial origins were reported in rivers. Deep marine waters were also suggested to represent 'older', more degraded and modified humic materials (Komada *et al.*, 2002; Hudson *et al.*, 2007).

1.1.3.4 Sources of surfactants

Natural surfactants are derived from multiple sources in the marine environment. Primary sources of surfactants in the open ocean are metabolic by-products of marine phytoplankton (extracellular release during all phases of growth) (Žutić *et al.*, 1981), products of zooplankton and protist grazing (Kujawinski *et al.*, 2002), bacterial degradation products (Hisatsuka *et al.*, 1971; Sieburth *et al.*, 1976; Rosenberg *et al.*, 1979; Hardy, 1982; Kurata *et al.*, 2016), material deposited from the atmosphere (i.e. wet and dry deposition such as rain and dust respectively) (Kurata *et al.*, 2016) and in situ photochemical degradation products of pre-existing organics (Tilstone *et al.*, 2010). In coastal regions additional surfactants of both natural origin (Frew *et al.*, 2006) and anthropogenic origin (Guitart *et al.*, 2007) may also be important.

For example, Salter (2010) reported two major sources of surfactants in the River Tyne Estuary and the coastal North Sea based on FDOM EEM analysis. These were an allochthonous source, being material derived from either terrestrial deposition or microbial degradation and an autochthonous source, being compounds derived from in-situ production of phytoplankton exudates.

One of the earliest studies of phytoplankton-derived surfactants was conducted by Žutić *et al*. (1981), in which surfactant production by six different marine phytoplankton species was measured during their growth in batch cultures. The results showed surfactant production in almost all growth stages (at various rates), with variable total production between different species and at different life stages. For example, *Cryptomonas* produced surfactants from the first day of the experiment (lag phase)[4] while *Skeletonema* released surfactants one week after the start of the experiment (Žutić *et al.*, 1981). The highest rate of surfactant production

[4] The growth dynamics of phytoplankton is characterized by four phases according to cell density, including a lag or induction phase in which little increase in cell density occurs. The next stage is the exponential phase in which cell density increases over the time. In the stationary phase the cell density is relatively constant and in the final, death phase, it decreases rapidly.

occurred after nearly two weeks of growth in *Cryptomonas* (late of stationary phase)[4] suggesting extracellular release due to cell lysis.

The study of natural surfactant slicks in the Sargasso Sea showed them to have formed from phytoplankton-derived organic matter (Sieburth and Conover, 1965). It was also suggested that high concentrations of carbohydrates determined in the SML might be associated with *Trichodesmium*-produced slicks in the Sargasso Sea (Sieburth and Conover, 1965).

Since then, there have been several studies of natural surfactant production by phytoplankton in both field and laboratory experiments (Table 1.4).

Table 1.4. Phytoplankton-produced surfactants during laboratory and field experiments

Sampling region	**Time**	**SA eq. Triton-X-100 (mgL^{-1})**	**Reference**
North Adriatic Sea	1985 - 1993	0.015 - 0.475	Vojvodić and Ćosović (1996)
North Adriatic Sea	May and Nov. 1992	0.07 - 0.16	Gašparović and Ćosović (1994)
Western Mediterranian	April, 1981	0.4	Ćosović (1985)
The coastal Adriatic Sea (polluted harbor along)	1976 - 1979	0.8 - > 10	Ćosović (1985)
Phytoplankton culture (*Prorocentrum micans*)	-	0.97	Vojvodić and Ćosović (1996)
North Adriatic Sea	Oct. 1979	0.97 - 1.96	Ćosović (1985)
Phytoplankton culture (*Dunaliella tertiolecta*)	-	1.95	Ćosović and Vojvodić (1989)
Phytoplankton culture (*Cafeteria sp.*)	-	2.58	Kujawinski *et al*. (2002)
Phytoplankton culture (*Paraphysomonas imperforata*)	-	3.23	Kujawinski *et al*. (2002)
Adriatic Sea, Rijeka Bay, poluted area	1977 -1 978	3.4 - >10	Ćosović (1985)
Phytoplankton culture (*Uronema sp.*)	-	5.8	Kujawinski *et al*. (2002)
Phytoplankton culture (*Cryptomonas sp.*)	-	6.5	Žutić *et al*. (1981)
Phytoplankton culture (*Skeletonema costatum*)		7	Žutić *et al*. (1981)
North Adriatic Sea	Aug. 1977 (bloom)	> 10	Žutić *et al*. (1981)
Phytoplankton culture (*Phaeodactylum tricornutum*)		18	Vojvodić and Ćosović (1996)
Southern Ocean (Iron fertilization experiment)	Feb. 2004	< 0.005 - 0.03 (ULW)	Croot et al. (2007)

For example, a field experiment was carried out to investigate an algal bloom impacts on air-sea gas transfer in the Southern Ocean. A high concentration of surfactants (~ 0.02 mg L^{-1} eq. T-X-100)[5] was found during the phytoplankton bloom, promoted by deliberately added iron (Southern Ocean Iron Fertilization Experiment, (EIFEX)) (Croot *et al.*, 2007). The highest surfactant concentration (up to 0.03 mg L^{-1} eq. T-X-100) was also reported at the end of phytoplankton bloom.

Fogg (1966) revealed phytoplankton extracellular production in natural environments and proposed two models including overflow and a passive diffusion model to describe the mechanism of this release. In the passive diffusion model, low molecular weight (LMW) photosynthetic products such as dissolved free amino acids (DFAAs) and sugars are released. However, active uptake of these products by bacterioplankton maintain the concentration gradient and promote the passive diffusion of the excretion from phytoplankton (Fogg, 1966).

The overflow release of high molecular weight (HMW) products by phytoplankton was the base of the overflow model. As the release of the photosynthetic products by phytoplankton costs less energy than storing them, especially under limited nutrient conditions, extracellular release of these products occurs at all phytoplankton growth stages (Fogg, 1966).

Frew *et al*. (1990) also found relatively high production of extracellular carbohydrates (27 – 47%) during the stationary phase[2] of phytoplankton growth in a series of laboratory experiments using natural seawaters from the Sargasso Sea.

Grazing by zooplankton and protists is another important source of natural surfactants in seawater. A two-phase laboratory system including protists and prey (bacterial suspension) was maintained to examine the possibility of surfactant production during protozoan grazing (Kujawinski *et al.*, 2002). The results showed that protozoans grazing on bacteria release soluble surfactants in concentrations comparable to those observed in association with phytoplankton blooms (Kujawinski *et al.*, 2002). It was proposed that protozoan grazing is a potentially important source of surfactants in marine ecosystems where protists are abundant, such as at the sediment-water interface and in microbial loop dominated oligotrophic regimes (Kujawinski *et al.*, 2002).

5 Triton-X-100: the non-ionic soluble surfactant polyoxyethylene t-octylphenol (or T-X-100)

Micro and macro-zooplankton were also shown to be a sink and source for surfactants. For example, the removal of significant amounts of total phytoplankton production (nearly 80%) via zooplankton sloppy feeding was reported (Sherr and Sherr, 1988). Release of surfactants during zooplankton grazing on organic exopolymer particles was also shown previously (Passow and Alldredge, 1999; Ling and Alldredge, 2003; Croot *et al.*, 2007).

The bacterial contribution to surfactant production is facilitated either by the degradation of biopolymeric materials or by formation of macromolecules via the condensation of low molecular weight organics (Nissenbaum, 1974). For example, it was shown that a range of bacteria such as *Pseudomonas*, *Bacillus*, *Mycobacterium* and *Acinetobacter* release natural surfactants as either extracellular products or attached to the cells during cell growth (Hisatsuka *et al.*, 1971; Rosenberg *et al.*, 1979).

Enrichment of bacteria, particularly amylolytic bacteria, within the SML compared to the sub-surface waters was also reported (Sieburth and Conover, 1965). This might indicate a lower contribution of lipids compared to carbohydrates to the SML structure than was thought previously (Sieburth and Conover, 1965; Kjelleberg and Håkansson, 1976; Williams *et al.*, 1986).

The so-called Bacterioneuston (bacteria in the SML) in slick and non-slick conditions was examined to identify dominant surfactant producers and surfactant degraders in the Strait of Florida (Kurata *et al.*, 2016). It was revealed that marine bacteria might control surfactant dynamics in the ocean, producing a variety of surfactants via multiple taxa ranging from *Pseudomonas*, *Bacillus* and *Acinetobacter* and *Rhodococcus* spp. The highest abundance of bacteria-produced surfactants was found in the near surface layer just under the SML (Kurata *et al.*, 2016). It was suggested that bacteria produce surfactants in organic-rich regions of the water column and that they accumulate at the sea surface by physical processes such as turbulence and bubble scavenging (Kurata *et al.*, 2016). Surfactant degradation by bacteria such as *Escherichia* spp. was also identified. However, the production pathways and transformations in the open ocean are yet to be revealed.

1.1.3.5 Distribution of surfactants

Seasonal and spatial variations in surfactant distributions were determined in previous research. For example, enhancement in surfactant concentrations during a phytoplankton bloom was suggested to be attributed to higher primary productivity in the bloom event in the Adriatic Sea

(Ćosović *et al.*, 1979; Zutic *et al.*, 1979; Zvonaric and Zutic, 1979; Ćosović *et al.*, 1985; Sakugawa and Handa, 1985a; Sakugawa and Handa, 1985b).

However, a lack of global in-situ surfactant level coverage due to difficulties in measuring surfactants in the field (such as ease of sample contamination and hardship of using the voltammetry technique at sea) and also the lack of a robust freezing protocol for the samples, led to the use of primary productivity as a proxy for biologically-derived surfactant distribution in the oceans (Goldman *et al.*, 1988; Asher, 1997; Tsai and Liu, 2003; Wurl *et al.*, 2011b).

For example, Asher (1997) also estimated oceanic surfactants from satellite-derived chlorophyll as a proxy for primary productivity and suggested lower amounts of surfactants in oligotrophic regions. Later, Wurl *et al.* (2011) suggested using primary productivity in conjunction with wind speed to predict global surfactant coverage and its spatial and temporal variabilities.

Based on the lowest threshold of primary productivity in the productive oceans (i.e. 15 mg C m^{-2} mth^{-1}) and depressions in the transfer velocity of CO_2, surfactant coverage was mostly proposed for the North Atlantic during the boreal summer and autumn (between ~ 60°N and ~ 40°N), in the subtropical Atlantic with nutrient-enriched upwelled waters, in the coastal waters off Africa and South America and also off the Falkland Islands in austral spring and summer. Of particular note, the rest of the Atlantic Ocean, including the central oligotrophic gyres between 30°N and 30°S was expected to be surfactant free (Tsai and Liu, 2003; Wurl *et al.*, 2011b).

Surfactants were also suggested to be more abundant in coastal regions because of freshwater discharge of terrestrial surfactants (Gašparović and Ćosović, 2001; Gašparović *et al.*, 2007).

Estimating the extent and coverage of natural surfactants via the application of remote sensing was not recommended as the surfactant coverage by soluble fractions in the absence of visible slicks is not detected by this technique (Liss *et al.*, 2005).

1.2 Air-sea gas exchange

Air-sea gas exchange is a globally relevant process that provides the link between marine biogeochemistry, ocean circulation and atmospheric composition.

The exchange flux (F) of a gas across the SML is the product of an air-sea gas concentration gradient (ΔC) and a gas transfer velocity (k_w):

$F = k_w \Delta C$ (equation: 1.2.1)

(Liss and Slater, 1974).

The most difficult parameter to quantify in equation 1.2.1 is k_w. The ratio of the diffusivity of the gas of interest (D) to the thickness of the water side diffusive boundary at the air-sea interface (z) define k_w (i.e. k_w=D/Z). Thus, increasing z decreases k_w and slows the gas exchange flux.

k_w can be interconverted between different gases based on the Schmidt number (S_c, i.e. the ratio of kinematic viscosity to the molecular diffusivity of each gas in question). To do this requires using an assumed or estimated "Schmidt number exponent", n, which is often assumed to be 0.5 for a wavy surface (Upstill-Goddard, 2006). The value of k_w is usually converted to k_{660} (i.e. the value of k_w for S_c = 660), being the value for CO_2 in seawater at 20°C (Upstill-Goddard, 2006).

The variables and underlying mechanisms that control the value of k_w are yet to be fully understood. Thus k_w remains the greatest challenge to quantifying the global air-sea exchanges of CO_2 and other climate active gases (Frew *et al.*, 2004; Takahashi *et al.*, 2009).

Various models have been proposed to describe gas exchange based on mostly molecular and turbulent diffusion. One of the simplest models is the two-layer (film) model in which the transfer process is mainly controlled by molecular diffusion while any production and destruction processes which occur in the film are slower than diffusion (Liss and Slater, 1974). It is also assumed that the concentration gradients of any gases in air and water below the diffusive boundary are zero due to efficient turbulent mixing by eddies. So, the dominant transport process in underlying water is a slow process of turbulent mixing, as compared to much more rapid molecular diffusion within the SML.

For low solubility gases such as carbon dioxide (CO_2), methane (CH_4) and sulphur hexafluoride (SF_6), the primary resistance to gas exchange in this model is transfer through the waterside thin film which is slower than through the air side (Le Quéré and Saltzman, 2013). However,

the thickness of the surface film varies with different degrees of turbulence; therefore assuming a constant film in the model is unrealistic (Le Quéré and Saltzman, 2013).

To overcome this, models such as the surface renewal model (Ledwell, 1984) have been proposed. This model assumes that surface water is consistently renewed by bulk water due to the presence of eddies approaching the surface and that this renewal restores surface conditions after any physical disruption. However, the model is rarely applied *in situ* because it is difficult to determine the renewal rate (Le Quéré and Saltzman, 2013).

There are other models proposed based on other parameters measurable in the field such as turbulent energy rate (Zappa *et al.*, 2007) or bubble mediated gas transfer (Woolf, 1997; McNeil and D'Asaro, 2007) but further discussion on these approaches are beyond the scope of this research.

1.2.1 *Surfactant control on air-sea gas exchange*

Soluble surfactants may exert greater control on air-sea gas exchange than was initially believed. This is because they reform more quickly at the interface after physical disruption than surface films composed of insoluble surfactants (Springer and Pigford, 1970).

Surfactants influence gas exchange by modifying the hydrodynamic characteristics of the interfacial layer (Frew *et al.*, 1990; Tsai 1998; Mckenna and McGills; 2004) via the dynamic damping of short wind (capillary) waves with subsequent reduced surface vorticity (Figure 1.7). They also dampen eddies approaching the surface by reducing surface tension and creating a stress opposite to the force of upward eddy transport.

Figure 1.7. Surfactant edge from Deep Ocean Gas Exchange Experiment (DOGEE II) in the North Atlantic Ocean. Credit to Robin Pascal.

So, as the thickness of viscous sublayer increases, the surface renewal weakens and turbulent length scale will be increased. All these modifications reduce k_w and hence air-sea gas exchange by capillary waves damping turbulent energy transfer (Davies, 1966; Metzger and Dobbins, 1967; Tsai, 1996; McKenna and McGillis, 2004; Liss *et al.*, 2005; Salter *et al.*, 2011).

Insoluble surfactants on the other hand influence air-sea gas exchange through a static mechanism. They form a monolayer physical barrier (Springer and Pigford, 1970) that increases mass transfer resistance at the sea surface (Liss and Martinelli, 1978) and disrupts molecular diffusion across the interface. However, this physical barrier tends to be dispersed under typical oceanic conditions of wind and waves (Goldman *et al.*, 1988). The effect is also most important for gases such as water vapour and ammonia (NH_3), for which mass transfer is controlled mainly by the gaseous phase than water side resistance (Springer and Pigford, 1970; Liss, 1983). Therefore, in evaluating the surfactant control of air-sea gas exchange in the marine environment the soluble surfactant effect is the most important.

There have been contradictory views on the effect of SML surfactants on k_w in the past. For example, Adamson (1990) and Asher (1997) suggested that forming a single-component film required to make a physical gas exchange barrier at the surface is impossible due to the presence

of mixed composition films (Liss *et al.*, 2005). On the other hand, surfactant control of gas exchange was previously underestimated because it was thought that surfactant-derived slicks only exist at low wind speeds and are disrupted at higher wind speeds (greater than 13 m s^{-1}), being dispersed by surface winds and waves (Broecker *et al.*, 1978; Liss, 1983; Tsai and Liu, 2003).

However, in agreement with a previous explanation by Goldman *et al*. (1988), Frew *et al*. (1990) consider soluble surfactants as important as insoluble fractions in controlling gas exchange at high wind speeds because they release back to the interface after physical disruption by bubble scavenging (Tsai and Liu, 2003).

Frew *et al*. (2002) also suggest that suppression of k_w is dependent on SML surfactant enrichment rather than bulk surfactant concentration, based on the results of a gas transfer experiment in a small annular wind-wave tank.

To highlight the importance of surfactants in air-sea gas exchange, an early global flux model for CO_2 (Berger and Herguera, 1992) showed a likely 6-fold suppression by surfactants. However full coverage of the global oceans with surfactants was considered unrealistic (Liss *et al.*, 2005).

A series of laboratory and field studies have been conducted to evaluate the suppression of air-sea gas exchange by surfactants using natural and synthetic surfactants (Table 1.5).

Synthesized surfactants including oleyl alcohol and Triton-X-100 (T-X-100) were chosen primarily in previous research because they are well characterized and studied under different conditions (Saylor, 2003). Also, alternative advantages of using oleyl alcohol is its similar characteristics to natural oceanic surfactants (Barger, 1991).

Table 1.5. Air-Sea gas transfer velocity (k_w) suppression controlled by natural and synthetic surfactants in laboratory and in-situ experiments

Laboratory studies	**k_w suppression**	**Reference**
Oceanic waters	~10% suppression in O_2 exchange	Goldman *et al.* (1988)
Coastal waters	~50% suppression in O_2 exchange	Goldman *et al.* (1988)
Phytoplankton exudates	~5% - 55% suppression in O_2 exchange	Frew *et al.* (1990)
Addition of soluble surfactant	Maximum of 90% reduction in O_2 exchange	Frew (1997)
California Bight surface water samples	k_w suppression in the presence of surfactants	Frew *et al.* (2002)
Coastal-Oceanic waters	Up to 51% suppression of k_w in CH_4 exchange	Pereira *et al.* (2016)
Oceanic waters (in-situ with fresh seawater)	Maximum of 25% of k_w suppression in CH_4 exchange	This study
In-situ studies		
Artificial slick of oleyl alcohol	~30% reduction in diffusion rate of CO_2	Brockmann *et al.* (1982)
Artificial slick of oleyl alcohol	~55% reduction in $SF_6/^3He$-derived k_{660}	Salter *et al.* (2011)
Artificial slick of oleyl alcohol	~24% - 39% reduction in DMS-derived k_{660}	Salter *et al.* (2011)

Table 1.5 shows that suppression of gas exchange in the presence of natural and artificial surfactants may typically approach 50% and even reach 85% (Broecker, 1978; Brockmann *et al.*, 1982; Asher and Pankow, 1986; Jähne *et al.*, 1987a; Goldman *et al.*, 1988; Salter *et al.*, 2011; Schneider-Zapp *et al.*, 2014; Pereira *et al.*, 2016). For example, spatiotemporal variability of k_w by natural surfactants was studied during a 20 km offshore transect in the North Sea using a custom built laboratory gas exchange tank (Pereira *et al.*, 2016). It was suggested that natural surfactants suppress k_w for CH_4 by between 14% and 51% relative to surfactant-free MilliQ water.

Some other laboratory measurements were also carried out to determine surfactant control on gas transfer as a function of wind speed. For example, Broecker (1978) measured gas transfer of CO_2 in the liquid phase using a wind-wave tunnel for clean and oleyl alcohol covered surfaces. They observed a four to five fold reduction in the gas transfer rate at a wind speed of 12.5 m s^{-1} in the film-covered surface compared to the clean surface (Broecker *et al.*, 1978).

Asher (1996) showed that k_w was reduced in the presence of insoluble synthetic surfactants (Triton) compared to clean water for insoluble helium (He) and relatively soluble CO_2 in a whitecap simulation tank (Liss *et al.*, 2005). He later, in agreement with Frew *et al*. (1990) assumed that the SML inhibits gas exchange by reducing k_w in the presence of both visible and invisible slicks (derived from soluble and insoluble surfactants). However, the quantification of this suppression under global oceanic conditions is yet to be understood (Asher, 1997).

Brockman *et al*. (1982) also reported a decrease in CO_2 exchange by 30% during artificial visible slick formation of oleic acid compared to non-slick conditions.

Some field experiments were also carried out to understand surfactant control on gas exchange in aquatic environments. For example, Salter *et al*. (2011) showed that phytoplankton derived surfactants suppress k_w by up to 55% during a mesocosm phytoplankton bloom experiment.

In northern Pacific and Atlantic Ocean CO_2 flux reduction by surfactants was reported throughout a year based on primary productivity (Tsai and Liu, 2003).

1.3 Objective of the thesis

The principal aim of this study is to examine the spatial variability of natural surfactants and associated components (e.g. CDOM) at the ocean basin scale (Atlantic Ocean), both in the SML and in depth profiles over the upper 100 metres of the water column. Such data are important to the evaluation of air-sea gas exchange but they have previously been lacking. The aims were achieved through participation in two Atlantic Meridional Transect cruises during 2014 (AMT24) and 2015 (AMT25). The results are discussed in the context of our current understanding of the environmental controls of air-sea gas exchange.

1.4 Thesis outline

In Chapter two, after a short introduction (section 2.1), section (2.2) describes the study region and identifies sampling stations (cruise map). Section 2.3 briefly describes major Atlantic Ocean water masses encountered on the AMT transects. Major ocean currents encountered are described in section 2.4. Sampling techniques for the SML and underlying water are in section 2.5. Analytical methods for SA and CDOM are described in section 2.6. In section 2.7, the gas exchange methodology including the structure of a custom-build gas exchange tank used in this work and the associated experimental method are outlined. Sections 2.8 - 2.10 describe relevant hydrographic data and statistical analyses used.

In Chapter three, sections 3.1 to section 3.5, present and discuss relevant ancillary data. Section 3.6 describes the distribution and spectral properties of CDOM in the SML and in the water column to a depth ~ 100 m. These data are used to assess the relationships between CDOM and biological and physiochemical parameters.

Chapter four examines SA in the SML and throughout the water column, and enrichment factors in the SML, in a range of Atlantic Ocean biogeochemical provinces. Associations of SA with other parameters including wind speed, chlorophyll, primary productivity temperature and salinity are examined.

Chapter five presents the results from the gas exchange tank experiment and discusses surfactant controls on k_w relative to surfactant-free MilliQ water.

Chapter 6 is a summary of Chapters three to five, highlighting the major findings and comparing these with previous results.

Finally, Chapter 7 includes conclusion and recommendations for future work.

Chapter 2. Materials and Methods

2.1 Introduction

This chapter describes the study region, sampling regime, analytical methods and sample processing used to determine spatial variations of natural surfactant activity (SA) and chromophoric dissolved organic matter (CDOM) in different oceanographic provinces of the Atlantic Ocean. It also summarises physiochemical characteristics of water masses via Temperature-Salinity (T-S) diagrams and describes surface water currents.

2.2 The study region and sampling stations

The aim of the Atlantic Meridional Transect (AMT) programme (http://www.amt-uk.org/) is to annually monitor the physical and biogeochemical properties of "oceanographic provinces" in the Atlantic ocean, defined by the regulation of phytoplankton distributions by hydrographic properties (Longhurst *et al.*, 1995; Reygondeau *et al.*, 2013). Since 1995, atmospheric and oceanic samples have been collected along AMT transects and examined for physical, optical and biogeochemical parameters (Robinson *et al.*, 2009). A typical AMT transect covers 13,500 km, crossing approximately 17 oceanographic provinces with distinct biological and physiochemical characteristics, from temperate regions to oligotrophic gyres and equatorial upwelling (Hooker *et al.*, 2000). To date the AMT programme has included 26 research cruises, the latest being between Immingham and the Falkland Islands during September-November 2016.

2.2.1 *Sampling pattern*

Sampling during an AMT cruise uses conductivity, temperature and depth (CTD) sensors attached to a stainless steel Niskin bottle rosette (Sea-Bird Electronics, SBE09 CTD; 24 x 20L PVC Niskin water bottles). This allows for the collection of water samples at predetermined depths throughout the water column. There are typically two casts per day. The first is

scheduled before dawn and the second at solar noon enabling the assessment of light-mediated biogeochemistry. Sampling is usually restricted to a maximum depth of 500 m due to time constraints, and with a particular focus on the euphotic zone.

AMT samples considered in this thesis were collected between ~50°N and ~50°S on two cruises of RRS *James Clark Ross*: AMT24 (21st Sept. - 6th Nov. 2014) and AMT25 (11th Sept. – 4th Nov. 2015). Consequently, sampling was in the boreal summer/autumn in the Northern Hemisphere and in the austral spring in the Southern Hemisphere. Both cruises departed from Immingham (UK), AMT24 terminating in Punta Arenas (Chile) and AMT25 terminating in Stanley, Falkland Islands (Figure 2.1).

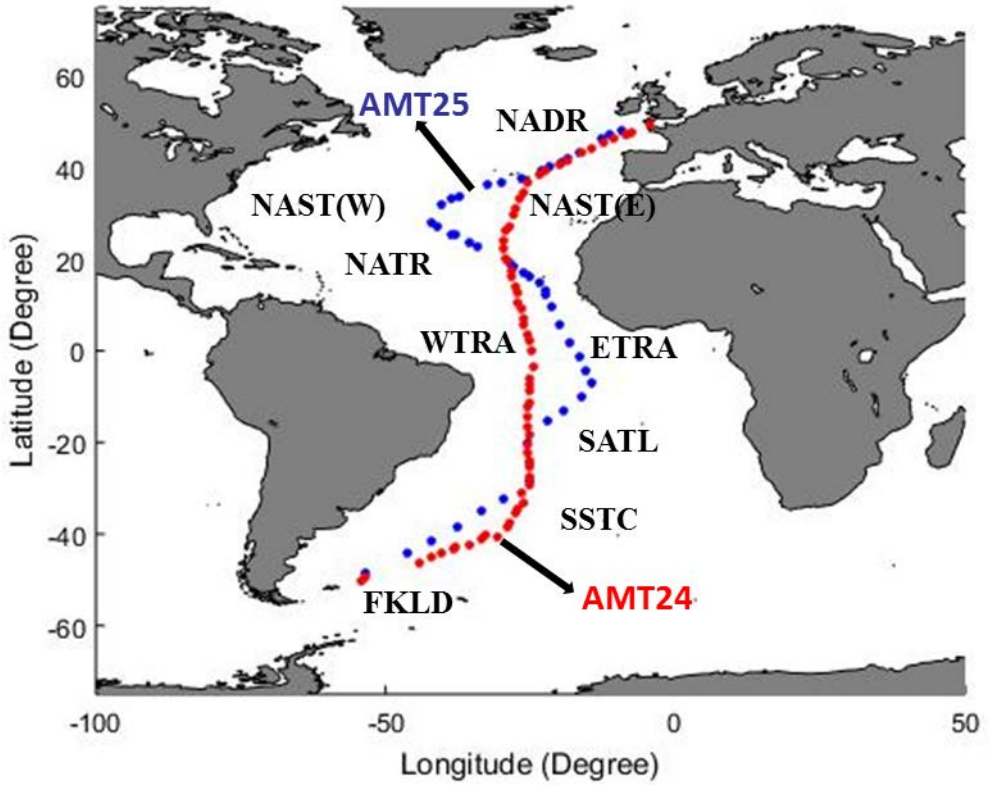

Figure 2.1. Map of the cruise transects. Filled circles in red represent sampling stations on AMT24 and in blue on AMT25. Oceanic provinces related to the AMT24 and AMT25 cruise tracks (Longhurst, 1995; Reygondeau *et al.*, 2013) are also shown. Provinces are: North Atlantic Drift region (NADR); North Atlantic Sub-Tropical (Eastern) (NAST (E)); North Atlantic Sub-Tropical (Western) (NAST (W)); North Atlantic Tropical (NATR); Western Tropical Atlantic (WTRA); Eastern Tropical Atlantic (ETRA); South Atlantic Gyral (SATL); South Sub-Tropical Convergence (SSTC); Southwest Atlantic Continental shelf (FKLD).

As Figure 2.1 shows, AMT24 and AMT25 followed slightly different courses. The principal difference was in the region from 40°N to 20°S, where there was a difference in longitude of ~ 13° between the two transects. This was due to deployment of moorings and deep CTDs arranged for other research groups on AMT25.

The Atlantic Ocean oceanographic provinces introduced by Longhurst (1995) were adopted in this study (Longhurst, 1995; Reygondeau *et al.*, 2013). Longhurst (1995) assessed seasonal chlorophyll satellite images using the Moderate Resolution Imaging Spectroradiometer (MODIS) from the Coastal Zone Colour Scanner (CZCS) satellite and compared them with regional archives of surface chlorophyll, mixed layer topography, seasonal wind stress, wind stress curl, oceanic surface heat flux, the distribution of observable oceanic frontal zones and phytoplankton ecology (Longhurst, 2010). Satellite-derived images of chlorophyll distribution on AMT24 and AMT25 are shown in Figure 2.2.

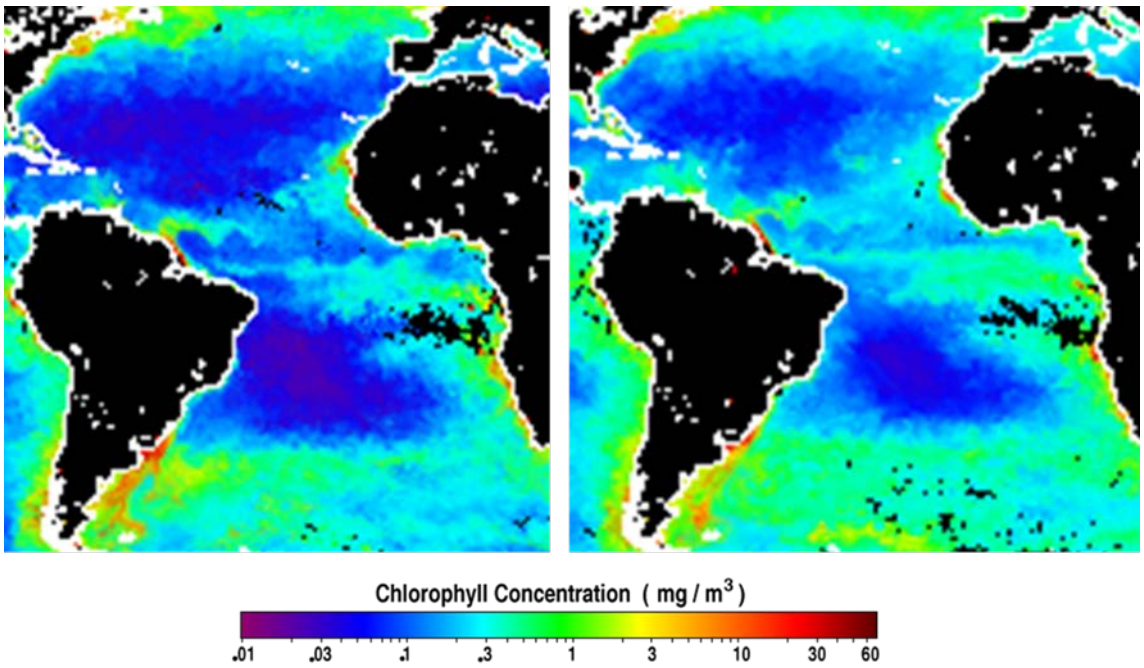

Figure 2.2. Satellite-derived images of chlorophyll distribution in the Atlantic Ocean. The data provided by NASA Earth Observatory for October 2014 (left) and 2015 (right). Available at: https://neo.sci.gsfc.nasa.gov/view.php?datasetId=MY1DMM_CHLORA (Accessed: 17 April 2017).

In general, the average chlorophyll concentration was higher on AMT24 (0.14 ± 0.17 mg m^{-3}) than on AMT25 (0.06 ± 0.10 mg m^{-3}). The maximum concentration of chlorophyll was observed in the European Continental Shelf Waters (ECSW) (~ 0.3 mg m^{-3}) and the minimum was found on North Atlantic Sub-tropical Region (NAST) (~ 0.1 mg m^{-3}) on both transects (Figure 2.2).

2.3 Water masses

Emery and Meincke (1986) identified four major water masses in the uppermost 500 m of the Atlantic Ocean: Atlantic Subarctic Upper Water (ASUW), which is the farthest north and is supplied by Subarctic and North Atlantic Intermediate Water (Wright and Worthington, 1970); Eastern and Western North Atlantic Central Water (ENACW and WNACW), in the eastern and western central north Atlantic Ocean respectively; and South Atlantic Central Water in the Southern Hemisphere (Table 2.1).

Table 2.1. Temperature-Salinity (T-S) characteristics of major water masses in the Atlantic Ocean determined by Emery and Meincke (1986)

Water masses (upper 500m, Atlantic Ocean)	Temperature (°C)	Salinity
Atlantic Subarctic Upper Water (ASUW)	0.0-4.0	34.0-35.0
Western North Atlantic Central Water (WNACW)	7.0-20.0	35.0-36.7
Eastern North Atlantic Central Water (ENACW)	8.0-18.0	35.2-36.7
South Atlantic Central Water (SACW)	5.0-18.0	34.3-35.8

In this study, water masses were identified by plotting T-S relationships derived from vertical CTD profiles (Aiken *et al.*, 2000; Hooker *et al.*, 2000) (Figure 2.3).

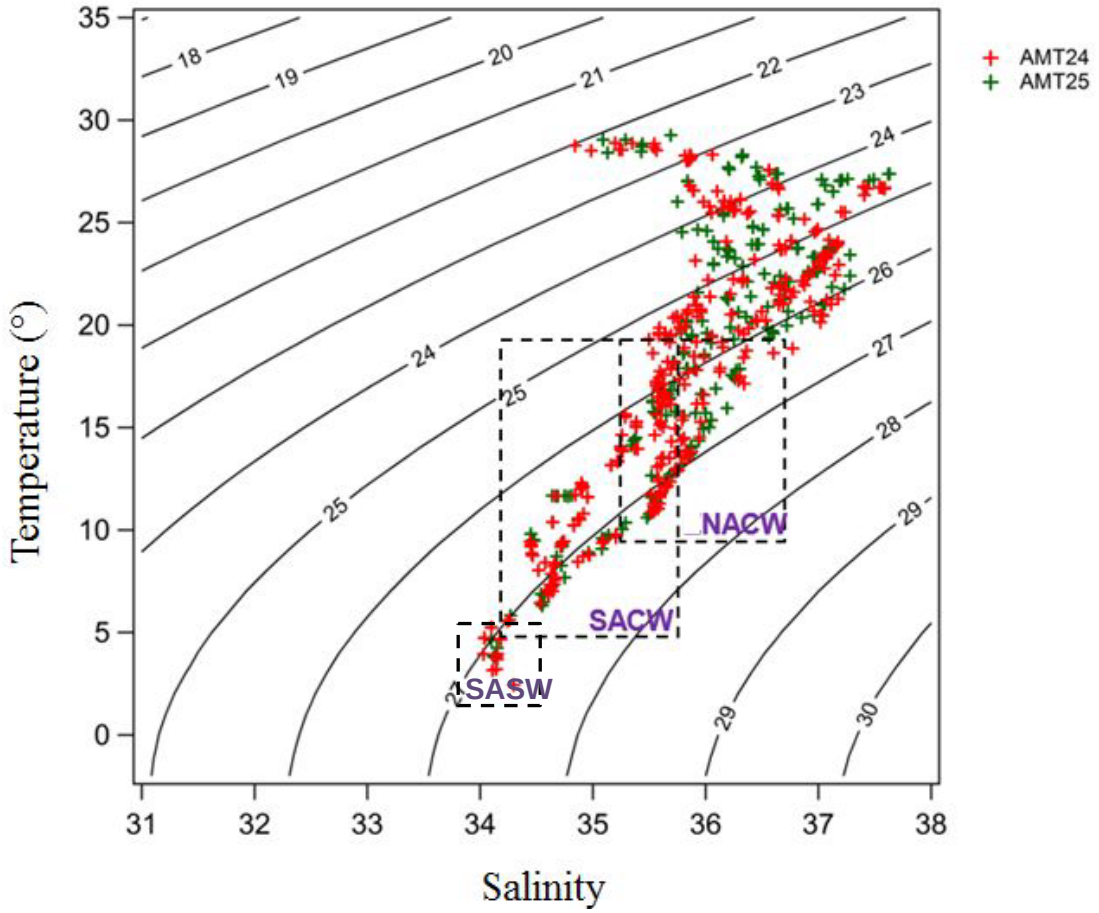

Figure 2.3. Temperature-Salinity (T-S) diagram showing water masses encountered during AMT24 (red symbol) and AMT25 (green symbol). The major identifiable water masses are North Atlantic Central Water (NACW), South Atlantic Central Water (SACW) and Sub-Antarctic Surface Water (SASW). The dashed boxes represent the corresponding boundaries of temperature and salinity. The lines show constant density.

North Atlantic Central Water (NACW) spans from ~50°N to ~10°N and from ~30°E to ~10°W, dominating northern equatorial areas, whereas SACW lies between ~10°N and 40°S and at the southerly boundary of NACW in the southern equatorial region (Sverdrup *et al.*, 1942; Wright and Worthington, 1970; Emery and Meincke, 1986; Aiken *et al.*, 2000). In general, SACW is more nutrient enriched and has lower salinity than NACW (Gardener, 1977).

From Figure 2.3 it is evident that northern and southern water masses can be distinguished easily by their distinct quasi-linear relationships between salinity and temperature. Proceeding from higher to lower latitudes, towards the tropical regions (most points outside the dashed boxes) coincides with rising temperature and salinity, except in the mid-latitude equatorial regions where high precipitation (Aiken *et al.*, 2000) and/or Amazon discharge influence salinity. Amazon water was characterised on previous AMT transects by temperatures ~28°C and salinities below 35.5 in the Boreal Autumn flowing easterly (North Equatorial Counter Current (NECC), see section 2.4) (Aiken *et al.*, 2000). West of the SACW boundary there is a small area showing inconsistency with the T-S relationship for the rest of the water mass, being characterised by a salinity ~34 and a temperature 3°C - 5°C (mostly evident on AMT24). The same was recorded by Aiken *et al*. (2000) on AMTs 1- 4 and Forster (2006) on AMTs 12-13. This low temperature, low salinity water might reflect Sub-Antarctic Surface Waters (SASW) transported northward by the Falkland Current (see section 2.4).

2.4 Atlantic Ocean surface circulation

The main ocean currents encountered during AMT24 and AMT25 are shown in Figure 2.4.

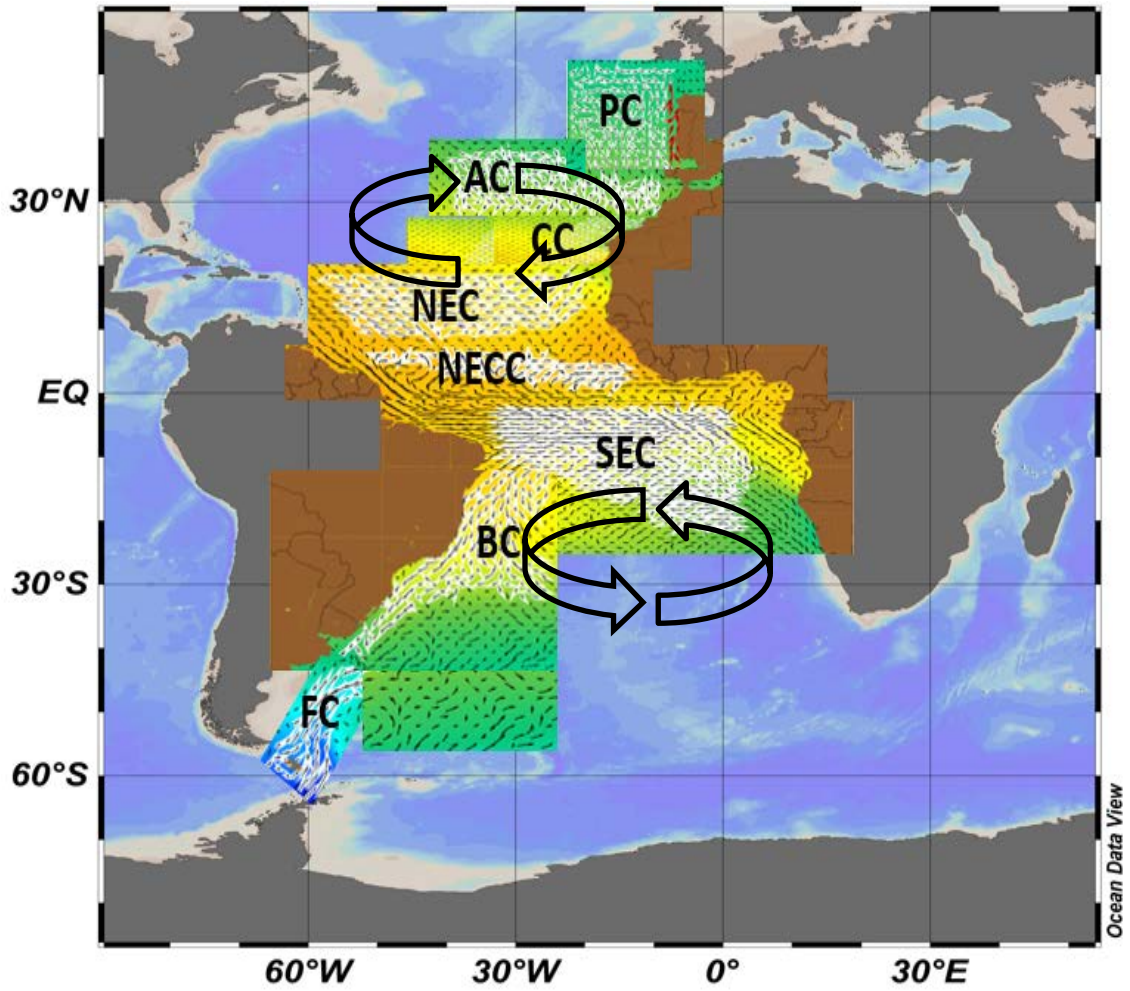

Figure 2.4. Atlantic Ocean surface currents encountered during AMT24 and AMT25: Letters refer to: Portugal current (PC); Azores Current (AC); Canary current (CC); North Equatorial Current (NEC); North Equatorial Counter Current (NECC); South Equatorial Current (SEC); Brazil Current (BC) and Falklands Current (FC), as defined by Hooker et al. (2000). The North Atlantic Gyre is a clockwise gyre between the northern temperate waters and the equatorial regions. The South Atlantic Gyre is an anti-clockwise gyre between the southern temperate waters and the equatorial regions.

The Atlantic Ocean comprises two main gyres: the northern Atlantic subtropical gyre (NAG) and the southern Atlantic subtropical gyre (SAG), each containing several current components (Aiken *et al.*, 2000). Both gyres are characterized by positively correlated high temperature and salinity (Hooker *et al.*, 2000).

The Azores Current (AC) component of the NAG is an eastward current to a depth of 1000 m. It originates in the Gulf Stream and flows within the region bounded by ~10°W and ~40°W and ~30°N and ~42°N. It has three branches which supply the northern boundary of the North

Equatorial Current (NEC) and the northern part of the Canary Current (CC) (Krauss *et al.*, 1990; Aiken *et al.*, 2000; Reverdin *et al.*, 2003). Another branch of the AC is the Portugal current (PC) which flows between 10°W and ~ 25°W and between 38°N and ~ 47°N.

The North Equatorial Current (NEC) flows westward, from the north west coast of Africa between ~10°N and 20°N, centred at 15°N (Fedoseev, 1970; Aiken *et al.*, 2000; Hooker *et al.*, 2000). Therefore, the northern part of the NEC is supplied by both AC and CC in the north-east Atlantic. The NEC can also be affected by west-coast African upwelling water (Fedoseev, 1970; Mittelstaedt, 1991).

The North Equatorial Counter Current (NECC) flows easterly between 3°N and 10°N (Hooker *et al.*, 2000). The current is supplied by the North Benguela Current (NBC) between 6°N and 8°N (Frew *et al.*, 1990; Wilson *et al.*, 1994), north of the South Equatorial Current (SEC) and south-westerly of the NEC. The current has seasonal variability with boreal summer and early autumn flow over the entirety of the tropics between 5°N and 10°N. However, the current disappears during the boreal spring due to strong winds in the northern hemisphere (Mittelstaedt, 1991; Wilson *et al.*, 1994; Aiken *et al.*, 2000). The eastward extension of the NECC reaches the African continent and supplies the Guinea Current (GC) while a northern branch of NECC also feeds the NEC (Richardson and Reverdin, 1987; Mittelstaedt, 1991). The surface interactions between the CC, NEC and NECC located between 15°N and 10°N gives rise to a surface cyclonic circulation (Mittelstaedt, 1991).

Major currents of the SAG are the South Equatorial Current (SEC), which crosses the equator, the Brazil Current (BC), the South Atlantic Current (SAC) and the Benguela Current (BenC) (Aiken *et al.*, 2000). The SEC is an westward current between ~ 4°N and ~ 25°S (da Silveira *et al.*, 1994; Aiken *et al.*, 2000; Hooker *et al.*, 2000). It is a complex current with 3 branches including a southern branch, the Southern South Equatorial Current (SSEC), a central branch, the Central South Equatorial Current (CSEC), which flows between 5-6°N and supplies the North Benguela Current (NBC), and finally a seasonal (austral summer/autumn) northern branch, the Northern South Equatorial Current (NSEC), which flows between 1°N and 3-5°S. The SSEC originates in the BenC and flows northward into the NBC between 10°S and 12°S, with some input into the Brazil Current (BC) (Aiken *et al.*, 2000; Hooker *et al.*, 2000).

The BC is a southerly flowing current at ~27°W which flows along the continental shelf and represents the western boundary of the SAG. (Peterson and Stramma, 1991). The most south-

westerly current encountered in this study is the Falkland Current (FC) which flows northward and is a branch of the Antarctic Circumpolar Current.

2.5 Sample collection and analytical methods

2.5.1 *Sampling the Sea Surface Microlayer (SML) and Sub-Surface Water (SSW)*

A total of 1479 samples were collected from 120 stations: 67 on AMT24 and 53 on AMT25 (Table A.2). The surface microlayer (SML) was sampled first, in triplicate twice daily, during pre-dawn (05.00 - 06.00 GMT) and solar noon (13.00 - 14.00 GMT) hydrocasts. A custom-made Garrett screen (Garrett, 1965) (width:60 cm, breadth: 60 cm, mesh:16, wire diameter: 0.36 mm, effective surface area: 2025 cm^2) was used, following a standard protocol (Cunliffe and Wurl, 2014).

Sampling took place from the deck of the ship, over the bow. The approximate deployment position was 8.3 metres above the sea surface. Sampling was only carried out when the ship was stationary, as recommended by Cunliffe and Wurl (2014), and following a visual inspection to establish that there were no ship-derived effluents that would contaminate the samples. No effluent was discharged from the ship 1 hour before arriving at the next sampling station so as not to disturb the surface and contaminate samples. This procedure was developed and evaluated by Salter *et al.* (2011) and used successfully in an investigation of air-sea gas exchange mediated by an artificial surfactant slick.

The need to sample from the ship's deck was dictated by cruise logistics and is the principal reason why the Garret Screen (Figure 2.5 A) was selected over alternative samplers such as the glass plate (see section 1.1.2), which cannot be deployed in this way. The Garret Screen has a number of other advantages, including ease of cleaning with 10% HCl or by baking at 450^oC for 6 hours, and the ability to accumulate relatively large sample volumes rapidly (15 ml/dip).

The screen was deployed horizontally, pre-rinsed in seawater and submerged just under the water surface for 5 seconds before being lifted back up through the SML. Based on multiple screen deployments, the Garrett screen used typically samples the uppermost 65-80 μm of the

sea surface (Pereira *et al.*, 2016). However, this may vary depending on both the oceanographic and meteorological conditions at the time of sampling (Cunliffe and Wurl, 2014).

The adhering small rectangular cells of seawater samples captured in the spaces of the wire mesh by means of surface tension were drained along one of the screen corners into pre-rinsed 15 ml high-density polyethylene (HDPE) tubes (Schneider-Zapp *et al*., 2014) (Figure 2.5 B) and stored in a cool box to minimize the possibility of photochemical degradation and/or biological modification prior to analysis. The HDPE tubes were previously shown to be inert to surfactant activity (Schneider-Zapp *et al.*, 2014; Pereira *et al.*, 2016).

(A)

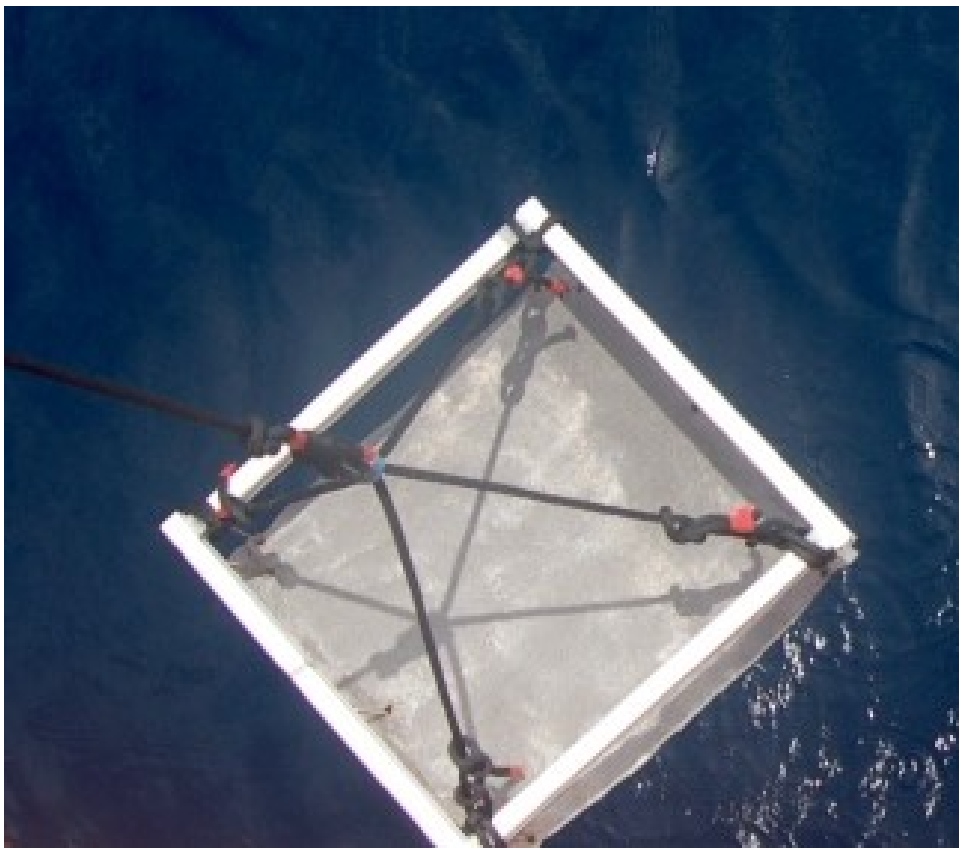

(B)

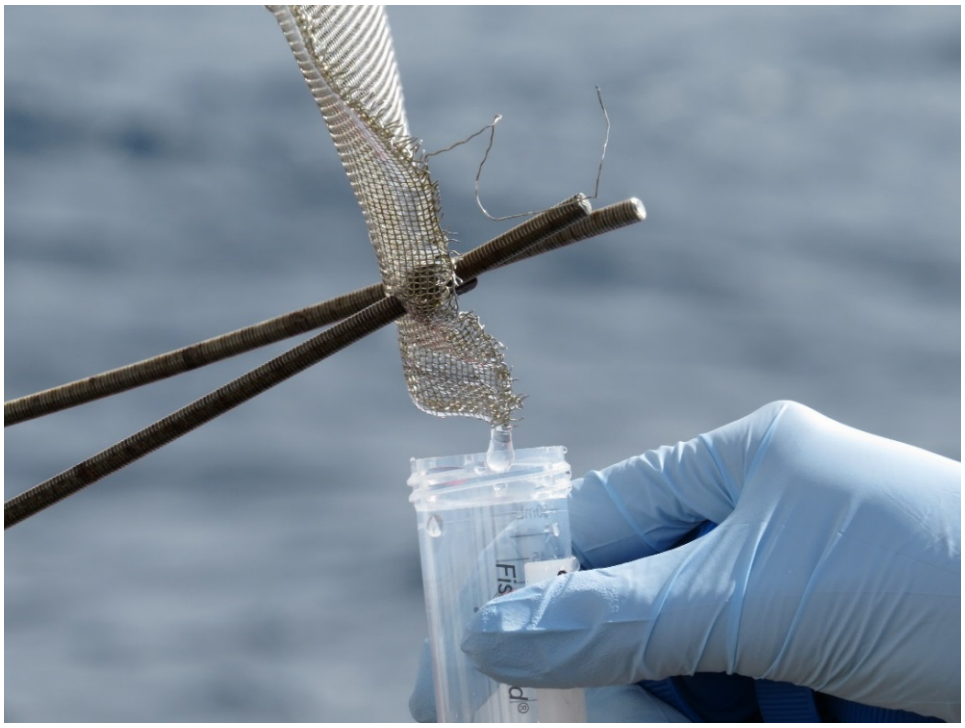

Figure 2.5. Garrett screen orientation during sampling on board *RRS* James Clark Ross: (A) Garrett Screen at the sea surface during AMT24: (B) Method of draining sample water from the Garrett Screen.

At high sea states the screen was deployed within wave troughs and in the case of any splash back, the samples were excluded.

Sub-Surface water (SSW) samples were routinely collected simultaneously via a hull-mounted "non-toxic" seawater inlet 7 m below the waterline and during each 500 m hydrocast (a total of 357 "non-toxic" SSW samples).

To investigate the vertical profile of CDOM in more detail (see section 3.6), at 14 stations on AMT24 and 13 stations on AMT25, 9 samples were collected: at the 5 selected light penetration depths (see section 2.4), at the base of the mixed layer, at the deep chlorophyll maximum (DCM) and at the oxygen (O_2) maximum and minimum depths (as indicated by an oxygen sensor on the CTD rosette). Sample allocations for the analysis of surfactant activity (SA) and CDOM absorbance (see sections 2.5.3 and 2.5.6) are shown in Figure 2.6.

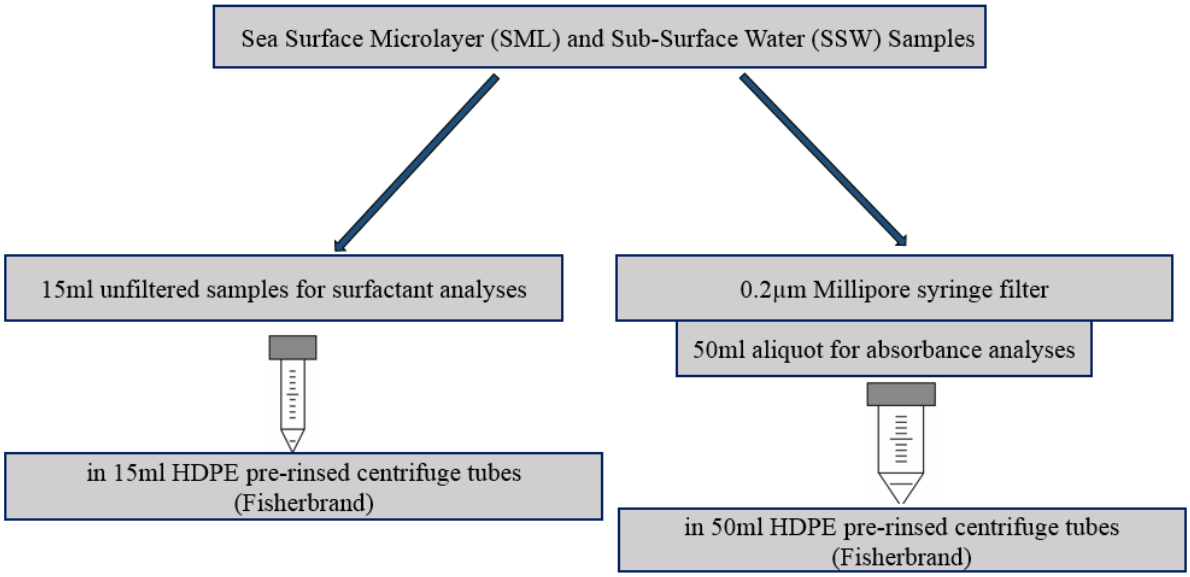

Figure 2.6. Sample collection and sample processing protocols for surfactant and CDOM absorbance on AMT24 and AMT25

In general, 7 samples were collected from each cast including 5 samples from various selected light penetration depths (97%; 55%; 33%, 14% and 1%). Samples were collected from the Niskin bottles using acid-washed silicon tubing that was pre-rinsed with excess sample.

Samples for SA determination were unfiltered because filtration can modify SA by removing insoluble and most absorbable compounds and/or releasing intracellular matter due to cell rupture (Žutić *et al.*, 1981; Ćosović *et al.*, 1985; Williams, 1986; Ćosović and Vojvodić, 1998; Schneider-Zapp *et al.*, 2014; Pereira *et al.*, 2016; Sabbaghzadeh *et al.*, 2017). Reduction in total

SA by ~13% in seawater samples (i.e. north Adriatic Sea) and ~70% in estuarine samples following filtration was reported previously (Ćosović and Vojvodić, 1998).

All samples for SA determination were analysed immediately following sample collection. Typically there was a maximum of 3 hours between sample collection and the final analysis for each cast. Samples were kept in the dark in a cool box after Gašparović *et al*. (2011), Salter *et al*. (2011) and Pereira *et al*. (2016). Schneider-Zapp *et al*. (2013) showed that untreated SA samples can be stored at 4°C in the dark for up to two weeks with little overall change.

Samples for CDOM determination were collected in 250 ml borosilicate volumetric flasks (analytical grade glassware, SCHOTT, GL 45, 250 ml, Fisher brand) pre-rinsed with excess sample. All glassware was pre-combusted at 450°C for 8 hours to remove any accumulated organic matter (Stubbins *et al.*, 2006). To minimize contamination during filtration, syringes and all containers were pre-rinsed with pure laboratory water (18.2 Ohm Milli-Q, Millipore System Inc., USA), hereinafter referred to as MilliQ, and a small aliquot of sample (~ 3 ml) prior to use. This procedure was repeated prior to each subsequent filtration. Powder free disposable gloves were worn during all sampling and sample processing.

After sample collection, sub-samples (20 ml) were transferred to a ground glass syringe (20 ml, SAMCO) and filtered (10 ml min^{-1}) through 0.22 µm surfactant-free single use Millipore syringe filters (MILLEX GP, Millipore, PES membrane).

CDOM samples were filtered based on previous protocols (Nelson *et al.*, 1998; Helms *et al.*, 2008; Nelson and Siegel, 2013). Unfiltered samples include particulate components such as picophytoplankton, bacteria, other organics and mineral grains, in addition to dissolved species that contribute to light attenuation and hence modify sample absorbance characteristics (Michaels and Knap, 1996; Nelson and Siegel, 2013). Particulate absorbance tends to become dominant at wavelengths > 360 nm, which importantly affects the calculation of spectral slope due to changed absorption characteristics (Stubbins *et al.*, 2006). For example, Nelson *et al.* (1998) reported 50% of total particulate absorption at 440 nm by detritus.

2.5.2 *SML thickness estimation*

SML thickness was determined in two ways, firstly by dipping the screen 10 times in one location and recording the total volume collected and secondly, by dipping the screen 10 times at 10 different spots around the ship and recording the total volume collected (Salter, 2010).

The SML thickness ranged between 185.2 and 340.7 µm with an overall average of 264.5 ± 35.6 µm on AMT24. The SML thickness was quite similar between the Northern and the Southern Hemisphere with an average of 258.0 ± 36.5 µm and 275.5 ± 31.8 µm respectively.

2.5.3 *Surfactant Activity (SA) determination by Alternating Current (AC) Voltammetry*

SA was analysed by sinusoidal alternating current (AC) voltammetry (797 VA Computrace, Metrohm, Switzerland). The method is the most convenient technique for surfactants with a wide range in hydrophobicity, i.e. from hydrophilic polysaccharides to strongly hydrophobic fatty acids (Gašparović and Ćosović, 1994; Vojvodić *et al.*, 1994). The method uses three electrodes: (i) reference electrode (saturated silver/silver chloride (Ag/AgCl)) saturated in 3 mol L^{-1} KCl solution; (ii) hanging mercury drop electrode (HMDE: renewable, non-polar hydrophobic surface) and (iii) platinum wire auxillary electrode (Ćosović and Vojvodić, 1982; Ćosović and Vojvodić, 1998; Cuscov and Muller, 2015).

In AC voltammetric analyses a constant potential (E) of -0.6V is applied between the HMDE and reference electrodes, giving an electrical double layer at the mercury-water interface while the water sample is stirred for some deposition period to adsorb surface active material to the electrode. The adsorbed compounds modify the electrical double layer at the mercury-water interface. The net effect of surfactant accumulation on the HMDE is to modify permittivity and thickness of the double layer, resulting in the depression of CC_i for the applied voltage (Cuscov and Muller, 2015).

Calibration was against the non-ionic soluble surfactant polyoxyethylene t-octylphenol (Triton-X-100 or T-X-100). T-X-100 is a simple, relatively small molecule (MW = 600 Da) that simulates the same absorption behaviour during AC voltammetry as does natural surfactant of the same activity (Ćosović and Vojvodić, 1998; Frka *et al.*, 2012; Cuscov and Muller, 2015). T-X-100 is chemically stable and is commercially available.

The change in capacitive current (ΔI) was calculated for a range of standard solutions with known concentrations of T-X-100 (50 µl, 55 µl, 110 µl, 220 µl, 480 µl, 1.05 ml, 2.95 ml, 5.80 ml and 9.90 ml of 2 mg L^{-1} T-X-100 solution added to the initial 10 ml of 0.55 mol L^{-1} NaCl). Standard solutions of T-X-100 were prepared fresh prior to each calibration. ΔI was then plotted as a function of T-X-100 concentration (mg L^{-1}) to derive a calibration curve. When determining SA it is important to select measurement conditions that ensure an absorption effect corresponding to the rising part of the calibration curve and below the surface saturation level (Ćosović and Vojvodić, 1982; Ćosović and Vojvodić, 1998) (Figure 2.7). Sample SA is expressed as a "T-X-100 (in mg L^{-1}) equivalent" (Ćosović and Vojvodić, 1998).

(a)

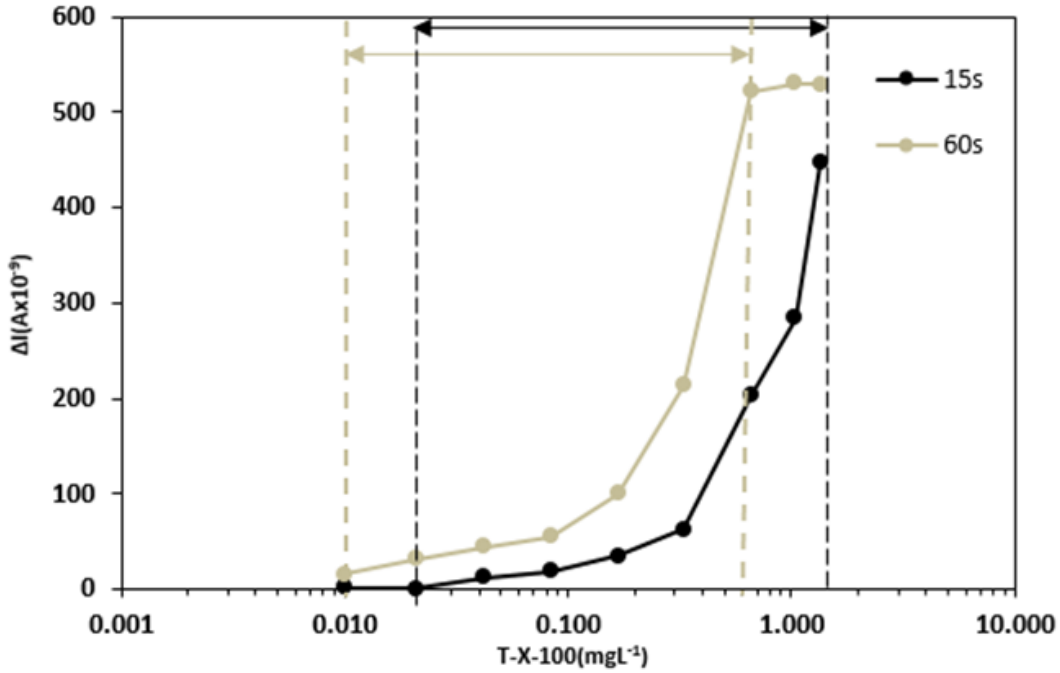

(b)

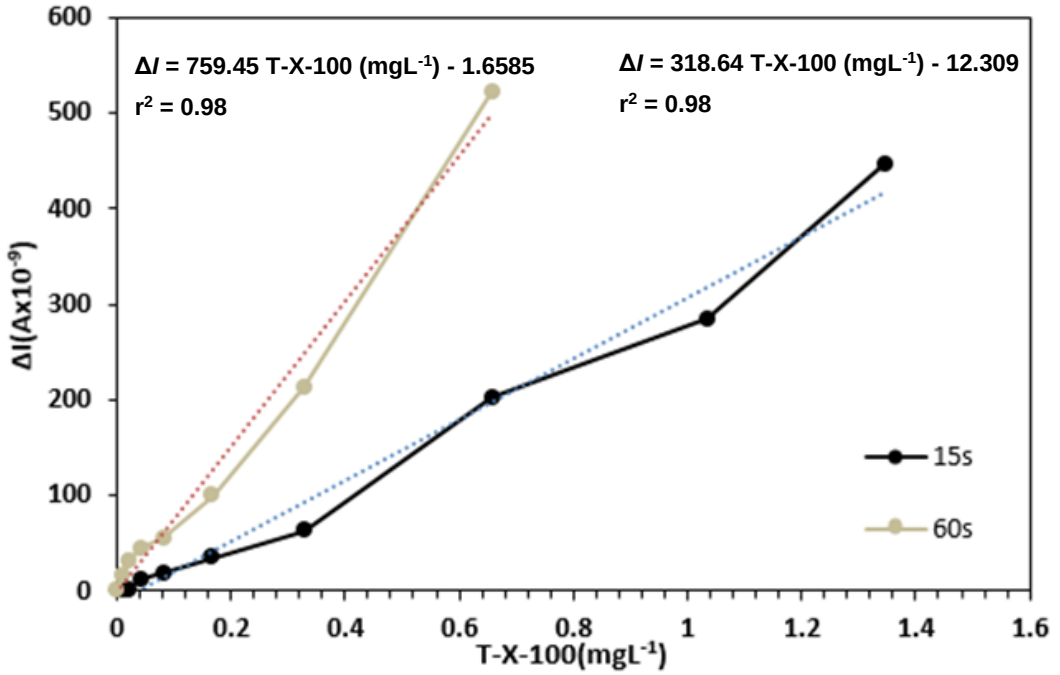

Figure 2.7. (a) Typical full calibration curve for T-X-100 for deposition times of 15s and 60s.The dashed lines and arrows represent the rising parts of each curve, which were used for calibration (b) and the dashed line represents the best linear fit. The best linear fit equation and r-squared (r^2) are also displayed. Note that the x-axis scale in (a) is logarithmic whereas in (b) it is linear.

Salt solution (3 mol L^{-1} NaCl) with an ionic strength lower than that of seawater (~ 0.7 mol L^{-1}) was selected as the blank/reference solution (Cuscov and Muller, 2015). Prior to use, solid sodium chloride (NaCl, FischerScientific, CAS: 7647-14-5, ≥ 99.0) was heated for 6 to 8 hours at 450°C to eliminate traces of organic matter. All blank and standard solutions were prepared from reagent grade chemicals.

The blanks run before and after each batch of samples and possible contamination of the blank and electrochemical cell was examined before each measurement. Suppression of CC_i above 10% of the maximum ΔI for surfactant absorption at saturation implies cell contamination or blank impurities. In that case the cell was acid washed and then heated at 450°C for 6 hours, a new blank solution was prepared and CC_i was re-evaluated. This process was also repeated for samples taken from the deepest Niskin bottle (i.e. 500 m) from each CTD cast as these were expected to have the lowest values of SA to better evaluate any potential contamination during sampling. The depression of the capacitive current (i.e. CC_i) is larger in samples of high SA (Figure 2.8).

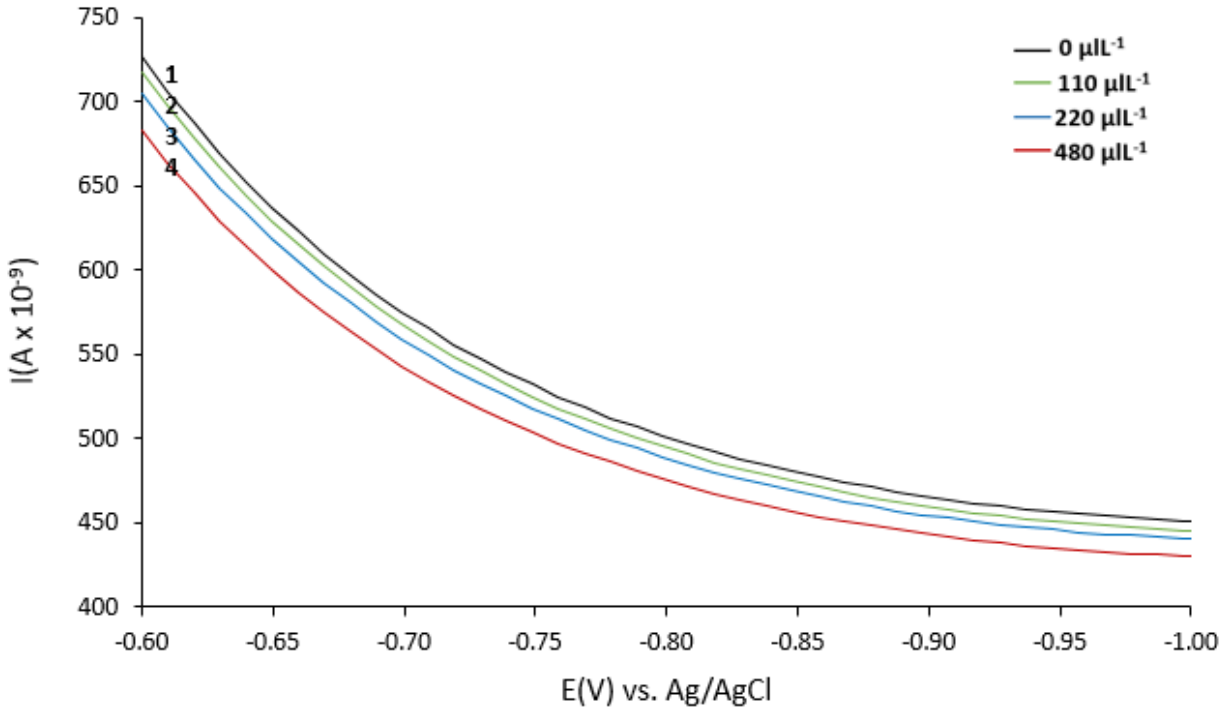

Figure 2.8. Current-potential curves for different concentrations of T-X-100: (1) 0 µl L^{-1}, (2) 110 µl L^{-1}, (3) 220 µl L^{-1} and (4) 480 µl L^{-1}. Supporting electrolyte: 0.55 M NaCl. Amplitude 10mV, frequency 75Hz.

For short deposition times (i.e. low surface coverage) the surface coverage is proportional to the deposition time. However, this will not be the case at longer deposition times because additional molecules will only be adsorbed with less spacing between them and the repulsive electrostatic interactions between adjacent molecules become apparent (i.e. decrease in the slope of the surface coverage) (Figure 2.9).

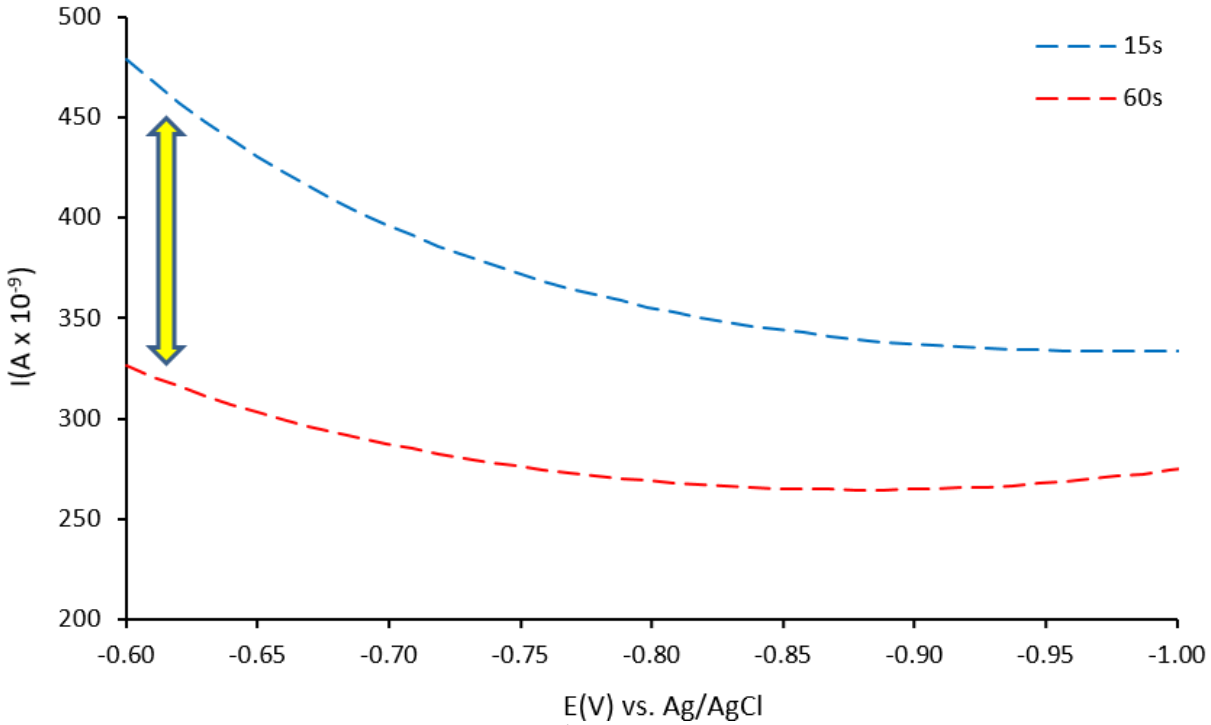

Figure 2.9. Current-voltage curves for 220 µl L^{-1} concentrations of T-X-100 for 15s (blue line) and 60s (red line) deposition times. Supporting electrolyte, 0.55 M NaCl; amplitude 10 mV; frequency 75Hz. The yellow arrow compares the difference between the intensity of the slope for the two deposition times.

The accumulation of surfactants is monitored by sweeping the potential from -0.6V to -1.0V (Schneider-Zapp *et al.*, 2014; Pereira *et al.*, 2016). As the standard in the literature is to use the current at -0.6V and because this enables comparison with other published data, E = -0.6V for SA measurements was employed. Therefore, SA includes the sum of the anionic and non-ionic components, as in previous studies of environmental water samples (Gašparović *et al.*, 2011; Wurl *et al.*, 2011b; Gašparović, 2012; Schneider-Zapp *et al.*, 2014; Pereira *et al.*, 2016).

The quantification of SA is by defining ΔI, the decrease in CC_i at E = - 0.6V relative to the baseline for pure, surfactant-free electrolyte (3mol L^{-1} NaCl): depending upon the expected value of SA in each sample:

$$\Delta I = I_s - I_b \qquad \text{(equation: 2.1);}$$

where I_s and I_b are the values of CC_i at E = -0.6V for the sample and the blank respectively (Ćosović and Vojvodić, 1982; Ćosović and Vojvodić, 1998).

Choosing an appropriate deposition time for the analyses is critical in any AC voltammetry technique. The deposition time should be long enough to provide satisfactory sensitivity for the

analyses, while avoiding saturation and absorption of any impurities present in the samples, such as cell walls and electrolytes.

This work used deposition times of both 15s and 60s for each individual sample to cover the range of SA in the oceanic samples and these were kept constant through all the measurements during both cruises. This is the standard technique established in the Oceans and Climate Research Group at Newcastle University, based on earlier methods (Ćosović and Vojvodić, 1982; Ćosović and Vojvodić, 1998), and used previously for offshore North Sea samples (Schneider-Zapp *et al.*, 2014; Pereira *et al.*, 2016).

Reduction in CC_i is related to the extent of surfactant absorption on HMDE during the deposition time. The HMDE became saturated at levels around 9.90 ml L^{-1} surfactant eq. T-X-100 and CC_i showed no further decrease (Figure 2.10).

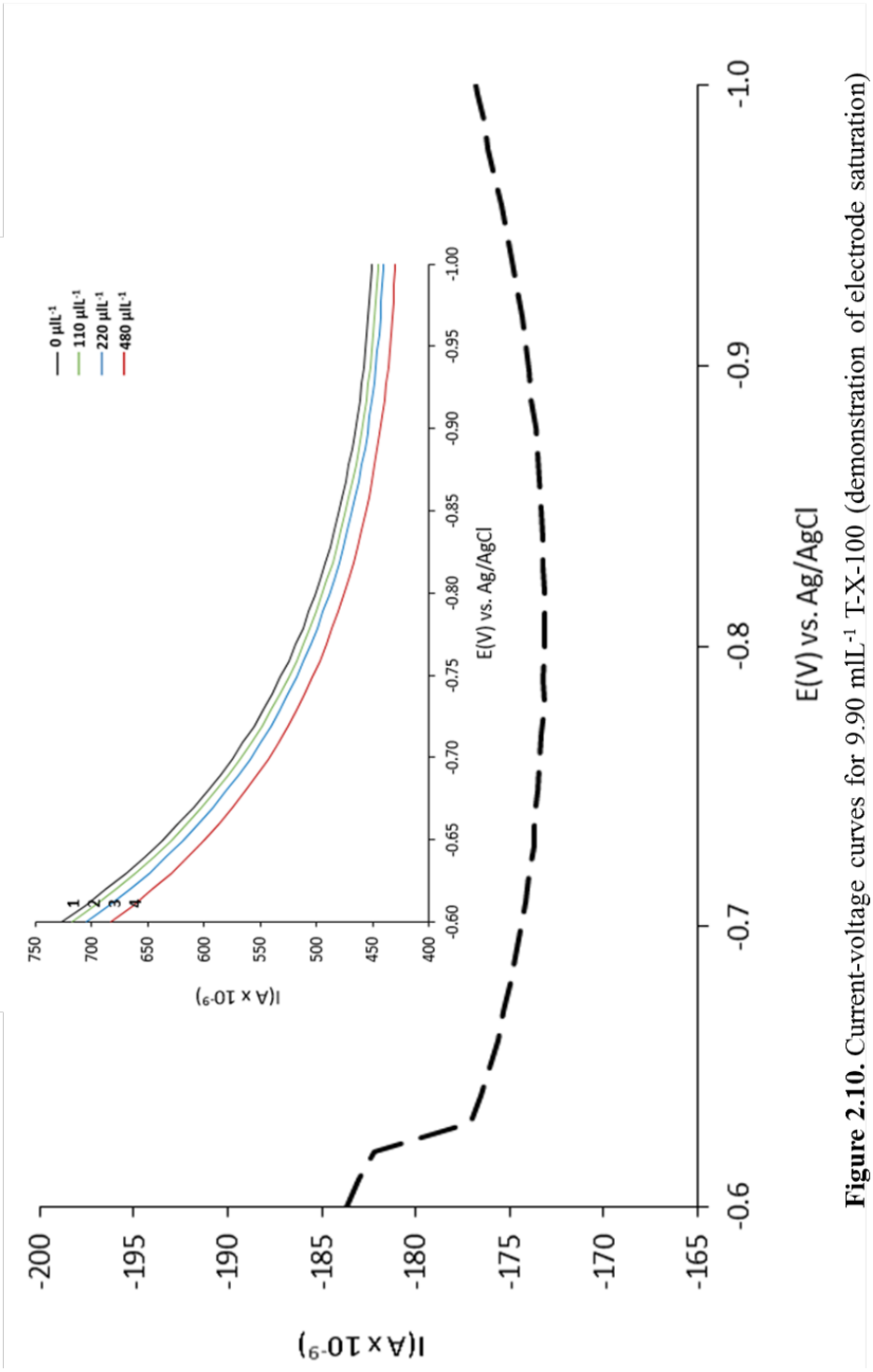

Figure 2.10. Current-voltage curves for 9.90 mlL^{-1} T-X-100 (demonstration of electrode saturation) Supporting electrolyte: 0.55 M NaCl. Amplitude 10mV, frequency 75Hz (Ćosović and Vojvodić, 1998)

If the electrode is saturated then appropriate dilution is required to bring the sample to within the measurable concentration range (Žutić *et al.*, 1981; Ćosović and Vojvodić, 1982; Ćosović and Vojvodić, 1998). Diluting the samples with high purity water and electrolyte will give better precision than reducing deposition time, which leads to decreased sensitivity (Ćosović and Vojvodić, 1998; Cuscov and Muller, 2015).

CC_i is influenced by the ionic strength of the sample. So, equal ionic strength between the samples was achieved by adding either MilliQ water or highly pure surfactant-free salt solution (3 mol L^{-1} NaCl) (FischerScientific) depending upon whether the initial salinity (S) of the sample was greater or lower than 35 (Ćosović and Vojvodić, 1998; Cuscov and Muller, 2015). All samples were therefore normalised to S = 35. The actual SA for a given sample was then recalculated using the dilution factor. The final volume of the sample in the cell was always maintained at 10 ml.

To enhance surfactant accumulation at the HMDE and increase the method sensitivity, the sample was stirred at 1000 rpm during deposition, in the standard 100 cm^3 Metrohm sample cell using a 10 cm Teflon stirrer bar (Ćosović and Vojvodić, 1982). All measurements were with the sample cell open to air and without de-aeration. Analyses were all in triplicate. Analytical precision was expressed as a standard error =100 $\sigma/\bar{x}$, where σ is the standard deviation of the mean (x) of the triplicate samples. Analytical precision was always better than ± 10% and was frequently better than ± 4%. The detection limit was 0.00995 mg L^{-1} T-X-100.

2.5.4 *Method modification for SA analyses at sea*

Some method modifications were required due to the possibility of the mercury drop detaching from the electrode at high sea states due to ship motion. To avoid this the equipment was installed on a custom-designed gimbal table (Figure 2.11).

Figure 2.11. 797 VA Computrace on the gimbal table during AMT25 (2015).

A gimbal table provides a platform such that and object can be fixed to it and allowed to rotate along different axes. This helps the object to remain upright while the ship is pitching or rolling.

Mercury drop size number gives the drop creation time in units of 40 ms. Presumably, there is an advantage of using a larger drop size because of higher surface absorption capacity for surfactants to be absorbed if the drop is sufficiently stable. With too large a drop size, the mercury drop becomes quite heavy which may affect the stability. For example, the typical mercury drop size (DS) used previously at Newcastle University (North Sea samples) was 7 (Pereira *et al.*, 2016) that was not stable enough under high sea states on AMT cruises (Figure 2.12).

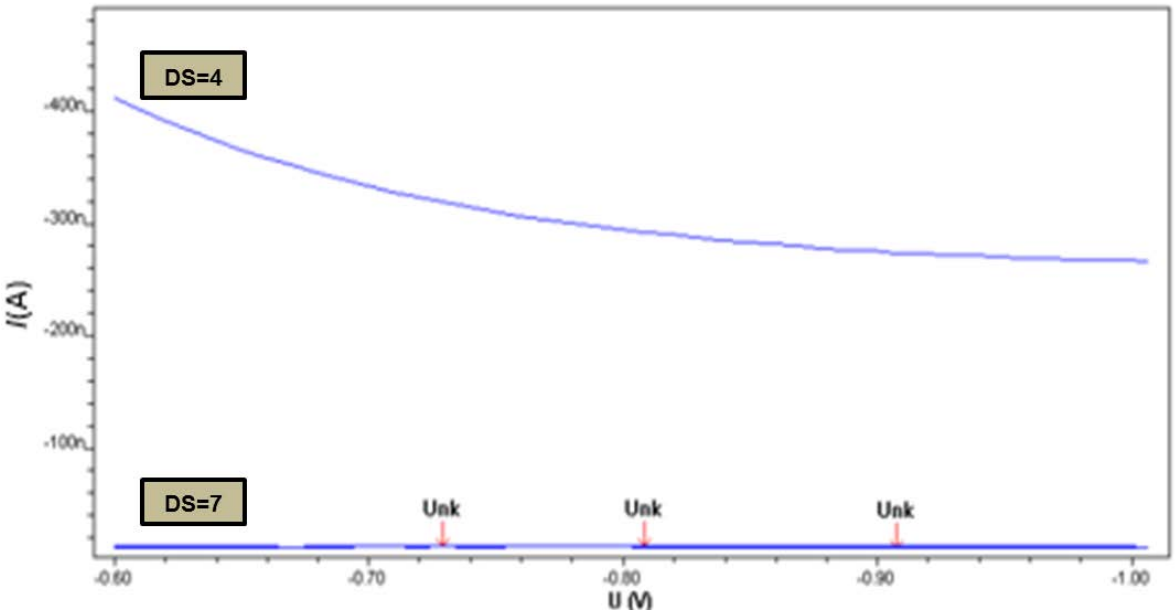

Figure 2.12. Current-potential curve derived from AC voltammetry with drop sizes (DS) of 4 and 7 on AMT24. Unk indicates inability to resolve the current

Figure 2.12 shows no response using DS = 7; the mercury drop has become unstable and fallen. A smaller drop (DS = 4) increases stability and makes it less likely to fall during the capillary measurement. However, it will make the analysis less sensitive unless the deposition time is increased. So, the medium mercury drop size of 4 with deposition of 15s and 60s was selected for all analyses (Cuscov and Muller, 2015).

2.5.5 *Enrichment factor (EF)*

To quantify the degree of surfactant enrichment in each SML sample relative to corresponding SSW sample, an enrichment factor (EF) was calculated as:

$EF = (Surfactants_{SML} / Surfactants_{SSW})$ (equation: 2.2);

Therefore, EF values >1 indicate surfactant enrichment in the SML whereas EF < 1 indicates surfactant depletion in the SML compared to the underlying waters.

To evaluate surfactant enrichment factors, data from the ship's non-toxic supply line at 7 m were used as the reference, as for CDOM optical properties (see section 2.5.6). Although 2 m data were also available from some CTD casts, this depth was not consistently sampled along transects (the shallowest depths in some CTD casts being 5 m or more). Also, a strong correlation between SA in the shallowest CTD sample (2 m) and SA in the corresponding 7m non-toxic sample was observed (Figure 2.13) hence, the latter were selected to determine SA EFs in the Atlantic Ocean and these 7 m data are subsequently referred to as sub-surface water (SSW).

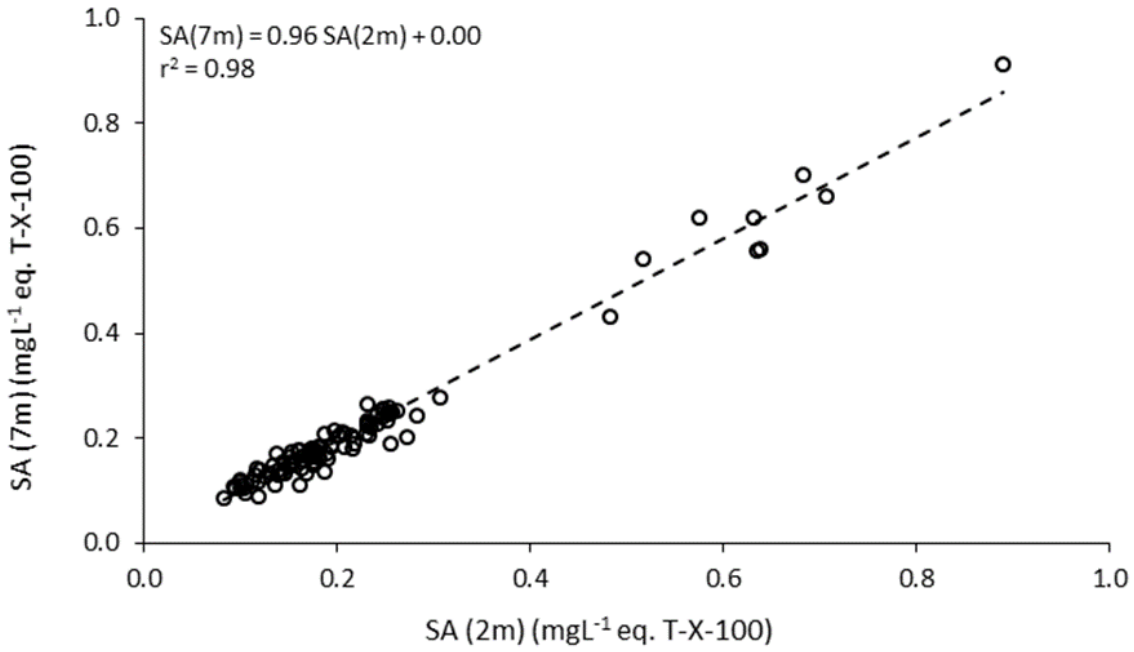

Figure 2.13. SA derived from the shallowest CTD samples (2m) and the corresponding 7m non-toxic sample. The dashed line represents the best linear fit. The regression model and r-squared (r^2) are also indicated.

So, EFs were calculated for all stations on AMT24 and AMT25 using SSW from 7 m depth.

2.5.6 *CDOM determination*

To maintain thermal equilibration between the samples (especially cooler, deep samples) and the reference solution, samples were stored at laboratory temperature (Kitidis *et al.*, 2006; Stubbins *et al.*, 2006) and in the dark for 1 hour prior to analysis to avoid artefacts arising from temperature differences (Miller *et al.*, 2002; Helms *et al.*, 2008).

Spectrophotometric analyses of CDOM were conducted using a UV-Visible high performance liquid core waveguide (LCW) spectrophotometer (Ultrapath UV, World Precision Instruments (WPI), Inc. USA) ideally suited to the analysis of low CDOM oceanic samples (Miller *et al.*, 2002) (Figure 2.14).

Figure 2.14. (Ultrapath) spectrophotometer with fibre-optic pathlength.
Source: https://www.wpiinc.com/products/spectroscopy-and-optics/upuv-ultrapath-system-ultraviolet-and-visible-light/

This instrument was used because using a 10 cm cuvette conventional spectrophotometer leads to significant errors in light absorption measurement at wavelengths > 360 nm for oceanic samples; previously CDOM absorption coefficients in the Atlantic Ocean determined in this way were below the detection limit of the spectrophotometer (Stubbins *et al.*, 2006).

The effective optical path lengths used were 50 cm on AMT24 and 200 cm on AMT25. It was necessary to use a shorter pathlength on AMT24 due to prior instrument damage. For this reason all results were normalized to the pathlength used in each case.

The detection limits of the LCW spectrophotometer at 50 and 200 cm path lengths were 0.0092 m^{-1} and 0.0023 m^{-1} respectively.

Filtered seawater samples (100 µl – 10 ml) (Miller *et al.*, 2002) were drawn into the Ultrapath sample cell using a peristaltic pump. Studies have shown that filtered and unfiltered CDOM gives the same/very similar results (Pereira *et al*., 2016).

To avoid artefacts from sample residue, wetted Ultrapath components were cleaned daily with 1 mL of Ultrapath Waveguide cleaning solution (WPI, USA) followed by 20 ml MilliQ.

Absorbance spectra were recorded over a range of wavelengths (275-700 nm) at 1nm resolution against a sodium chloride (NaCl) reference (0.5 M NaCl solution) following Nelson *et al*. (2007). The reference solution closely matched sample salinity to within ±1 (34 to 37). The artificial seawater was prepared using granular NaCl (Fisher Scientific, CAS: 7647-14-5, ≥ 99.0) baked at 400°C for 6-8 hours to remove any organic contamination (Miller *et al.*, 2002; Helms *et al.*, 2008). Instrument baseline values were recorded before and after processing of a CTD cast, to monitor instrument drift, which was also monitored by checking the absorbance spectra of MilliQ water regularly. In the case of any observed high absorbance while running MilliQ, the sample cell was cleaned and the procedure repeated until successful.

Baselines recorded on the same day usually agreed to within ± 0.00005 absorbance units at 275 nm. Collected spectra were all corrected for dark current by setting the shutter in the closed position and taking dark spectra. Measurements were made in triplicate within 3 hours of collection. Naperian absorption coefficients, a_λ, were then calculated following:

$$a_\lambda = 2.303A/l \qquad \text{(equation: 2.3);}$$

where a_λ is sample absorbance at wavelength λ (corrected for the blank (reference) and temperature offset), A is the absolute absorbance and l is the fibre-optic pathlength (m). The effective pathlength for each optical cell was 49.78 ± 0.5 cm and 204.01 ± 1.0 cm for 50 and 200 cm pathlengths respectively.

CDOM absorbance is highest at short wavelengths (280 - 450 nm) and decreases exponentially towards longer wavelengths (Twardowski *et al.*, 2004). Typically, no absorbance is measurable at wavelengths > 600 nm (Figure 2.15).

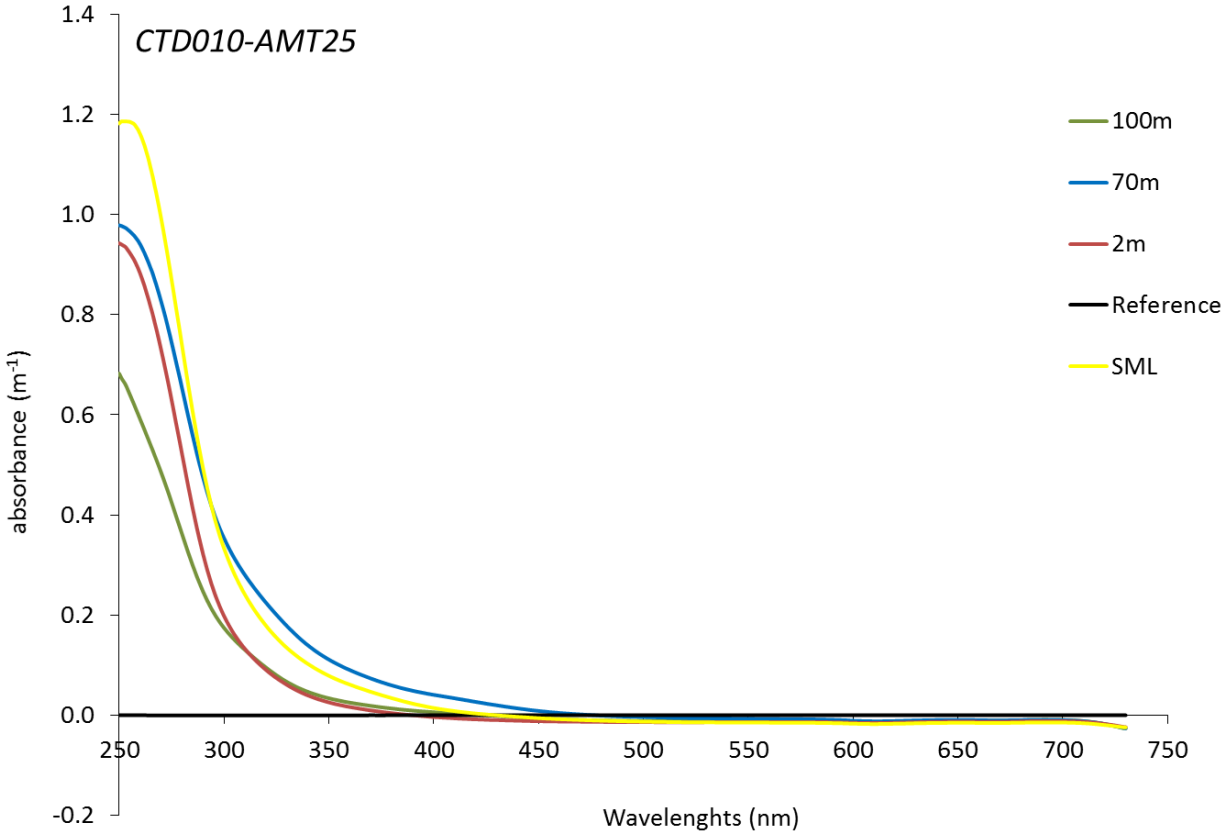

Figure 2.15. A typical CDOM absorbance-wavelength curve for a wavelength range 250 nm to 730 nm. Samples from SML, 2, 70 and 100 m were collected during CTD cast number 10 on AMT25. The black line represents the reference/blank absorbance.

However, a typical CDOM absorbance spectrum is a featureless (i.e. without distinctive feature) trend and low overall resolution (Figure 2.15) led to absorbance measurements at discrete wavelengths or a range of wavelength bands to better determine CDOM, after Kalbitz *et al.* (1999), Hautala *et al.* (2000) and Helms *et al.* (2008).

2.5.6.1 Refractive index and offset correction

Differences in the refractive indices (RI) of a seawater sample and the Milli-Q reference can lead to systematic errors because the effective optical pathlength of the LCW varies with the refractive index of the solution (Miller *et al.*, 2002). Miller et al. (2002) therefore recommended the use of sodium chloride (NaCl) solution as a reference against seawater samples and adjusted the NaCl concentration of their reference to match that of their seawater samples, using a refractometer. Given that salinities along AMT transects generally vary from 35 to 37 (Aiken *et al.*, 2000), it was initially assumed that a NaCl solution of salinity of 36 (36.005 g L^{-1} NaCl) would be a practical reference, because the concentration dependence of the refractive index effect over the 35-37 salinity range is negligible , (i.e. the change in refractive index is 0.0138%

per PSU) (Tan and Huang, 2015). However, closer inspection of absorbance spectra recorded against the NaCl reference showed consistent negative offsets at longer wavelengths (675-695 nm) indicating possible errors caused by differences in the wavelength dependence of the refractive indices of seawater and NaCl reference, respectively.

It was therefore necessary to investigate the wavelength dependence of absorbance of saline solutions obtained by subtracting the absorbance spectrum of a Milli-Q reference from absorbance spectra of artificial seawater and NaCl solution (S = 36) respectively after Dickson (1990) and Grasshoff *et al.* (2009).

The apparent absorbance of NaCl (S = 36) (solution B) showed negative values at long wavelengths (-0.13 at 730 nm), an approximately linear increase towards the UV, followed by a roughly exponential increase towards shorter wavelengths (~ 0.15 at 250 nm). Absorbance for artificial seawater (solution D) showed a similar pattern, but with significantly higher values at wavelengths below 600 nm (Figure 2.16).

At wavelengths above 300 nm, apparent absorbance increased with increasing salinity, showing a maximum increase of 0.003 per unit salinity at 325 nm.

These results agree favourably with Nelson *et al.* (2007) who reported the same salinity dependence at 325 nm and found that the refractive index of seawater varied linearly with salinity over the entire ocean salinity range.

To account for changes in sample salinity during AMT24 and AMT25, the apparent absorbance of the artificial seawater reference was calculated by interpolation to sample salinity as follows:

$$A_{\lambda,ref,SS} = A_{\lambda,ref,35} + (A_{\lambda,ref,37} - A_{\lambda,ref,35}) / (37-35) \times (SS-35) \quad \text{(equation: 2.4)}$$

where $A_{\lambda,ref,35}$ and $A_{\lambda,ref,37}$ denote the apparent absorbances at wavelength λ and salinities 35 and 37 respectively, and SS denotes sample salinity. To account for the use of NaCl solution as a reference during AMT 24 and 25, spectral correction factors, F_λ, were calculated by subtracting the absorbance of artificial seawater at sample salinity $A_{\lambda,ref,SS}$ from the absorbance of NaCl (S = 36), $A_{\lambda,NaCl,36}$: $F_\lambda = A_{\lambda,NaCl,36} - A_{\lambda,ref,SS}$.

The maximum F_λ for salinity 36 occurred at 280 nm (0.057; Figure 2.16). Absorbance spectra, referenced to artificial seawater matched to sample salinity, were then obtained by subtracting F_λ from sample absorbance.

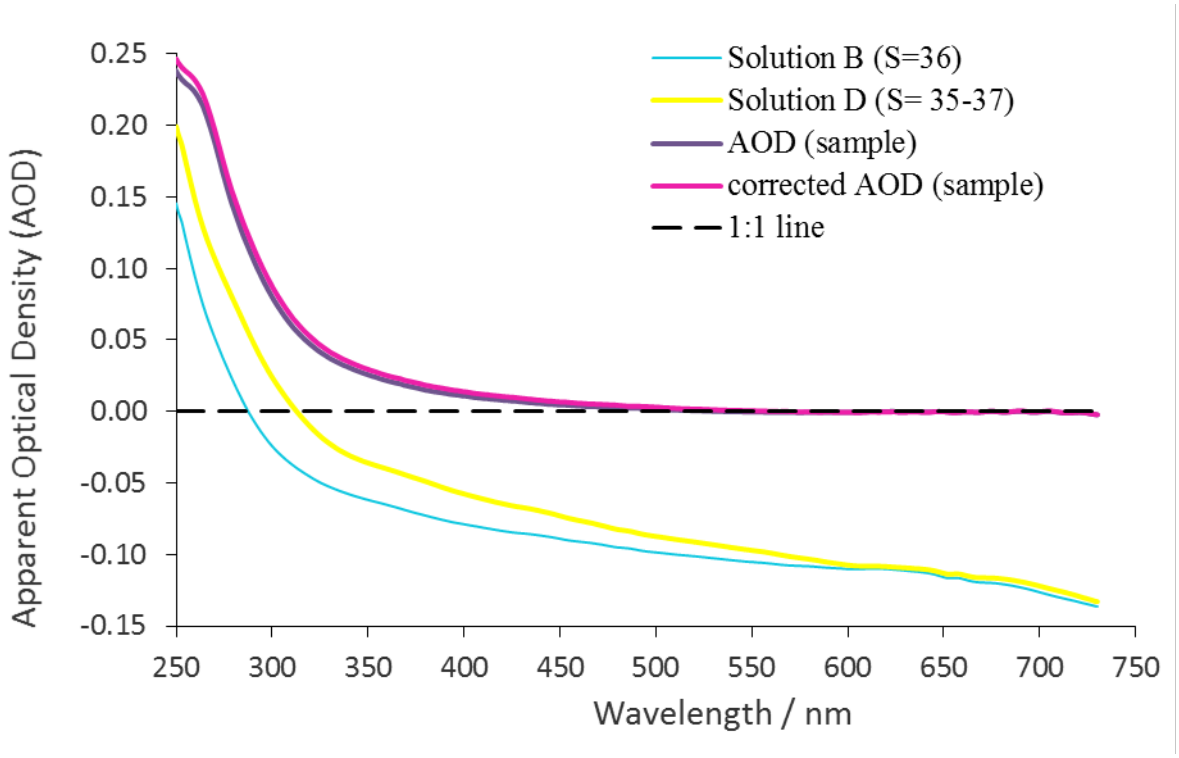

Figure 2.16. The difference in absorbance spectra over a range of wavelengths before and after refractive index (RI) correction. NaCl solution of salinity 36 (solution B) (blue), artificial seawater with interpolated salinity of 35 to 37 (solution D) (yellow), apparent optical density of the sample (purple), sample apparent optical density after offset correction (pink) and 1:1 line (black).

2.5.6.2 Data processing

For this study CDOM absorption coefficient was calculated at 300 nm wavelength (a_{300}) because CDOM dominates at this wavelength (Kitidis *et al.*, 2006; Stubbins *et al.*, 2006; Helms *et al.*, 2008; Pereira *et al.*, 2016). Also, the measurement of absorption coefficient at longer wavelengths (i.e. > 400 nm) may be problematic for most spectrophotometers (Helms *et al.*, 2008).

2.5.6.2.1 Spectral slope ratio (SR)

Characterisation of CDOM properties such as chemical structure and source can be informed by using spectral slope values and specific spectral slope ratios that are not CDOM concentration dependant (Brown, 1977). Spectral slope determination over a narrow wavelength range is more efficient with less variation than over a longer wavelength range (Brown, 1977). Therefore, two distinct spectral slope regions (i.e. 275-295nm and 350 -

400nm) were selected, after Carder *et al*. (1989) and Helms *et al*. (2008). The spectral slope ratio (S_R) was calculated using a log linear fit of an exponential function in MS Excel to the absorption spectrum over two pre-defined wavelength ranges as following:

S_R = Slope (ln absorbance at wavelength 275:295) / Slope (ln absorbance at wavelength 350:400) (i.e. $S_{275-295}$ / $S_{350-400}$) (equation: 2.5);

(Helms *et al*., 2008). Using spectral slopes over these two defined wavelength ranges avoids using absorption spectra close to the detection limit of the instrument. These wavelength ranges are very sensitive indicators of the photochemical transformation of CDOM, changes in its molecular weight and source (Helms *et al.*, 2008).

However, using non-linear fits may cause a bias in slope ratio. To test for this, a log-linear fit procedure was applied to a sample subset. No discernible differences were found by using either a log linear or nonlinear fit (Stedmon *et al.*, 2000; Twardowski *et al.*, 2004; Helms *et al.*, 2008). Helms *et al*. (2008) pointed that the variation between log transform linear regression and nonlinear regression fit was less than 1%. This was most likely due to the wavelength (λ) ranges in Helms *et al*. (2008) being much shorter than in this study.

Variations in organic matter molecular weight can also be evaluated using E_2:E_3, the absorption ratio for the wavelengths 250 nm and 365 nm. There is an inverse correlation between E_2:E_3 ratio and molecular weight because of stronger light absorption by high molecular weight material at longer wavelengths (De Haan and De Boer, 1987; Peuravuori and Pihlaja, 1997; Helms *et al.*, 2008).

2.6 Gas exchange methodology

Estimates of carbon dioxide (CO_2) transfer velocity (k_w) were made on large volume (93 L) surface water samples collected at 13 stations between 26th September and 26th October 2014 during AMT24 by Dr Ryan Pereira (Newcastle University, now at Heriot-Watt University) using a fully automated closed air-water gas exchange tank (Figure 2.17).

These k_w estimates were coordinated with SA and CDOM measurements presented in this thesis and are used subsequently (Chapter 5) to aid interpretation of the wider implications of the SA and CDOM distributions observed in the Atlantic Ocean SML. Therefore, while detailed

descriptions of the gas exchange tank methodology and k_w derivation is outside the scope of this thesis, a brief description is provided here to give some context. Full details, including tank design, operation and cleaning procedures are given in Schneider Zapp *et al*. (2014). Principal features of the exchange tank are shown in Figure 2.17.

(a)

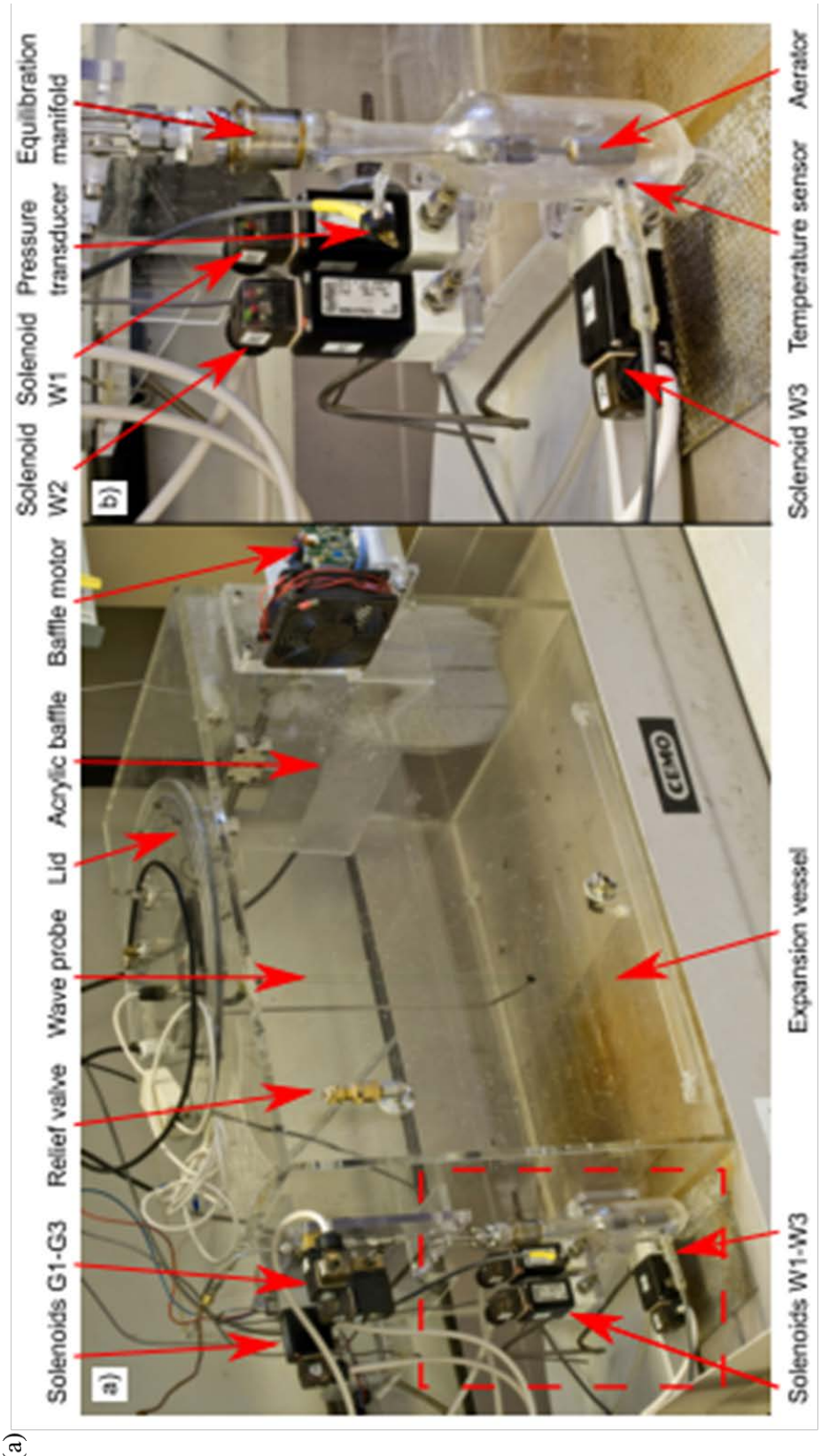

Figure 2.17. (a), major features of the custom-designed gas exchange tank used on AMT24; (b), schematic of the gas exchange tank and ancillary analytical system, reproduced from Schneider-Zapp *et al.* (2014).

(b)

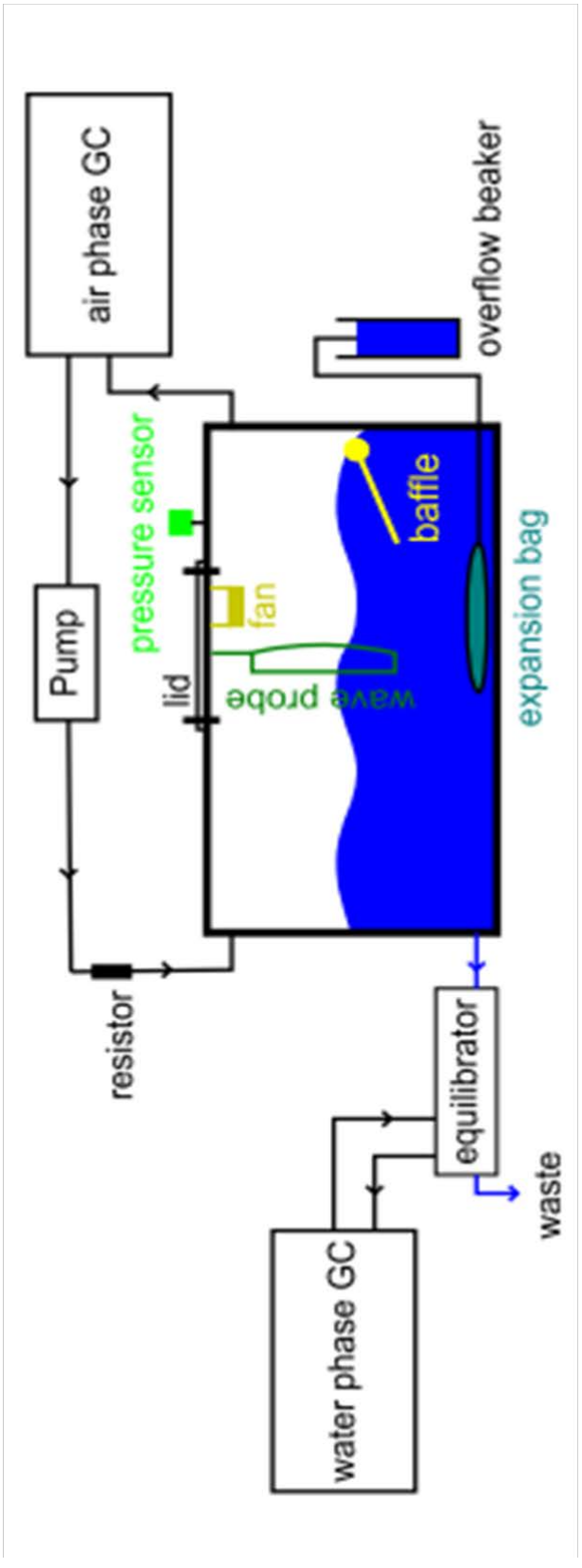

Figure 2.17. (continued) (a), major features of the custom-designed gas exchange tank used on AMT24; (b), schematic of the gas exchange tank and ancillary analytical system, reproduced from Schneider-Zapp *et al.* (2014).

In brief, the cleaned acid-washed tank was filled with ~ 93 L of seawater via the ship non-toxic seawater supply (inlet at 7m). It is not practical to collect the required sample volume from the SML using the Garrett Screen (Pereira *et al.*, 2016). A 1.1 L subsample of ambient seawater was decanted into a sealed glass bottle and enriched with methane (CH_4) and sulphur hexafluoride (SF_6) by equilibration. This gas-enriched sub-sample was then added to the tank water and the final volume recorded. Adding the sub-sample creates a gradient of gas partial pressures between the tank air and water phases, which drives measurable air-water gas exchange during the experiment. Then the tank was sealed.

Two sequential fixed levels of baffle frequency (0.60 and 0.75 Hz) were used, controlled by user designed software in Newcastle University. However, in some experiments it was found that 0.75 Hz had the potential to create bubbles and so all reported results are for the baffle frequency of 0.60 Hz in this study.

During an experimental run, samples of tank headspace and water, the latter automatically equilibrated with compressed air, are analysed for CH_4 and SF_6 by gas chromatography. The changes in tank headspace and water gas partial pressure with time are used to derive k_w estimates for CH_4 at the baffle speed. These data are then converted to equivalent values for CO_2 in seawater at 20^{o}C (k_{660}) using diffusivity-based relations (Schmidt number). Schmidt numbers were obtained from Wanninkhof *et al*. (1992) after Schneider-Zapp *et al*. (2014) to aid comparison under different physical conditions.

The ratio of k_{660} of the sample to that of corresponding surfactant-free MilliQ water; film factor (R_{660}') was calculated as a means of minimising variability in the results due to ship movement.

Surfactant-free MilliQ water (sample blank) was therefore run prior to each seawater sample. The value of k_{660} for the sample blank was then normalized to the k_{660} value of an 'installation blank' (surfactant-free MilliQ water) measured prior to the cruise while the ship was in port.

This correction factor was applied to each sample:

k_{660} sample = k_{660} sample x [k_{660} installation MilliQ / k_{660} sample MilliQ] (equation: 2.6).

Results were discarded if the correction factor was greater than 30% (Schneider-Zapp *et al.*, 2014; Pereira *et al.*, 2016).

2.6.1 *Wind speed measurement*

Wind speeds were measured from the ship's anemometer located on the top of the foremast at ~ 20.8 m height above sea level and logged on the ship's computer every 10 minutes. The true wind speed and direction were corrected for the ship's heading by the respective vector. Wind speeds were finally corrected to U_{10n}, the corresponding wind speed at reference height of 10 m corrected to neutral stability (Nightingale *et al.*, 2000).

2.6.2 *SML thickness versus wind speed*

The relative standard deviation (RSD) of the SML measurements was better than 20%, showing that the data are tightly clustered around the mean.

SML thickness showed an inverse relationship with wind speed during this study, although the relationship is rather weak (Figure 2.18).

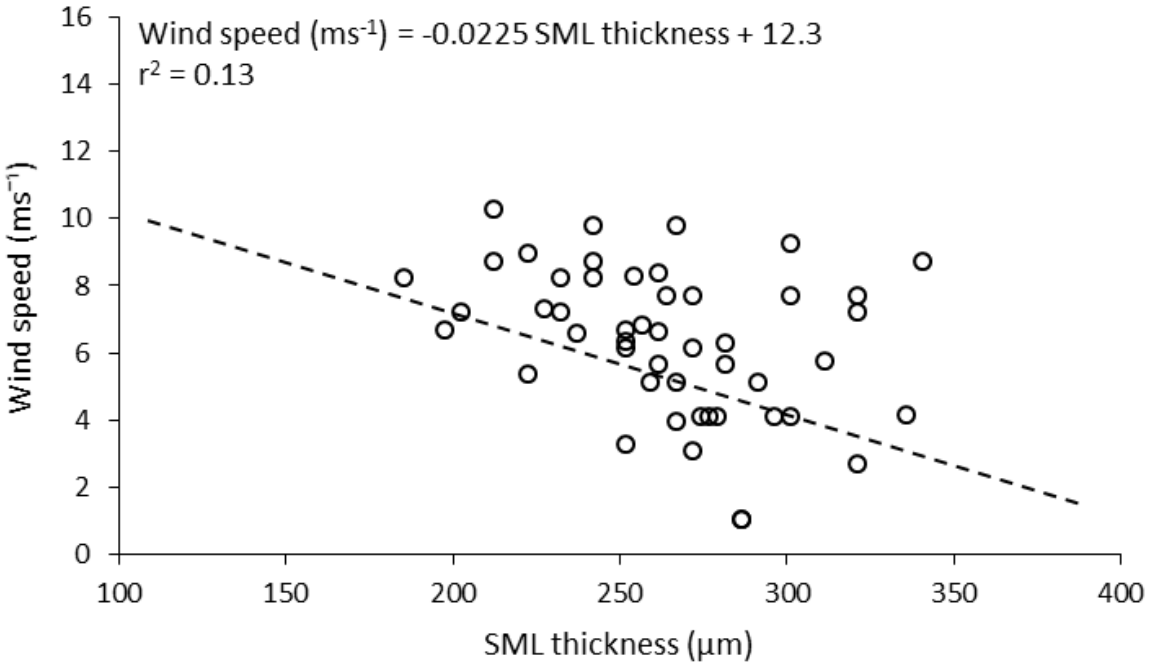

Figure 2.18. SML thickness against wind speed in the Atlantic Ocean. Data are available for AMT24 only.

Although the inverse correlation between SML thickness and wind speed was significant (p = 0.010) the small r-squared value (i.e. r^2 = 0.13) due to the scatter of the data (Figure 2.18) implies that wind speed alone cannot be used to predict SML thickness. Other factors such as wind generated turbulence, waves and bubbles are likely to also be important in controlling SML thickness (Wurl *et al.*, 2011b; Cunliffe *et al.*, 2013).

2.7 Statistical analysis

Statistical analyses were established based on sample size; if the sample size was small (i.e. less than 30 data points), a parametric test (i.e. two sample t-test) was used to analyse similarity between the datasets for normally distributed samples. Nonparametric tests (i.e. Mann-Whitney) were conducted for non-normally distributed data. For large sample sizes (i.e. greater than 30 data points), the Central Limit Theorem[6] was considered for normality of the datasets. Statistical differences were accepted as significant for a probability of less than 0.05 (i.e. $p < 0.05$).

Statistical analysis and illustrations were performed with Microsoft excel 2013, Ocean Data View (ODV4), MATLAB R2016a and Minitab17.

2.8 Hydrographic variables

This section gives a broad outline of temperature, salinity and density during this study. The distributions of these characteristics during previous AMT transects were described by Aiken *et al*. (2000) and Robinson *et al*. (2006). The hydrography during AMT24 and AMT25 did not vary from the typical salinity and temperature climatology for September - November in the study area.

In-situ temperature and salinity were logged from the ship's thermosalinograph (in-line with the non-toxic seawater supply) and the CTD probe to investigate vertical hydrographic structure of the water column.

[6] According to the Central Limit Theorem, the distribution of means will follow a Gaussian distribution (i.e. normal bell shaped distribution) if the sample size is large enough (i.e. more than 30 data points).

Distributions of surface temperature, salinity and Sigma-T (σ_t), seawater density (derived from S and T) expressed as density (kg L^{-1}) – 1000 kg L^{-1}, were relatively similar on the two transects (Figure 2.19).

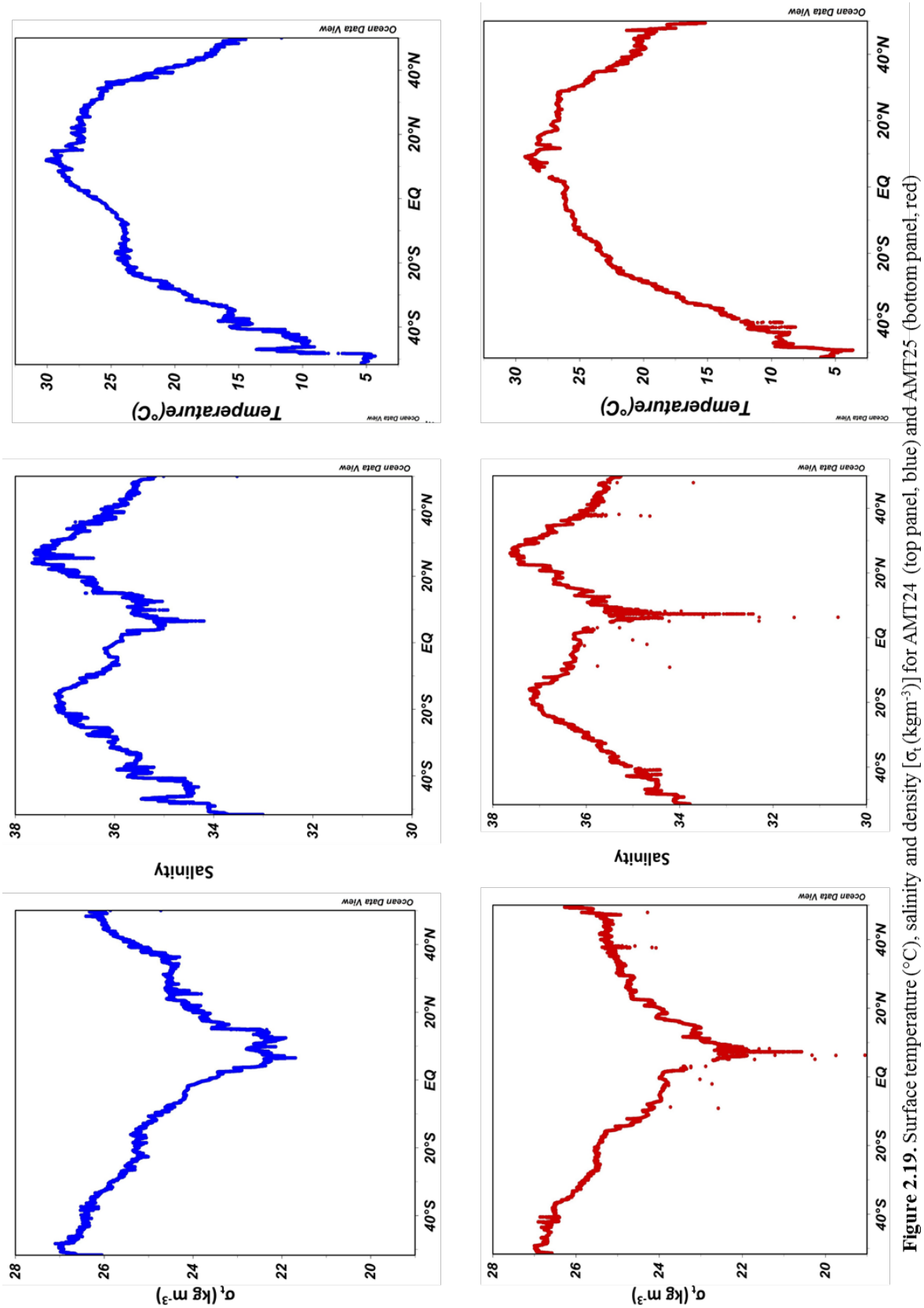

Figure 2.19. Surface temperature (°C), salinity and density [σ_t (kgm^{-3})] for AMT24 (top panel, blue) and AMT25 (bottom panel, red)

Surface water in the tropical and equatorial regions has low σ_t due to low salinity and the high temperatures. In the northern hemisphere equatorial region, the highest temperature is associated with a sharp decline in salinity, which may reflect some dilution of the salinity by precipitation (Aiken *et al*., 2000; Hooker *et al*., 2000).

Temperature reaches a plateau in the northern hemisphere tropics (~ 28° N) and remains above 20°C until it decreases towards the higher latitudes in the southern hemisphere. The coastal upwelling off the west coast of Africa is not clear from the surface temperature profile because the cruise tracks are too far from this region (Figure 2.19).

Salinity shows a similar pattern; increasing from higher to lower latitudes. Salinity maxima were observed in the tropics (37 - 37.5) in association with high surface temperature typical of the regions. Salinity minima of ~ 32 – 34 were observed around ~ 5°N on both cruises in association with salinity decreases in the underlying water (Figure 2.19), indicating some upwelling of low salinity upwelled water to the surface and/or the signature of excess precipitation at the Equator. However, this is not very clear from the temperature plot (Figure 2.19).

Highest σ_t occurs at high latitudes in both hemispheres and declines sharply to < 22 in the equatorial region (i.e. 10°N) due to the higher temperatures (Figure 2.19).

Depth profiles of S, T and σ_t are shown in Figure 2.20.

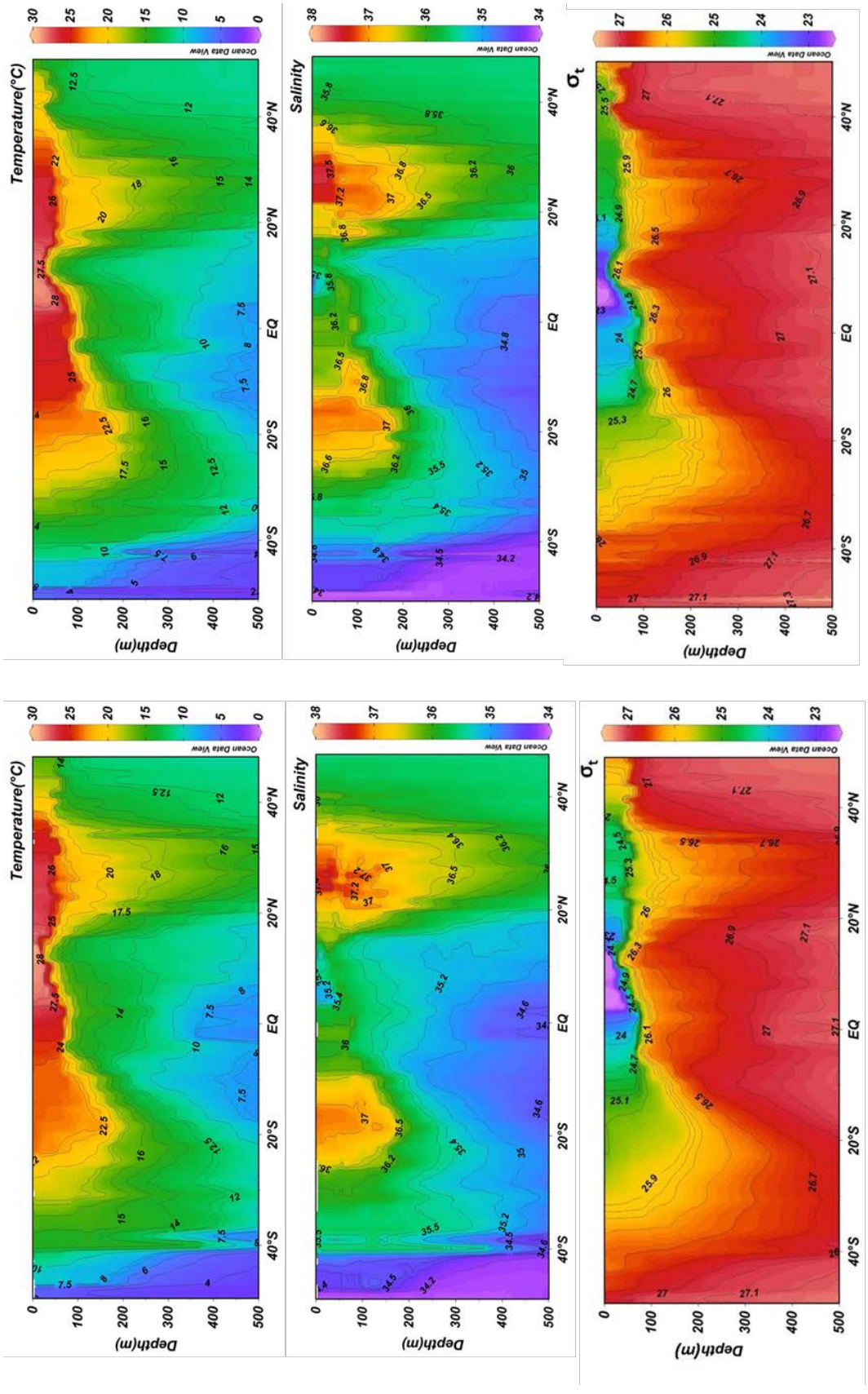

Figure 2.20. Latitudinal cross section of temperature (°C), salinity and density (σ_t) on AMT24 (right) and AMT25 (left)

The main features of the North Atlantic Gyre (NAG) and the Southern gyre (SAG) between ~35°N and ~20°S are the high surface temperatures which declined through the water column associated with the tropical regions (Figure 2.20).

Clearly seen in the temperature profile is cool (and low salinity) water south of ~ 42°S. Low temperature and salinity around the equatorial regions may result from equatorial upwelling on both cruises (Figure 2.19). Upwelling African coastal water was especially discernible on AMT25 (see section 2.2) but it does not show clearly on the temperature and salinity plots (Figure 2.20).

Along the full extent of both transects σ_t increases with depth. The lower values in the Northern and Southern Gyres are observable to ~ 300 m depth. This is due to high solar radiation penetration in these surface optically clear waters and also high temperature at depth due to convergence. These less dense waters extend deeper in the Southern Hemisphere, crossing further into the central gyre (Figure 2.19). Minima in σ_t are also found between 10°N and the equator to a depth ~ 50 m associated with low salinity and high temperature. This may reflect the influence of Amazon outflow carried by the NECC (see section 2.4) (Aiken *et al*., 2000; Hooker *et al*., 2000) and is more noticeable on AMT24 than on the more eastward AMT25 (see section 2.2).

In the high latitudes, north of 40°N and south of 40°S around the European and South-West American continental shelves there is less vertical contrast in σ_t. These variations in density down to 500 m allowed Hooker *et al*. (2000) to identify 17 distinct biogeochemical provinces along AMT transects.

2.8.1 *Dissolved oxygen profile in the Atlantic Ocean*

As for salinity (S) and temperature (T), the latitudinal distributions of dissolved oxygen to 500 m depth were similar during AMT24 and AMT25 (Figure 2.21).

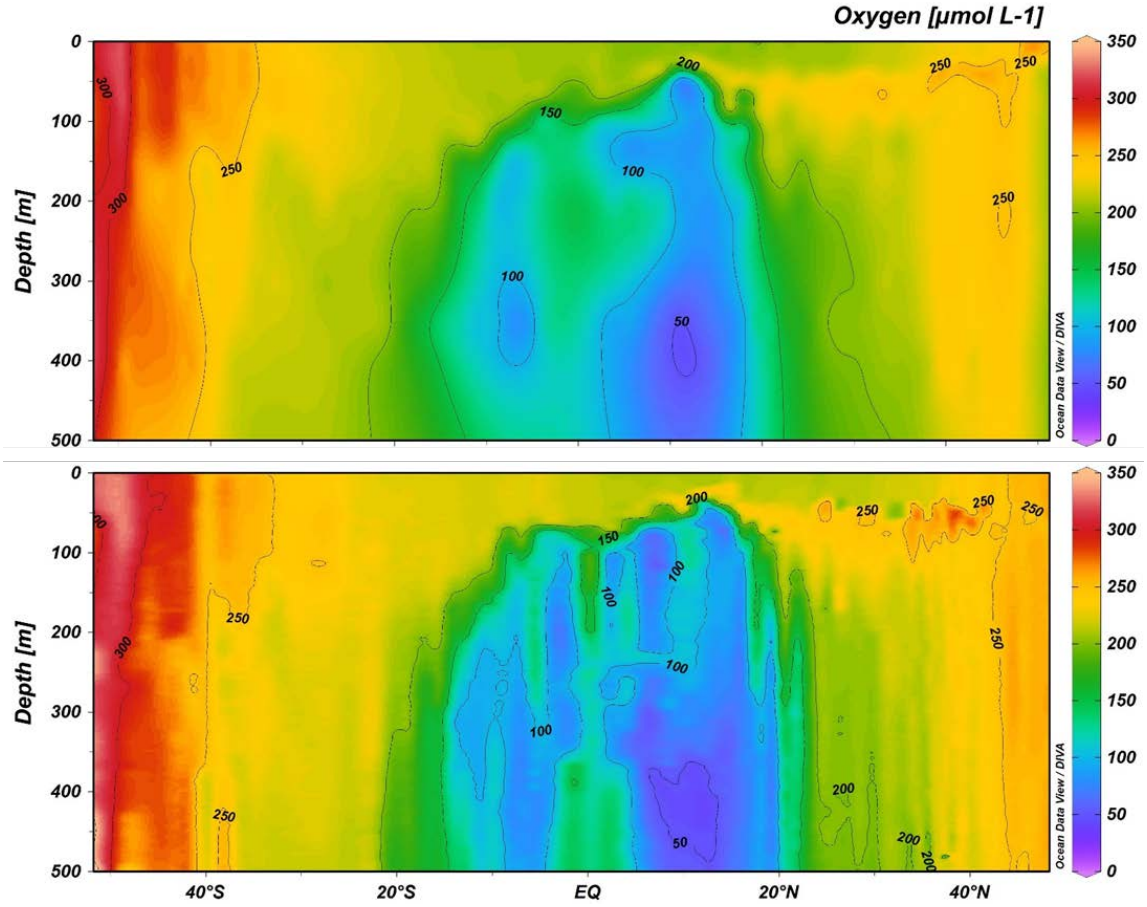

Figure 2.21. Latitudinal cross section of dissolved oxygen (µg L^{-1}) on AMT24 (top) and AMT25 (bottom)

There was a distinct oxygen minimum (~ 100 µmol L^{-1}) between ~ 20°N and ~ 10°S. However, concentrations were slightly higher around the equator. Maximal oxygen was at high latitudes, especially south of 40°S where it is associated with the spring phytoplankton bloom.

2.8.2 *Nutrients*

Samples were analysed for nutrients on board using a Bran and Luebbe segmented flow colorimetric Auto-analyser after Woodward and Rees (2001) and Hydes et al. (2010).

2.8.3 *Mixed Layer Depth (MLD)*

Mixed layer depth (MLD) is a boundary between the mixed layer of the surface and stratified deeper layer (Longhurst *et al.*, 1995; de Boyer Montégut *et al.*, 2004).

Mixed layer determination was adapted from Hooker et al (2000), an approach valid for previous AMT cruises. According to their model, the pycnocline or thermocline starts where gradients of three out of four continuous depths are greater than 0.035 kgm^{-3} for σ_t or 0.1°C/m in temperature (Hooker *et al.*, 2000). In areas with lower gradients the threshold values were increased to 0.1 kg m^{-3} for σ_t or 0.5°C/m in temperature from surface water (i.e. the reference).

Hooker et al. (2000) however found strong compatibility between MLD derived from temperature and density. So, it was suggested that MLD determination based only on temperature is reliable enough (Hooker *et al.*, 2000).

During this study, the gradients in temperature were thus derived to identify the MLD after Hooker *et al*. (2000). It was revealed that the mixed layer determination in this way is consistent with the depth of the mixed layer identified during sampling based on temperature profile by the ship's system within the analytical error of ± 0.1. So, the MLD presented in this study were derived from on board temperature profiles during sampling.

2.9 Summary

Table 2.2 summarises the analyses, methods and relevant references. Also listed are colleagues who provided their raw data, which had not been published at the time of writing. Data interpretations throughout the entire thesis are those of the author alone.

Table 2.2. Summary of the analyses, methods and references included in this thesis

	Cruise No.			
Analyses	**AMT24**	**AMT25**	**Method**	**Reference**
Primary productivity	✓	×	Tilstone *et al*. (2009), (2015)	Tilstone, PML
Phytoplankton community and distribution	✓	✓	Tarran *et al*. (2006)	Tarran, PML
Phytoplankton pigments	✓	✓	Zapata *et al*. (2000)	Airs and Cummings, PML
Nutrients	✓	✓	Woodward and Rees (2001), Hydes *et al*. (2010)	Woodward, PML
Chlorophyll	✓	✓	Welschmeyer (1994)	Thomas, BODC - Bargery, LPU
Surfactants	✓	✓	Ćosović and Vojvodić (1998)	Thesis author
Chromophoric Dissolved Organic Matter (CDOM)	✓	✓	Helms *et al*. (2008)	Thesis author
Gas transfer velocity (k_w)	✓	×	Schneider-Zapp *et al*. (2014)	Pereira, HWU
PML	Plymouth Marine Laboratory			
BODC	British Oceanography Data Centre			
LPU	Liverpool University			
HWU	Heriot Watt Unversity			

Chapter 3. Biological and optical properties of water masses in the Atlantic Ocean

3.1 Introduction

This Chapter presents and discusses ancillary data (latitudinal distributions of phytoplankton communities, chlorophyll, primary production and nutrients) collected during AMTs 24 and 25 from ~ 50°N to ~ 50°S and between ~ 5°W and ~ 55°W, (see section 2.2) and which support interpretation of the surfactant data discussed in Chapter four.

To assess dissolved organic matter (DOM) biogeochemical characteristics, optical properties of the chromophoric fraction of DOM (chromophoric dissolved organic matter, CDOM) in the SML, in SSW (7m) and throughout the water column to ~ 100 m are presented. Relatively little is known about CDOM distributions and variability at ocean basin scales; therefore, using a framework of biogeochemical provinces is advantageous for identifying CDOM variability.

3.2 Chlorophyll distribution and primary productivity in the Atlantic Ocean

Satellite-derived surface chlorophyll images reveal rather similar chlorophyll distributions during the two cruises and a strong similarity to the distribution of phytoplankton abundance (see section 3.4).

Concentrations were lower in the oligotrophic regions, about 0.1 mg m^{-3}, and higher in temperate waters in the Northern Hemisphere and in tropical regions; ~ < 1 mg m^{-3}. The highest concentration of chlorophyll on both transects was observed at high latitudes in the Southern Hemisphere, ~ 1 mg m^{-3} (Figure 3.1).

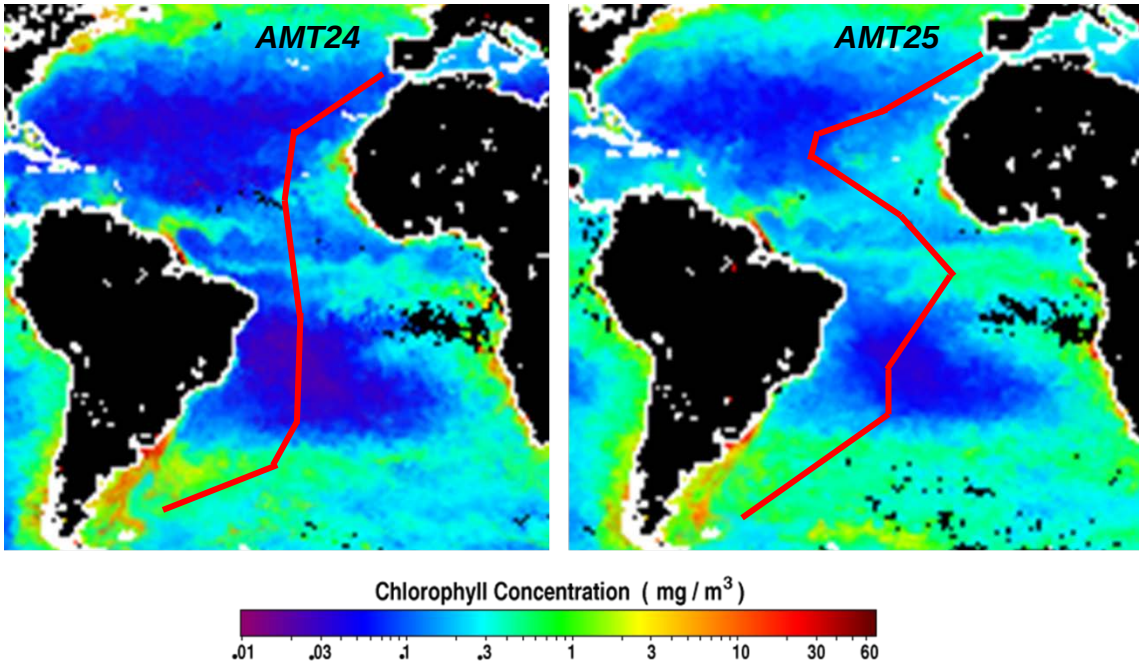

Figure 3.1. Satellite-derived (AQUA/MODIS) images of chlorophyll distribution in the Atlantic Ocean. The data are provided by NASA Earth Observatory for October 2014 (left) and 2015 (right). https://earthobservatory.nasa.gov/GlobalMaps/view.php?d1=MY1DMM_CHLORA. The red lines represent the cruise track.

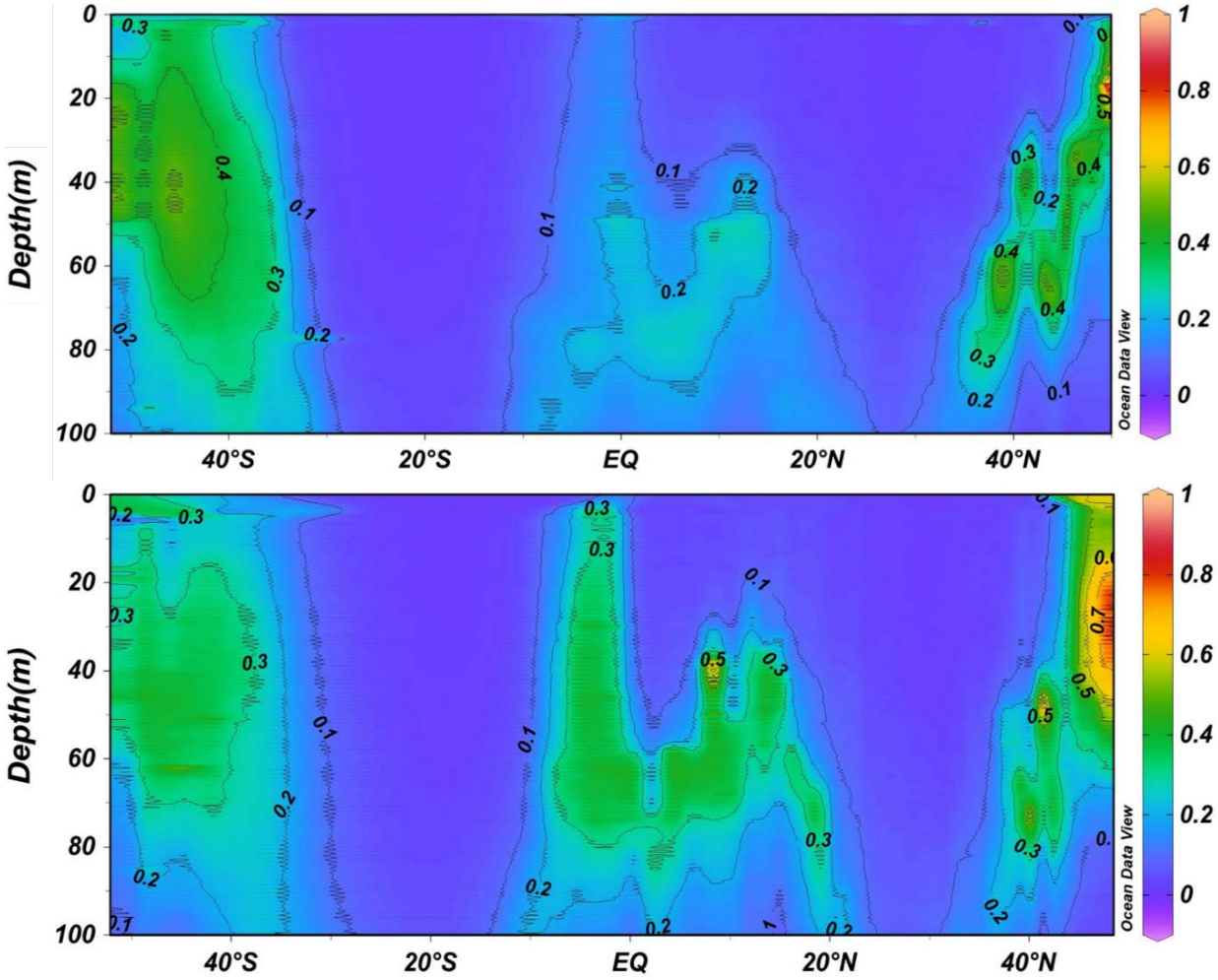

Figure 3.2. Latitudinal cross section of chlorophyll (mg m^{-3}) in the Atlantic Ocean. The data are derived from a fluorescence sensor fitted on the CTD rosette on AMT24 (top) and AMT25 (bottom).

Chlorophyll concentrations in the upper 100 m of the water column averaged 0.049 ± 0.084 mg m^{-3} (range: 0.00 - 1.08 mg m^{-3}) on AMT24 and 0.046 ± 0.079 mg m^{-3} (range: 0.00 - 0.93 mg m^{-3}) on AMT25. However, the chlorophyll concentration was not constant with depth and the chlorophyll maximum was more intense during AMT25 in the Northern latitudes (Figure 3.2).

Chlorophyll maxima occurred around 40°N and 40°S with a shallow euphotic zone (~ 65 m) and in the tropics between 20°N and 10°S where the average of euphotic zone depth was ~75 m. Chlorophyll reached a maximum ~ 0.7 mg m^{-3} at about 30 m depth north of 40°N on AMT25 compared to lower chlorophyll concentrations (~ 0.4 mg m^{-3}) on AMT24. The concentration of chlorophyll was about 0.3 mg m^{-3} south of 40°S on both transects (Figure 3.2). In the tropical region, chlorophyll was more uniform with depth, ~ 0.2 mg m^{-3} and ~ 0.3 mg m^{-3} on AMT24 and AMT25 respectively.

In the oligotrophic regions around 30°N and 20°S, chlorophyll was mostly undetectable or close to the detection limit on both cruises (Figure 3.2). The euphotic zone was deepened in these regions with ~ 100 m depth in the Northern Hemisphere and ~ 120 m depth in the Southern Hemisphere.

The overall distribution of primary productivity also corresponded to chlorophyll and phytoplankton distribution (see section 3.4). The average total primary productivity for depths ≤ 100 m was 0.48 ± 0.41 mg C $m^{-3}d^{-1}$, with a range of 0.02 - 1.70 mg C m^{-3} d^{-1} (Figure 3.3).

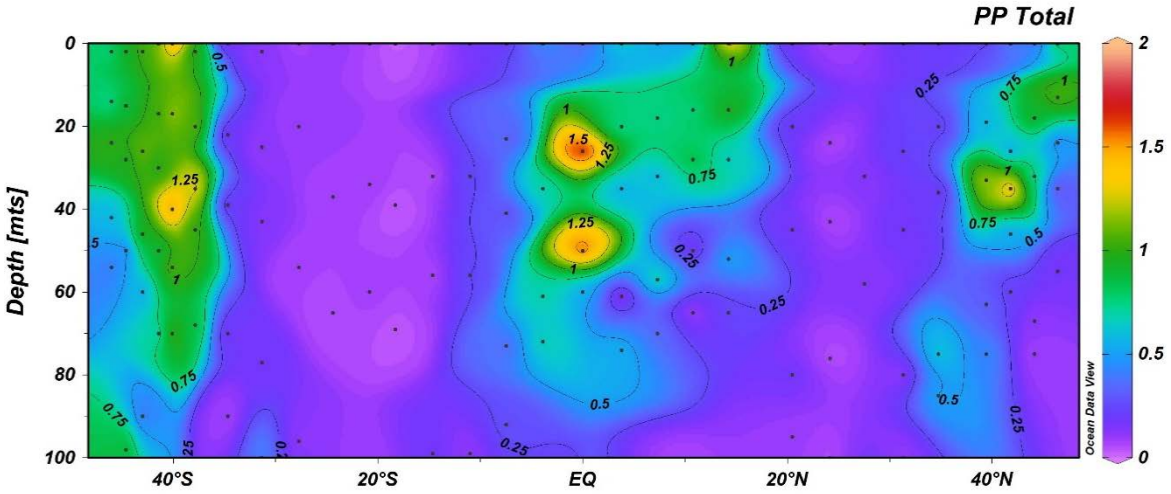

Figure 3.3. Total primary productivity (PP Total) (mg C m^{-3} d^{-1}) in the water column on AMT24 The data are available for AMT24 only. Black dots represent sampling locations.

Productive regions around 40°N with an average of 0.54 ± 0.39 mg C m^{-3} d^{-1} in a range of 0.08 - 1.47 mg C m^{-3} d^{-1} and 40°S with an average of 0.90 ± 0.30 mg C m^{-3} d^{-1} in a range of 0.39 - 1.56 mg C m^{-3} d^{-1} corresponded to chlorophyll maxima and were also associated with a phytoplankton bloom (high coccolithophores numbers) in the region (see section 3.4).

Another maximum in primary productivity was found around the equatorial region between 10°N and 10°S (0.57 ± 0.38 mg C m^{-3} d^{-1} in a range of 0.03 - 1.70 mg C m^{-3} d^{-1}) in association with nutrient-enriched upwelling waters.

Primary productivity minima were observed in the oligotrophic gyres of the Northern Hemisphere (between 30°N and 10°N) and the Southern Hemisphere (between 10°S and 38°S) corresponding to chlorophyll minima and a less abundant phytoplankton distribution (see section 3.4). Averages of 0.33 ± 0.36 mg C m^{-3} d^{-1} in a range of 0.04 - 1.40 mg C m^{-3} d^{-1} in the Northern gyre and 0.25 ± 0.33 mg C m^{-3} d^{-1} in a range of 0.02 - 1.29 mg C m^{-3} d^{-1} in the Southern gyre were observed.

3.3 Nutrient distributions in the Atlantic Ocean

Vertical nutrient distributions were broadly similar on both cruises (p > 0.05), with higher concentrations at high latitudes (i.e. north of 40°N and south of 40°S) and in the tropics between about 20°N and 10°S, mostly at depths shallower than 40m. The most abundant nutrients were

silicate (ranged between 0.07 and 49.71 µM) and nitrate + nitrite (up to ~ 34.54 µM), phosphate (range from 0.01 to 2.38 µM) and nitrite (maximum of 0.37 µM) being lower (Figure 3.4).

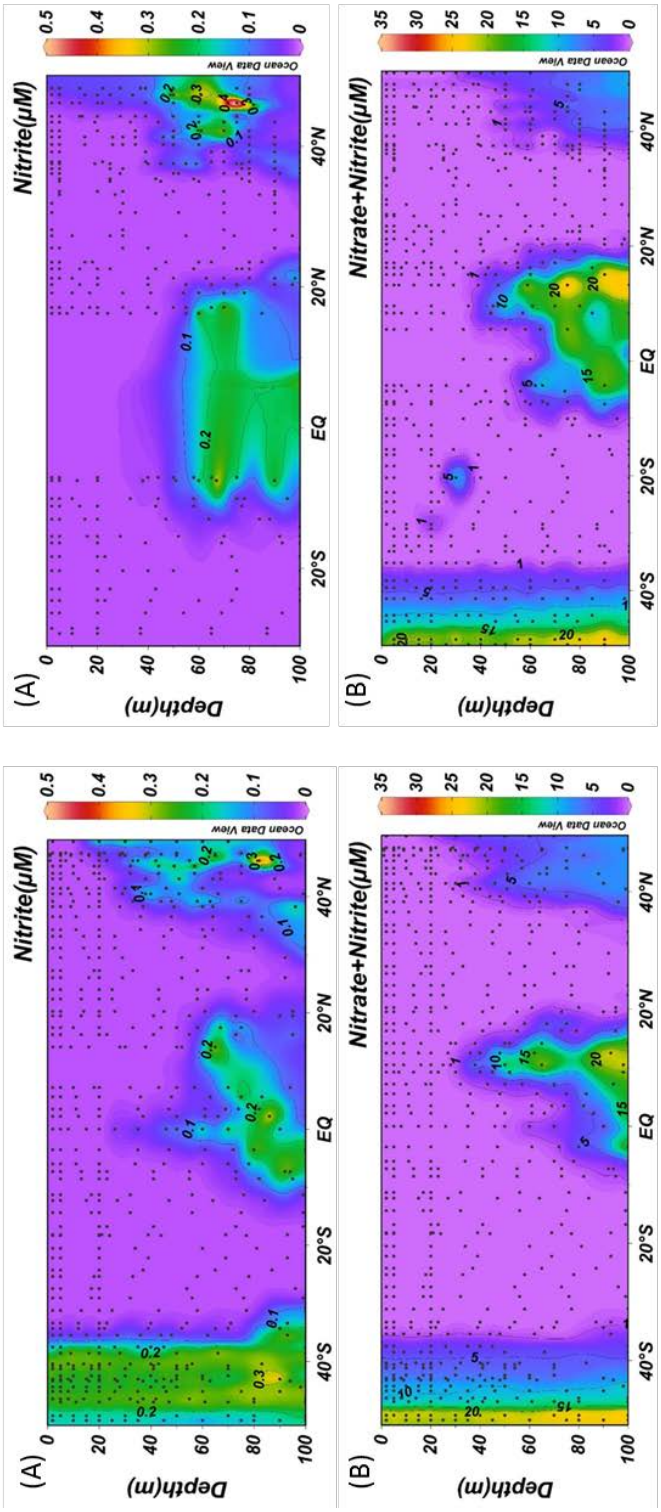

Figure 3.4. Contour plots of nutrient distribution in the Atlantic Ocean. Nitrite (A), nitrate + nitrite (B), phosphate (C) and silicate (D) in the top 100m depth. Data derived from AMT24 (left) and AMT25 (right). Black dots represent sampling stations. For the better resolution the scales bars are different.

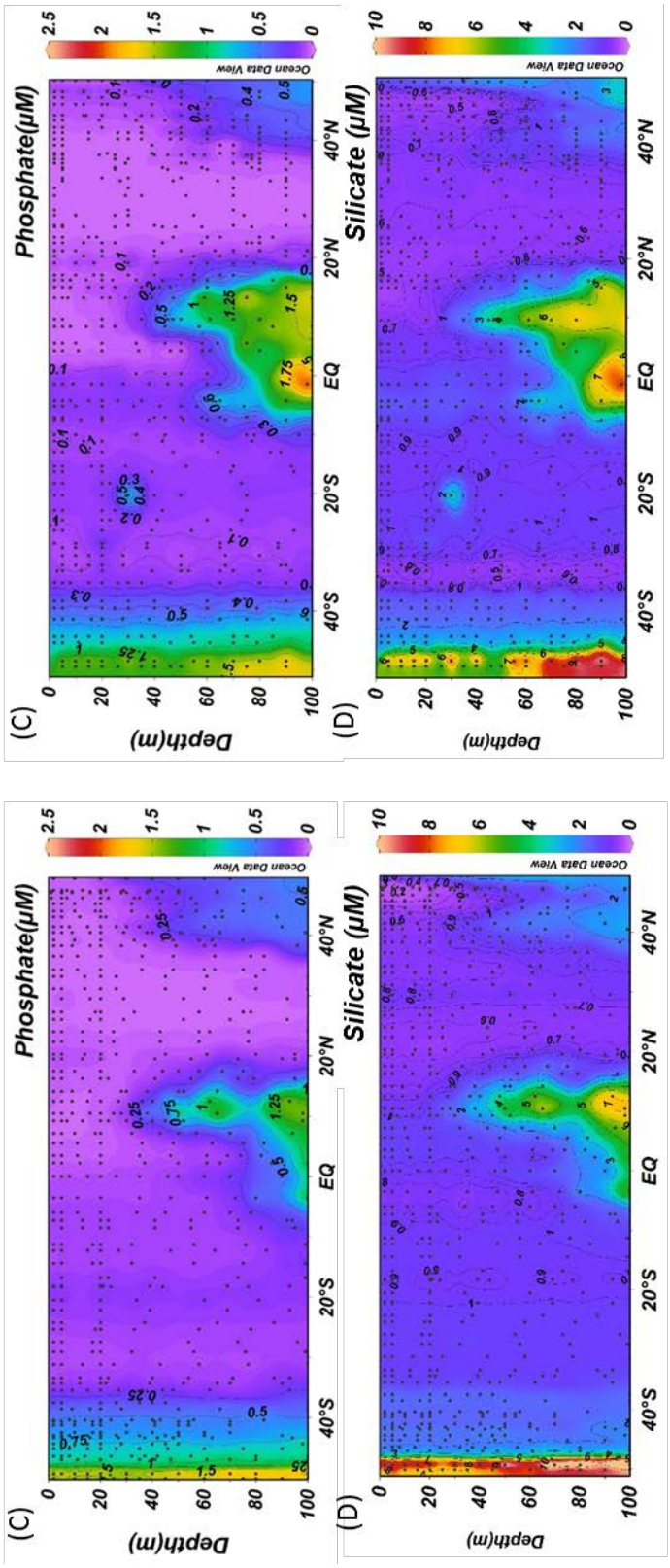

Figure 3.4. (continued) Contour plots of nutrient distribution in the Atlantic Ocean. Nitrite (A), nitrate + nitrite (B), phosphate (C) and silicate (D) in the top 100m depth. Data derived from AMT24 (left) and AMT25 (right). Black dots represent sampling stations. For the better resolution the scales bars are different.

Surface temperate waters in the Northern Hemisphere were characterized by low concentrations of nutrients. However, below the nutricline at about 40 m depth, nutrient concentrations were higher (Figure 3.4).

In the northern and southern Atlantic gyre (i.e. NAG and SAG), NO_2^- and NO_3^- were almost fully depleted. PO_4^{3-} showed a similar pattern in the northern gyre but slightly higher concentrations (~ 0.2 µM) in the southern gyre. SiO_4^{2-} concentrations were also low in the gyres: ~ 0.6µM in the northern gyre and ~ 0.9 µM in the southern gyre (Figure 3.4).

In the upwelling region between 20°N and 10°S nutrients followed almost the same pattern between the surface and ~50 m depth (nutricline), with low concentrations of SiO_4^{2-} and PO_4^{3-} and undetectable levels of NO_2^- (Figure 3.4). The enhancement of nutrients within the water column in this region might be evidence of the equatorial upwelling.

At high southern latitudes (i.e. south of 40°S), nutrient distribution in top 100 m was more homogenous (Figure 3.4). SiO_4^{2-} concentration ranged between 4 and 10 µM, there was < 2 µM of PO_4^{3-} and ~ 0.2 µM of NO_2^-, but the latter was observed only on AMT24 (Figure 3.4).

3.4 Phytoplankton abundances in the Atlantic Ocean

In general, phytoplankton community structure and abundance varied latitudinally and with depth, with the highest phytoplankton occurences at high latitudes, in northern and southern hemisphere temperate waters, and in sub surface waters in tropical and equatorial upwelling regions around deep chlorophyll maxima (i.e. ~ 60 – 80m depth), reflecting similar distributions of nutrients (see section 3.3).

The dominant phytoplankton size classes in the Atlantic Ocean are picophytoplankton (0.2 – 2.0 µm) and nanoplankton (2.0 – 20 µm) (Zubkov *et al.*, 2000b; Teira *et al.*, 2005).

In the oligotrophic regions with low nutrient availability between 35°N and 35°S, the phytoplankton was dominated by picophytoplankton whereas in the mesotrophic zone with moderate nutrients north of 35°N and south of 35°S, nanoeukaryotes including cryptophytes were abundant in this study, in agreement with Aiken *et al*. (2009).

Major picoplankton species included autotrophic cyanobacteria such as *Prochlorococcus* sp. and *Synechococcus* sp. and also heterotrophic bacteria (Sieburth, 1979; Zubkov *et al.*, 2000b; Tarran *et al.*, 2006) (Figure 3.5).

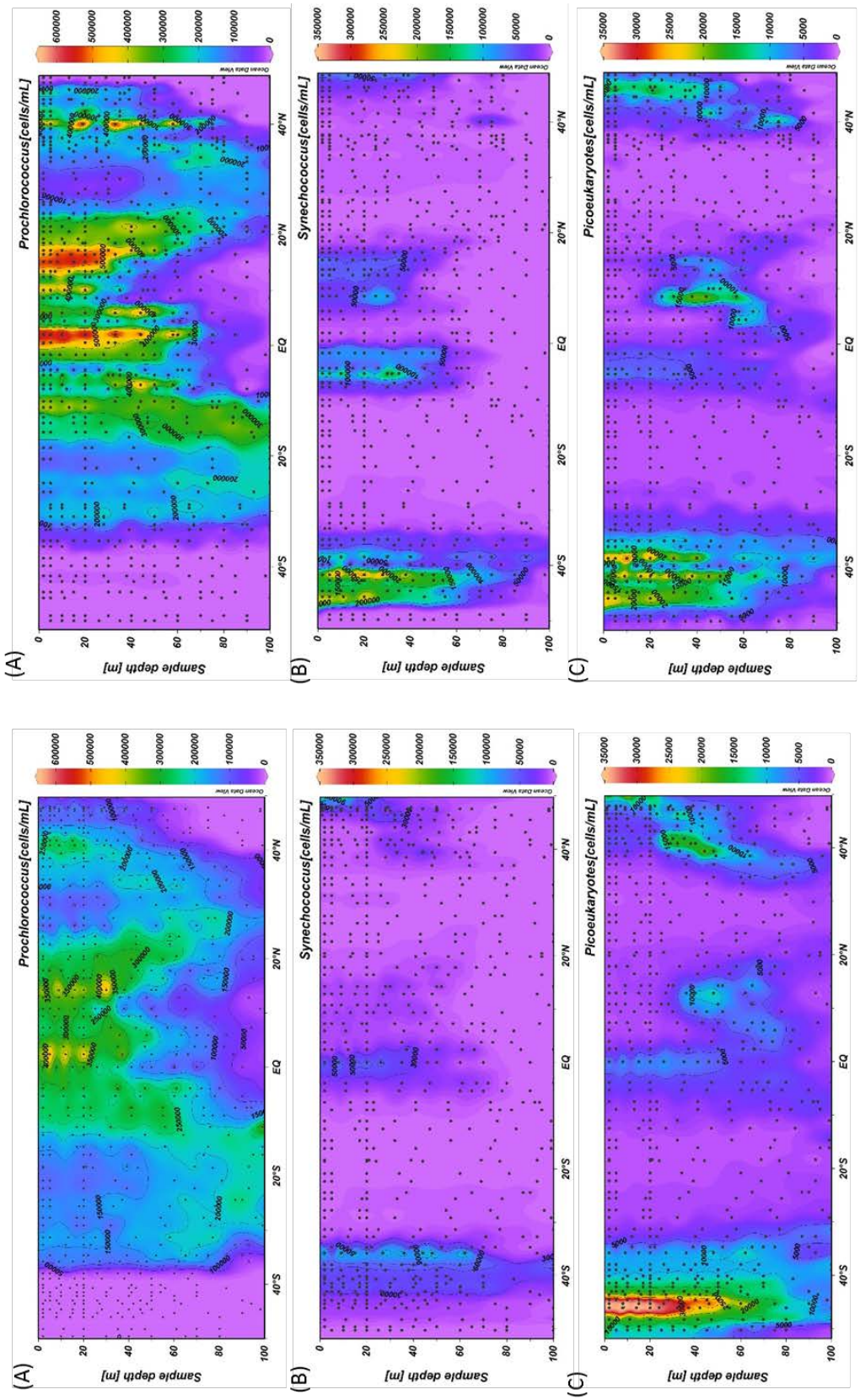

Figure 3.5. Contour plots of phytoplankton distributions in the Atlantic Ocean. Distribution of prochlorococcus (A), synechococcus (B), picoeukaryotes (C), cocolithophores (D), cryptophytes (E) and nanoeukaryotes (F) in the top 100 m depth. Data derived from AMT24 (left) and AMT25 (right). Black dots represent sampling stations.

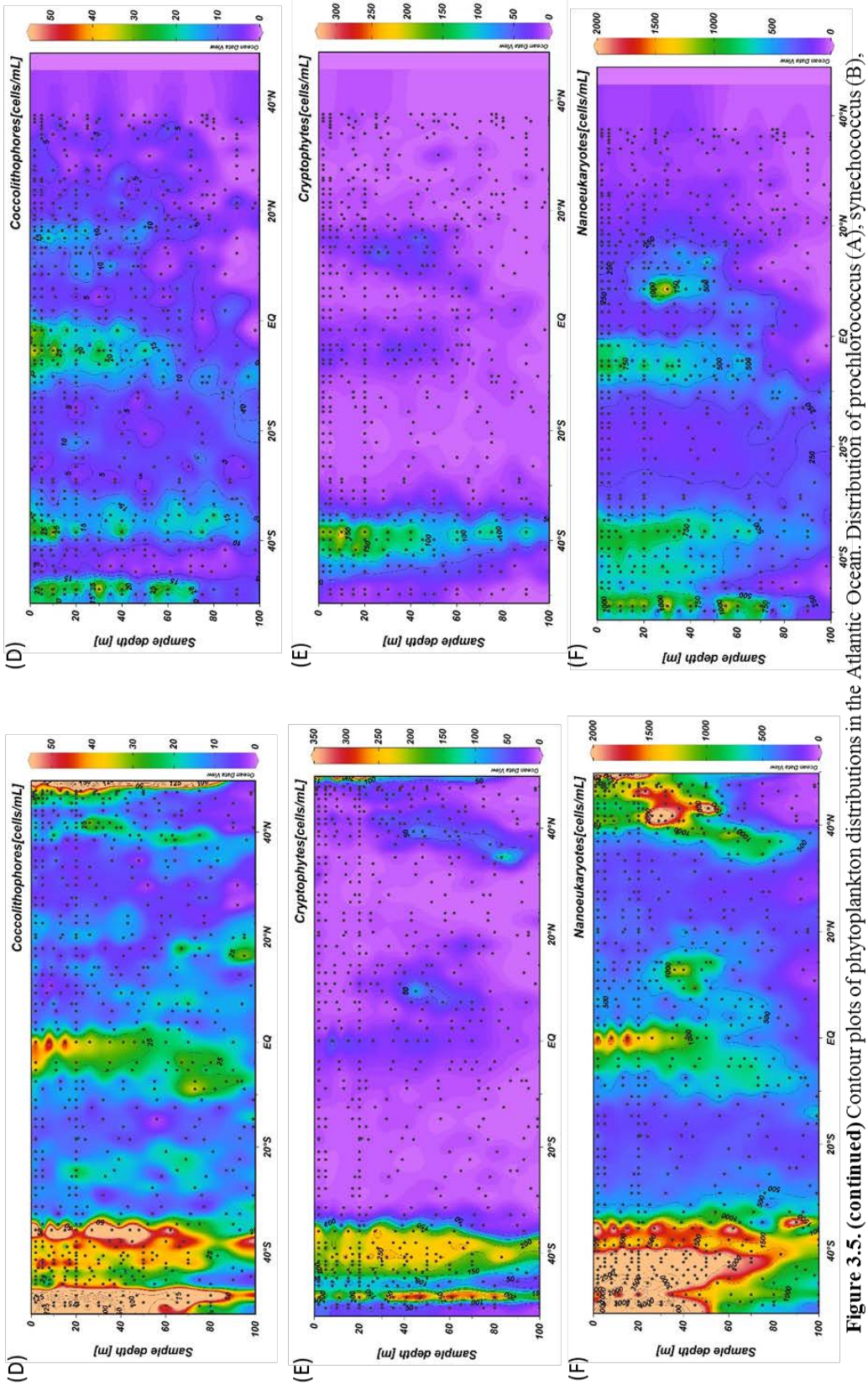

Figure 3.5. (continued) Contour plots of phytoplankton distributions in the Atlantic Ocean. Distribution of prochlorococcus (A), synechococcus (B), picoeukaryotes (C), cocolithophores (D), cryptophytes (E) and nanoeukaryotes (F) in the top 100 m depth. Data derived from AMT24 (left) and AMT25 (right). Black dots represent sampling stations.

Prochlorococcus was the most abundant picoplankton species throughout the water column on both transects between ~50°N and ~ 38°S, including the northern and southern gyres. *Prochlorococcus* dominated the oligotrophic gyres (NAST and SATL; average of 150,000 cells ml^{-1}) characterised by low nutrient availability (see section 3.3) and temperatures below 20°C.

It has been suggested that the latitudinal distribution of *Prochlorococcus* is temperature dependent and that low temperatures (14 - 17°C) limit its distribution (Olson *et al.*, 1990). However, although *Prochlorococcus* were absent south of 38°S where the surface water temperature decreased to ~14°C they were detected down to 60m at 47°N where the temperature was ~ 16°C (Figure 3.5; see also section 2.8). High *Prochlorococcus* abundance in oligotrophic waters implies that their growth is not substantially nutrient dependent. It was pointed out earlier that *Synechococcus* and picoeukaryote abundances might be more strongly controlled by nutrient availability than *Prochlorococcus* (Vaulot *et al.*, 1995). Maximal *Prochlorococcus* cell numbers (600,000 cells ml^{-1}) were found above 60 m depth in the equatorial region between 20°N and the equator. This distribution presumably reflects the influence of the subsurface equatorial current that transports nutrient-enriched waters from deep water towards the surface (Zubkov *et al.*, 2000b). However, their distribution is more uniform in the euphotic zones of oligotrophic waters compared to the equatorial region (Figure 3.5).

Synechococcus was found in very low abundance over the full extent of both transects. The highest concentration of *Synechococcus* was found in the West African (Mauritanian) upwelling mainly on AMT25 (Figure 3.5). *Synechococcus* was absent in the Atlantic gyres but was more abundant at high latitudes temperate waters (i.e. the northern and southern end of transects) with temperature < 10°C (Olson *et al.*, 1988; Olson *et al.*, 1990; Campbell and Vaulot, 1993) and higher nutrient concentrations. It has been suggested that *Synechococcus* has a greater nutrient dependence than does *Prochlorococcus* and it has been observed that the abundance of *Synechococcus* generally increases around 40 – 80m depth in the equatorial region where nutrient-enriched water is transported to the surface (Zubkov *et al.*, 2000b).

Picoeukaryotes were less abundant on both cruises, with the highest cell numbers of ~ 30,000 cells ml^{-1} at the northern and the southern ends of the transects throughout the water column and in between ~ 20 m and ~ 80 m in the equatorial regions (Figure 3.5).

Higher phytoplankton abundances are reported for areas with relatively shallow pycnoclines and nitraclines (rate of maximum change in NO_3^- with depth), such as in northern and southern

temperate waters, whereas in the Atlantic oligotrophic gyres with a deeper nitracline (> 90 m), phytoplankton are less abundant (Heywood *et al.*, 2006; Tarran *et al.*, 2006).

In southern hemisphere temperate waters, phytoplankton distributions were vertically extended because of greater water column mixing as compared to more stratified waters in the same latitudes of the Northern Hemisphere. Also, water stratification in the Northern Hemisphere during the late boreal summer caused the phytoplankton to be mostly distributed below the surface, as also found earlier (Tarran *et al.*, 2006).

The least abundant eukaryotic phytoplankton are coccolithophores, which are often undetectable by flow cytometry (Tarran *et al.*, 2006). Maxima of only about 300 cells ml^{-1} were found at the northern and southern end of the transects. Coccolithophores also showed a maximum on AMT24 north of 40°N, at around 20 m depth, which coincided with a peak in chlorophyll (see section 3.2).

Picoeukaryotes also showed the highest concentrations in the same area as *Synechococcus* (i.e. temperate water at either end of transect and at 40 – 80 m depth in the equatorial region) although they were much less numerous than *Prochlorococcus* and *Synechococcus*. In general, high numbers of picoeukaryotes coincided with *Synechococcus* between 30°S and 50°S and an absence of *Prochlorococcus*.

In the Southern Hemisphere, picoeukaryotes disappeared completely in the oligotrophic waters of the SAG but rose again from nearly 30°S to the Falkland Islands shelf, suggestive of a nutrient dependent species (Figure 3.5).

Overall, different picoplankton communities were observed between mesotrophic[7] waters in temperate regions where *Synechococcus* and picoeukaryotes dominated, compared to the northern and southern oligotrophic waters where *Prochlorococcus* were particularly abundant, while concentrations of both *Synechococcus* and picoeukaryotes were much lower, as also found earlier (Zubkov *et al.*, 2000b).

From temperate to subtropical zones, seasonal stratification persists in autumn, associated with a shallow mixed layer (~ 50m) with the presence of phytoplankton in the thermocline. However, in tropical waters, a permanently stratified water column on either side of the equator is

[7] Mesotrophic waters with the moderate trophic state contain more dissolved nutrients than the oligotrophic waters but less than eutrophic waters.

associated with a deep mixed layer and very low chlorophyll (~ 0.05 mg m^{-3}) (Aiken *et al.*, 2000).

The depth-integrated biomass of heterotrophic bacteria previously showed similarity with picophytoplankton abundances at all latitudes in the Atlantic Ocean while they were most dominant in the temperate and equatorial waters and least abundant in the Atlantic oligotrophic gyres (Robinson *et al.*, 2006).

Although no data are available for heterotrophic bacterial distributions for this study it has been suggested that the maximal occurrence of DOM-dependent heterotrophic bacteria is in the productive regions of temperate waters at the northern end of the transects, in upwelling regions and in the frontal system between the Brazil and Falkland currents at the southern end of the transects, as previously reported along AMT transects at the same time of year (Zubkov *et al.*, 1998). In oligotrophic regions such as Atlantic northern and southern gyres, by comparison, the distribution of heterotrophic bacteria is limited by the growth of *Prochlorococcus* and their limited excretion of DOM (Zubkov *et al.*, 1998). Also, heterotrophic bacterial numbers and biomass maxima are observed in temperate and equatorial waters and shift southwards in April-May (Zubkov *et al.*, 2000a). Zubkov *et al.* (2000a) also concluded that heterotrophic nanoplankton control the growth of heterotrophic bacteria by consuming their total daily production throughout the Atlantic Ocean.

3.5 CDOM distributions in the Atlantic Ocean

The distributions of CDOM and its optical properties (i.e. spectral slopes and slope ratios) (see section 2.5.6) in the SML and the water column show some distinct and contrasting features (Figure 3.6). The figure shows a small subset of the actual data (i.e. 42 profiles, see section 4.2.4). The purpose of figure 3.6 is to illustrate the consistent contrast between the SML and SSW for CDOM properties that warrants the SML being discussed separately.

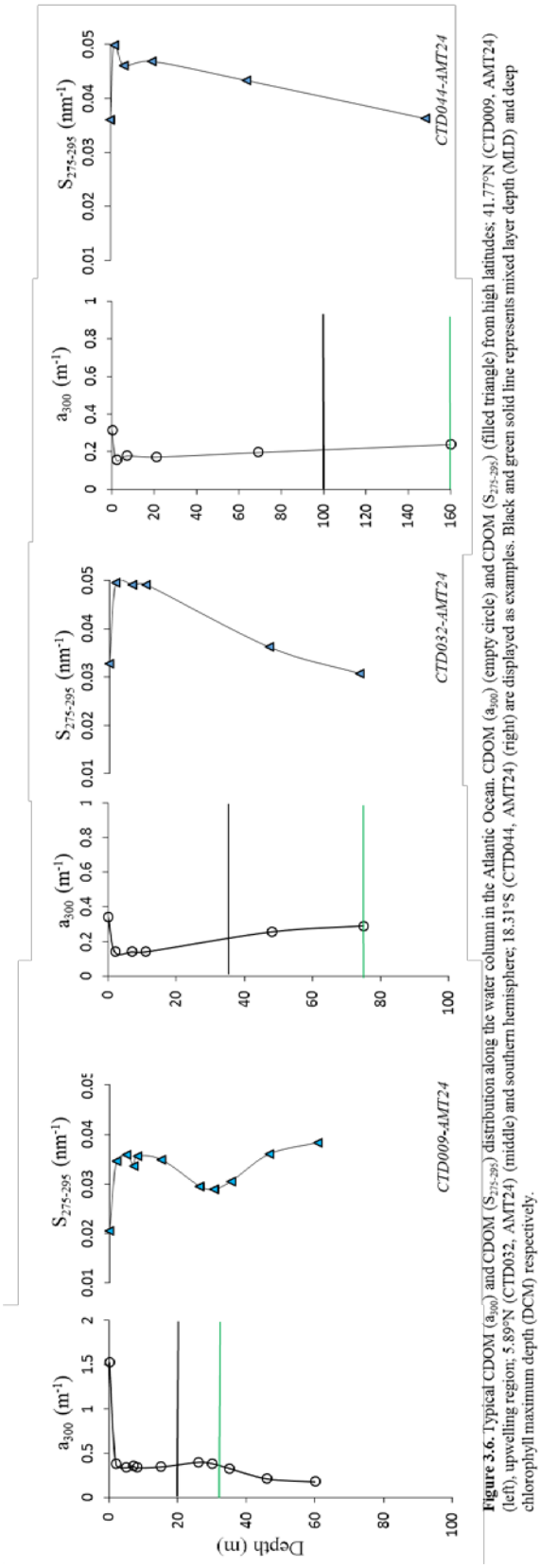

Figure 3.6. Typical CDOM (a_{300}) and CDOM ($S_{275-295}$) distribution along the water column in the Atlantic Ocean. CDOM (a_{300}) (empty circle) and CDOM ($S_{275-295}$) (filled triangle) from high latitudes; 41.77°N (CTD009, AMT24) (left), upwelling region; 5.89°N (CTD032, AMT24) (middle) and southern hemisphere; 18.31°S (CTD044, AMT24) (right) are displayed as examples. Black and green solid line represents mixed layer depth (MLD) and deep chlorophyll maximum depth (DCM) respectively.

In general, CDOM (a_{300}) was higher in the SML compared to the underlying waters with statistically significant difference observed at high latitudes ($p < 0.05$) in contrast to $S_{275-295}$ which is lower in the SML relative to the underlying waters. Moreover, CDOM (a_{300}) and $S_{275-295}$ did not show any changes in the mixed layer or deep chlorophyll maximum[8] (DCM) in the water column. So, based on these results, it is concluded that the distinct pattern of high CDOM-low spectral slope SML relative to the underlying water exists and these contrasts might apply to the whole data set in the Atlantic Ocean.

Data were therefore grouped into two categories for subsequent discussion: (a) samples in the SML and (b) samples from the water column (depth ≤ 100m).

3.5.1 *The latitudinal distribution of CDOM and its optical properties in the SML*

The mean, standard deviation and range of CDOM spectral parameters in the SML over the full extent of the two transects (i.e. AMT24 and AMT25) with respect to their oceanographic provinces is represented in Table 3.1.

[8] A deep chlorophyll maximum depth (DCM) is a sub-surface depth in which the concentration of chlorophyll is maximum in the oceans.

Table 3.1. The mean, standard deviation and range of CDOM optical properties within the SML in the Atlantic Ocean CDOM (a_{300}), $S_{275-295}$, $S_{350-400}$ and S_R on AMT24 (A) and AMT25 (B) with respect to oceanographic provinces are represented. The 8 provinces are: European Continental Shelf Water (ECSW, 50-48°N), North Atlantic Drift Region (NADR, 48-42°N), North Atlantic Subtropical (NAST, 42-25°N), North Atlantic Tropical (NATR, 25-10°N), Western and Eastern Tropical Atlantic (W/ETRA, 10°N-5°S), South Atlantic Gyre (SATL, 5-42°S), South Subtropical Convergence Zone (SSTC, 42-45°S) and Southwest Atlantic Shelfs or Falkland Islands (FKLD, 45-50°S). Sample numbers are indicated. NA represents 'not applicable'.

(A)

Provinces	Sample No.	(a_{300}) (m^{-1})	$S_{275-295}$ (nm^{-1})	$S_{350-400}$ (nm^{-1})	S_R
***ECSW* (50-48°N)**	1	1.04 ± 0.00 (NA)	0.020 ± 0.000 (NA)	0.017 ± 0.000 (NA)	1.19 ± 0.000 (NA)
***NADR* (48-42°N)**	7	0.87 ± 0.27 (0.59-1.42)	0.025 ± 0.002 (0.022-0.028)	0.017 ± 0.001 (0.015-0.020)	1.45 ± 0.23 (1.19-1.77)
***NAST* (42-25°N)**	11	0.52 ± 0.03 (0.16-1.52)	0.030 ± 0.006 (0.020-0.043)	0.014 ± 0.006 (0.000-0.025)	1.86 ± 0.49 (1.17-2.65)
***NATR* (25-10°N)**	9	0.58 ± 0.02 (0.24-1.15)	0.027 ± 0.008 (0.008-0.038)	0.030 ± 0.012 (0.015-0.055)	1.07 ± 0.44 (0.15-1.71)
***(W)TRA* (10°N-5°S)**	6	0.38 ± 0.03 (0.33-0.43)	0.032 ± 0.000 (0.031-0.033)	0.021 ± 0.006 (0.017-0.035)	1.59 ± 0.35 (0.92-1.87)
***SATL* (5-42°S)**	23	0.35 ± 0.13 (0.22-0.82)	0.033 ± 0.004 (0.023-0.042)	0.019 ± 0.009 (0.011-0.054)	1.90 ± 0.56 (0.72-2.70)
***SSTC* (42-45°S)**	5	0.34 ± 0.01 (0.32-0.36)	0.030 ± 0.001 (0.028-0.032)	0.022 ± 0.001 (0.013-0.039)	1.58 ± 0.57 (0.77-2.19)
***FKLD* (48-50°S)**	2	0.34 ± 0.02 (0.32-0.36)	0.025 ± 0.001 (0.025-0.026)	0.014 ± 0.002 (0.012-0.016)	1.81 ± 0.27 (1.61-2.00)

Table 3.1. (continued) The mean, standard deviation and range of CDOM optical properties within the SML in the Atlantic Ocean CDOM (a_{300}), $S_{275-295}$, $S_{350-400}$ and S_R on AMT24 (A) and AMT25 (B) with respect to oceanographic provinces are represented. The 8 provinces are: European Continental Shelf Water (ECSW, 50-48°N), North Atlantic Drift Region (NADR, 48-42°N), North Atlantic Subtropical (NAST, 42-25°N), North Atlantic Tropical (NATR, 25-10°N), Western and Eastern Tropical Atlantic (W/ETRA, 10°N-5°S), South Atlantic Gyre (SATL, 5-42°S), South Subtropical Convergence Zone (SSTC, 42-45°S) and Southwest Atlantic Shelfs or Falkland Islands (FKLD, 45-50°S). Sample numbers are indicated. NA represents 'not applicable'.

(B)

Provinces - n	Sample No.	(a_{300}) (m^{-1})	$S_{275-295}$(nm^{-1})	$S_{350-400}$(nm^{-1})	S_R
***ECSW* (50-48°N)**	1	0.64 ± 0.00 (NA)	0.026 ± 0.000 (NA)	0.018 ± 0.000 (NA)	1.49 ± 0.000 (NA)
***NADR* (48-42°N)**	4	0.62 ± 0.11 (0.55-0.79)	0.028 ± 0.003 (0.024-0.031)	0.017 ± 0.000 (0.017-0.018)	1.61 ± 0.18 (1.36-1.76)
***NAST* (42-25°N)**	16	0.30 ± 0.01 (0.24-0.68)	0.037 ± 0.004 (0.028-0.040)	0.017 ± 0.001 (0.014-0.021)	2.17 ± 0.40 (1.70-3.09)
***NATR* (25-10°N)**	9	0.40 ± 0.04 (0.33-0.49)	0.037 ± 0.002 (0.033-0.040)	0.023 ± 0.006 (0.016-0.032)	1.72 ± 0.43 (1.03-2.22)
***(E)TRA* (10°N-5°S)**	4	0.42 ± 0.01 (0.31-0.58)	0.036 ± 0.003 (0.033-0.041)	0.018 ± 0.002 (0.016-0.021)	2.02 ± 0.36 (1.54-2.34)
***SATL* (5-42°S)**	13	0.37 ± 0.15 (0.26-0.82)	0.037 ± 0.005 (0.023-0.043)	0.015 ± 0.002 (0.011-0.018)	2.56 ± 0.65 (1.56-3.60)
***SSTC* (42-45°S)**	2	0.32 ± 0.08 (0.26-0.38)	0.033 ± 0.000 (0.032-0.033)	0.017 ± 0.000 (0.017-0.017)	1.93 ± 0.04 (1.90-1.96)

The total average CDOM (a_{300}) in the SML was 0.45 ± 0.23 m^{-1} and ranged from 0.16 to 1.52 m^{-1}. Results were statistically similar between AMT24 (average of 0.47 ± 0.28 m^{-1}) and AMT25 (average of 0.41 ± 0.13 m^{-1}) (Two Sample t-test, testing H_0: the two means are equal against H_A: at least one mean is different; As μ1 - μ2 = 0.0617, $t_{95\%\ CI\ (2)\ 101}$ = 1.53, H_0 is accepted [p = 0.128]). CDOM (a_{300}) varied between 0.16 – 1.52 m^{-1} over both transects (Figure 3.7).

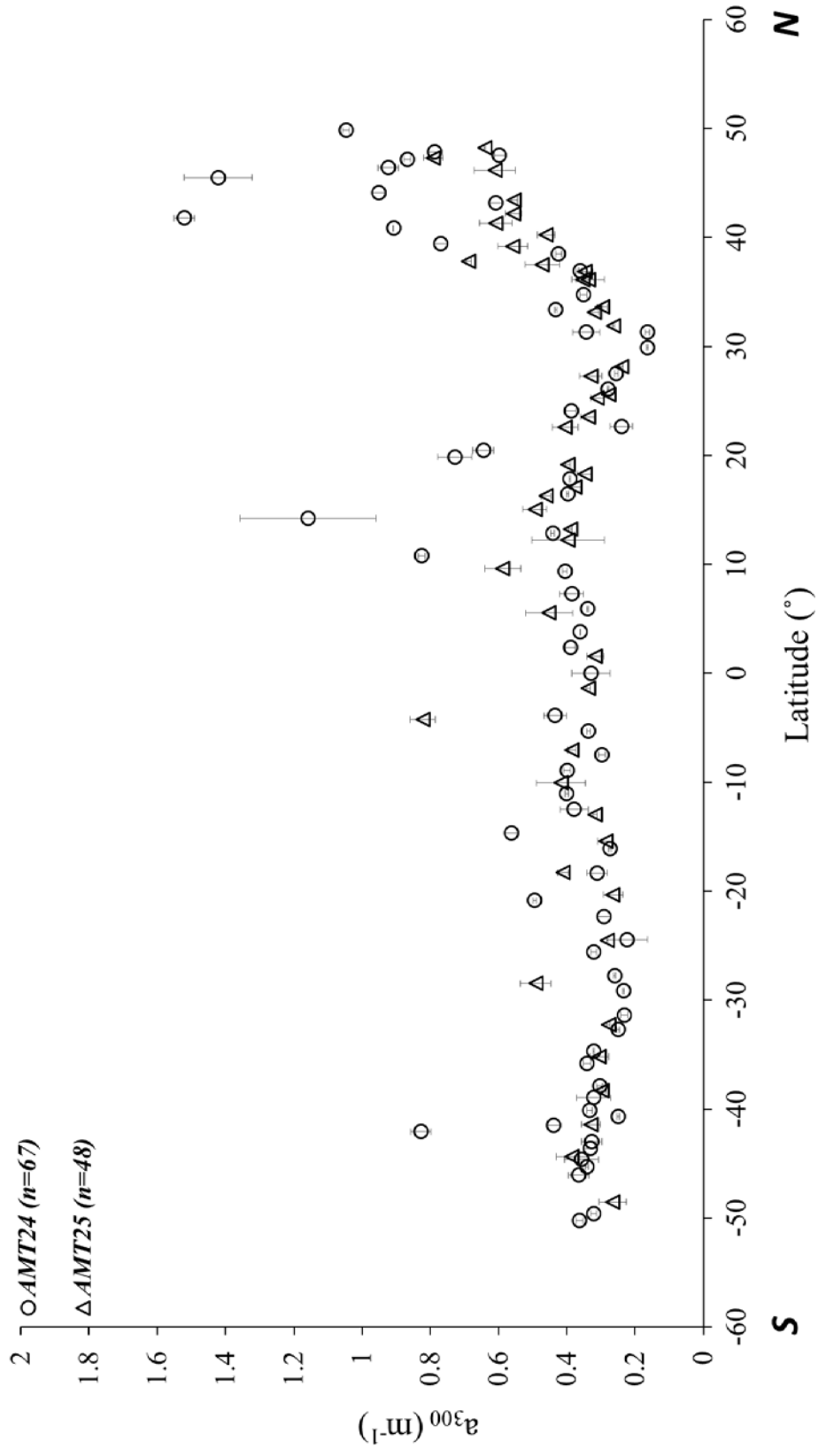

Figure 3.7. Latitudinal distribution of CDOM (a_{300}) in the SML on AMT24 (circle) and AMT25 (triangle) Error bars represent the standard deviation of the mean for each sample. Sample numbers (n) are also indicated. Southern latitudes are represented by negative values.

The most notable features of the data common to both transects within the SML, were distinct CDOM (a_{300}) maxima between 50°N and 40°N (ECSW and NADR), on AMT24 (0.96 ± 0.30 m^{-1}) and AMT25 (0.60 ± 0.10 m^{-1}). There were also small CDOM (a_{300}) maxima between 20°N and 10°N in the tropics (NATR) on AMT24 (0.65 ± 0.27 m^{-1}) and AMT25 (0.40 ± 0.05 m^{-1}).

CDOM (a_{300}) decreased significantly to almost a half (0.44 ± 0.27 m^{-1}) of its values at higher latitudes towards NAST, indicating a transition to low CDOM waters of the oligotrophic NAG during both cruises (Two-Sample t-test, testing H_0: the two means are equal against H_A: at least one mean is different; As μ1 - μ2 = 0.3520 and 0.2434, $t_{95\%\ CI\ (2)\ 16\ and\ 18}$ = 2.04 and 3.36, H_0 is rejected [p = 0.04 and 0.004] for AMT24 and AMT25 respectively).

CDOM (a_{300}) increased again into the productive and nutrient-enriched tropical regions (NATR; 25-10°N) on both cruises (see Table 3.1).

While Figure 3 shows a few isolated high CDOM (a_{300}) values, due to the stringent precautions taken to exclude contamination during sampling, it is most likely that these are real values.

Mann (2010) also observed high surface CDOM (a_{280}) distributions (1.0 - 1.1 m^{-1}) at 50°N on the UK shelf during AMT18 (Oct – Nov. 2008), although these samples were not from the SML. He also observed a reduction in surface CDOM to less than 0.45 m^{-1} towards the northern and the southern Atlantic gyres during AMT18. High concentrations of CDOM (a_{280}) around 10°N and 10°S (ranged from 0.55 to 0.65 m^{-1}) at 100 – 130 m depth were also reported (Mann, 2010).

In agreement with the present results, Nelson *et al*. (2007) also reported the lowest surface CDOM (a_{325}) (< 0.1 m^{-1}) values in the central Atlantic subtropical gyre due to CDOM photodegradation and high CDOM absorption measurements (up to ~ 0.7 m^{-1}) in the coastal areas of the North Atlantic influenced by the terrestrial inputs.

In concurrence, Siegel *et al*. (2002) found the CDOM absorption coefficient (a_{440}) of total CDOM and detrital material to be maximal at high latitude polar waters of the Northern Hemisphere using satellite ocean colour data. Absorption decreased significantly towards the oligotrophic gyres but local absorption maxima were also reported in equatorial upwelling regions of the global oceans (Siegel *et al.*, 2002).

On both cruises CDOM (a_{300}) in the Southern Hemisphere SML was lower than in the Northern Hemisphere SML, but with a significant difference observed only on AMT24 (Two-Sample t-test, testing H_0: the two means are equal against H_A: at least one mean is different; As $\mu 1 - \mu 2 = 0.2373$, $t_{95\%\ CI\ (2)\ 42} = 3.86$, H_0 is rejected [$p = 0.000$]). Averages of Northern Hemisphere CDOM (a_{300}) were 0.58 ± 0.34 m^{-1} on AMT24 and 0.43 ± 0.13 m^{-1} on AMT25, compared to the Southern Hemisphere CDOM (a_{300}) averages of 0.35 ± 0.11 m^{-1} on AMT24 and 0.36 ± 0.13 m^{-1} on AMT25.

The Southern Hemisphere biogeochemical provinces SATL (5 - 42°S), SSTC (42 - 45°S) and FKLD (48 - 50°S) showed no significant differences in CDOM (a_{300}) on either cruise. Southern Hemisphere CDOM (a_{300}) was also not statistically different between the two cruises (Two-Sample t-test, testing H_0: the two means are equal against H_A: at least one mean is different; As $\mu 1 - \mu 2 = -0.0160$, $t_{95\%\ CI\ (2)\ 46} = -0.42$, H_0 is accepted [$p = 0.674$]).

Average $S_{275\text{-}295}$ was 0.030 ± 0.005 nm^{-1} (range 0.020 - 0.043 nm^{-1}) on AMT24 and 0.036 ± 0.004 nm^{-1} (range 0.023 - 0.044 nm^{-1}) on AMT25 (Figure 3.8).

Contrary to CDOM (a_{300}) values, the highest $S_{275\text{-}295}$ (nm^{-1}) values were encountered in the oligotrophic gyres (centered on 30°N and ~ 20°S) with an average of about 0.04 nm^{-1} whereas the lowest measured $S_{275\text{-}295}$ (< 0.03 nm^{-1}) were found north of 40°N and south of 40°S, statistically similar between the two cruises ($p > 0.05$) (Figure 3.8).

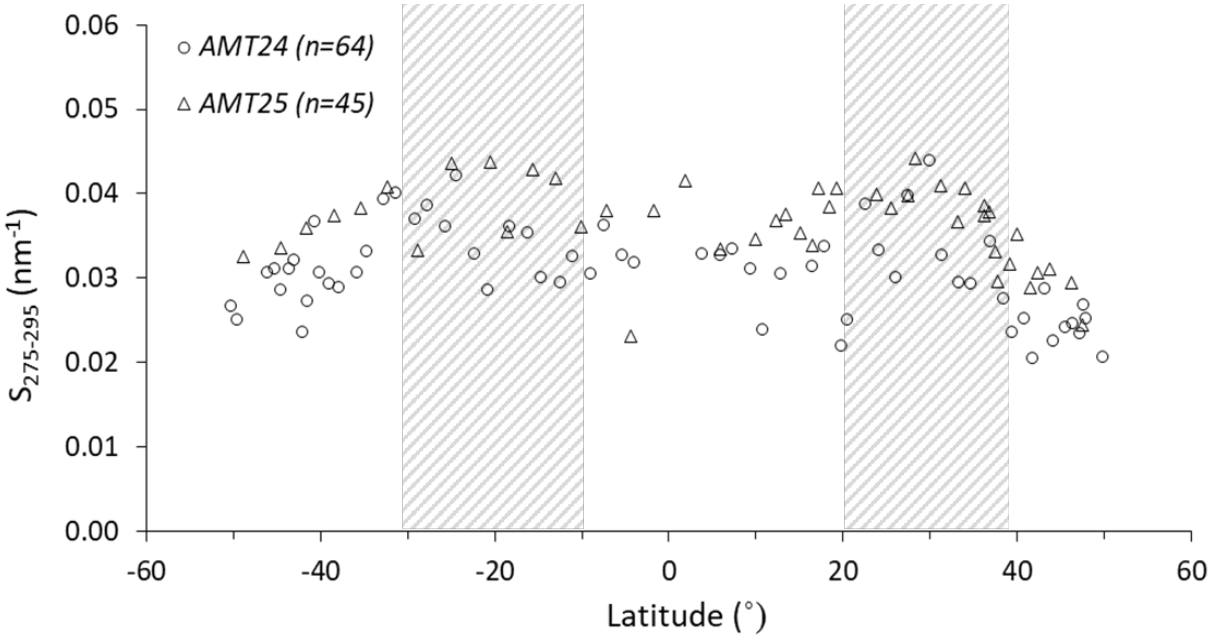

Figure 3.8. Latitudinal distributions of $S_{275-295}$ in the SML on AMT24 (circles) and AMT25 (triangles). The hatched regions indicate the northern and southern oligotrophic gyres with high $S_{275-295}$. Negative latitudes are south of the Equator.

Average $S_{275-295}$ (nm^{-1}) was higher in the Southern Hemisphere than in the Northern Hemisphere during both cruises but with a significant difference observed only on AMT24 (AMT24 Northern Hemisphere, 0.030 ± 0.006 nm^{-1} (n = 32); AMT24 Southern Hemisphere, 0.032 ± 0.004 nm^{-1} (n = 32, t-test, p = 0.04)); (AMT25 Northern Hemisphere, 0.036 ± 0.004 nm^{-1} (n = 33); AMT25 Southern Hemisphere, 0.037 ± 0.005 nm^{-1} (n = 16, t-test, p = 0.44)).

The highest average of $S_{350-400}$ (nm^{-1}) (see section 2.5.6) within the SML on both cruises was observed on NATR (AMT24; 0.030 ± 0.012 nm^{-1}, n = 9 in a range of 0.015 - 0.055 nm^{-1} and AMT25; 0.023 ± 0.006 nm^{-1}, n = 9 in a range of 0.016 - 0.032 nm^{-1}) (see Table 3.1).

A significant difference was also observed between $S_{350-400}$ in the oligotrophic NAST compared to more productive NATR, consistent on both cruises (AMT24; p = 0.003 and AMT25; p = 0.02). $S_{350-400}$ was similar (p > 0.05) between the remaining provinces on AMT24. However $S_{350-400}$ was significantly different between the equatorial region (i.e. WTRA) and the Southern Gyre (SATL) (p = 0.01) and also between SATL and SSTC (p = 0.004) on AMT25 (see Table 3.1).

The average of $S_{350-400}$ in the Northern Hemisphere was similar between the cruises (AMT24; 0.020 ± 0.009 nm^{-1} and AMT25; 0.019 ± 0.004 nm^{-1}), however, the average of Southern Hemisphere $S_{350-400}$ on AMT25 was lower than the average of the Southern Hemisphere S_{350-}

$_{400}$ on AMT24 (AMT24; 0.019 ± 0.008 nm^{-1} and AMT25; 0.015 ± 0.002 nm^{-1}) but the difference was not statistically significant ($p > 0.05$).

The total average of S_R in the SML (see section 2.5.6) was 1.65 ± 0.54 in a range of 0.15 - 2.70 and 2.11 ± 0.56 in a range of 1.03 - 3.60 (excluding the outliers) on AMT24 and AMT25 respectively (Table 3.1). The highest S_R (i.e. $S_R > 2$) was found in the oligotrophic regions of the NAST and the SATL. S_R in the SML was low with an average of < 1.5 around the European continental shelf (i.e. ECSW) on both transects (Table 3.1).

3.5.2 *CDOM enrichment factors (EF) in the Atlantic Ocean*

CDOM (a_{300}) in SSW was distributed similarly to CDOM (a_{300}) in the SML consistently between both transects (Figure 3.9).

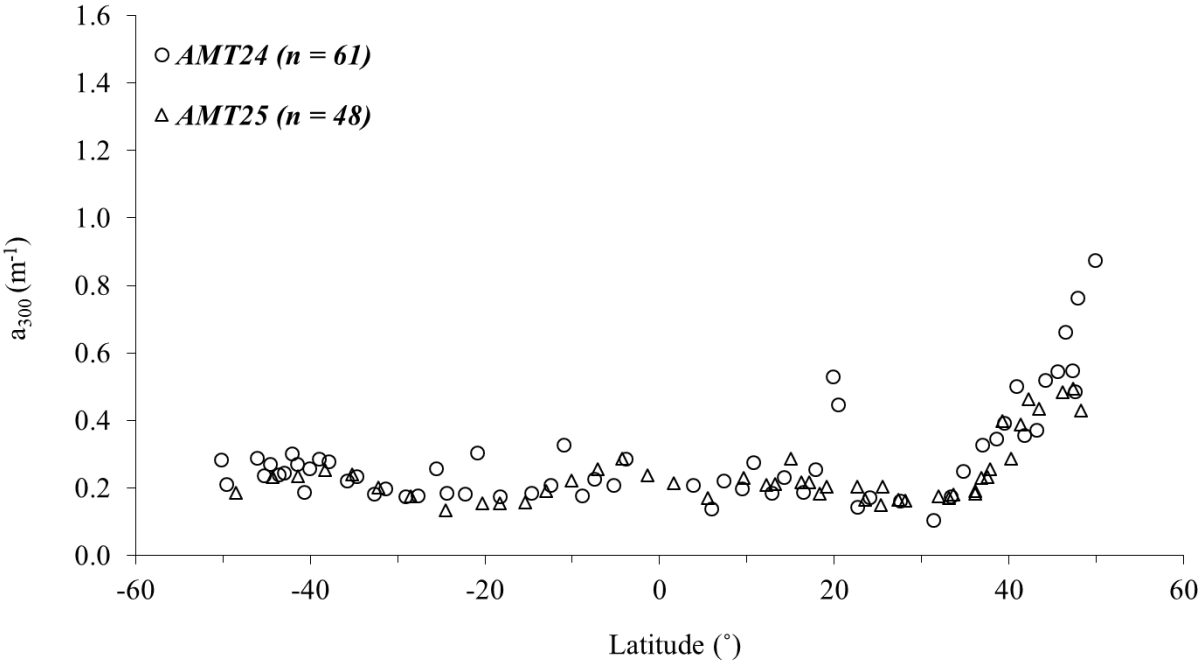

Figure 3.9. Latitudinal distribution of CDOM (a_{300}) in SSW (7m) on AMT24 (circles) and AMT25 (triangles). Sample numbers (n) are also indicated. Negative latitudes are south of the Equator line.

There was a strong positive relationship between SML CDOM (a_{300}) and SSW CDOM (a_{300}) (Pearson correlation coefficient (r) = 0.805, $p < 0.001$, n = 103).

The results are in agreement with previous studies that showed statistically significant relationships between values in the SML and corresponding subsurface water of CDOM (a_{305}),

DOC and dimethylsulfide (DMS) in the Pacific/Yellow Sea (Yang *et al.*, 2005; Yang *et al.*, 2006; Yang *et al.*, 2009).

SSW CDOM (a_{300}) was in the range 0.10 - 0.87 m^{-1} on AMT24 and 0.13 - 0.50 m^{-1} on AMT25 with maxima observed at north of 40°N on both transects (AMT24, 0.57 ± 0.17 m^{-1} ; AMT25, 0.44 ± 0.03 m^{-1}).

SSW CDOM (a_{300}) was significantly higher overall in the Northern Hemisphere than in the Southern Hemisphere (AMT24 Northern Hemisphere SSW CDOM (a_{300}), 0.35 ± 0.19 m^{-1}; Southern Hemisphere SSW CDOM (a_{300}), 0.23 ± 0.04 m^{-1}; AMT25 Northern Hemisphere SSW CDOM (a_{300}), 0.25 ± 0.10 m^{-1}; Southern Hemisphere SSW CDOM (a_{300}), 0.20 ± 0.04 m^{-1}) (Mann Whitney, testing H_0: $n_1 = n_2$ against H_A: $n_1 \neq n_2$; As $n_1 - n_2$ = 0.1119 (AMT24) and 0.8761 (AMT25) with %95 CI, H_0 is rejected [p = 0.040 0 (AMT24) and p = 0.000 0 (AMT25]).

To investigate possible accumulation or depletion of CDOM within the SML with respect to SSW, the enrichment factor (EF) of CDOM was calculated: $EF_{(CDOM)} = CDOM_{(SML)} / CDOM_{(SSW)}$. EF > 1 indicates enrichment of CDOM in the SML and EF < 1 indicates depletion. EFs for CDOM (a_{300}) showed similar variability on both transects and were >1 for all sampling stations (Figure 3.10).

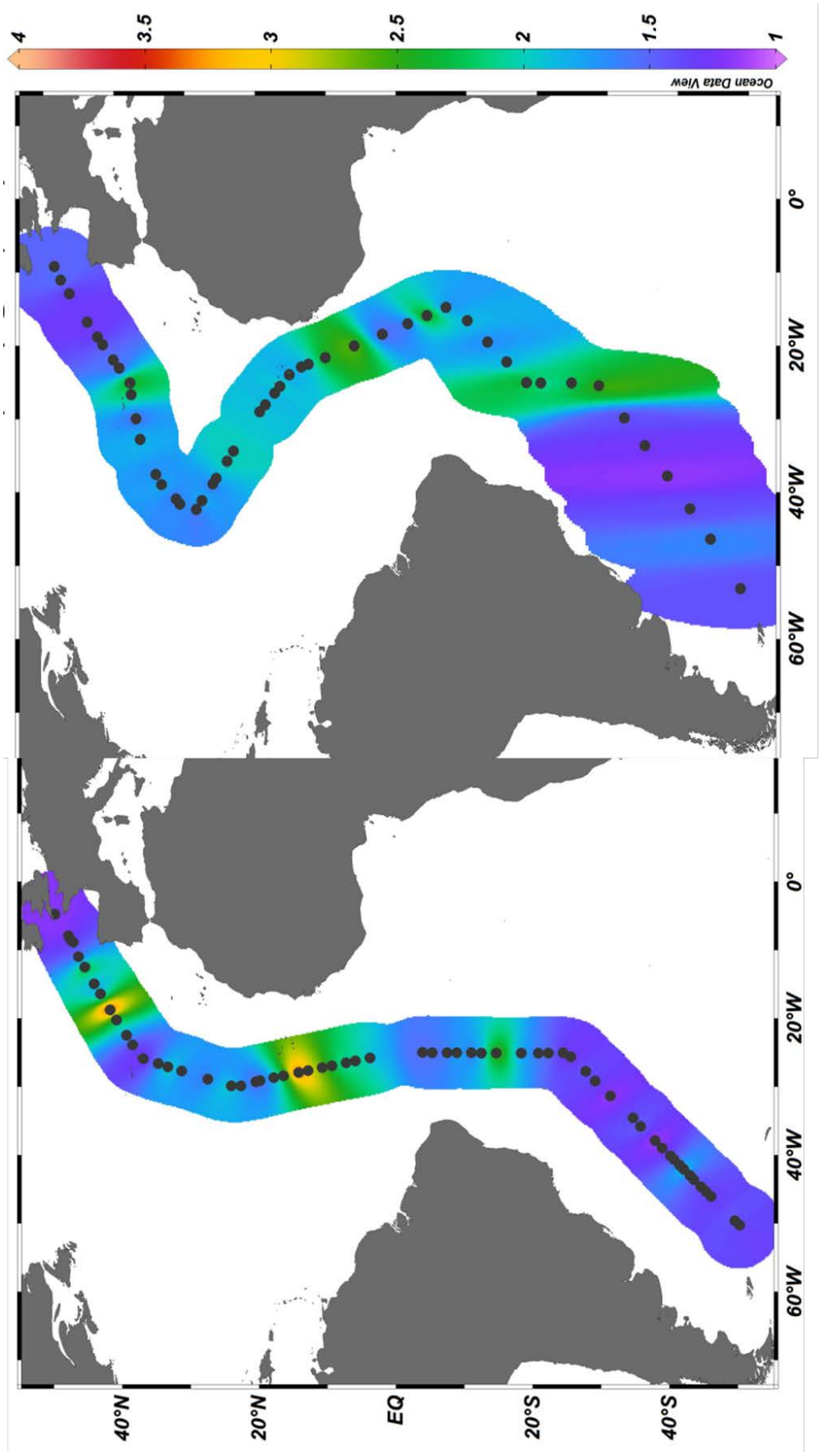

Figure 3.10. Enrichment factor of CDOM (a_{300}) in the Atlantic Ocean.AMT24 (left) and AMT25 (right). Black dots represent sampling locations.

During both cruises three bands of high CDOM (a_{300}) EF were observed centered on ~ 42°N in NADR, 10°N in WTRA and 15°S (Figure 3.10). Average CDOM (a_{300}) EF values were 1.73 ± 0.72 (range 1.03 - 3.03) on AMT24 and 1.63 ± 0.47 (range 1.16 - 2.87) on AMT25.

Enriched CDOM in the SML on both cruises is in agreement with Galgani and Engel (2016) who observed CDOM (a_{325}) enrichments in the SML in upwelling regions off the coast of Peru. The SML enrichment factors ranged between 0.40 and 2.80 with a median EF (a_{325}) = 1.20, (Galgani and Engel, 2016), as compared to the range of 1.03 and 3.03 found in this study.

The results from the current study also agree with those of Tilstone *et al*. (2010) who found CDOM (a_{300}) maxima in the SML with concentrations more than twice those of sub-surface waters (2.0 m depth) off the Iberian Peninsula. CDOM was also observed to be enriched in the SML (EF = 1.84) compared to the underlying waters in Jiazhou Bay, China during autumn and winter (Zhang and Yang, 2013).

The relationship between EF CDOM (a_{300}) and CDOM absorption characteristics was investigated, but no significant linear regressions between EF CDOM (a_{300}) and either $S_{275-295}$, $S_{350-400}$ or S_R were found ($p > 0.05$) .

3.5.3 *SML CDOM (a_{300})-SSW CDOM (a_{300}) association*

Further investigation revealed that SML CDOM (a_{300}) has a strong positive relationship (r^2 = 0.64) with SSW CDOM (a_{300}) (Pearson correlation coefficient; r = 0.80, $p < 0.001$, n = 103) (Figure 3.11).

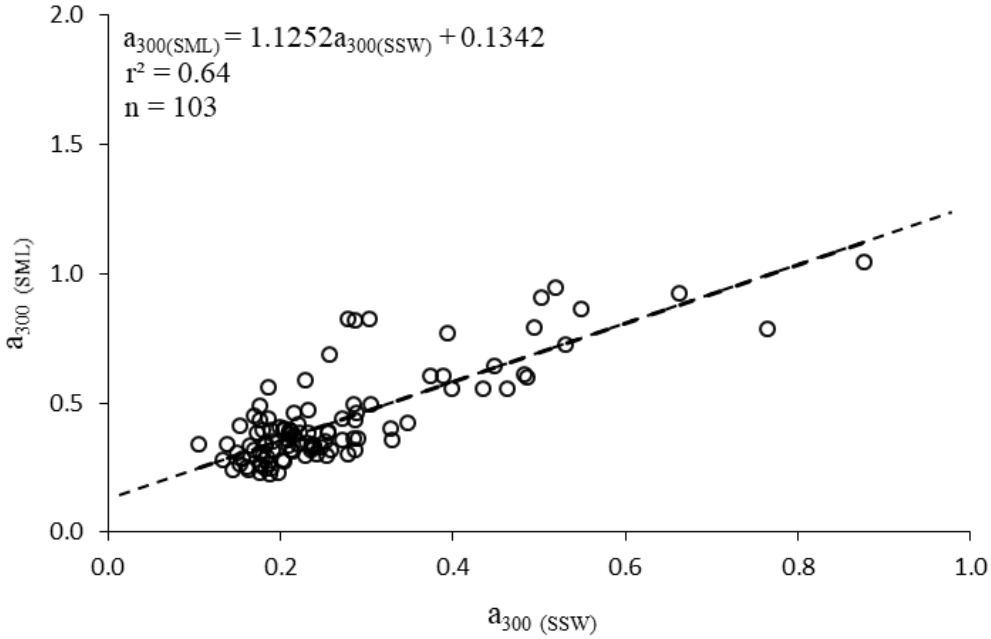

Figure 3.11. CDOM (a_{300}) in the SML against CDOM (a_{300}) in SSW (7m)
The line represents the best fit linear relationship. The linear equation and r-squared are also shown. Sample number (n) is indicated.

Although, the r-squared value (r^2) was not great due to probably the clustering of the data at the low value of absorption (Figure 3.11). This indicates a direct dependency of SML CDOM on organic matter availability in the underlying waters (Zhang and Yang, 2013).

3.5.4 *CDOM profile within the water column in the Atlantic Ocean*

In general, CDOM (a_{300}) decreased below the SML at all latitudes during AMT24 and AMT25. It ranged from 0.10 - 0.87 m^{-1} on AMT24 and 0.13 - 0.55 m^{-1} on AMT25 at depths shallower than 100 m, with a statistically significant difference between two cruises (p = 0.003, n = 583) (Table 3.2).

Table 3.2. The mean, standard deviation and range of CDOM absorption characteristics within the water column (2m ≤ Depth ≤ 100m) on (A) AMT24 and (B) AMT25 in the Atlantic Ocean. CDOM (a_{300}), $S_{275-295}$, $S_{350-400}$ and S_R with respect to oceanographic provinces were represented. The provinces are: European Continental Shelf Water (ECSW, 50-48°N), North Atlantic Drift Region (NADR, 48-42°N), North Atlantic Subtropical (NAST, 42-25°N), North Atlantic Tropical (NATR, 25-10°N), Western and Eastern Tropical Atlantic (W/ETRA, 10°N-5°S), South Atlantic Gyre (SATL, 5-42°S), South Subtropical Convergence Zone (SSTC, 42-45°S) and Falkland Islands (FKLD, 48-50°S). Sample numbers (n) were also indicated.

(A)

Provinces	Sample No.	(a_{300}) (m^{-1})	$S_{275-295}$ (nm^{-1})	$S_{350-400}$ (nm^{-1})	S_R
***ECSW* (50-48°N)**	8	0.69 ± 0.08	0.023 ± 0.001	0.017 ± 0.003	1.29 ± 0.15
		(0.62 - 0.87)	(0.022 - 0.024)	(0.016 - 0.024)	(0.93 - 1.41)
***NADR* (48-42°N)**	62	0.42 ± 0.09	0.031 ± 0.003	0.018 ± 0.005	1.76 ± 0.50
		(0.25 - 0.76)	(0.024 - 0.033)	(0.009 - 0.035)	(0.90 - 3.36)
***NAST* (42-25°N)**	68	0.30 ± 0.10	0.035 ± 0.007	0.013 ± 0.006	3.49 ± 2.54
		(0.10 - 0.52)	(0.023 - 0.053)	(0.001 - 0.024)	(1.30 - 7.30)
***NATR* (25-10°N)**	45	0.32 ± 0.14	0.037 ± 0.009	0.022 ± 0.011	2.03 ± 1.19
		(0.14 - 0.62)	(0.020 - 0.051)	(0.006 - 0.057)	(0.67 - 3.79)
***WTRA* (10°N-5°S)**	29	0.23 ± 0.07	0.040 ± 0.007	0.018± 0.008	2.46 ± 1.03
		(0.13 - 0.45)	(0.024 - 0.050)	(0.007 - 0.048)	(1.00 - 6.78)
***SATL* (5-42°S)**	100	0.22 ± 0.04	0.039 ± 0.006	0.017 ± 0.014	3.43 ± 2.23
		(0.14 - 0.35)	(0.027 - 0.052)	(0.003 - 0.074)	(0.62 - 6.77)
***SSTC* (42-45°S)**	23	0.25 ± 0.02	0.035 ± 0.002	0.017 ± 0.009	2.57 ± 1.10
		(0.22 - 0.29)	(0.032 - 0.037)	(0.008 - 0.038)	(0.98 - 4.41)
***FKLD* (48-50°S)**	8	0.22 ± 0.02	0.031 ± 0.001	0.013 ± 0.003	2.42 ± 0.49
(AMT24)		(0.20 - 0.28)	(0.029 - 0.033)	(0.009 - 0.018)	(1.78 - 3.16)

Table 3.2. (continued) The mean, standard deviation and range of CDOM absorption characteristics within the water column (2m ≤ Depth ≤ 100m) on (A) AMT24 and (B) AMT25 in the Atlantic Ocean. CDOM (a_{300}), $S_{275-295}$, $S_{350-400}$ and S_R with respect to oceanographic provinces were represented. The provinces are: European Continental Shelf Water (ECSW, 50-48°N), North Atlantic Drift Region (NADR, 48-42°N), North Atlantic Subtropical (NAST, 42-25°N), North Atlantic Tropical (NATR, 25-10°N), Western and Eastern Tropical Atlantic (W/ETRA, 10°N-5°S), South Atlantic Gyre (SATL, 5-42°S), South Subtropical Convergence Zone (SSTC, 42-45°S) and Falkland Islands (FKLD, 48-50°S). Sample numbers (n) were also indicated.

(B)

Provinces	Sample No.	(a_{300}) (m^{-1})	$S_{275-295}$ (nm^{-1})	$S_{350-400}$ (nm^{-1})	S_R
***ECSW* (50-48°N)**	7	0.43 ± 0.01	0.032 ± 0.000	0.016 ± 0.000	1.96 ± 0.07
		(0.42 - 0.44)	(0.031 - 0.032)	(0.016 - 0.017)	(1.85 - 2.04)
***NADR* (48-42°N)**	27	0.46 ± 0.04	0.032 ± 0.001	0.017 ± 0.001	1.89 ± 0.09
		(0.34 - 0.55)	(0.029 - 0.034)	(0.014 - 0.018)	(1.68 - 2.13)
***NAST* (42-25°N)**	67	0.26 ± 0.09	0.041 ± 0.008	0.015 ± 0.003	2.86 ± 0.09
		(0.14 - 0.46)	(0.028 - 0.052)	(0.010 - 0.022)	(1.68 - 4.89)
***NATR* (25-10°N)**	42	0.27 ± 0.10	0.041 ± 0.008	0.016 ± 0.002	2.62 ± 0.58
		(0.16 - 0.51)	(0.023 - 0.051)	(0.012 - 0.018)	(1.63 - 4.19)
***WTRA* (10°N-5°S)**	21	0.24 ± 0.08	0.041 ± 0.008	0.015± 0.002	2.68 ± 0.36
		(0.15 - 0.49)	(0.026 - 0.050)	(0.012 - 0.018)	(1.84 - 3.14)
***SATL* (5-42°S)**	66	0.22 ± 0.05	0.044 ± 0.005	0.013 ± 0.002	3.42 ± 0.98
		(0.13 - 0.35)	(0.031 - 0.053)	(0.008 - 0.017)	(2.28 - 6.43)
***SSTC* (42-45°S)**	10	0.21 ± 0.03	0.036 ± 0.001	0.013 ± 0.002	2.74 ± 0.53
		(0.18 - 0.24)	(0.034 - 0.038)	(0.011 - 0.015)	(2.30 - 3.28)

This is in agreement with Galgani and Engel (2016) who also observed higher CDOM (a_{325}) in the SML compared to the underlying waters in upwelling waters off the coast of Peru.

The average CDOM absorbance of 0.29 ± 0.12 m^{-1} agrees closely with values of 0.35 ± 0.10 m^{-1} obtained from AMTs 9, 10 and 11 to a depth of 300 m (Kitidis *et al.*, 2006). However, their results were slightly higher than the mean CDOM absorption coefficient in this study due to their unfiltered samples.

CDOM absorption coefficients for oceanic samples with an average CDOM (a_{300}) < 0.50 m^{-1} were reported for the Mid-Atlantic Bight, the western tropical Atlantic and the Sargasso Sea (Siegel and Michaels, 1996; Del Vecchio and Blough, 2004).

Stubbins *et al*. (2006) reported average CDOM (a_{300}) of 0.19 ± 0.03 for filtered surface water samples from the entire euphotic zone (i.e. > 100m depth) collected on AMT15 (September and October 2004) between the UK and Cape Town (South Africa).

CDOM (a_{300}) measurements within the water column also showed a maximum between 50°N and 35°N, with an AMT24 average of 0.41 ± 0.12 m^{-1} (range 0.17 - 0.87 m^{-1}) and an AMT25 average of 0.36 ± 0.10 m^{-1} (range 0.17 - 0.54 m^{-1}) (Figure 3.12).

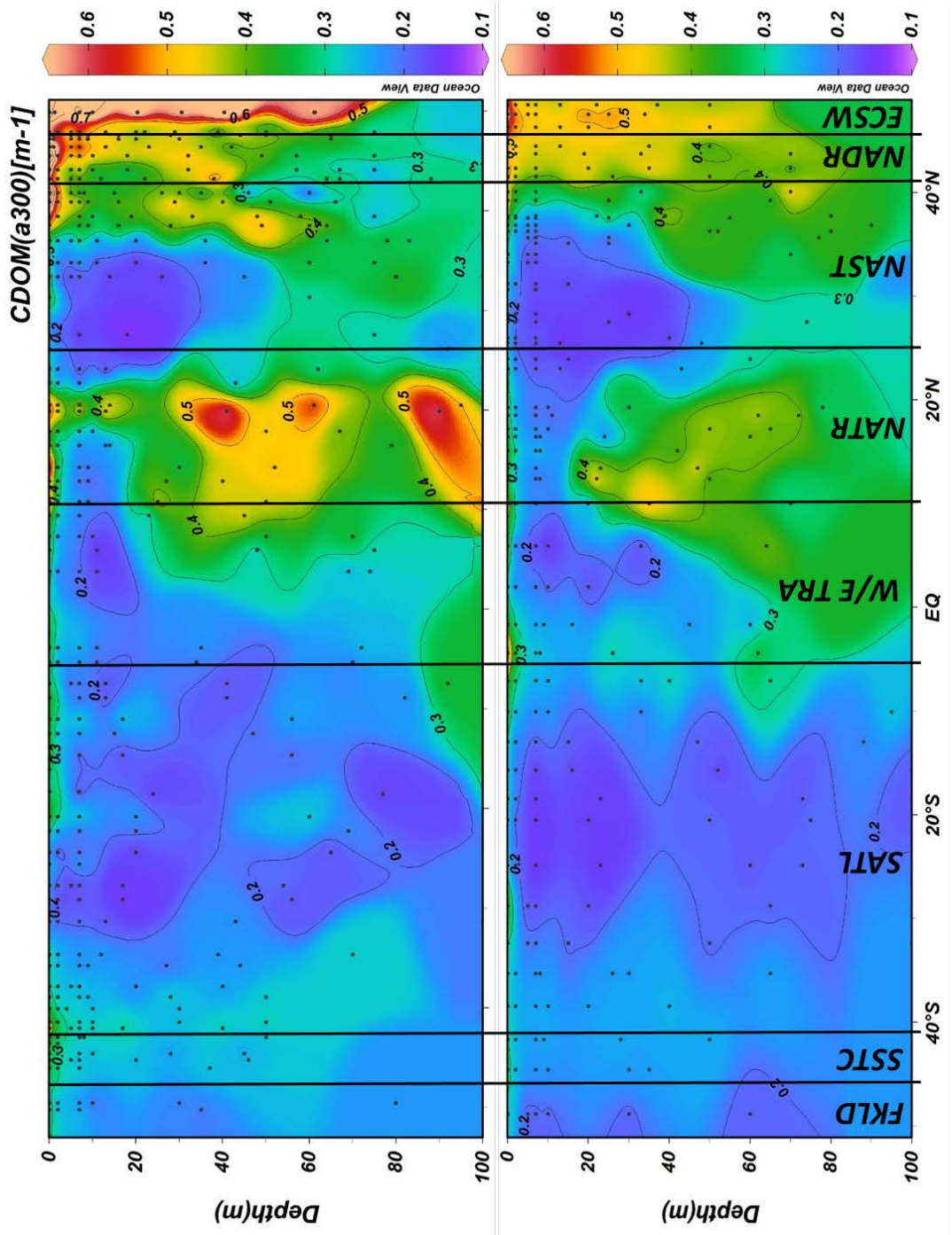

Figure 3.12. Water column profile of CDOM (a_{300}) (m^{-1}) in the Atlantic Ocean. CDOM (a_{300}) during AMT24 (top) and AMT25 (bottom) are displayed. Black dots represent latitude and depth of individual samples. Biogeochemical provinces including: European Continental Shelf Water (ECSW), North Atlantic Drift Region (NADR), North Atlantic Subtropical Region (NATR), North Atlantic Tropical Region (NATR), Western/Eastern Tropical Atlantic (W/E TRA), South Atlantic Gyre (SATL), South Subtropical Atlantic (SSTC) and Falkland Islands (FKLD) are displayed.

At high latitudes in the Northern Hemisphere (i.e. ECSW and NADR), CDOM (a_{300}) maxima in the water column were typically encountered shallower than 70 m, with a surface MLD ~ 25 m and DCM at around 50 m during both cruises in this study.

The current study shows the notable increase in CDOM absorbances from the base of the mixed layer in the Northern Hemisphere between 45°N and 25°N in water deeper than 60 m. In the tropical-equatorial region (between 20°N and 5°S), CDOM (a_{300}) maxima were encountered below 20 m depth. Average values were 0.31 ± 0.14 m^{-1} (range 0.13 - 0.62 m^{-1} on AMT24 and 0.27 ± 0.10 m^{-1} (range 0.15 - 0.51 m^{-1}) on AMT25 (Figure 3.12). In agreement with the current study, maxima in CDOM (a_{300}) (> 0.6 m^{-1}) were measured between 30 m and 80 m depth at the same latitudes (Kitidis *et al.*, 2006).

In the oligotrophic regions between 35°N and 20°N a smooth distribution and lower CDOM (a_{300}) values were observed throughout the water column (AMT24, 0.24 ± 0.11 m^{-1}, range, 0.10 - 0.56 m^{-1} ; AMT25, 0.19 ± 0.05 m^{-1}, range, 0.14 - 0.37 m^{-1}). The position of the DCM had deepened to ~100 m in the vicinity of the oligotrophic NAG while the MLD was still shallow (~ 35 m). It was also noticed that at depths shallower than 50 m in this region, CDOM depletion might occur as CDOM (a_{300}) decreased to less than 0.1 m^{-1} in some samples (Figure 3.12).

In concurrence, the central oligotrophic gyres of the Atlantic, Indian and Pacific Ocean showed CDOM minima in previous research (Carder *et al.*, 1989; Nelson and Siegel, 2002; Siegel *et al.*, 2002; Siegel *et al.*, 2005a; Siegel *et al.*, 2005b; Kitidis *et al.*, 2006; Kowalczuk *et al.*, 2013)

In the Southern Hemisphere, CDOM (a_{300}) was lower than the Northern Hemisphere (AMT24, 0.22 ± 0.04 m^{-1}, range of 0.14 - 0.35 m^{-1}; AMT25, 0.21 ± 0.04 m^{-1}, range 0.13 - 0.35 m^{-1} (see Table 3.2).

In the oligotrophic South Atlantic gyre (SAG) between 10°S and 30°S, CDOM (a_{300}) values were more homogenous within the water column with lower concentrations (AMT24, 0.20 ± 0.04 m^{-1}, range 0.14 - 0.32 m^{-1}; AMT25, 0.18 ± 0.02 m^{-1}, range 0.13 - 0.27 m^{-1}) compared to lower latitudes in the Northern Hemisphere. The DCM had deepened in this region (DCM > 100 m) and reached almost 140 m on AMT24. Overall, CDOM (a_{300}) distributions in the water column are less variable with depth in both the NAG and SAG with a deep DCM and low surface chlorophyll values.

At higher latitudes in the Southern Hemisphere (south of 30°S) a shallower DCM (~ 50 m) might have resulted in slightly higher CDOM (a_{300}) values within the water column compared to the lower latitudes of the South Atlantic (AMT24, 0.24 ± 0.03 m^{-1}, range 0.17 - 0.31 m^{-1}; AMT25, 0.22 ± 0.02 m^{-1}, range 0.18 - 0.25 m^{-1}).

Water column CDOM (a_{300}) values in the Northern Hemisphere changed significantly along the cruise transects between the provinces whereas the water column CDOM (a_{300}) in the Southern Hemisphere was more homogenous and changed statistically less between the provinces.

CDOM (a_{300}) was also found to be significantly different between the Northern and the Southern Hemisphere, consistently on the two cruises in agreement with Kitidis *et al*. (2006) (Two-Sample t-test, testing H_0: the two means are equal against H_A: at least one mean is different; As µ1 - µ2 = 0.1238 (AMT24) and 0.0841 (AMT25), $t_{95\%\ CI\ (2)\ 251}$ = 11.39 (AMT24) and $t_{95\%\ CI\ (2)\ 218}$ = 8.04 (AMT25), H_0 is rejected for AMT24 and AMT25 [$p < 0.001$]). Northern Hemisphere CDOM (a_{300}) was 0.35 ± 0.14 m^{-1} and 0.30 ± 0.11 m^{-1} compared to Southern Hemisphere CDOM (a_{300}) of 0.22 ± 0.04 m^{-1} and 0.21 ± 0.04 m^{-1} on AMT24 and AMT25 respectively.

3.5.4.1 Further investigation of CDOM optical properties in the Atlantic Ocean

In agreement with Kowalczuk *et al*. (2013), the distribution of CDOM (a_{300}) and $S_{275-295}$ show a significant inverse correlation in the Atlantic Ocean both in the SML and throughout the water column (Pearson correlation coefficient (r) = -0.77, $p < 0.001$, n = 114 (SML) and r = -0.83, $p < 0.001$, n = 584 (water column)). The average of $S_{275-295}$ throughout water column (i.e. ≤ 100 m) is significantly higher than in the SML of the Atlantic Ocean (Two-Sample t-test, testing H_0: the two means are equal against H_A: at least one mean is different; As µ1 - µ2 = 0.00450 3, $t_{95\%\ CI\ (2)\ 188}$ = -7.05, H_0 is rejected [$p < 0.001$]).

In concurrence, Galgani and Engel (2016) found higher $S_{275-295}$ in underlying waters (~ 20 cm), ranging from 0.017 to 0.043 nm^{-1} compared to between 0.012 and 0.038 nm^{-1} in the SML, in the upwelling region off the coast of Peru, but the difference was not statistically significant. Zhang and Yang (2013) also found lower $S_{350-400}$ in the SML than in sub-surface waters for almost all sampling stations along offshore transects in Jiaozhou Bay, China.

The total average of $S_{275-295}$ within the water column was rather similar on both cruises (AMT24 $S_{275-295}$, 0.036 ± 0.007 nm^{-1}; range 0.020 - 0.053 nm^{-1}; AMT25 $S_{275-295}$, 0.040 ± 0.007 nm^{-1};

range 0.023 - 0.053 nm^{-1}). CDOM spectral slope values with the inverse relationship with CDOM absorption coefficient were reported typically for oceanic samples (Bricaud *et al.*, 1981; Nelson *et al.*, 1998; Nelson *et al.*, 2004; Nelson *et al.*, 2007; Nelson *et al.*, 2010).

$S_{275-295}$ was compared between the hemispheres to further investigate its latitudinal/regional variability. Similar to results from the SML (see section 3.5.1), average Southern Hemisphere $S_{275-295}$ was higher than for the Northern Hemisphere observed on both cruises (AMT24 Northern Hemisphere $S_{275-295}$, 0.034 ± 0.007 nm^{-1}, n = 200; AMT24 Southern Hemisphere $S_{275-295}$, 0.038 ± 0.005 nm^{-1}, n = 141; AMT25 Northern Hemisphere $S_{275-295}$, 0.039 ± 0.007 nm^{-1}, n = 158; AMT25 Southern Hemisphere $S_{275-295}$, 0.042 ± 0.005 nm^{-1}, n = 82) with significant difference (Two-Sample t-test, testing H_0: the two means are equal against H_A: at least one mean is different; As µ1 - µ2 = -0.0038 05 (AMT24) and -0.0032 84 (AMT25), $t_{95\%\ CI\ (2)\ 338}$ = -5.35 (AMT24) and $t_{95\%\ CI\ (2)\ 222}$ = -3.84 (AMT25), H_0 is rejected for AMT24 and AMT25 [p < 0.001]).

To further assess the spatial signal of the quantity and composition of organic matter in the Atlantic Ocean, $S_{275-295}$ values in the SML and the water column were compared. In total, the average SML $S_{275-295}$ was 0.033 ± 0.005 nm^{-1} (AMT24 SML $S_{275-295,}$ 0.030 ± 0.005 nm^{-1}, range 0.020 – 0.043 nm^{-1}; and AMT25 $S_{275-295,}$ 0.036 ± 0.004 nm^{-1}, range 0.023 - 0.044 nm^{-1}, lower than average $S_{275-295}$ within the water column (depth ≤ 100m) with an average of 0.038 ± 0.007 nm^{-1} (AMT24 $S_{275-295}$, 0.035 ± 0.007 nm^{-1}, range 0.020 - 0.053 nm^{-1}; AMT25 $S_{275-295}$, 0.040 ± 0.007 nm^{-1}, range 0.023 - 0.052 nm^{-1}).

$S_{275-295}$ maxima were found in the oligotrophic region of the NAG above ~ 50 m depth, above ~20 m depth in the equatorial region between 20°N and the Equator and also in low latitudes in the SAG (north of 40°S), consistent between the two cruises (Figure 3.13).

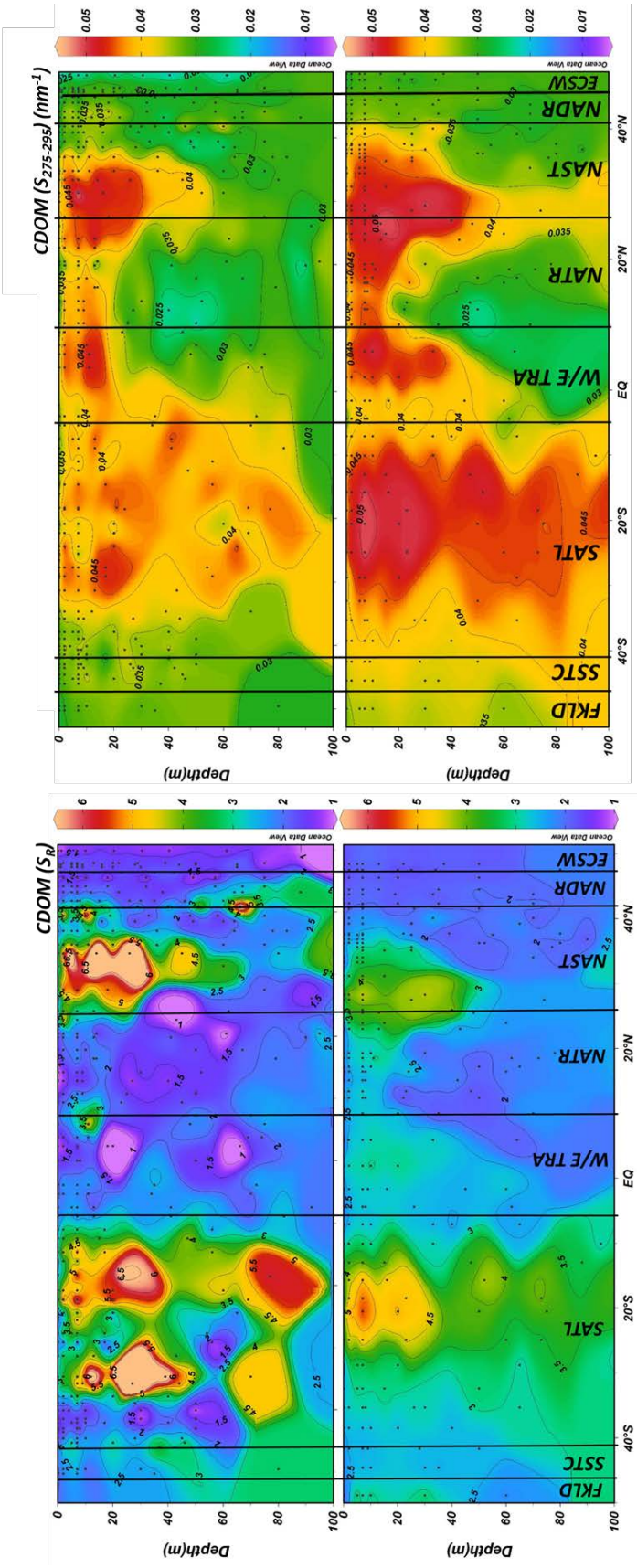

Figure 3.13. Distribution of CDOM ($S_{275-295}$) (right) and CDOM (S_R) (left) in the water column of the Atlantic Ocean. AMT24 (top) and AMT25 (bottom) were displayed. Black dots represent latitude and depth of individual samples.

In the oligotrophic region of the NAG (35°N - 20°N) (depth ≤ 50 m) $S_{275-295}$ maxima were found with an average of 0.041 ± 0.007 nm^{-1} (range 0.027 - 0.053 nm^{-1}) on AMT24 and 0.046 ± 0.004 nm^{-1} (range 0.031 - 0.052 nm^{-1}) on AMT25. Second $S_{275-295}$ maxima were found in SAG between 10°S and 30°S, with an average of 0.042 ± 0.005 nm^{-1} (range 0.026 - 0.051 nm^{-1}) on AMT24 and 0.047 ± 0.003 nm^{-1} (range 0.037 - 0.052 nm^{-1}) on AMT25. The last $S_{275-295}$ maxima was above 20 m in the tropical region (between 20°N and the Equator) with an average of 0.037 ± 0.008 nm^{-1} (range 0.020 - 0.050 nm^{-1}) on AMT24 and an average of 0.040 ± 0.008 nm^{-1} (range 0.023 - 0.050 nm^{-1}) on AMT25.

$S_{275-295}$ was lower at high latitudes (~ 40°N and ~ 40°S) within the water column and also in the tropical and equatorial region in the Northern Hemisphere waters below ~ 20 m depth (Figure 3.13).

$S_{350-400}$ on the other hand showed a homogenous distribution within the water column (depth ≤ 100 m) with some high $S_{350-400}$ values observed at single depths mainly on AMT24. $S_{350-400}$ within the water column was in the range 0.001 - 0.074 nm^{-1} and 0.008 - 0.022 nm^{-1} on AMT24 and AMT25 respectively (Table 3.2).

S_R within the water column was in the range 0.62 - 7.30 on AMT24 and 1.63 - 6.43 on AMT25 (see Table 3.2). S_R maxima were observed mostly in the oligotrophic NAST, primarily at depths shallower than ~ 60 m and at all depths in SAG. S_R minima (~2) were found at the northern end of transects and in the tropical and the equatorial region within the water column deeper than 20 m (Figure 3.13). This is in agreement with Kowalczuk *et al.* (2013), who found the lowest S_R values (S_R ~ 2.0) in the western European continental shelf in the upper 100 m and also at the southern edge of the transect about 50°S in the top 50 m.

Overall, the average of S_R during this study is in agreement with S_R reported by Kowalczuk *et al*. (2013), who report an average of 3.09 ± 0.05 in the mixed layer of the Atlantic Ocean during AMT20 (2010). Zhang and Yang (2013) reported S_R ranging between 0.8 and 2.3 and increased with CDOM photodegradation in Jiaozhou Bay, China.

Also, in agreement with Galgani and Engel (2016), S_R was significantly lower in the SML (1.88 ± 0.58, range from 0.15 to 3.60) compared to the sub-surface waters (3.00 ± 1.35, range from 0.85 to 7.86) (Two-Sample t-test, testing H_0: the two means are equal against H_A: at least one mean is different; As μ1 - μ2 = 1.090, $t_{95\%\ CI\ (2)\ 140}$ = -7.54, H_0 is rejected [$p < 0.001$]). In

contrast, Tilstone *et al*. (2010) found higher S_R in the SML associated with higher $S_{275\text{-}295}$, indicative of CDOM photobleaching in oceanic samples off the Iberian Peninsula.

3.5.5 *The presence of mycosporine-like amino acids (MAA)*

A typical UV/visible absorption spectrum for CDOM was presented and discussed in section 2.5.6. However, in SML samples around 15°N a prominent absorption shoulder between 325 and 350 nm was observed in the CDOM absorbance vs wavelength plots (Figure 3.14).

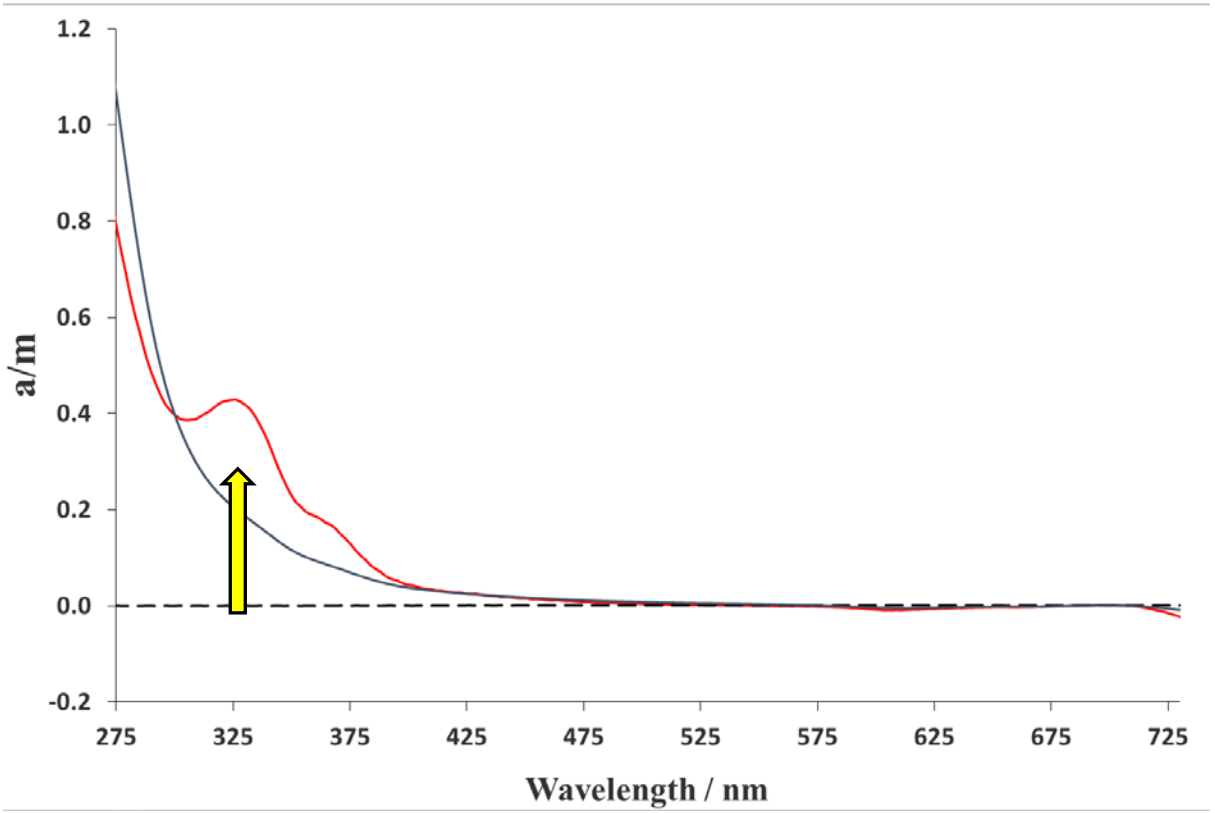

Figure 3.14. Absorbance vs wavelength plot (in red) of an SML sample (CTD026, AMT24: Lat. 16.43°N; Long. 28.4°S) showing a distinct shoulder at 325-350 nm. The grey line represents the absorbance vs wavelength plot for corresponding sub-surface water. The dashed line represents the artificial seawater reference.

Tilstone *et al*. (2010) also reported such a prominent absorption shoulder at short wavelengths, suggestive of the presence of mycosporine-like amino acids (MAA) in the dissolved optical fraction of organic matter off the Iberian Peninsula. The MAA enrichment in the SML of up to 290 µg L^{-1} during slick formation coincided with abundance of dinoflagellates (Tilstone *et al.*, 2010).

Also, a strong correlation between CDOM absorption coefficient and MAA concentration may indicate that MAA compounds might have similar optical properties, contributing to total CDOM absorption in the ocean (Tilstone *et al.*, 2010).

Whitehead and Vernet (2000) also observed MAA to be present in oceanic samples during a red tide off the upwelling coast of California.

A prominent absorption ~ 280 nm in some samples from the UK shelf regions associated with *coccolithophores* bloom has been reported previously (Mann 2010).

However, the samples containing MAAs in this study were mostly observed in the SML around 15°N in the NATR during both cruises (4 samples in total). The presence of MAA was not frequent in other provinces and CDOM dominates the spectral absorbance within the SML at other locations.

3.5.6 *CDOM absorption coefficient – spectral slope relationship*

Overall there was a significant inverse relationship between CDOM (a_{300}) and $S_{275\text{-}295}$ both in the SML ($r^2 = 0.60$, n = 114) and in the water column ($r^2 = 0.69$, n = 584) (Figure 3.15).

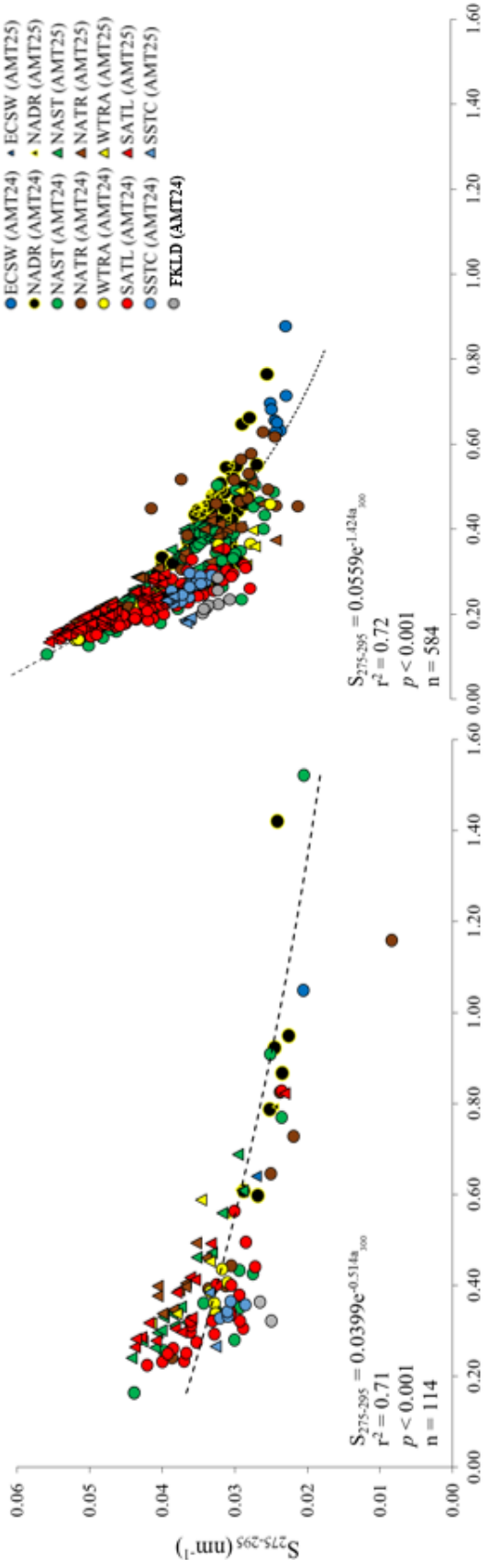

Figure 3.15. The distribution of CDOM (a_{300}) against CDOM ($S_{275-295}$) in the SML (left) and the water column (2m ≤ depth ≤ 100m) (right) during AMT24 and AMT25
The legend lists the distinct oceanographic provinces in the Atlantic Ocean. Sample numbers (n) are also indicated. The dashed line represent the best linear fit. The linear equation, r-squared (r^2) and probability of the correlation (p) are provided.

In general, $S_{275-295}$ decreased with increasing CDOM (a_{300}) consistently on the two cruises while the highest average values of $S_{275-295}$ i.e. 0.044 and 0.054 nm^{-1} coincided with the lowest CDOM (a_{300}) i.e. 0.16 and 0.10 m^{-1} in the SML and the water column respectively.

The highest values of CDOM (a_{300}), associated with the lowest $S_{275-295}$, were observed in the waters off the UK coast (ECSW) and in NADR during both cruises whereas the highest $S_{275-295}$ values are associated with the lowest CDOM (a_{300}) as recorded in the oligotrophic waters of the SATL on both cruises (Figure 3.15).

A significant negative correlation ($p < 0.001$, n = 114) between CDOM (a_{300}) and $S_{275-295}$ was found in the SML, with the strongest linear relationship observed in the NATR ($r^2 = 0.89$, n = 18). A significant negative correlation was also found between CDOM (a_{300}) and $S_{275-295}$ in the water column ($p < 0.001$ n = 584).

3.5.7 *CDOM-Chlorophyll association*

Phytoplankton are the principal source of biologically-derived CDOM in the marine environment (Carder *et al.*, 1989; Kowalczuk, 1999).

Phytoplankton were distributed in deeper waters at lower latitudes (excluding the equatorial upwelling region) and within the mixed layer at higher latitudes (depth ≤ 100m) in this study (see section 3.4). Given that CDOM in the open ocean is mainly derived from phytoplankton (Carder *et al.*, 1989; Kowalczuk, 1999), the relationship between CDOM (a_{300}) and chlorophyll- a as an overall indicator of phytoplankton abundances was examined. CDOM (a_{300}) showed a positive relationship with chlorophyll-a. Although the *p*-value vale was significant (Pearson correlation coefficient (r) = 0.40, $p < 0.001$, n = 661), the linear regression model cannot be used to predict CDOM absorption coefficient based on chlorophyll-a with any significant degree of accuracy as the r^2 value was only 15%. To investigate further, the data were split to two groups i.e. SML and SSW (= 7m) (Figure 3.16).

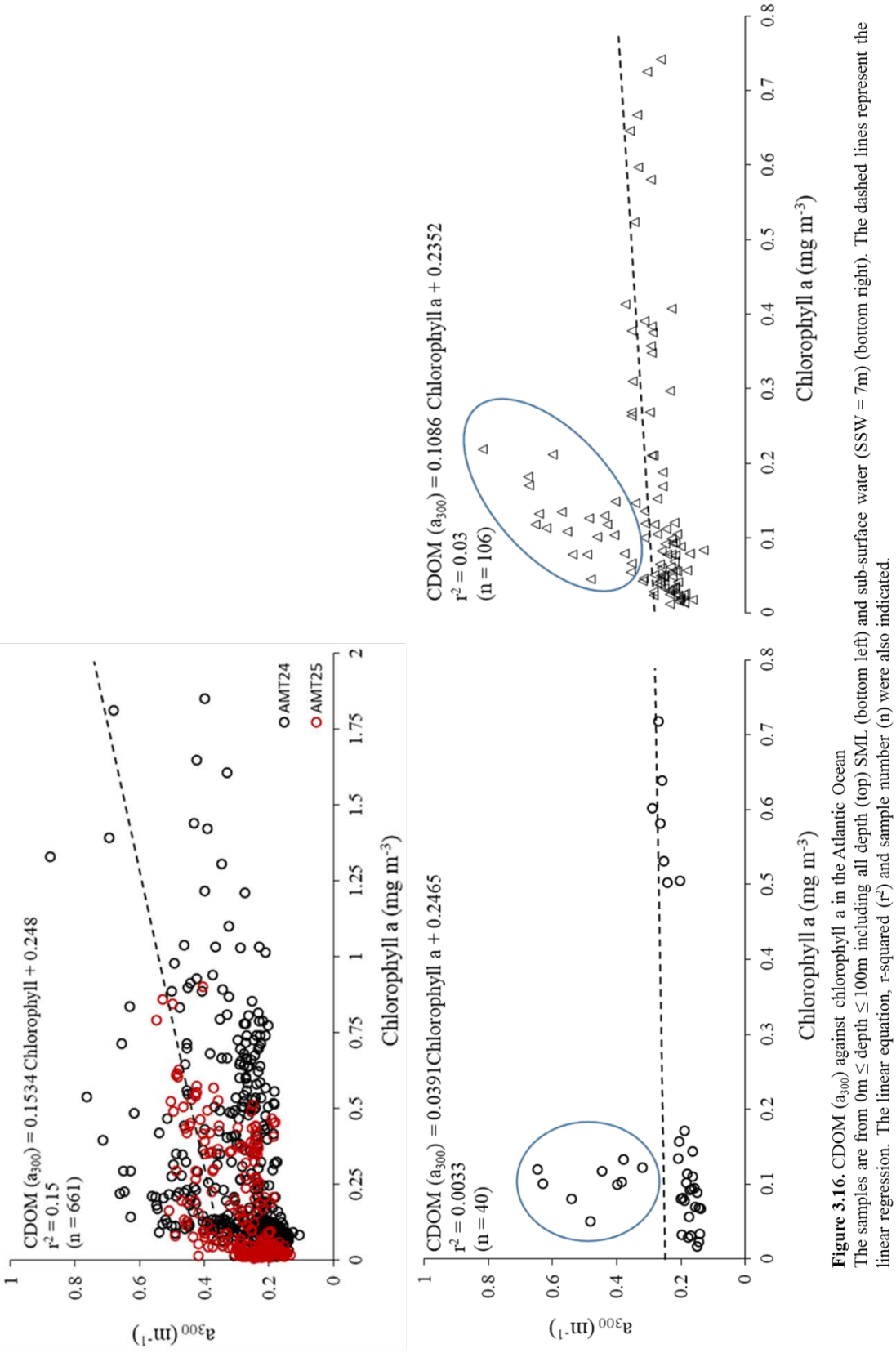

Figure 3.16. CDOM (a_{300}) against chlorophyll a in the Atlantic Ocean
The samples are from 0m ≤ depth ≤ 100m including all depth (top) SML (bottom left) and sub-surface water (SSW = 7m) (bottom right). The dashed lines represent the linear regression. The linear equation, r-squared (r^2) and sample number (n) were also indicated.

This showed that there are two distinct patterns with respect to the chlorophyll-a and CDOM association in the Atlantic Ocean. The water masses at high latitudes mainly in the Northern Hemisphere (i.e. ECSW and NADR; circled in Figure 3.16) differ markedly from the general data trends in both the SML and SSW. The correlation between CDOM and chlorophyll-a improves significantly in the absence of these water masses (Pearson correlation coefficient (r), SML (r) = 0.88 and SSW (r) = 0.64, $p < 0.001$; Figure 3.17).

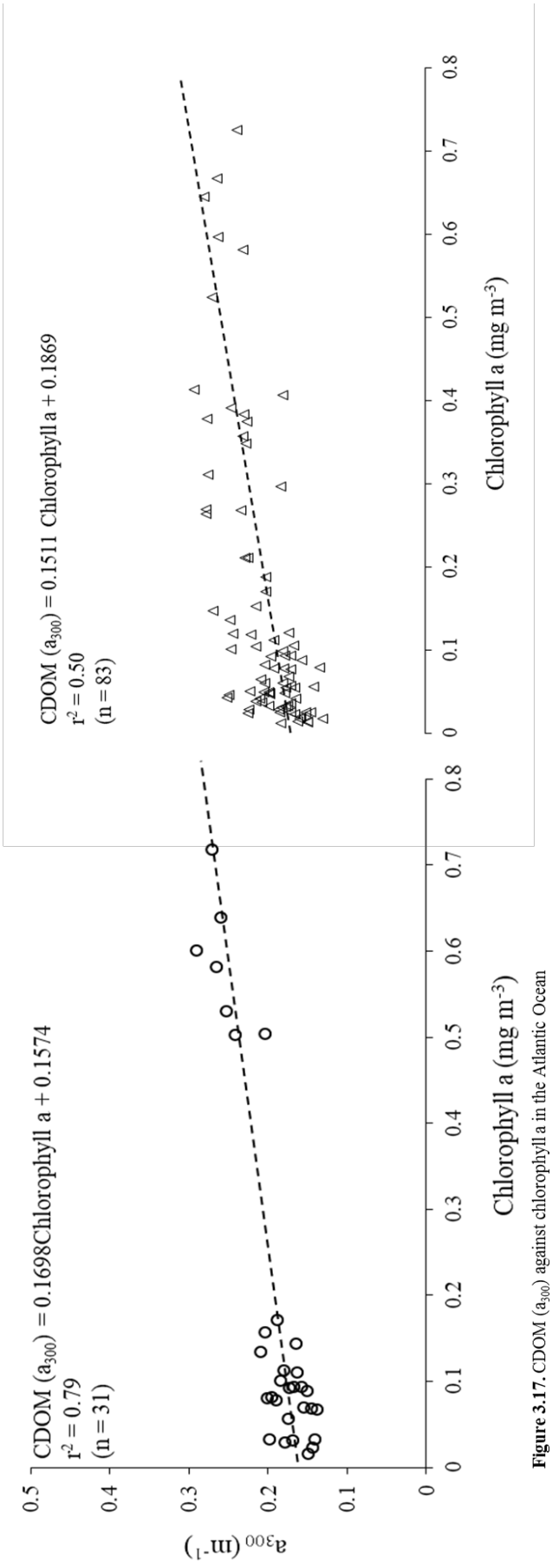

Figure 3.17. CDOM (a_{300}) against chlorophyll a in the Atlantic Ocean
The samples are from SML (left) and sub-surface water (SSW = 7m) (right). The dashed lines represent the linear regression. The linear equation, r-squared (r^2) and sample number (n) were also indicated.

The linear regression model can then be used to predict the CDOM absorption coefficient in the SML using chlorophyll-a as a proxy with a nearly 80% accuracy. However, the model is province-dependent, and is applicable for the open ocean where there are no alternative sources of CDOM such as riverine or terrestrial input. In addition, in the ECSW and NADR there might be additional factors controlling CDOM distribution.

Kitidis *et al*. (2006) also observed regional/spatial co-dependence of CDOM and chlorophyll-a in the Atlantic Ocean. A statistically significant correlation was found between CDOM and chlorophyll-a in relation to phytoplankton abundance at the base of the mixed layer at lower latitudes and in the mixed layer at higher latitudes (Kitidis *et al.*, 2006). However, overall the linear regression between CDOM and chlorophyll-a was not strong ($r^2 \sim 0.20$) on AMT 9, 10 and 11, suggesting that chlorophyll-a cannot be used as a quantitative proxy for CDOM distribution (Kitidis *et al.*, 2006).

Nelson *et al*. (1998) found no clear correlation between CDOM (a_{300}) and chlorophyll-a concentration ($r^2 = 0.45$, $p > 0.05$), even with low CDOM (a_{300}) of 0.20 m^{-1} coinciding with high chlorophyll-a (0.30 mg m^{-3}) during a phytoplankton spring bloom in the Sargasso Sea.

The $S_{275-295}$ vs chlorophyll-a relationship was also improved by excluding the samples from high latitudes in the Northern Hemisphere (Figure 3.18).

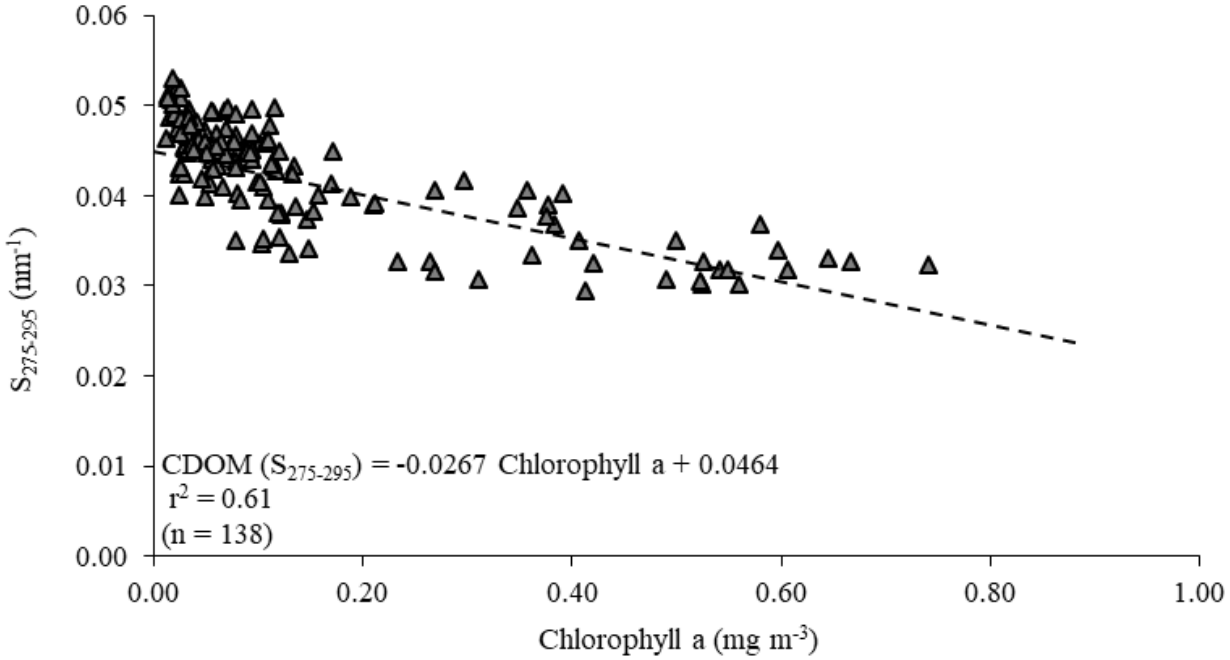

Figure 3.18. $S_{275-295}$ – chlorophyll a relationship in the SML and the SSW during AMT24 and AMT25. The dashed line represents the linear regression of the data along with the linear regression equation, correlation coefficient and number of the samples.

The Pearson correlation coefficient of r = -0.79 showed a strong negative correlation between CDOM spectral slope and chlorophyll-a concentration in the SML and the SSW samples ($p < 0.001$). The linear regression showed that the degree of the model accuracy is high based on r^2 value ($r^2 = 0.61$) (Figure 3.18).

3.5.8 *Changes in CDOM optical properties related to physiochemical indicators*

CDOM optical properties including CDOM (a_{300}) and $S_{275-295}$ were compared with salinity, water temperature and wind speed in the SML, the SSW (7 m) and the water column (depth ≤ 100 m).

Overall, CDOM (a_{300}) showed inverse correlations with salinity and temperature in the SML, SSW and the deeper water column, but these were not statistically significant (AMT24 salinity, $r^2 = 0.018$, $p = 0.275$, n = 65, AMT25 salinity $r^2 = 0.000$, $p = 0.876$, n = 65; AMT24 temperature, $r^2 = 0.024$, $p = 0.292$, n = 47, AMT25 temperature, $r^2 = 0.006$, $p = 0.604$, n = 47) (Table 3.3).

Table 3.3. Pearson correlation coefficient (r) between CDOM (a_{300}) and $S_{275\text{-}295}$ in the SML, the SSW (7m) and the water column (depth ≤ 100m) with salinity (r_S) and temperature (r_T) during AMT24, AMT25 and the total samples. Significant correlation ($p < 0.05$) are marked with star. Negative values represent inverse correlation. Sample number (n) are also indicated.

AMT24				**AMT25**				**Total**			
SML	r_S	r_T	n	***SML***	r_S	r_T	n	***SML***	r_S	r_T	n
CDOM $a_{(300)}$	-0.13	-0.02	66	CDOM $a_{(300)}$	-0.15	-0.07	47	CDOM $a_{(300)}$	-0.16	-0.03	113
$S_{275\text{-}295}$	0.30	0.13	64	$S_{275\text{-}295}$	0.37	0.35	45	$S_{275\text{-}295}$	0.36*	0.25	109
SSW				***SSW***				***SSW***			
CDOM $a_{(300)}$	-0.21	-0.16	61	CDOM $a_{(300)}$	-0.39	-0.37	49	CDOM $a_{(300)}$	-0.28	-0.25	110
$S_{275\text{-}295}$	0.44*	0.43*	61	$S_{275\text{-}295}$	0.65*	0.63*	49	$S_{275\text{-}295}$	0.53*	0.57*	110
Water column				***Water column***				***Water column***			
CDOM $a_{(300)}$	-0.19	-0.19	321	CDOM $a_{(300)}$	-0.30	-0.36	200	CDOM $a_{(300)}$	-0.24*	-0.26*	521
$S_{275\text{-}295}$	0.38*	0.50*	321	$S_{275\text{-}295}$	0.48*	0.58*	200	$S_{275\text{-}295}$	0.44*	0.55*	521

Galgani and Engel (2016) also found a decrease in CDOM absorbance with increasing salinity, temperature and wind speed with stronger dependency within the SML compared to underlying waters of the upwelling region off the coast of Peru.

Kitidis *et al*. (2006) also reported that CDOM (a_{350}) decreased with increasing salinity while CDOM levels decreased at salinity greater than 33.0, suggestive of CDOM removal due to photodegradation.

CDOM spectral slope, an indicator of CDOM history including its source, molecular weight and degradation (Helms *et al.*, 2008), increased at higher salinity and temperature with significant dependency observed in the SSW and the water column although the correlation are still relatively small (Table 3.3).

In agreement with this study, Kitidis *et al*. (2006) also found that $S_{290-350}$ increased with salinity and temperature in the surface waters (< 7m) of the Atlantic Ocean, attributed to CDOM photodegradation due to high solar radiation.

Moreover, CDOM, in general, showed a negative correlation with wind speed while CDOM (a_{300}) and $S_{275-295}$ decreased at high wind speed (U_{10}) with statistically significant correlation observed between wind speed and $S_{275-295}$ (Table 3.4).

Table 3.4. Correlation between CDOM optical properties in the SML and wind speed (U_{10}) during AMT24, AMT25 and the total samples. The numbers represent Pearson correlation coefficient. Significant correlation ($p < 0.05$) are marked with star. Negative values represent inverse correlation. Sample numbers (n) are indicated.

AMT24			AMT25			Total		
SML	U_{10}	n	SML	U_{10}	n	SML	U_{10}	n
CDOM $a_{(300)}$	-0.39	63	CDOM $a_{(300)}$	-0.26	43	CDOM $a_{(300)}$	-0.37*	106
$S_{275-295}$	-0.49	63	$S_{275-295}$	-0.89*	43	$S_{275-295}$	-0.76*	106

Galgani and Engel (2016) also found a positive correlation between $S_{275\text{-}295}$ and both salinity and temperature in the SML and underlying waters but did not show any correlation with wind speed for the upwelling region off the coast of Peru.

However, it should be pointed that the range of wavelengths on which CDOM spectral slope values are calculated is important as it might show different behaviour towards salinity and temperature. For example, Kitidis *et al*. (2006) found that CDOM spectral slope decreases with higher salinity if the slope is calculated above 350 nm whereas CDOM increases with salinity for spectral slopes calculated below 350 nm as in this study.

3.6 Summary

To discern dynamics and chemical characteristics of DOM including sources, sinks and transformations in the Atlantic Ocean, the optical properties of CDOM in the SML, in subsurface water (SSW = 7m) and in the deeper water column (≤ 100m) were determined in a range of biogeochemical provinces on two cruises of AMT. Characterization of CDOM via its optical properties enhances our understanding of organic matter composition in the marine environment and assists in identifying any modification of DOM in the SML or throughout the water column.

CDOM generally showed a SML maximum over the full extent of the transects, with a more homogenous distribution in the water column, but with the exception of high latitudes in the Northern Hemisphere (i.e. around 40°N) and in the equatorial region, with possible local CDOM production or terrestrial deposition in the vicinity of the continental shelves and/or equatorial upwelling systems.

Other biological characteristics of the Atlantic Ocean including phytoplankton community structure, chlorophyll, nutrient distributions and primary productivity in the Atlantic Ocean with respect to the biogeochemical provinces were discussed in this Chapter. Relationships of CDOM with chlorophyll-a revealed the distinct pattern in Atlantic biogeochemical provinces. A better correlation was observed in the lower latitudes of the tropical and the equatorial regions compared to the higher latitudes in the Northern Atlantic hemisphere in the vicinity of the European continental shelves (see section 3.5.7).

Chapter 4. Surfactants in the Atlantic Ocean surface microlayer and underlying water

4.1 Introduction

In this Chapter, the three following datasets are presented and discussed; total surfactant activity (SA) in the sea surface microlayer (SML) and in the water column (depth ≤ 100m) and surfactant enrichment factors (EFs) in the Atlantic Ocean. These first comprehensive surfactant measurement at ocean basin scales are important because as discussed (see section 1.2.1) surfactants are one of the major controls of the air-sea exchange of climate active gases such as CO_2.

4.2 Results

4.2.1 *Surface distributions of surfactants in the Atlantic Ocean*

In this section measurements of surfactant activity (SA) in the SML along two Atlantic Meridional Transect (AMT) cruises between 50°N and 50°S: AMT24 (2014) and AMT25 (2015) (section 2.2) are discussed.

Average SA in the SML was 0.34 ± 0.19 mg L^{-1} eq. T-X-100 (range 0.13 – 1.00 mg L^{-1} eq. T-X-100) on AMT24 and 0.47 ± 0.38 mg L^{-1} eq. T-X-100 (range 0.12 - 1.77 mg L^{-1} eq. T-X-100) on AMT25.

Wurl *et al*. (2011 b) reported SA values of 0.49 ± 0.40 mgL^{-1} eq. T-X-100 in the SML (range: 0.10 - 1.57 mg L^{-1} eq. T-X-100) for several oceanic regions including the north Pacific, the subtropical north Pacific and the Arctic. Although the ranges in SA during this study were within those given by Wurl *et al*. (2011b) (except for the upper limit of SA of 1.76 mg L^{-1} eq. T-X-100 on AMT25), there are some important differences. The details of the SA distributions varied between the Atlantic Ocean biogeochemical provinces in this study, which was not shown by the earlier more broad based synthesis which predicted similar SA (and EF) ranges for areas of comparable trophic status in different ocean basins (Wurl *et al.*, 2011b).

Frew *et al*. (2002) reported that SA in the SML ranged from 0.05 to 3.00 mg L^{-1} eq. T-X-100 in coastal and oceanic samples from the Sargasso Sea-Middle Atlantic Bight. They found significantly lower SA in oligotrophic oceanic samples, with a maximum of 0.15 mg L^{-1} eq. T-X-100 compared to more eutrophic coastal samples where SA reached as high as 3.00 mg L^{-1} eq. T-X-100 (Frew *et al.*, 2002).

SA in the SML was also considerably lower in oceanic samples of the northern Adriatic Sea (i.e. average of 0.083 mg L^{-1} eq. T-X-100) (Gašparović *et al.*, 2011) compared to this study. Although, the data were reported on a yearly basis and SA maxima were observed in August and at the beginning of November.

Ćosović and Vojvodić (1982) also reported higher SA for the SML (range; 0.10 - 2.50 mg L^{-1} eq. T-X-100) compared to the SSW samples (maximum 60 m depth) (range; 0.01 - 1.00 mg L^{-1} eq. T-X-100) in the Northern Adriatic Sea. SA also showed seasonal dynamics with the

highest SA values measured in the late summer and autumn associated with a phytoplankton bloom (Ćosović and Vojvodić, 1998).

Croot *et al*. (2007) reported SA values in the Southern Ocean during an iron fertilisation experiment (to promote a phytoplankton bloom) ranging from < 0.005 to 0.03 mg L^{-1} eq. T-X-100 with general SA enrichment observed in the SML. The highest SA values (> 0.02 mg L^{-1} eq. T-X-100) were also recorded at the end of the phytoplankton bloom (Croot *et al.*, 2007).

Latitudinal SA distributions on AMT24 and AMT25 were broadly similar. While the SA maximum at 40°N was present in both the SML and the SSW, other details of SML SA were not reflected in the SSW data. Excluding the SA maxima, there was a discernible trend of progressively decreasing SA from the north to the south on both transects, both in the SML and in SSW (Figure 4.1).

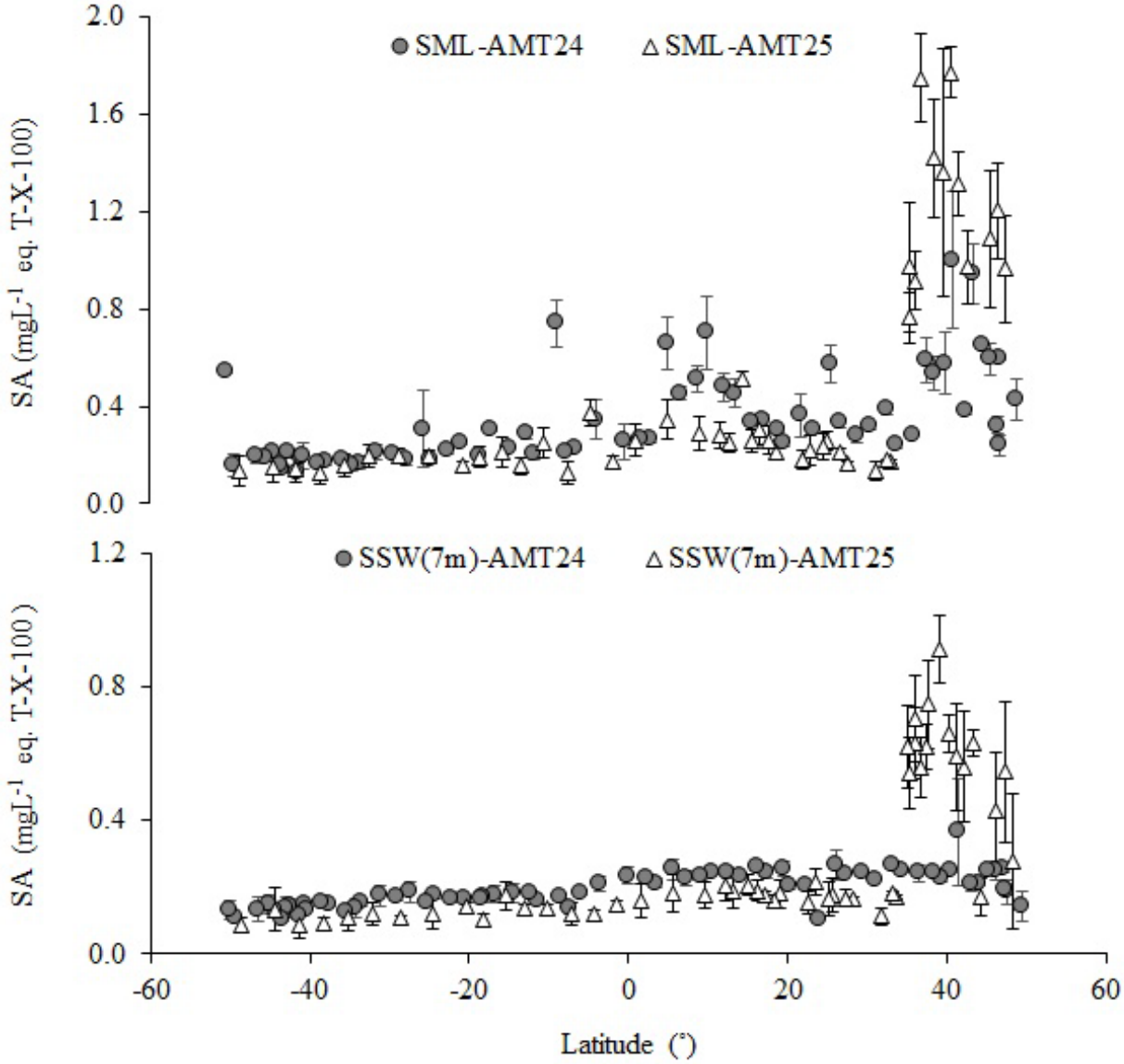

Figure 4.1. Latitudinal distribution of SA in the SML (top) and in SSW (7m depth) (bottom) along AMT24 and AMT25 in the Atlantic Ocean. Negative values of latitude represent the Southern Hemisphere. Bars display standard deviation of the mean. Note that the scales on y-axis are different for the two plots.

Given that the two transects differed by up to 13° of longitude between ~ 40°N and 20°S (see section 2.2), it seems that there are only comparatively small longitudinal SA gradients across a substantial fraction of the Atlantic Ocean. The most notable features of the data, common to both transects and in both the SML and in SSW, were distinct SA maxima centred on ~ 40°N, in NADR (AMT24, SML 1.00 ± 0.28 mg L^{-1} eq. T-X-100, SSW 0.36 ± 0.15 mg L^{-1} eq. T-X-100; AMT25, SML 1.76 ± 0.10 mg L^{-1} eq. T-X-100, SSW 0.58 ± 0.16 mg L^{-1} eq. T-X-100) (Figure 4.1).

On AMT24 only, there were also two small SA maxima that were exclusive to the SML, centred around 26°N between NAST and NATR provinces with an average of 0.57 ± 0.07 mg L^{-1} eq. T-X-100 and at ~10°N in WTRA, (0.70 ± 0.14 mg L^{-1} eq. T-X-100) (Figure 4.1). It was also noticeable that the ranges in wind speed (U_{10}) between 36°N and 26°N (6.69 ± 1.33 m s^{-1}) and between 12°N and 9°N (3.91 ± 0.71 m s^{-1}) on AMT24 were somewhat higher than on AMT25 (4.77 ± 1.14 m s^{-1} ; 1.26 ± 0.35 m s^{-1} respectively). Also, as Figure 4.2. shows, salinity was comparatively low at ~10°N on both transects, but it was also about two salinity units lower during AMT24 (Salinity ~ 32) than during AMT25 (Salinity ~ 34) at this location.

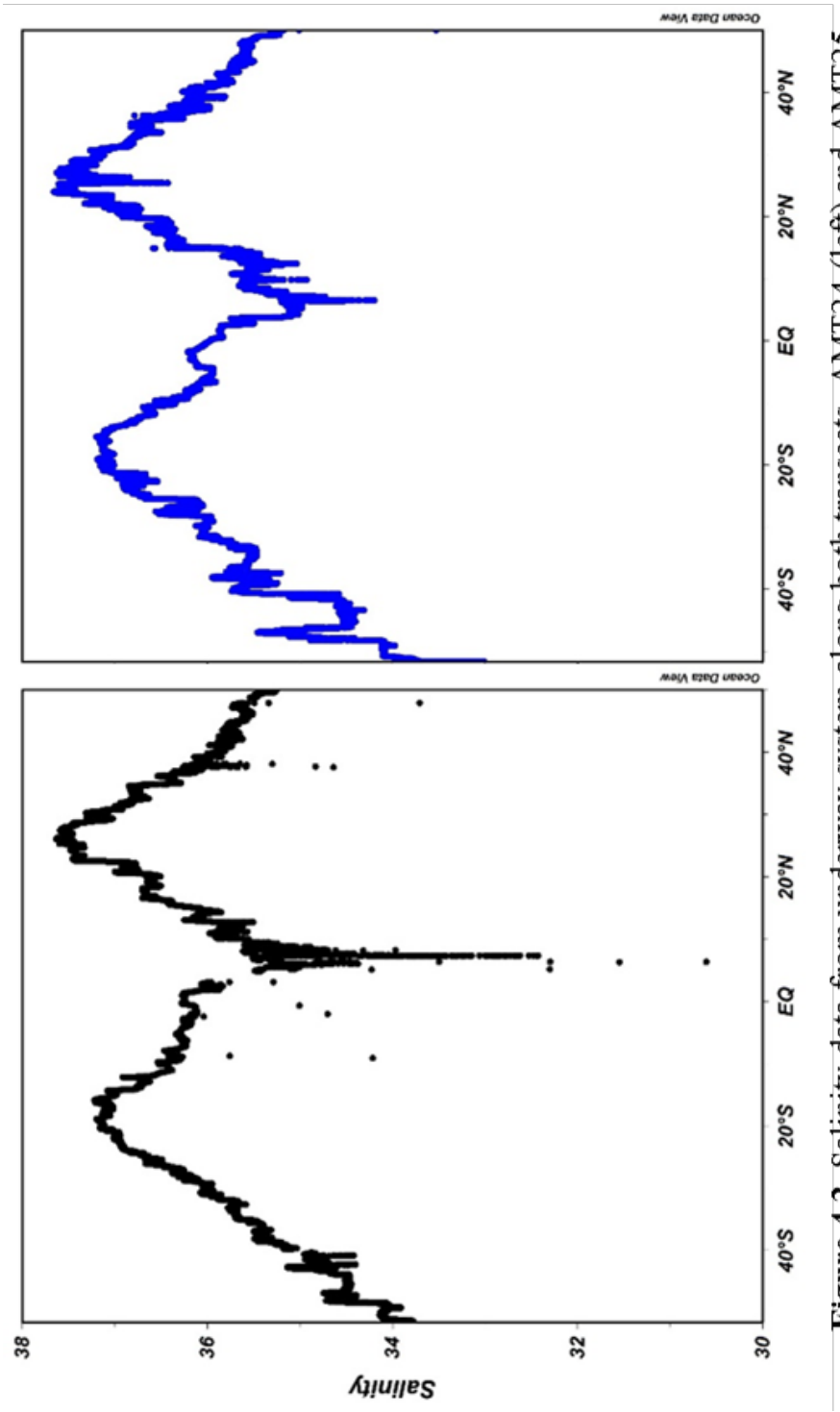

Figure 4.2. Salinity data from underway system along both transects, AMT24 (left) and AMT25 (right).

Additionally, high SA was observed at ~50°S in Falkland Islands (FKLD) (0.54 ± 0.01 mg L^{-1} eq. T-X-100) during AMT24. Evidence for this feature during AMT25 was either absent or comparatively limited (Figure 4.1).

An average SA in the Atlantic Ocean was found to be statistically higher in the SML compared to the SSW and as high as a factor of two on AMT25 (Two Sample t-test, testing H_0: the two means are equal against H_A: at least one mean is different; As µ1 - µ2 = 0.1319, $t_{95\%\ CI\ (2)\ 293}$ = 6.74, H_0 is rejected [$p < 0.001$]).

Average SA was also compared between the northern and the southern hemispheres for both transects (Table 4.1). The Atlantic Northern and Southern Hemisphere showed different SA ranges during this study. An average of SA in the SML and the SSW was statistically higher (as high as three times) in the Northern Hemisphere than in the Southern Hemisphere {(Two Sample t-test, testing H_0: the two means are equal against H_A: at least one mean is different; As µ1 - µ2 = 0.2107 and 0.4360, $t_{95\%\ CI\ (2)\ 57\ and\ 31}$ = 5.44 and 4.63, H_0 is rejected [$p < 0.001$] for SML AMT24 and AMT25 respectively) (Two Sample t-test, testing H_0: the two means are equal against H_A: at least one mean is different; As µ1 - µ2 = 0.0772 and 0.2366, $t_{95\%\ CI\ (2)\ 53\ and\ 35}$ = 9.43 and 5.94, H_0 is rejected [$p < 0.001$] for SSW AMT24 and AMT25 respectively)}.

Table 4.1. The mean, standard deviation and ranges of SA (SML) and SA (SSW) in the northern hemisphere and the southern hemisphere along AMT24 and AMT25 in the Atlantic Ocean.

Cruise No.	Date	Hemispheres	SA (SML) (mgL^{-1} eq. T-X-100)	SA (7m) (mgL^{-1} eq. T-X-100)
AMT24	Sep.-Nov. 2014	Northern	0.47 ± 0.20* (0.23-1.00)	0.23 ± 0.04 (0.10-0.36)
AMT24	Sep.-Nov. 2014	Southern	0.22 ± 0.10 (0.12-0.63)	0.15 ± 0.02 (0.10-0.20)
AMT25	Sep.-Nov. 2015	Northern	0.61 ± 0.51 (0.13-1.76)	0.35 ± 0.23 (0.11-0.91)
AMT25	Sep.-Nov. 2015	Southern	0.18 ± 0.06 (0.12-0.37)	0.12 ± 0.02 (0.08-0.17)

**Standard deviation*

() range of concentrations

On AMT24 average Northern Hemisphere SA was more than twice as high in the SML and about 1.5 times as high in SSW as in the Southern Hemisphere. On AMT25 Northern Hemisphere SA was also about three fold higher than in the Southern Hemisphere, both in the SML and in SSW. The differences in SML SA and SSW SA between the hemispheres were statistically significant (t-test, $p < 0.05$) on both cruises (Table 1.4).

4.2.2 *Surfactant enrichment factors (EF) in the Atlantic Ocean*

Further investigations showed that there is a broad significant positive correlation (Pearson correlation coefficient (r) = 0.85; $p < 0.001$, n = 205) between SML SA and corresponding SSW SA that implies a consistent SA enrichment in the SML compared to the corresponding underlying waters in the Atlantic Ocean (Figure 4.3). This is similar to the relationship found for CDOM (a_{300}) (Figure 3.11).

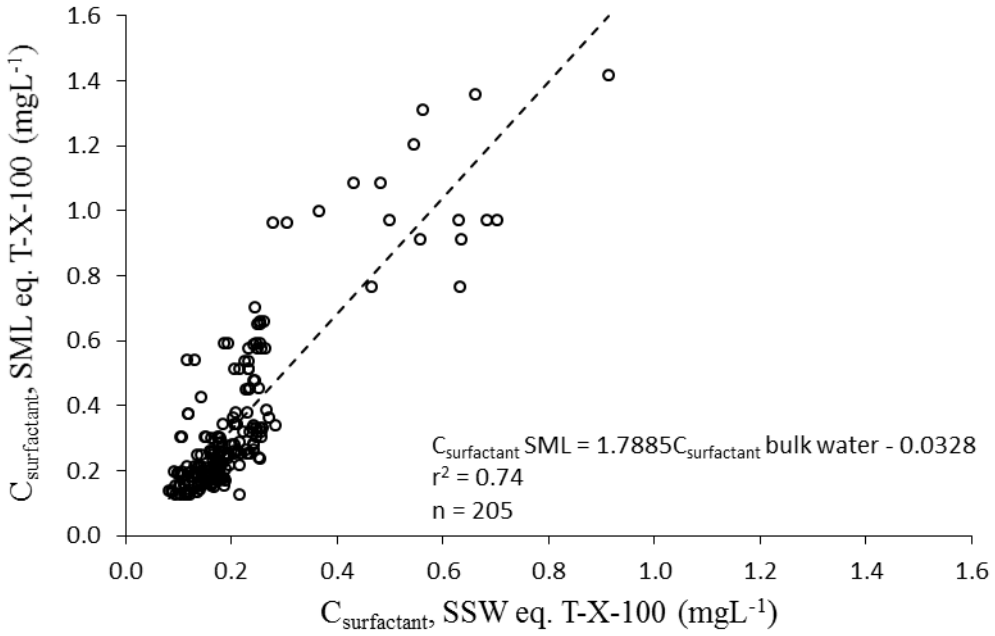

Figure 4.3. Surfactant activity (SA) in the sea surface microlayer against sub-surface Water (SSW = 7m) in the Atlantic Ocean. The dashed line represents the best linear fit. The r-squared (r^2) value of the linear fit and sample numbers are also indicated.

SA was enriched in the SML (EF > 1; see section 2.5.5) at 64 of 66 and 45 of 47 sampling locations during AMT24 and AMT25 respectively; the remaining four values of EF being ~ 0.96 ± 0.01 (Figure 4.4).

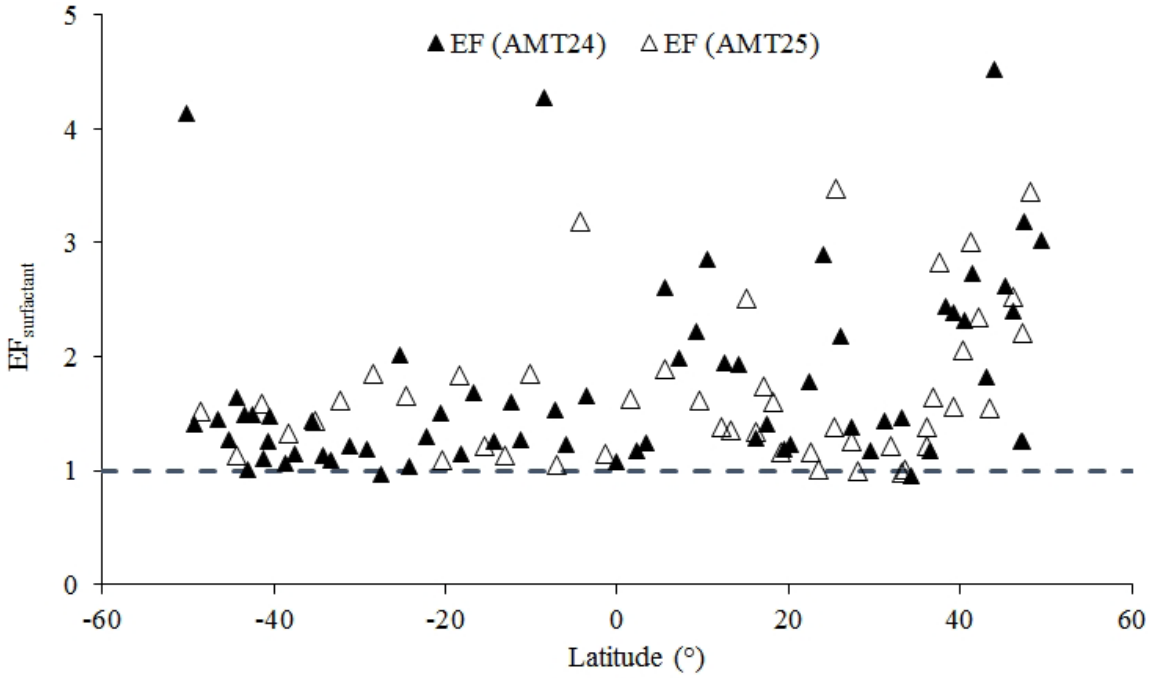

Figure 4.4. Latitudinal distribution of SA enrichment factors (EFs) in the SML of the Atlantic Ocean. AMT24 (filled triangle) and AMT25 (empty triangle). The dashed line represents the same concentration of surfactants in the SML and the SSW (i.e. EF = 1). Negative values of latitude represent the Southern Hemisphere.

Overall, EFs were an average of 1.74 ± 0.79 (range; 0.95 - 4.25) on AMT24 and 1.68 ± 0.65 (range; 0.97 - 3.47) on AMT25. The results were statistically similar between the two transects (Two Sample t-test, testing H_0: the two means are equal against H_A: at least one mean is different; As µ1 - µ2 = 0.061, $t_{95\%\ CI\ (2)\ 111} = 0.43$, H_0 is accepted [$p = 0.667$]). SA enrichment in the SML (i.e. EF > 1) in almost all sample locations in the current study confirms the findings of Wurl *et al*. (2011b) who showed surfactant enrichments in most oceanic samples. They suggested surfactant levels varying between 0.21 and 0.81 mg L^{-1} eq. T-X-100 with enrichment factors of 1.1 – 5.6 in the global oceans, based not on direct measurements but on primary productivity and wind speed proxies (Wurl *et al.*, 2011b).

EF maxima were observed at the same latitudes as the SML SA maxima (Figure 4.1), to the north of ~ 40°N (ECSW and NADR) on both transects. Another small EF maximum was centred around 10°N with an average of 1.70 ± 0.57 on AMT24 and 1.64 ± 0.72 on AMT25. An additional EF maximum at ~50°S (FKLD) (4.14 ± 0.2) during AMT24 was also observed at the same latitude as the SML SA maximum; however, this feature was absent during AMT25 (Figure 4.4 and Table 4.2).

The overall average of surfactant EFs in the Atlantic Northern Hemisphere was higher than the Atlantic Southern Hemisphere with a statistically significant difference observed on AMT24 only (Two Sample t-test, testing H_0: the two means are equal against H_A: at least one mean is different; As µ1 - µ2 = 0.445, $t_{95\%\ CI\ (2)\ 64} = 2.34$, H_0 is rejected [$p = 0.023$]).

The average Northern Hemisphere SA EF was 2.11 ± 0.92 (range; 0.96 - 4.52) on AMT24 and 1.75 ± 0.70 (range; 0.97 - 3.47) on AMT25, as compared to average Southern Hemisphere SA EFs of 1.51 ± 0.67 (range; 0.97 - 4.15) on AMT24 and 1.53 ± 0.52 (range; 1.05 - 3.19) on AMT25. Surfactant EF variations between the biogeochemical provinces are shown in Table 4.2.

Table 4.2. Surfactants enrichment factors (EF (SA)) in the biogeochemical Atlantic provinces. Mean, standard deviation and ranges of SA EFs on AMT24 and AMT25. The provinces are: European Continental Shelf Water (ECSW), North Atlantic Drift Region (NADR), North Atlantic Subtropical (NAST), North Atlantic Tropical (NATR), Western and Eastern Tropical Atlantic (W/ETRA), South Atlantic Gyre (SATL), South Subtropical Convergence Zone (SSTC) and Falkland Islands (FKLD).

	EF (SA)	
Provinces	**AMT24**	**AMT25**
ECSW (50-48°N)	3.02 ± 0.20	3.44 ± 0.45
NADR (48-42°N)	2.44 ± 1.16 (1.25 - 4.52)	2.09 ± 0.50 (1.54 - 2.52)
NAST (42-25°N)	1.78 ± 0.63 (0.96 - 2.73)	1.65 ± 0.69 (0.97 - 3.00)
NATR (25-10°N)	1.70 ± 0.57 (1.18 - 2.88)	1.64 ± 0.72 (1.01 - 3.47)
W/ETRA (10°N-5°S)	1.85 ± 0.68 (1.08 - 2.86)	1.89 ± 0.77 (1.14 - 3.19)
SATL (5-42°S)	1.43 ± 0.66 (0.97 - 4.27)	1.47 ± 0.30 (1.05 - 1.85)
SSTC (42-48°S)	1.39 ± 0.20 (1.01 - 1.64)	1.32 ± 0.27 (1.12 - 1.51)
FKLD (48-50°S)	4.14 ± 0.2	-

SA EFs from the same trophic (productivity) levels but different locations have been compared previously and revealed that surfactant enrichments are independent of location (Wurl *et al.*, 2011b). For example, surfactant EFs in the oligotrophic regions of the Arctic (2.7 ± 1.3) were not significantly different from EFs of waters of similar productivity in the North Pacific (2.3 ± 1.2) (Wurl *et al.*, 2011b). Dissolved organic carbon (DOC) enrichments have been also reported to be independent of location, time and wind state (Carlson, 1983).

A summary of SML SA and EFs reported for global aquatic environments compared to the current study are presented (Table 4.3).

Table 4.3. SA and EFs in the oceanographic regions with contrasting trophic states

Sampling region	Trophic states	Time (Month. Year)	EF (SA) (Ave ± SD.)	Range	SML SA (mgL^{-1} eq. T-X-100) (Ave. ± SD.)	Range	Reference
Atlantic Ocean	Oceanic	Sept-Nov. 2014	1.8 ± 0.8	1.0 - 4.5	0.34 ± 0.19	0.13 - 1.00	This study
Atlantic Ocean	Oceanic	Sept-Nov. 2015	1.6 ± 0.6	1.0 - 3.5	0.47 ± 0.40	0.12 - 1.76	This study
North Adriatic	Eutrophic	-	-	1.6 - 2.1		0.19 - 0.32 ($mgdm^{-3}$)	Marty *et al*. (1988)
Labrador Fjords	Oligotrophic	Nov. 2008	4.1 ± 1.0	-	-	-	Wurl *et al*. (2011)
Saanich Inlet	Eutrophic	Nov. 2008	2.3 ± 1.1	-	-	-	Wurl *et al*. (2011)
North Pacific	Oceanic	Jun. 2009	2.9 ± 1.3	1.1 - 5.3	0.43 ± 0.32	0.19 - 1.48	Wurl *et al*. (2011)
North Pacific	Offshore	Jun. 2009	1.7 ± 0.6	1.0 - 2.5	0.26 ± 0.03	0.23 - 0.32	Wurl *et al*. (2011)
Hawaii	Oligotrophic	Aug-Sep. 2009	2.5 ± 1.3	-	-	-	Wurl *et al*. (2011)
Subtropical North Pacific (HI)	Oceanic	Aug-Sep. 2009	2.3 ± 1.2	1.4 - 5.6	0.81 ± 0.44	0.29 - 1.57	Wurl *et al*. (2011)
Subtropical North Pacific (HI)	Coastal (offshore)	Aug-Sep. 2009	1.7 ± 1.1	0.6 - 4.4	0.32 ± 0.16	0.11 - 0.67	Wurl *et al*. (2011)
Saanich Inlet	Nearshore	Jun-Sep. 2008	1.9 ± 0.6	-	0.62 ± 0.54	0.10 - 4.98	Wurl *et al*. (2011)
Saanich Inlet	Nearshore	May. 2009	1.9 ± 1.0	0.5 - 5.6	0.62 ± 0.54	0.10 - 4.98	Wurl *et al*. (2011)
Vancouver Island	Offshore	May-Jun. 2009	1.8 ± 0.9	0.6 - 3.5	0.61 ± 0.39	0.24 - 1.26	Wurl *et al*. (2011)
Vancouver Island	Coastal (nearshore)	May-Jun. 2009	2.5 ± 1.3	0.7 - 4.5	0.71 ± 0.52	0.19 - 0.1	Wurl *et al*. (2011)
California (CA)	Offshore	Sept. 2008	1.8 ± 1.1	0.6 - 5.0	0.40 ± 0.13	0.20 - 0.82	Wurl *et al*. (2011)
Arctic (AC)	Coastal (nearshore)	Oct.-Nov. 2009	4.8 ± 1.1	1.4 - 5.6	0.24 ± 0.02	0.21 - 0.27	Wurl *et al*. (2011)
Arctic (AC)	Offshore	-	2.0 ± 0.4	3.2 - 5.9	0.27 ± 0.07	0.17 - 0.41	Wurl *et al*. (2011)
Arctic(AC)	Oceanic	Oct.-Nov. 2009	2.7 ± 1.3	1.5 - 2.6	0.21 ± 0.09	0.10 - 0.38	Wurl *et al*. (2011)
Middle Adriatic Sea	Coastal	May-Oct	3.4 ± 1.4	1.4 - 5.1	-	-	Frka *et al.* (2009)
River Tyne	Estuary	May-Sept.2007	-	0.8 - 8.0	-	0.35 - 1.12	Salter (2010)
North Sea	Coastal	-	-	1.2 - 20	-	0.01 - 0.3 (ULW)	Salter (2010)
Adriatic Sea	Oceanic	April 1978 - Jan. 1980	≤ 2.5		-	0.32 - 0.64 ($mgd^{-1}m^{-3}$)	Ćosović and Vojvidić (1982)
North Adriatic Sea	Oceanic	Aug.-June (1989 - 1993)	-		-	0.06 - 0.4 (ULW, 0.5m depth, filtered samples)	Ćosović and Vojvidić (1989)
Adriatic Sea	Oceanic	Fab. 1998 -Jan. 2000	-	-	-	0.04 - 0.16 ($mgd^{-1}m^{-3}$)	Gašparović and Ćosović (2001)
Adriatic Sea	Oceanic -culture media		-	-	-	0.015 - 0.475 ($mgd^{-1}m^{-3}$)	Vojvidić and Ćosović (1996)
Sargasso Sea-Middle Atlantic Bight	Coastal	1993 - 1994	-	-	-	1.5 - 3	Frew *et al*. (2002)
Sargasso Sea-Middle Atlantic Bight	Oceanic	1994 - 1994	-	-	-	0.05 - 0.15	Frew *et al*. (2002)
Norwegian fjords	Coastal - Oceanic	July 2001 - Jun. 2003	-	1.2 - 2.8		0.075 - 0.138 (ULW)	Gašparović *et al*. (2007)
Southern Ocean (Iron release)	Oceanic	Feb. 2004	-	-	-	0.005 - 0.03 (ULW)	Croot *et al*. (2007)
Kirka River	riverine	May-Oct.	-	-	0.30 ± 0.13 ($mgd^{-1}m^{-3}$) (ULW)	-	Frka *et al*. (2009)
Kirka River	riverine	Winter	-	-	0.06 ± 0.02 ($mgd^{-1}m^{-3}$) (ULW)	-	Frka *et al*. (2009)
Santa Barbara Channel	Oceanic	Sept. 2008	-	0.57 - 7.1	-	0.11 - 0.637 (ULW)	Wurl *et al*. (2009)
Northern Adriatic Sea	Oceanic	Feb. 1998 - Jan. 2003	1.06		0.35 ± 0.10 ($mgCL^{-1}$)	0.15 - 0.67 ($mgCL^{-1}$) (Depth fractionated)	Gašparović (2012)
Northern Adriatic Sea	Oceanic	Feb. 2005 - Aug. 2010	1.03		0.27 ± 0.08 ($mgCL^{-1}$)	0.15 - 0.48 ($mgCL^{-1}$) (Depth fractionated)	Gašparović (2012)
Northern Adriatic Sea	Mesotrophic-Oceanic	Feb. 1998 - Jan. 2003	1.08		0.37 ± 0.12 ($mgCL^{-1}$)	0.09 - 0.66 ($mgCL^{-1}$) (Depth fractionated)	Gašparović (2012)
Northern Adriatic Sea	Mesotrophic-Oceanic	Feb. 2005 - Aug. 2010	1.1		0.32 ± 0.10 ($mgCL^{-1}$)	0.09 - 0.64 ($mgCL^{-1}$) (Depth fractionated)	Gašparović (2012)
Northern Adriatic Sea	Oceanic	2001 - 2002			0.083	0.042 - 0.145	Gašparović *et al*. (2011)
North Sea	Offshore coastal transect	Jan. 2012 - Dec. 2013	-	~1.0 - 1.9	-	0.08 - 0.38	Pereira *et al*. (2016)

SA in the SML and its EFs from both transects during the current study were mostly within the range of 0.21 - 0.81 mg L^{-1} eq. T-X-100 and 1.1 - 5.6 respectively suggested for oceanic regions (Wurl *et al.*, 2011b).

Table 4.3 shows that in general, samples from eutrophic coastal waters tend to have higher ranges in SA in the SML and lower SA enrichment factors than oligotrophic open oceans. For example, SA EF ≤ 2.5 were reported for the Adriatic Sea between April and January (Ćosović and Vojvodić, 1982). The averages EFs of 1.7 ± 0.7 and 4.9 ± 2.4 in non-slick and slick samples respectively were however observed at Santa Barbara Channel, a highly productive area (Wurl *et al.*, 2009).

A five year study of surfactants in the northern Adriatic Sea also revealed average SA EFs of 1.3 in oceanic filtered samples (Gašparović, 2012), slightly lower than SA EFs found in the current study but not significantly ($p < 0.05$).

Salter (2010) reported SA in a range 0.35 and 1.12 mg L^{-1} eq. T-X-100 with EFs between 0.8 and 8.0 during May and September 2007 in the River Tyne estuary. SA EFs were also reported between 1.2 and 20.0 along a 20 km offshore transect in the North Sea (Salter, 2010). These very high EFs presumably are linked to inputs of terrestrially derived surfactant in this region. Pereira *et al.* (2016) reported SA EFs ranged ~ 1.0 to 1.9 using the same transects in the North Sea between January 2012 and December 2013, which is significantly lower than the earlier study by Salter (2010), which sampled the same stations.

SA EFs were also inversely correlated with SA in the SSW whilst high EFs were mostly observed when SA in the SSW was < 0.4 mg L^{-1} eq. T-X-100 (Figure 4.5).

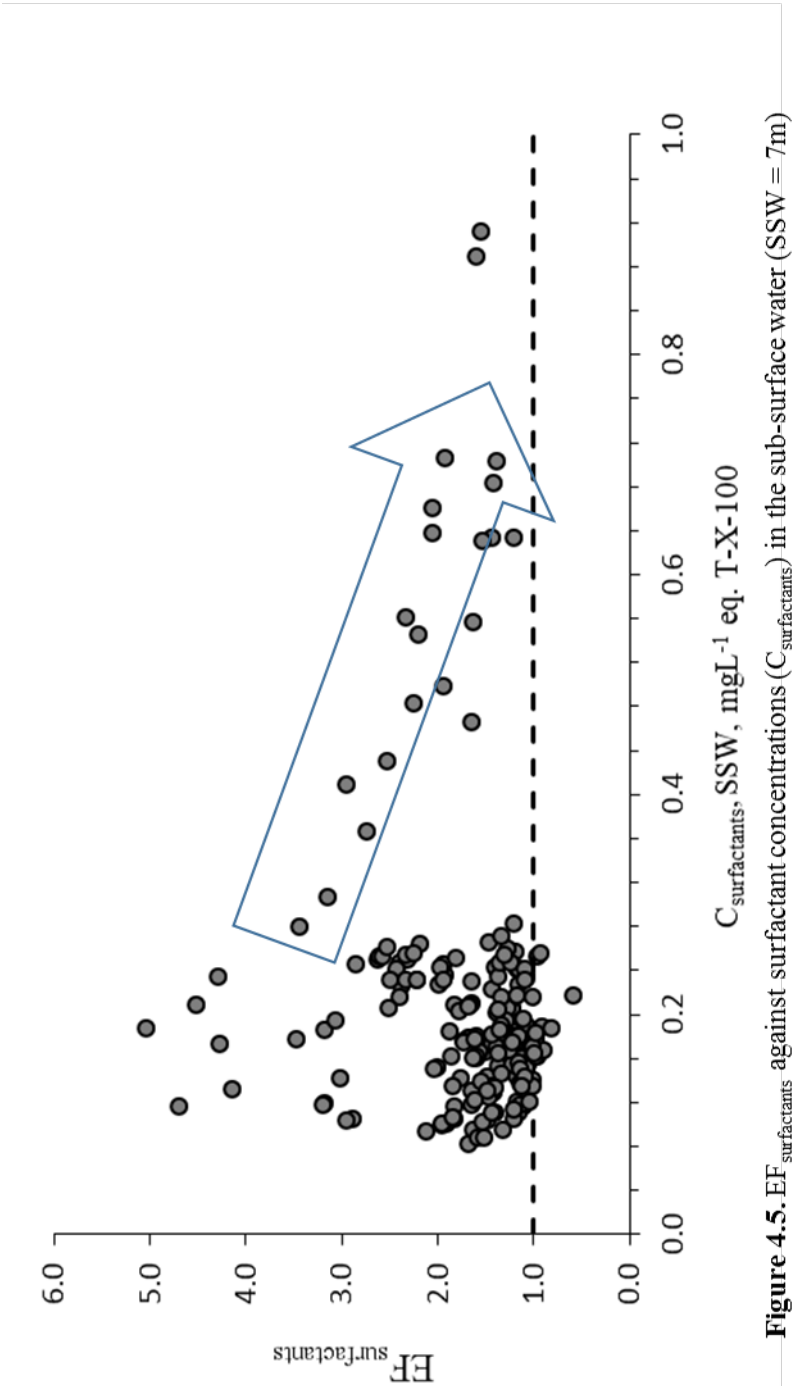

Figure 4.5. $EF_{surfactants}$ against surfactant concentrations ($C_{surfactants}$) in the sub-surface water (SSW = 7m) Dashed line represents the equal concentration in the sea surface microlayer (SML) and the corresponding sub-surface water (SSW). The arrow displays $EF_{surfactants}$ reduction beyond a threshold value of $C_{surfactants}$ (0.4 mgL^{-1} eq. T-X-100) in the SSW.

It is also noticeable that when SSW SA exceeded this threshold, EFs were mostly less than 2.6 in the Atlantic oceanic samples (Figure 4.5).

The consistent observations of low EFs coincident with high SA in the subsurface waters is also supported by Wurl *et al.* (2011), who reported EF values < 2.7 for SA values in the subsurface waters > 0.6 mg L^{-1} eq. T-X-100.

4.2.3 *Depth distributions of surfactants in the Atlantic Ocean*

Surfactants in the open oceans are derived from diverse sources, for example phytoplankton production and bacterial degradation (see Chapter 1). Hence, important features of the SA distributions are likely to relate to these sources.

Depth profiles of SA in this study are mainly focused on the top 100 m because this is the region where most light-dependent biological activity occurs (Zubkov *et al.*, 1998). It has been reported previously that heterotrophic[9] bacteria have higher metabolic activities shallower than 100m and that their contribution to production decreases to 10 - 20% of total bacterial production in water deeper than 100 m. Also, autotrophic [10] phytoplankton are mostly distributed at depths shallower than 200 m (Zubkov *et al.*, 1998). So, SA depth profiles were routinely sampled between surface waters and 100m depth on both cruises.

The average value of SA in top 100m of the water column (and including the SML) was 0.21 ± 0.10 mg L^{-1} eq. T-X-100 (range 0.09 – 1.00 mg L^{-1} eq. T-X-100) on AMT24 and 0.31 ± 0.28 mg L^{-1} eq. T-X-100 (range 0.06 - 1.77 mg L^{-1} eq. T-X-100) on AMT25.

There were no discernible differences in SA depth profiles within provinces so profiles for all stations are not shown. Figure 4.6 summarises typical SA profiles for each oceanographic province sampled, with station locations identified on the map.

[9] heterotroph; an organism that obtains nourishment from the ingestion and breakdown of organic matter

[10] autotroph; an organism capable of synthesizing organic nutrients directly from simple inorganic compounds such as carbon dioxide and inorganic nitrogen

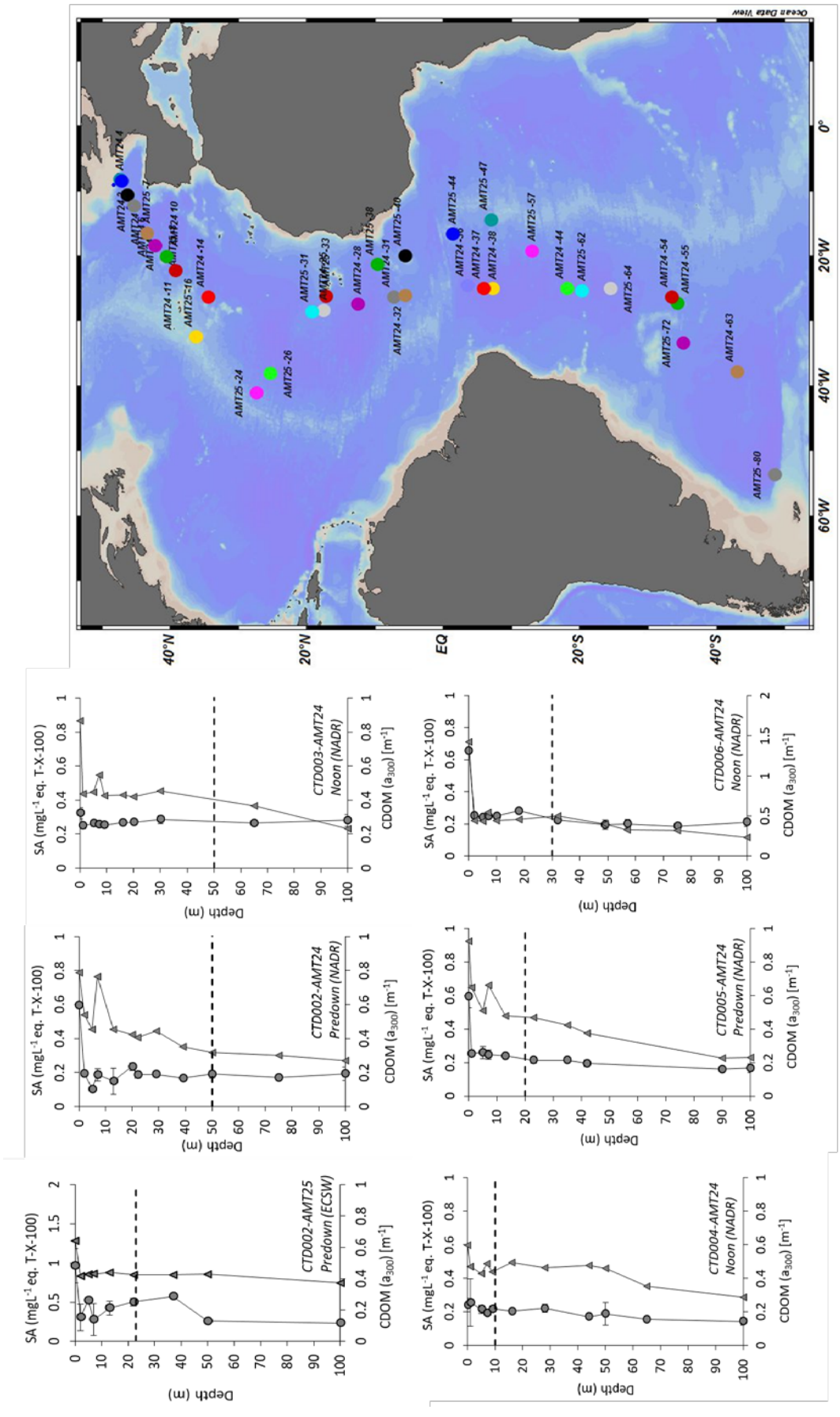

Figure 4.6. Sampling locations for surfactants depth profile determination during AMT24 and AMT25 (right) and typical depth profile of surfactants (circle) and chromophoric dissolved organic matter (CDOM) (triangle) in the biogeochemical provinces of the Atlantic Ocean (left). The provinces are European Continental Shelf Water (ECSW), North Atlantic Drift Region (NADR), North Atlantic Sub-Tropical Region (NAST), North Atlantic Tropical Region (NATR), Western Tropical Atlantic (WTRA), South Atlantic Gyre (SATL), South Sub-Tropical Convergence (SSTC) and Falkland Shelves (FKLD). Dashed line represents mixed layer depth MLD (m). Error bars represent standard deviation from the mean.

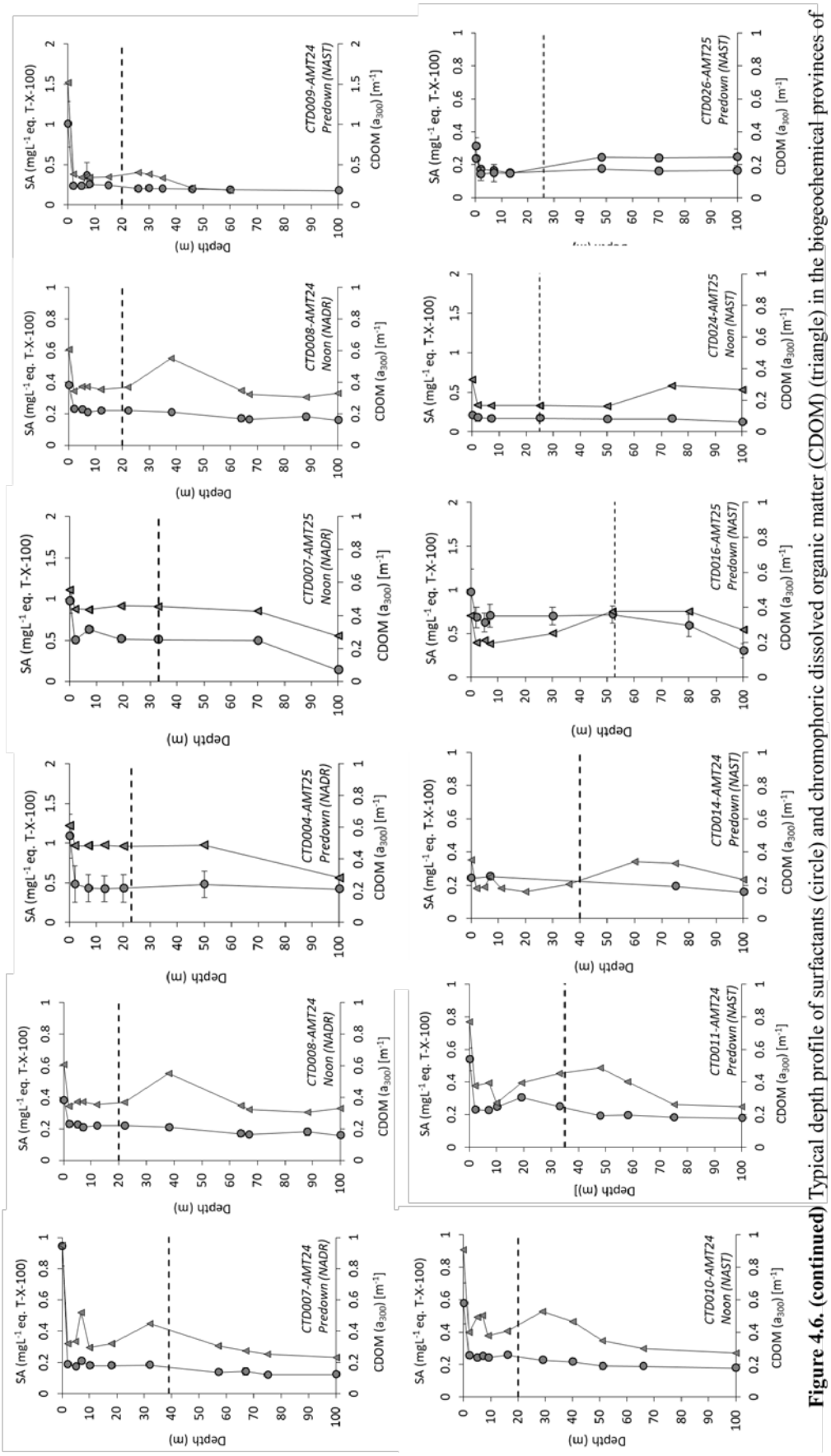

Figure 4.6. (continued) Typical depth profile of surfactants (circle) and chromophoric dissolved organic matter (CDOM) (triangle) in the biogeochemical provinces of the Atlantic Ocean. The provinces are European Continental Shelf Water (ECSW), North Atlantic Drift Region (NADR), North Atlantic Sub-Tropical Region (NAST), North Atlantic Tropical Region (NATR), Western Tropical Atlantic (WTRA), South Atlantic Gyre (SATL), South Sub-Tropical Convergence (SSTC) and Falkland Shelves (FKLD). Dashed line represents mixed layer depth MLD (m). Error bars represent standard deviation from the mean.

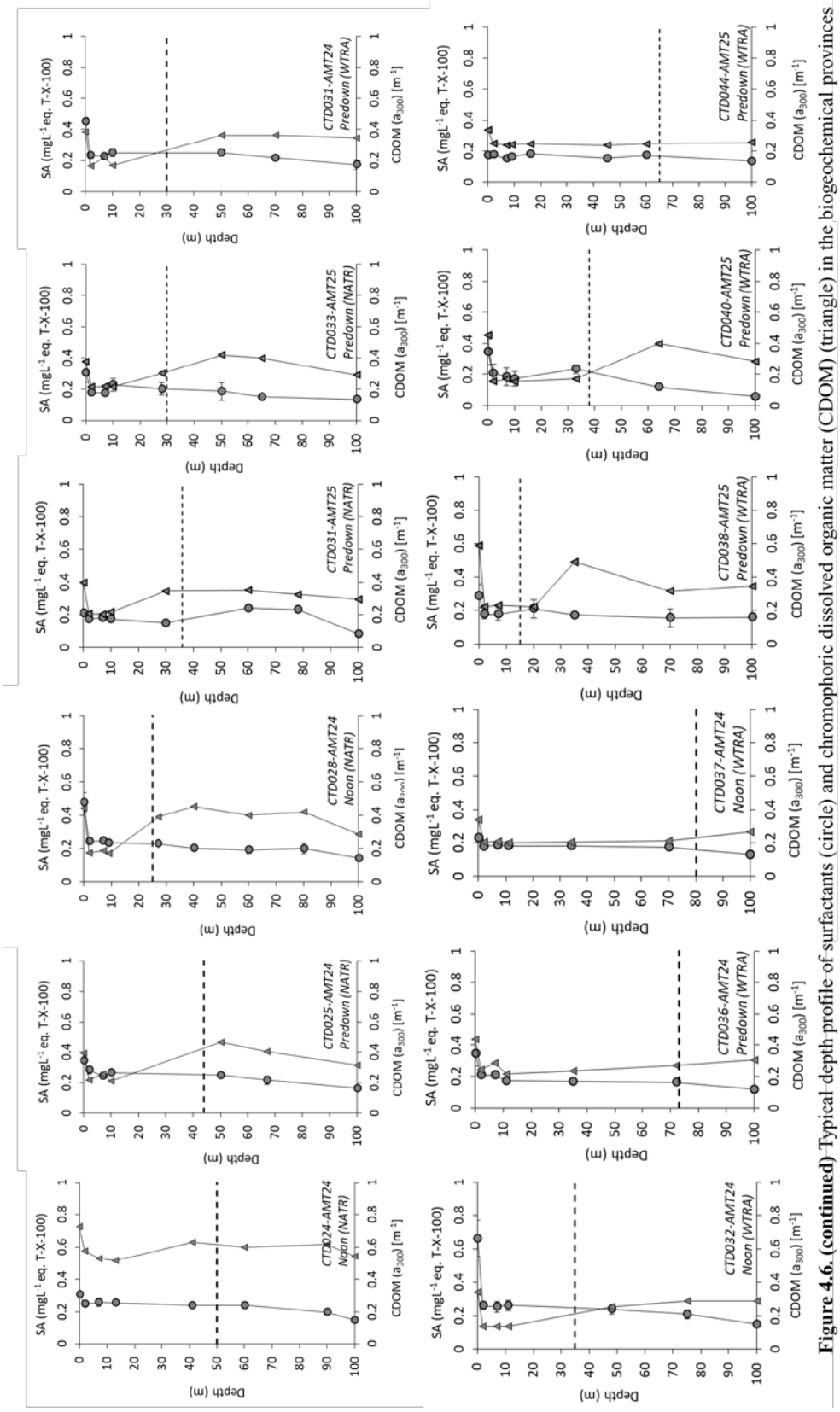

Figure 4.6. (continued) Typical depth profile of surfactants (circle) and chromophoric dissolved organic matter (CDOM) (triangle) in the biogeochemical provinces of the Atlantic Ocean. The provinces are European Continental Shelf Water (ECSW), North Atlantic Drift Region (NADR), North Atlantic Sub-Tropical Region (NAST), North Atlantic Tropical Region (NATR), Western Tropical Atlantic (WTRA), South Atlantic Gyre (SATL), South Sub-Tropical Convergence (SSTC) and Falkland Shelves (FKLD). Dashed line represents mixed layer depth MLD (m). Error bars represent standard deviation from the mean.

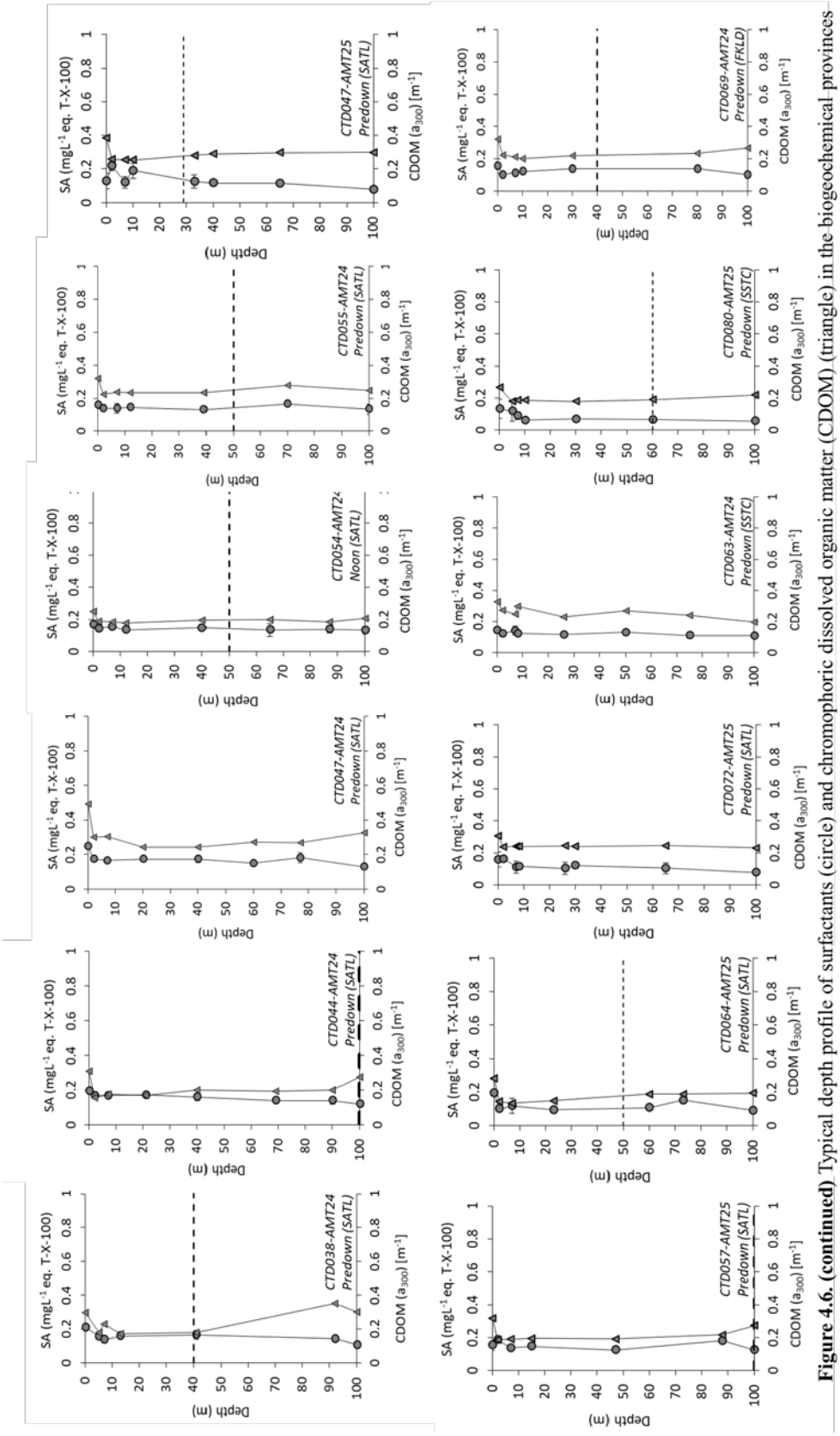

Figure 4.6. (continued) Typical depth profile of surfactants (circle) and chromophoric dissolved organic matter (CDOM) (triangle) in the biogeochemical provinces of the Atlantic Ocean. The provinces are European Continental Shelf Water (ECSW), North Atlantic Drift Region (NADR), North Atlantic Sub-Tropical Region (NAST), North Atlantic Tropical Region (NATR), Western Tropical Atlantic (WTRA), South Atlantic Gyre (SATL), South Sub-Tropical Convergence (SSTC) and Falkland Shelves (FKLD). Dashed line represents mixed layer depth MLD (m). Error bars represent standard deviation from the mean.

Figure 4.6 also shows that vertical SA distributions are also rather similar between oceanographic provinces as well as within them. Typically, SA declined steeply below the SML and was then rather constant from sub-surface waters down to 100 m depth.

In agreement with the current study, Ćosović *et al*. (1985) also found SA maxima in the SML, and a decline in SA through the water column to a depth of 100 m in the western Mediterranean Sea and in coastal waters of the Adriatic Sea.

Notably, samples collected from the DCM were not elevated in SA relative to other samples. Associated CDOM profiles follow the same general trend, with CDOM maxima in the SML, a sharp decrease into sub-surface waters and approximately constant values below this (Figure 4.6).

For further investigation, the data were split into two subgroups; above and below the base of the mixed layer, and SA distributions within the water column were examined accordingly. On both cruises and in all biogeochemical provinces SA was always higher above (shallower) than below (deeper) the base of the mixed layer (Table 4.4). However, the difference was not statistically significant (Two Sample t-test, testing H_0: the two means are equal against H_A: at least one mean is different; As µ1 - µ2 = 0.0671 and 0.1186, $t_{95\%\ CI\ (2)\ 8}$ = 2.27 and 1.38, H_0 is accepted [p = 0.060 and 0.206] on AMT24 and AMT25 respectively).

Table 4.4. Average and standard deviation of SA mg L^{-1} eq. T-X-100 above (shallower) (A-MLD) and below (deeper) (B-MLD) the base of the mixed layer in each individual biogeochemical province on AMT24 and AMT25 in the Atlantic Ocean

	SA (mgL^{-1} eq. T-X-100)	
Biogeochemical province	**A-MLD**	**B-MLD**
	AMT24	
ECSW	-	-
NADR	0.28 ± 0.15 (0.17 - 0.94)	0.18 ± 0.03 (0.11 - 0.28)
NAST	0.31 ± 0.15 (0.22 - 1.00)	0.19 ± 0.01 (0.16 - 0.23)
NATR	0.27 ± 0.10 (0.10 - 0.70)	0.19 ± 0.04 (0.13 - 0.26)
WTRA	0.25 ± 0.11 (0.16 - 0.66)	0.18 ± 0.04 (0.11 - 0.25)
SATL	0.17 ± 0.06 (0.09 - 0.74)	0.13 ± 0.02 (0.10 - 0.20)
SSTC	0.13 ± 0.03 (0.09 - 0.21)	0.12 ± 0.01 (0.10 - 0.14)
FKLD	0.16 ± 0.14 (0.10 - 0.54)	0.11 ± 0.01 (0.10 - 0.14)
	AMT25	
ECSW	0.49 ± 0.24 (0.27 - 0.96)	0.35 ± 0.18 (0.23 – 0.57)
NADR	0.57 ± 0.30 (0.13 - 1.31)	0.28 ± 0.16 (0.06 - 0.49)
NAST	0.52 ± 0.38 (0.11 - 1.77)	0.27 ± 0.18 (0.08 - 0.75)
NATR	0.21 ± 0.06 (0.15 - 0.51)	0.15 ± 0.05 (0.08 - 0.23)
WTRA	0.18 ± 0.06 (0.09 - 0.37)	0.14 ± 0.04 (0.05 - 0.21)
SATL	0.13 ± 0.04 (0.07 - 0.25)	0.10 ± 0.03 (0.05 - 0.20)
SSTC	0.10 ± 0.03 (0.06 - 0.16)	0.08 ± 0.03 (0.05 - 0.13)
FKLD	-	-

Average SA above the base of the mixed layer decreased gradually from higher latitudes to lower latitudes in the Northern Hemisphere. This decline continued towards the Southern Hemisphere (i.e. a steady meridional gradient), SA decreasing by almost 50% from NADR and NAST towards SSTC on AMT24 and by almost six-fold on AMT25 (Table 4.4). Around the Falkland Islands, there was a slight increase in average SA compared to the adjacent SSTC province (data available for AMT24 only) (Table 4.4).

SA below the base of the mixed layer showed a constant trend, as above the base of the mixed layer, with a discernible decrease from higher latitudes towards lower latitudes in the Northern and Southern Hemisphere, although the changes from higher to lower latitudes were smaller than for SA above the base of the mixed layer (Table 4.4). The differences in SA above and below the base of the mixed layer were however not statistically significant on either cruise (t-test, $p > 0.05$).

High SA above the base of the mixed layer was also reported previously with no statistically significant difference from deeper waters below the base of the mixed layer to 200 m depth (Gašparović and Ćosović, 2001; Croot *et al.*, 2007; Wurl *et al.*, 2009). For example, Wurl *et al.* (2009) found higher SA above the base of the mixed layer (0.33 ± 0.20 mg L^{-1} eq. T-X-100) compared to the deeper waters (0.18 ± 0.07 mg L^{-1} eq. T-X-100) in the Santa Barbara channel while, the difference was not statistically significant ($p > 0.05$).

Croot *et al*. (2007) also reported a significantly higher SA around the base of mixed layer compared to the deeper waters during the Southern Ocean Iron fertilization experiment, suggestive of in-situ biological production in accordance with a greater abundance of phytoplankton in euphotic zone.

It is evident from the contour plot of SA distribution along the full extent of both transects to 100 m depth that in general, some “surfactant production zones” exist in the Atlantic Northern Hemisphere (Figure 4.7).

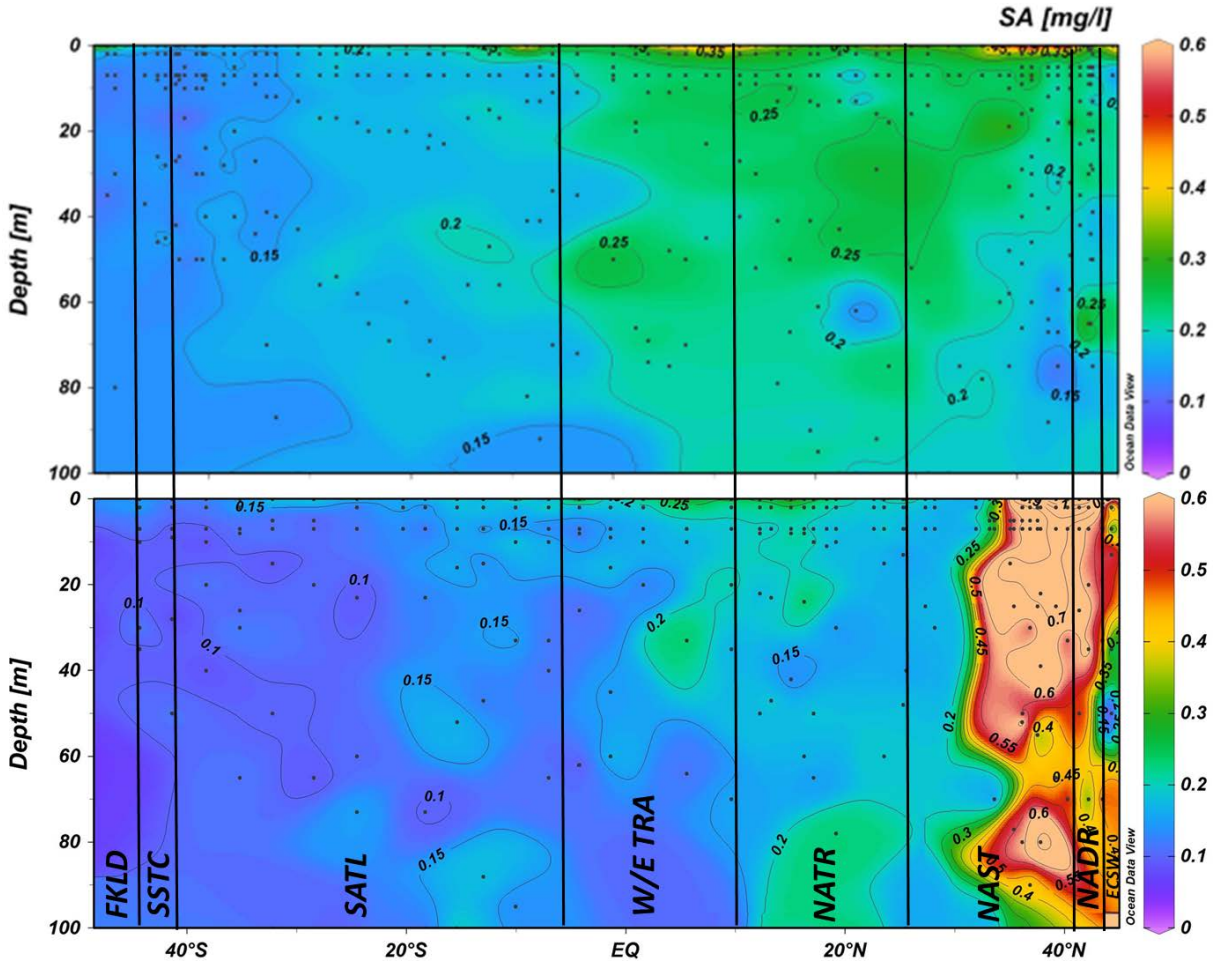

Figure 4.7. Contour plot of SA water column profile to 100m depth over the full extent of the transects on AMT24 (top) and AMT25 (bottom) in the Atlantic Ocean

As for the SML, overall, SA was higher in the Northern Hemisphere than in the Southern Hemisphere on both cruises. Northern Hemisphere SA was 1.5 times higher (0.24 ± 0.11 mg L^{-1} eq. T-X-100, range of 0.10 - 1.00 mg L^{-1} eq. T-X-100) than Southern Hemisphere SA (0.16 ± 0.06 mg L^{-1} eq. T-X-100, range of 0.09 - 0.74 mg L^{-1} eq. T-X-100) on AMT24. On AMT25, Northern Hemisphere SA was almost three times higher (0.36 ± 0.29 mg L^{-1} eq. T-X-100, range of 0.05 - 1.77 mg L^{-1} eq. T-X-100) than Southern Hemisphere SA (0.12 ± 0.04 mg L^{-1} eq. T-X-100, range of 0.05 - 0.37 mg L^{-1} eq. T-X-100). The SA difference between the hemispheres was statistically significant on both cruises (Two Sample t-test, testing H_0: the two means are equal against H_A: at least one mean is different; As µ1 - µ2 = 0.0824 and 0.2348, $t_{95\%\ CI\ (2)\ 399\ and\ 237}$ = 10.21 and 11.54, H_0 is rejected [$p < 0.001$] on AMT24 and AMT25 respectively).

The main feature of the SA depth distribution was that the high surface SA observed to the north of 35°N on AMT25 is present to 100m depth with an average (0.57 ± 0.31 mg L^{-1} eq. T-X-100) that is almost two times higher than on AMT24 (0.24 ± 0.13 mg L^{-1} eq. T-X-100). This difference was statistically significant (t-test $p < 0.05$). SA was also somewhat lower between the equator and 35°N on AMT25 (0.20 ± 0.11 mg L^{-1} eq. T-X-100) than on AMT24 (0.24 ± 0.08 mg L^{-1} eq. T-X-100).

The Atlantic Northern Gyre (42 - 25°N) also showed higher SA (0.22 ± 0.03 mg L^{-1} eq. T-X-100 and 0.39 ± 0.25 mg L^{-1} eq. T-X-100 on AMT24 and AMT25 respectively) than the Atlantic Southern Gyre (5 - 42°S) (0.16 ± 0.02 mg L^{-1} eq. T-X-100 and 0.12 ± 0.04 mg L^{-1} eq. T-X-100 on AMT24 and AMT25 respectively).

At 10 stations (5 stations on each cruise) deeper sampling was carried out to a maximum of 500m, with typically 4 of 7 samples above 100 m. These showed only small SA variability at most, within the deeper water column (Figure 4.8).

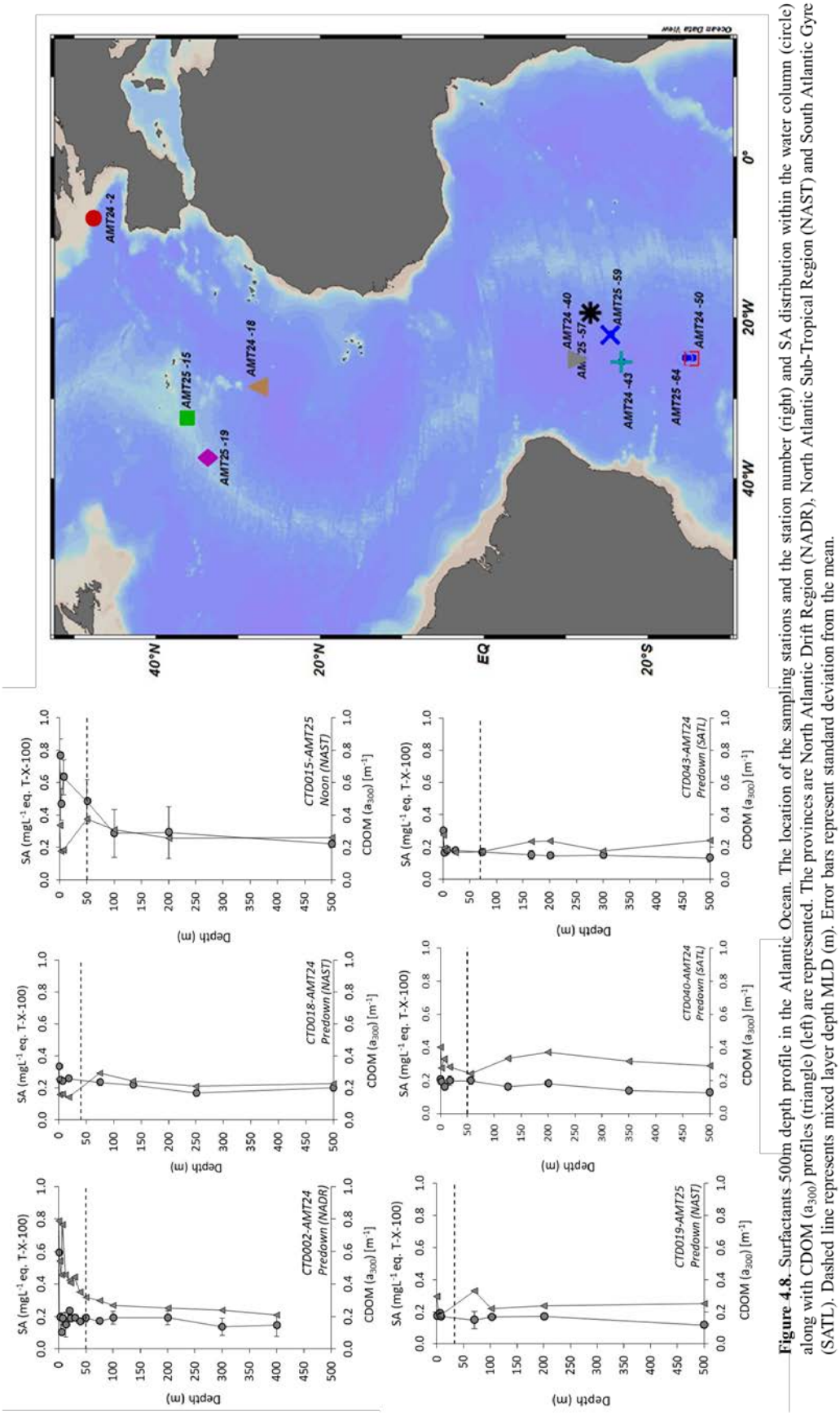

Figure 4.8. Surfactants 500m depth profile in the Atlantic Ocean. The location of the sampling stations and the station number (right) and SA distribution within the water column (circle) along with CDOM (a_{300}) profiles (triangle) (left) are represented. The provinces are North Atlantic Drift Region (NADR), North Atlantic Sub-Tropical Region (NAST) and South Atlantic Gyre (SATL). Dashed line represents mixed layer depth MLD (m). Error bars represent standard deviation from the mean.

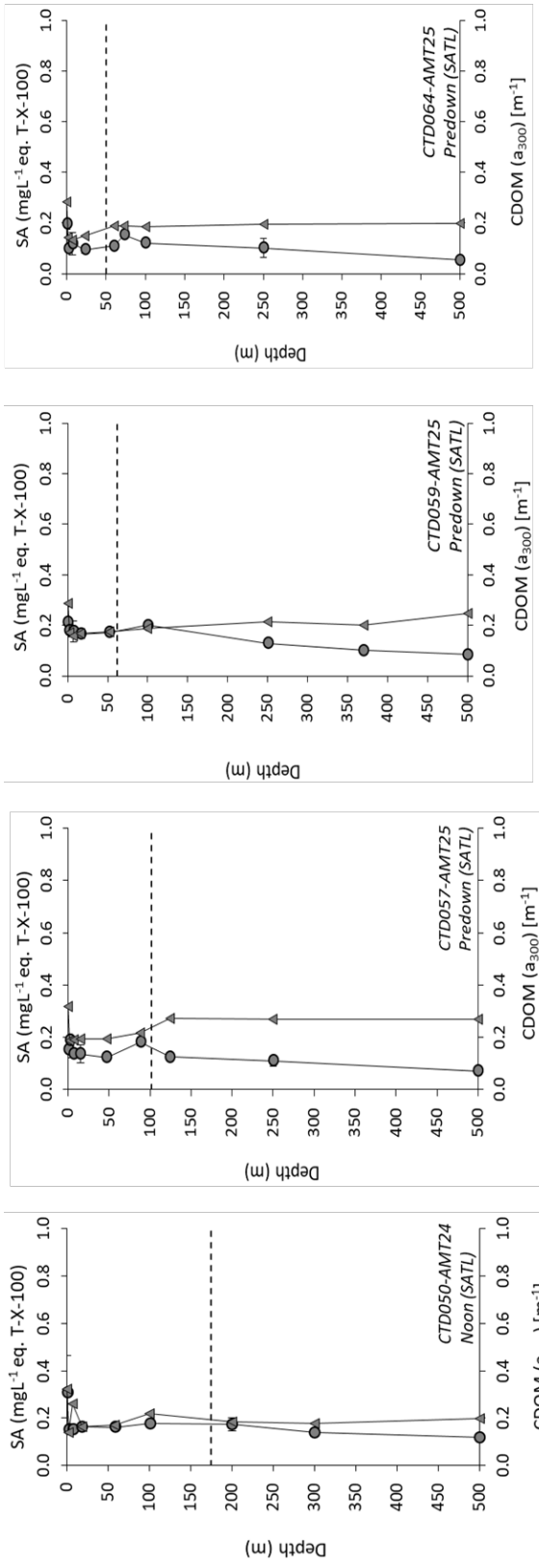

Figure 4.8. (continued) Surfactants 500m depth profile in the Atlantic Ocean. SA distribution within the water column (circle) along with CDOM (a_{300}) profiles (triangle) are represented. The provinces are North Atlantic Drift Region (NADR), North Atlantic Sub-Tropical Region (NAST) and South Atlantic Gyre (SATL). Dashed line represents mixed layer depth MLD (m). Error bars represent standard deviation from the mean.

CDOM showed a similar pattern to SA to 500m, with no significant changes in absorbance with depth. These profiles of SA and CDOM do not show any evidence of variability between Atlantic biogeochemical provinces (Figure 4.8).

4.2.4 *Association of surfactants and wind speed (U_{10n}) in the Atlantic Ocean*

The average values of wind speed normalised to 10 m height and corrected for atmospheric stability (U_{10n}) were 6.95 ± 2.17 m s^{-1} (range 0.65 - 12.93 m s^{-1}) on AMT24 and 4.94 ± 1.44 m s^{-1} (range 0.29 - 7.25 m s^{-1}) on AMT25. Evidently, surfactants were typically present in SML at all values of U_{10n} up to the highest recorded (~ 13 m s^{-1}) on both transects (Figure 4.9).

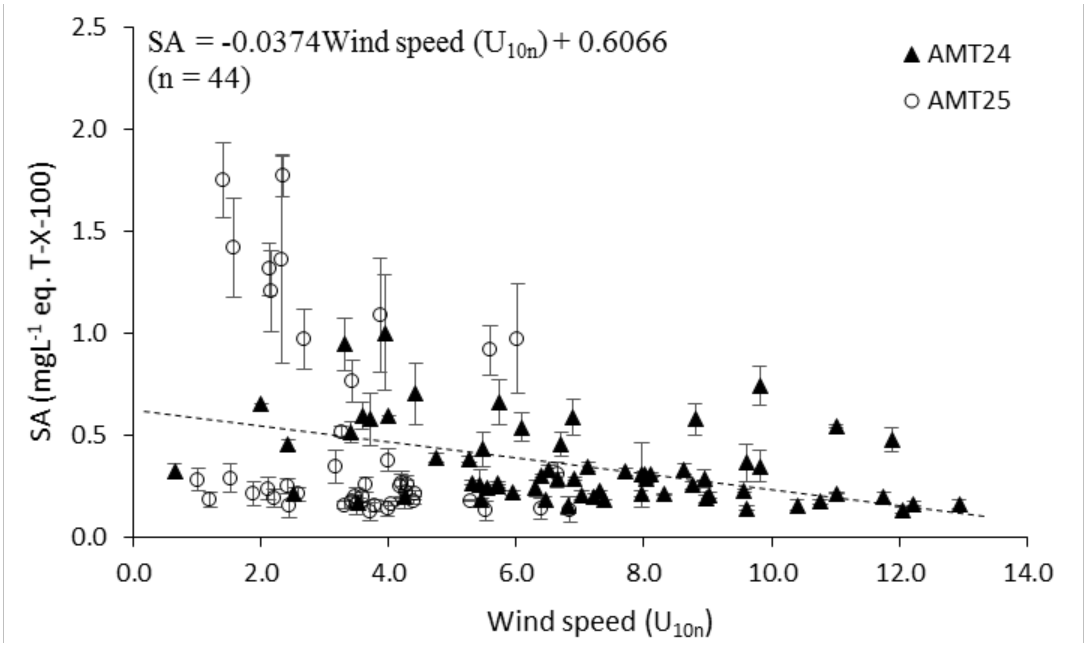

Figure 4.9. SA in the SML vs wind speed in the Atlantic Ocean. The data were derived from AMT24 (filled triangles) and AMT25 (circles). The dashed line represents the linear regression with linear equation present. The bars display the standard deviation of the mean. The sample numbers are also displayed.

Surfactant distributions in the SML showed an inverse correlation with wind speed under the sampling conditions encountered during this research (Figure 4.9) (Pearson correlation coefficient (r) = -0.318, p = 0.001). Although this result was significant, a linear regression showed that the model could not be used to predict surfactant distributions based on wind speed with any significant degree of confidence as the r^2 value was only 0.10 (Figure 4.9). This is consistent with a previous study by Wurl *et al.* (2011) who found no evidence of a significant relationship between surfactant distributions (and their enrichment factors in the SML) with wind speed in either the North Pacific or the Arctic Oceans.

Surfactants were also enriched in the SML compared to the corresponding sub-surface waters (i.e. EF > 1) at all wind speeds up to the maximum ~ 13 m s^{-1} observed in the current study (Figure 4.10). These results, showing high EF values at high wind speeds, are contrary to a previous prediction that high EFs for SA and other SML components poleward of both 30°N and 30°S in the Atlantic Ocean would be precluded at wind speeds > 12 m s^{-1} (Wurl *et al.*, 2011b) due to physical surface disturbance.

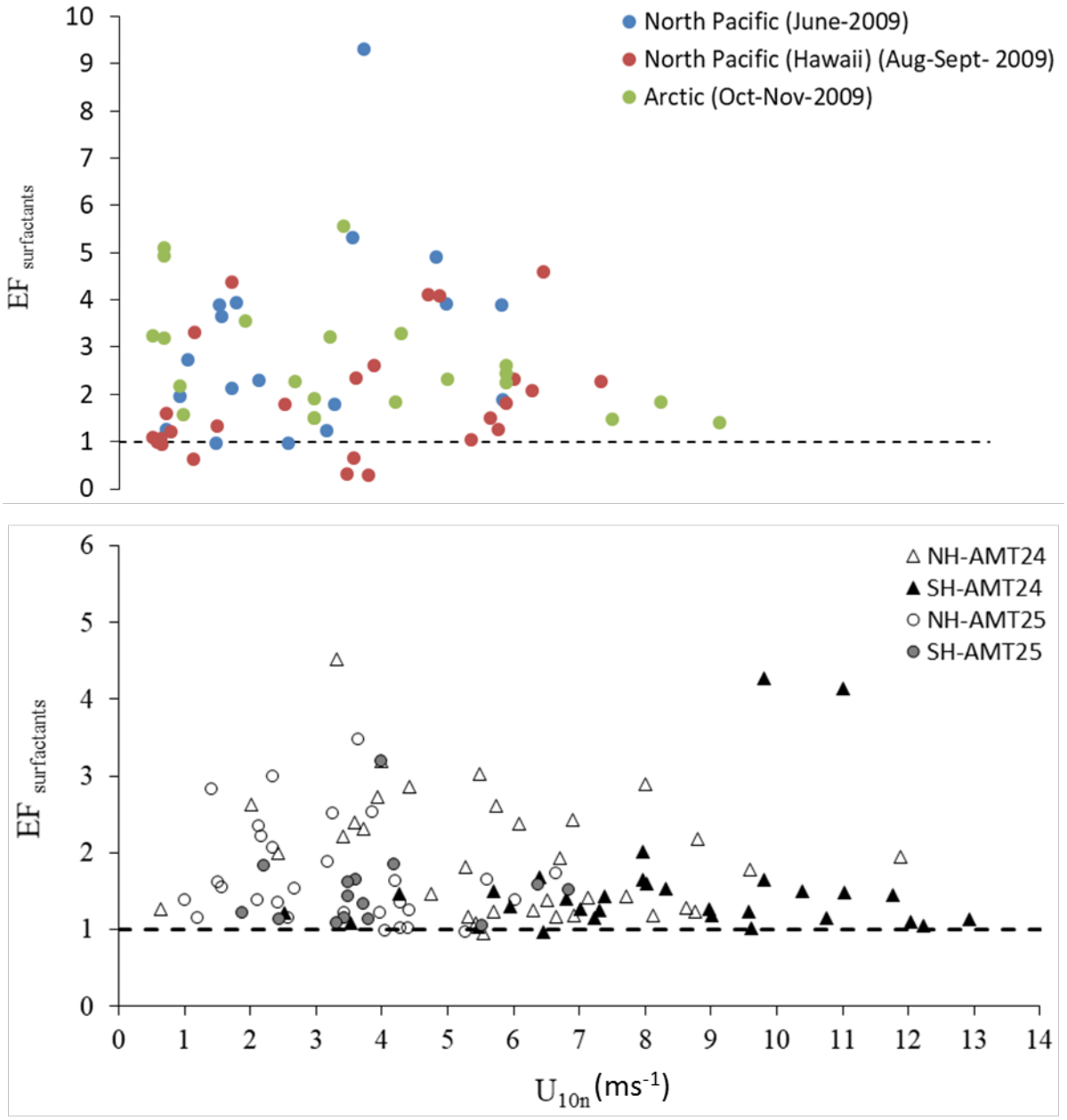

Figure 4.10. Surfactants enrichment factor ($EF_{Surfactants}$) against wind speed (U_{10n}) (ms^{-1}) in the Atlantic Ocean (bottom) and other oceanic sampling locations (top). The data along both transects (i.e. AMT24 and AMT25) split between the Northern Hemisphere (NH) and the Southern Hemisphere (SH) are represented. The dashed lines show EF = 1. The other global oceans data were kindly provided by Oliver Wurl.

In agreement with the current study, Reinthaler *et al.* (2008) also found SML enrichments in dissolved organic carbon (DOC) and amino acids at wind speeds greater than 7.5 m s^{-1}. They also reported the second highest enrichment of DOC (EF = 2.1) and dissolved free amino acids (DFAA) (EF = 2.6) at their highest recorded wind speeds (9.7 m s^{-1}) in the open Atlantic and the western Mediterranean Sea (Reinthaler *et al.*, 2008).

It should be pointed that SML stability at high wind speed represents invisible slicks whereas visible slicks will disrupt at wind speeds higher than 4 m s^{-1} (see section 1.1).

Carlson (1983) observed dissolved organic carbon (DOC) enrichment in the SML at wind speeds up to 8 m s^{-1}, however, there was no discernible influence of wind speed or wave state on DOC enrichment factors. It was suggested that accumulation and depletion processes were in balance (Carlson, 1983).

Frew *et al*. (2004) suggested that surfactant enrichments in the SML would be suppressed at wind speeds greater than 6 – 8 ms^{-1} during a field study.

Obernosterer *et al*. (2008) found an inverse correlation between SML particulate organic matter enrichment and wind speed in the South Pacific Ocean. However, it was suggested that wind speed history (i.e. at least 6 hours recorded wind speeds prior to measurements) is more important than instantaneous winds concerning SML enrichments. In agreement, Tilstone *et al*. (2010) also found high concentrations of chlorophyll-a at low wind speeds off the Iberian Peninsula.

The correlation between SA EFs and wind speed were not statistically significant on either transect (Pearson correlation coefficient (r) = -0.175, p = 0.164 and n = 65 on AMT24 and r = -0.165, p = 0.285 and n = 44 on AMT25 respectively).

The lack of any strong correlation between SA and wind speed during the current study is in agreement with the data from the Pacific and Arctic oceans (Figure 4.10).

4.2.5 *Relationships between SA and biological variables*

Chlorophyll-a has been used previously as a proxy for phytoplankton productivity to investigate any possible relationship with SA in the marine environment (Wurl *et al.*, 2009; Wurl *et al.*, 2011b). Therefore, the relationships between chlorophyll-a and SA were investigated for both cruises (Figure 4.11).

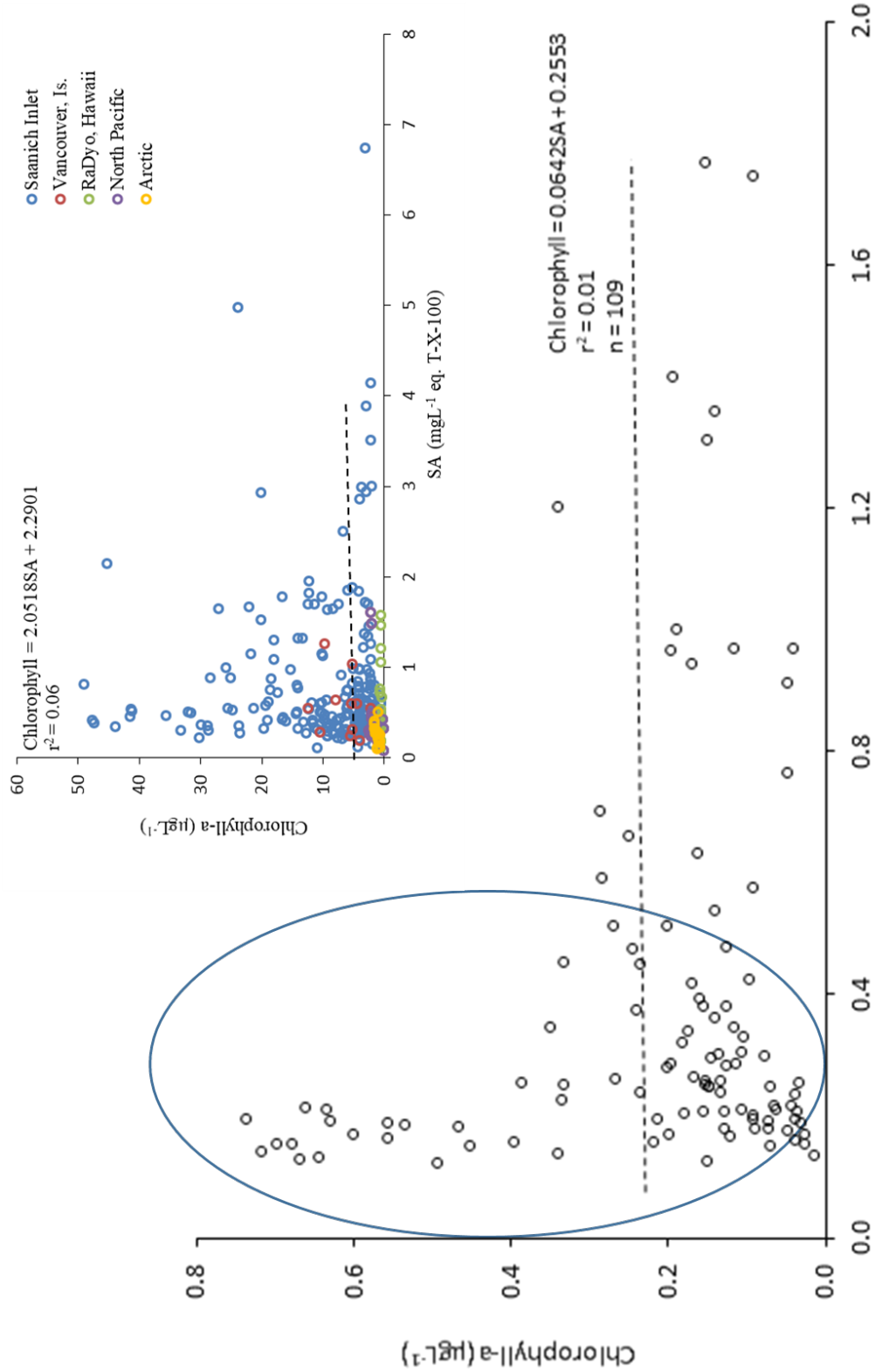

Figure 4.11. SA association with chlorophyll-a (μgL^{-1}) for the surface samples (SML) in the Atlantic Ocean. SA and chlorophyll relationship in other sampling locations is shown in the insert. Dashed lines represent the best linear fit. The linear regression model, r-squared (r^2) and sample number (n) are also indicated. The data points are combined from both cruises. The data excluding the Atlantic Ocean kindly provided by Oliver Wurl.

Overall, a positive relationship was found between chlorophyll-a and SA during this study but the correlation was not statistically significant (Pearson correlation coefficient (r) = 0.117, p = 0.226, n = 109). This is in agreement with earlier results from coastal and oceanic locations including Saanich inlet, Vancouver Island, Hawaii, North Pacific and Arctic (Wurl *et al.*, 2011b) (insert in Figure 4.11).

In concurrence with results from this study, the vertical distribution of surfactants did not correlate with fluorescence or chlorophyll in the Southern Ocean during an iron fertilisation experiment (Croot *et al.*, 2007). Wurl *et al*. (2009) also noticed no correlation between fluorescence and SA in the water column in the Santa Barbara Channel. However, they reported a positive correlation between fluorescence and SA above the base of the mixed layer (Wurl *et al.*, 2009). Pereira *et al.* (2016) also found no clear relationship between SA and chlorophyll-a in the coastal waters of the North Sea, suggesting that primary productivity is not a good proxy for SA. Gašparović *et al*. (2011) also found no significant correlation between chlorophyll-a and surfactants in the northern Adriatic Sea.

However, there are some contradictory results reported by Salter (2010) who found a strong positive relationship between SA and chlorophyll-a (r^2 = 0.76) during a phytoplankton bloom in a mesocosm experiment and also on a 20 km offshore coastal North Sea transect suggesting that phytoplankton produced surfactants were dominant at the sample location. This is probably because of only one phytoplankton species being dominant in the bloom event.

There is a cluster of the data points within the oval in Figure 4.11 showing that with increasing chlorophyll to a maximum of 0.8 µg L^{-1}, SA does not exceed 0.4 mg L^{-1} eq. T-X-100. For samples with SA above this threshold chlorophyll-a is below ~ 0.3 µg L^{-1}. The latter samples are mostly from higher latitudes on both transects (i.e. ECSW and NADR) and it may be that these include an SA component deriving from terrestrial sources not associated with chlorophyll-a, such as riverine humics (Figure 4.11).

Samples from the DCM in this study also did not show higher SA compared to the reminder of the water column, in contrast to the results of Wurl *et al*. (2009) who found higher SA in the DCM of the Santa Barbara channel, perhaps due to phytoplankton sinking through the water column.

Although it is widely assumed that natural surfactants in the oceans derive mainly from primary production, no strong correlation was observed between total primary productivity and SA in this study (Pearson correlation coefficient (r) = 0.005, p = 0.962, n = 80) (Figure 4.12).

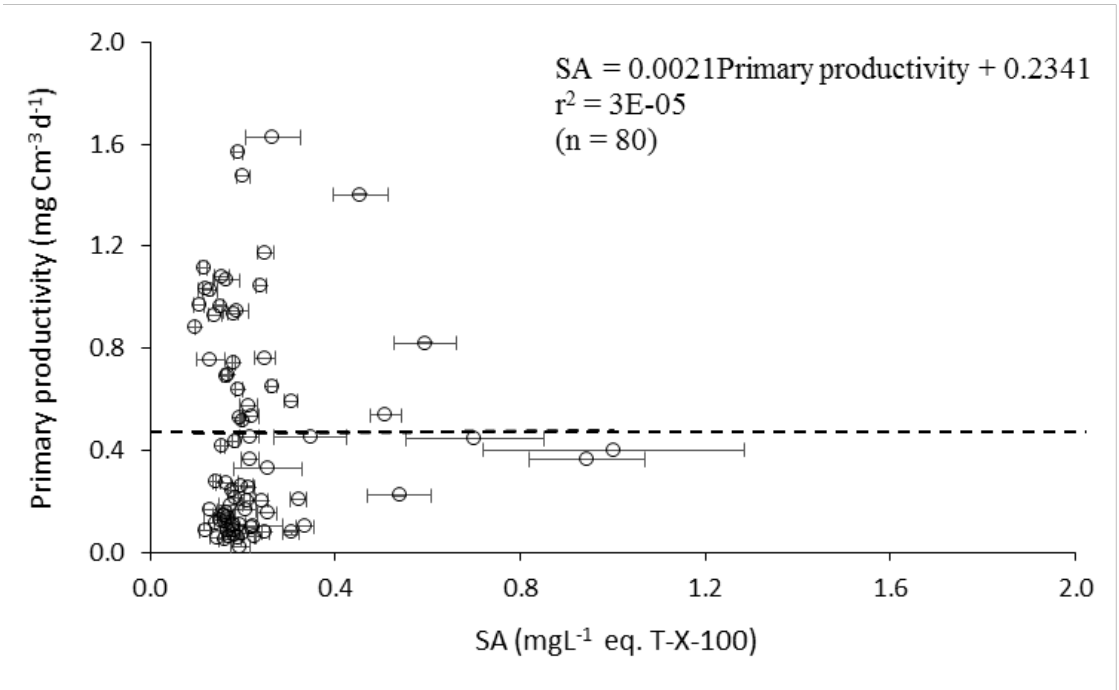

Figure 4.12. Primary productivity against SA in the Atlantic Ocean. The data are all depth and available for AMT24 only. Linear regression model, r-squared (r^2) and sample numbers are also indicated. The dashed line represents the best linear fit. Error bars display the standard deviation of the mean.

This was in contrast to Salter (2010) who found positive correlations between primary productivity and SA in the River Tyne Estuary and the coastal waters of the North Sea with the highest SA recorded during a phytoplankton bloom. Further, SA in the northern Adriatic Sea were found to be highly dependent on phytoplankton community production (Gašparović and Ćosović, 2001).

However, Wurl and Holmes (2008) showed that temporal variations in dissolved organic carbon (DOC), total dissolved carbohydrates (TDC), transparent exopolymer particles (TEP) and suspended particulate matter enrichment in the SML relative to corresponding sub-surface waters in oceanic samples is poorly correlated with biological parameters such as chlorophyll-a and primary productivity.

4.2.6 *SA-nutrients association*

Nutrient distributions in the SML and through the water column showed an inverse relationship with SA in the Atlantic Ocean (Figure 4.13).

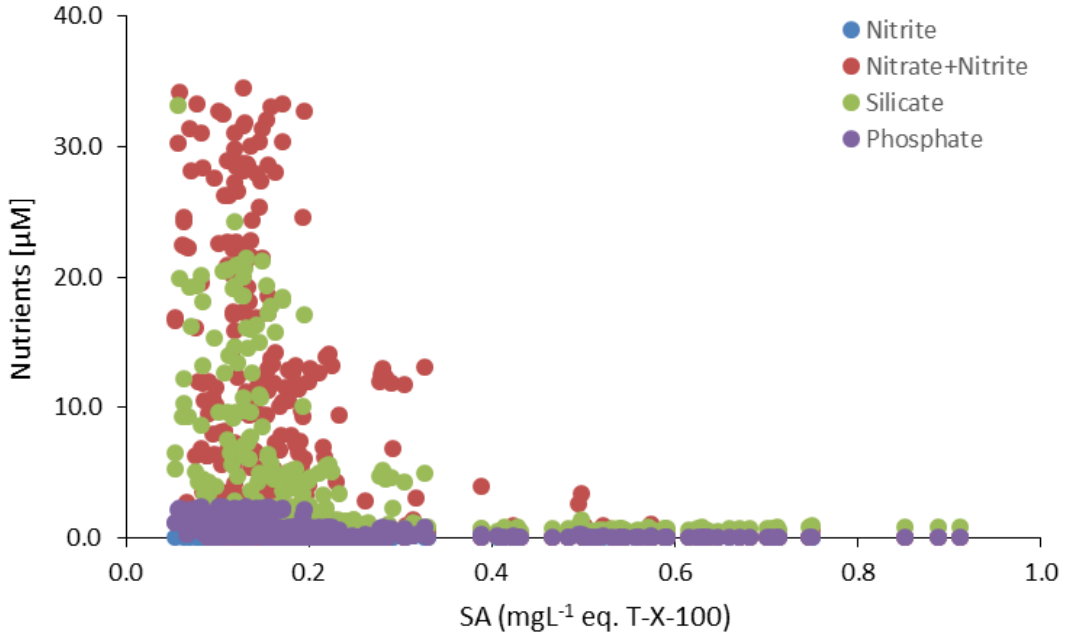

Figure 4.13. SA - nutrient association in the Atlantic Ocean. Nutrients are: nitrite (blue), nitrate + nitrite (red), silicate (green) and phosphate (purple). The data are extracted from AMT24 and AMT25 irrespective of depth.

Spearman rank correlation coefficients were statistically significant: phosphate, r = -0.61, $p < 0.001$, n = 638; silicate; r = -0.54, $p < 0.001$, n = 633; nitrate + nitrite; r = -0.46, $p < 0.001$, n = 628; nitrite; r = -0.23, $p < 0.001$, n = 552. However, the linear regression shows that nutrient distributions cannot be used to satisfactorily predict SA distributions (r^2 was not better than 0.12). Even by excluding low SA values, this correlation does not markedly improve ($r^2 \sim 0.15$).

4.2.7 *Association of SA with CDOM in the Atlantic Ocean*

To explore if CDOM can be used as a proxy for SA determination in oceanic waters, the relationship between SA and CDOM was investigated.

Overall, vertical profiles of SA and CDOM in the Atlantic Ocean showed the same trends (see section 4.2.3). Maximal SA and CDOM were observed within the SML and neither changed

significantly with depth below the sub-surface waters. There were positive linear relationships between SA and CDOM for both transects (Figure 4.14).

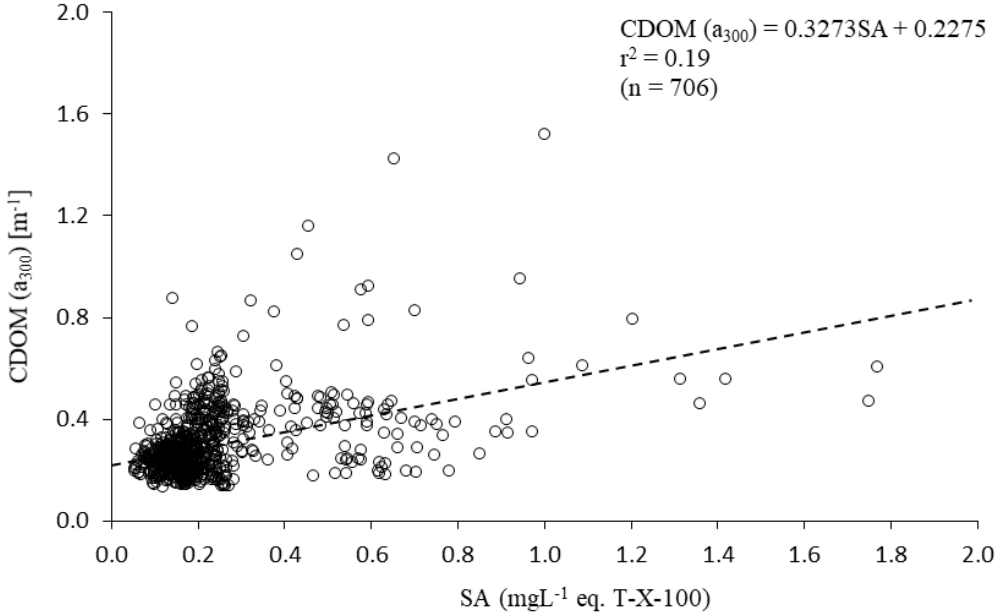

Figure 4.14. SA and CDOM relationship in the Atlantic Ocean along AMT transects. Data are from AMT24 and AMT25. Dashed line represents the best linear fit. The linear regression model, r-squared (r^2) value and sample number are indicated.

Although the correlation was significant (Pearson correlation coefficient (r) = 0.433, $p < 0.001$), a linear regression showed that the model could not be used to predict surfactant extent based on CDOM with any significant degree of confidence as the r^2 value was only 0.20 (Figure 4.14).

4.2.8. *Association of SA with hydrographic indicators in the Atlantic Ocean*

There was no general correspondence between SA and either salinity or temperature in the SML or SSW during the current study [(SA (SML) versus salinity; AMT24, $r^2 = 0.000$, $p = 0.843$, n = 64 - AMT25, $r^2 = 0.001$, $p = 0.840$, n = 44) (SA (SSW) versus salinity; AMT24, $r^2 = 0.112$, $p = 0.008$, n = 61 - AMT25, $r^2 = 0.002$, $p = 0.753$, n = 47) (SA (SML) versus temperature; AMT24, $r^2 = 0.090$, $p = 0.016$, n = 64 - AMT25, $r^2 = 0.025$, $p = 0.307$, n = 44) and (SA (SSW) versus temperature; AMT24, $r^2 = 0.341$, $p = 0.000$, n = 61 - AMT25, $r^2 = 0.006$, $p = 0.584$, n = 47)]. Neither salinity nor temperature was found to be confidently predict SA ($r^2 < \sim 0.35$).

In contrast, Salter (2010) found an inverse correlation between SA and salinity in the River Tyne estuary in agreement with Hunter and Liss (1982) who observed SA decrease with salinity

in four UK estuaries. However, the salinity gradients are larger in estuaries compared to the open ocean during the current study and the strong correlations found previously reflect high SA inputs from rivers.

4.3 Summary

Measurements of SA in the Atlantic Ocean, both in the SML and in SSW during AMT24 and AMT25 shows consistent SA enrichment in the SML.

Surfactants are enriched in the SML to a wind speed of at least 13 m s^{-1}, so that SA in the SML should be decoupled from the ambient wind speed.

At ocean basin scales with diverse biogeochemical regimes variability in surfactant sources will likely to be maximal and include temporal components as well as additional effects from advection and mixing, challenging the use of primary productivity and associated proxies for predicting surfactant distributions.

Chapter 5. Surfactant control of gas transfer velocity (k_w) in the Atlantic Ocean: in-situ gas exchange experiments during AMT24

5.1 Introduction

This chapter presents the results of gas exchange experiments carried out using a custom-designed gas exchange tank (Schneider-Zapp *et al.*, 2014) during AMT24 and compares the results with those from identical experiments in the North Sea (Pereira *et al.*, 2016) to help evaluate surfactant suppression of k_w across a range of Atlantic Ocean biogeochemical provinces. North Sea and AMT24 data were generated by Dr Ryan Pereira (Newcastle, now at Heriot-Watt University), the latter during the NERC RAGNARoCC project that also funded this PhD. The data were used to aid interpreting how SA distributions in the Atlantic Ocean SML may impact air-sea gas exchange. SA data and all interpretations in this chapter are solely those of the author.

The fully automated, closed air-water gas exchange tank was built to determine surfactant control of k_w in the laboratory using un-amended seawater (Schneider-Zapp *et al.*, 2014). Water-side turbulence is set with an automated baffle. Changes in the partial pressures of selected climate-active gases (CH_4, N_2O, SF_6) in tank air and water during the experiment (i.e. 3.25 h, the duration of a typical experiment) are determined by two in-line gas chromatographs (see section 2.6). For direct comparison, derived k_w values are normalised to a constant Schmidt number of 660 (Wanninkhof *et al.*, 1993; Wanninkhof *et al.*, 1997) for each selected level of fixed turbulence (Schneider-Zapp *et al.*, 2014).

5.2 Results

5.2.1 *R_{660} evaluation of the Atlantic Ocean samples*

In the earlier North Sea study k_w was estimated at baffle frequencies of 0.6 Hz, 0.7 Hz and 0.75 Hz but the strongest linear relationships between R_{660} (ratio of sample k_{660} to the corresponding k_{660} of surfactant-free MilliQ water) and SA was found for baffle frequencies of 0.6 Hz and 0.7 Hz due to potential interference from bubbles at 0.75 Hz (Pereira *et al.*, 2016). In this work due to time constraints it was decided to use k_w estimated at 0.6 Hz only. Due to further problems with the analysis of SF_6 (N_2O was not measured), the k_{660} and R_{660}' estimates discussed here were all derived from CH_4 data at 0.6 Hz.

The average value of CH_4 k_{660} (0.6 Hz) was 8.50 ± 0.82 cm h^{-1} (range 6.85 - 9.83 cm h^{-1}) equivalent to a wind speed ~ 5.50 - 6.60 m s^{-1} after Nightingale *et al*. (2000). R_{660}' ranged from 0.68 ± 0.02 to 0.98 ± 0.04 cm h^{-1} on AMT24 (Table 5.1).

Table 5.1. k_{660} and R_{660}' of CH_4 during AMT24. The data derived from the gas exchange tank. Water-side turbulence setting at 0.6Hz. The negative latitudes represent the Atlantic southern hemisphere. The data are represented in average and standard deviation.

Date	Station No.	Latitude (°)	Longitude (°)	CH_4 (K_{660})	CH_4 (R_{660}')
26/09/2014T10:07:00	S003	47.18	-8.81	8.49	0.85 ± 0.03
29/09/2014T13:05:00	S008	43.17	-16.42	8.11	0.81 ± 0.02
30/09/2014T13:04:00	S010	40.84	-20.21	8.08	0.81 ± 0.02
03/10/2014T13:04:00	S015	33.35	-27.09	9.19	0.92 ± 0.04
04/10/2014T13:03:00	S017	29.89	-28.16	8.10	0.81 ± 0.03
09/10/2014T14:04:00	S028	12.84	-27.64	7.49	0.75 ± 0.04
10/10/2014T14:04:00	S030	9.36	-26.92	8.22	0.82 ± 0.04
15/10/2014T14:04:00	S039	-8.91	-25.04	6.85	0.68 ± 0.02
20/10/2014T14:04:00	S048	-22.31	-25.06	9.28	0.93 ± 0.03
21/10/2014T14:02:00	S050	-25.59	-25.03	9.03	0.90 ± 0.02
22/10/2014T14:04:00	S052	-29.15	-25.27	8.41	0.84 ± 0.02
23/10/2014T15:01:00	S054	-32.71	-26.63	9.35	0.93 ± 0.04
26/10/2014T15:06:00	S060	-40.68	-32.10	9.83	0.98 ± 0.04

Evidently, the values of R_{660}' are below 1.0 because of the suppression of k_w by surfactants. These results are within the reported natural range for k_{660} in the presence of surfactants of 5.81 - 70.17 cm h^{-1} (Asher, 2009).

Values of k_{660} in the range 8.02 ± 0.33 to 13.04 ± 0.51 cm h^{-1} were found using the same system with the same baffle frequency for water samples from a 20km offshore transect in the North Sea (Pereira *et al.*, 2016). Corresponding values of CH_4 R_{660} were reported in the range 0.49 ± 0.02 to 0.82 ± 0.03 (Pereira *et al.*, 2016).

So, the average CH_4 R_{660}' suppression to the maximum of 25% in the presence of natural surfactants in the current study were within the range of 10% to 90% suppression of k_w reported for both oceanic and coastal waters in the presence of natural and synthetic surfactants in laboratory tank and field experiments (Broecker, 1978; Brockmann *et al.*, 1982; Jähne *et al.*, 1987a; Jähne *et al.*, 1987b; Goldman *et al.*, 1988; Frew, 1997; Bock *et al.*, 1999; Salter *et al.*, 2011; Schneider-Zapp *et al.*, 2014; Pereira *et al.*, 2016).

For example, Goldman *et al*. (1988) and McKenna and McGillis (2004) reported the magnitude of suppression of gas transfer ranged between 36% and 47% using artificial surfactants (i.e. oleyl alcohol) during laboratory experiments. Salter *et al*. (2011) reported an average k_w suppression ~ 34% for wind speeds of between 4.95 and 10.75 m s^{-1} with a maximum of suppression as high as 41% during a dual tracer release experiment in the North Atlantic.

Suppression of k_{660} of oxygen (O_2) by 55% to 65% in the presence of natural surface films was reported during tank experiments using coastal waters from the southwestern Baltic Sea (Schmidt and Schneider, 2011). It was suggested that the seasonal variability of water column productivity in the Baltic Sea may drive changes in the thickness and composition of surface films, resulting in variability in the suppression of gas transfer (Schmidt and Schneider, 2011).

5.2.2 *Association of R_{660}' with SA and CDOM: a comparison between the Atlantic Ocean and North Sea*

The results show a significant suppression of CH_4 R_{660}' as a function of SA in the SML, in both the Atlantic Ocean (AMT24) and in the North Sea (Dove Time Series) ($p = 0.018$ and $p < 0.001$ respectively, Figure 5.1). Average CH_4 R_{660}' suppression was 14.0 ± 6.9% (range 1.8 - 30.0%) for the Atlantic Ocean, somewhat less than the value of 35.8 ± 10.3% (range 18.0 - 51.0%) found for the North Sea (Pereira *et al.*, 2016).

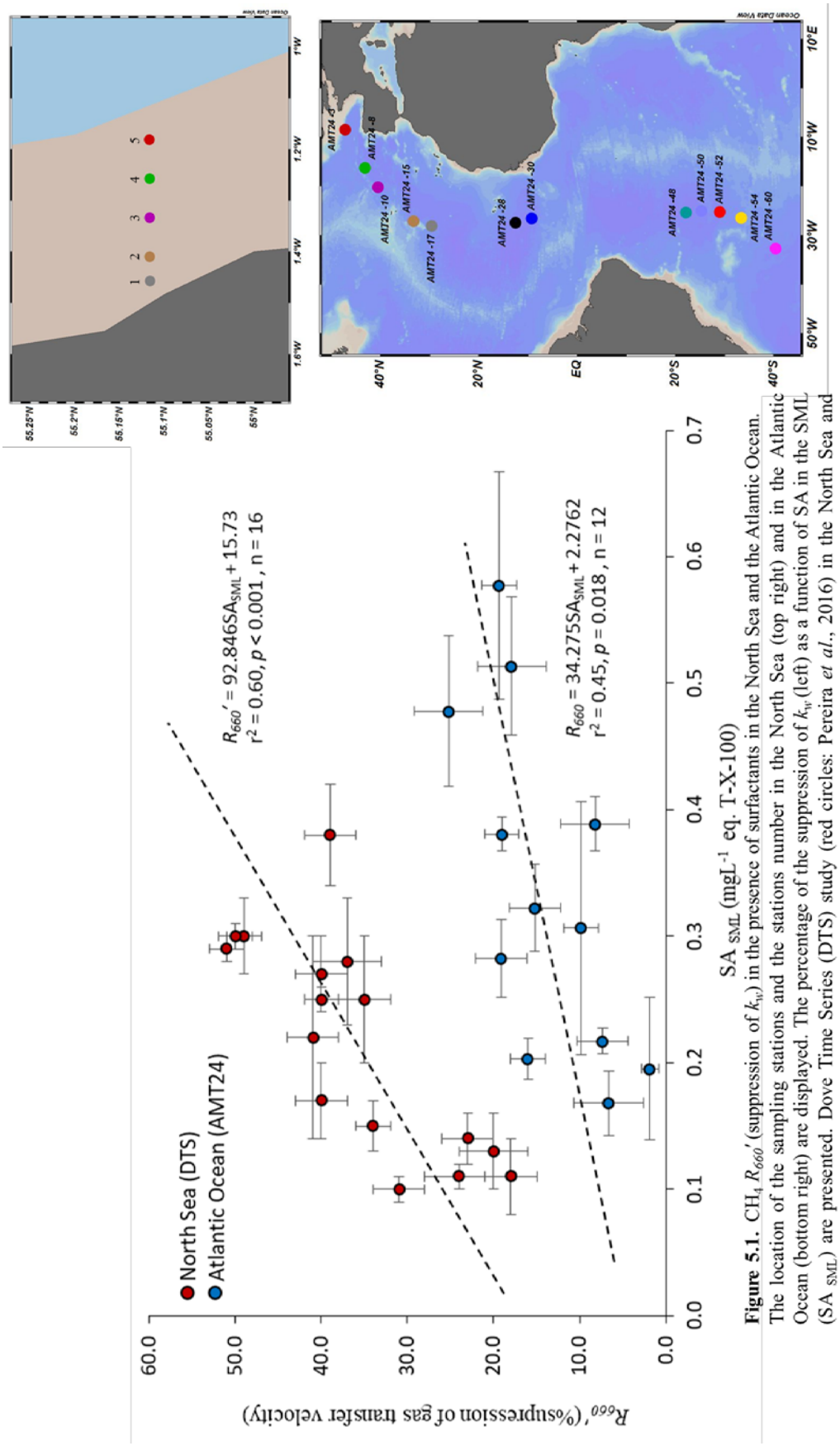

Figure 5.1. CH_4 R_{660}' (suppression of k_w) in the presence of surfactants in the North Sea and the Atlantic Ocean. The location of the sampling stations and the stations number in the North Sea (top right) and in the Atlantic Ocean (bottom right) are displayed. The percentage of the suppression of k_w (left) as a function of SA in the SML (SA_{SML}) are presented. Dove Time Series (DTS) study (red circles: Pereira *et al.*, 2016) in the North Sea and AMT24 (blue circles) in the Atlantic Ocean. The dashed line represents the linear fit described by the equation, with the corresponding value of the correlation coefficient (r^2). $p < 0.05$ gives the probability of significant correlation. The samples number (n) are also indicated.

Table 5.2. Air-Sea gas transfer velocity (k_w) suppression controlled by natural and synthetic surfactants in laboratory and in-situ experiments

	k_w suppression	Reference
Laboratory studies		
Oceanic waters	~10% suppression in O_2 exchange	Goldman *et al.* (1988)
Coastal waters	~50% suppression in O_2 exchange	Goldman *et al.* (1988)
Phytoplankton exudates	~5% - 55% suppression in O_2 exchange	Frew *et al.* (1990)
Addition of soluble surfactant	Maximum of 90% reduction in O_2 exchange	Frew (1997)
Addition of synthetic soluble surfactant (0.1 mM T-X-100)	Maximum of 60% reduction in O_2 exchange	Bock *et al.* (1999)
California Bight surface water samples	k_w suppression in the presence of surfactants	Frew *et al.* (2002)
Coastal-Oceanic waters	Up to 51% suppression of k_w in CH_4 exchange	Pereira *et al.* (2016)
Oceanic waters (in-situ with fresh seawater)	Maximum of 25% of k_w suppression in CH_4 exchange	This study
In-situ studies		
Artificial slick of oleyl alcohol	~30% reduction in diffusion rate of CO_2	Brockmann *et al.* (1982)
Artificial slick of oleyl alcohol	~55% reduction in $SF_6/^3He$-derived k_{660}	Salter *et al.* (2011)
Artificial slick of oleyl alcohol	~24% - 39% reduction in DMS-derived k_{660}	Salter *et al.* (2011)

T-X-100 is the abbreviation for synthetic surfactant of Triton-X-100

Table 5.2 compares the AMT24 results with those of other studies of k_w suppression by surfactants including the North Sea experiment.

The plausible explanation of the difference between the degree of k_w suppression for the North Sea and the Atlantic Ocean is that variability in the composition of the surfactant pool as well as SA influences k_w suppression.

To investigate k_w suppression with respect to organic matter composition in more detail, the relationship between CH_4 R_{660}' and CDOM (a_{300}) was examined. An inverse linear relationship was observed between CH_4 R_{660}' and CDOM (a_{300}) in the SML and in SSW, however, the relationship is not statistically significant (Figure 5.2).

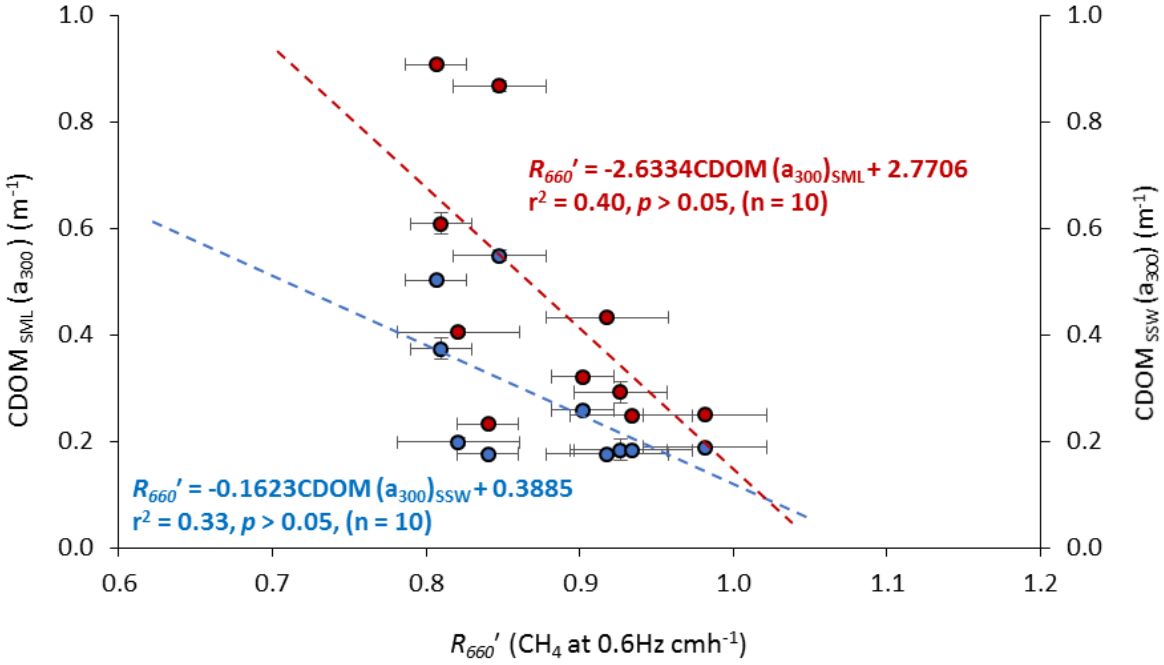

Figure 5.2. CH_4 R_{660}' against CDOM absorption coefficient (a_{300}). CDOM (a_{300}) (m^{-1}) in the SML (red) and in the SSW (blue) during AMT24. The dashed lines represent the linear fit described by the equation, with the corresponding value of the correlation coefficient (r^2). $p < 0.05$ gives the probability of significant correlation. The sample numbers are also indicated.

The results from the current study support the recent conclusion from the North Sea that CDOM is not an effective proxy for predicting k_w (Pereira *et al.*, 2016). In that study CH_4 R_{660} did not show a statistically significant relationship with total CDOM absorbance i.e. ($a_{250-450}$) (CH_4 R_{660} versus SML Total CDOM ($a_{250-450}$); $r^2 = 1 \times 10^{-5}$, $p = 0.992$ and SSW Total CDOM ($a_{250-450}$); $r^2 = 0.11$, $p = 0.250$, n = 13).

However, further investigation during this study revealed a statistically significant inverse correlation between CH_4 R_{660}' and EF (a_{300}) on AMT24 (Pearson correlation coefficient; r = -0.80, $p = 0.002$, n = 12) (Figure 5.3).

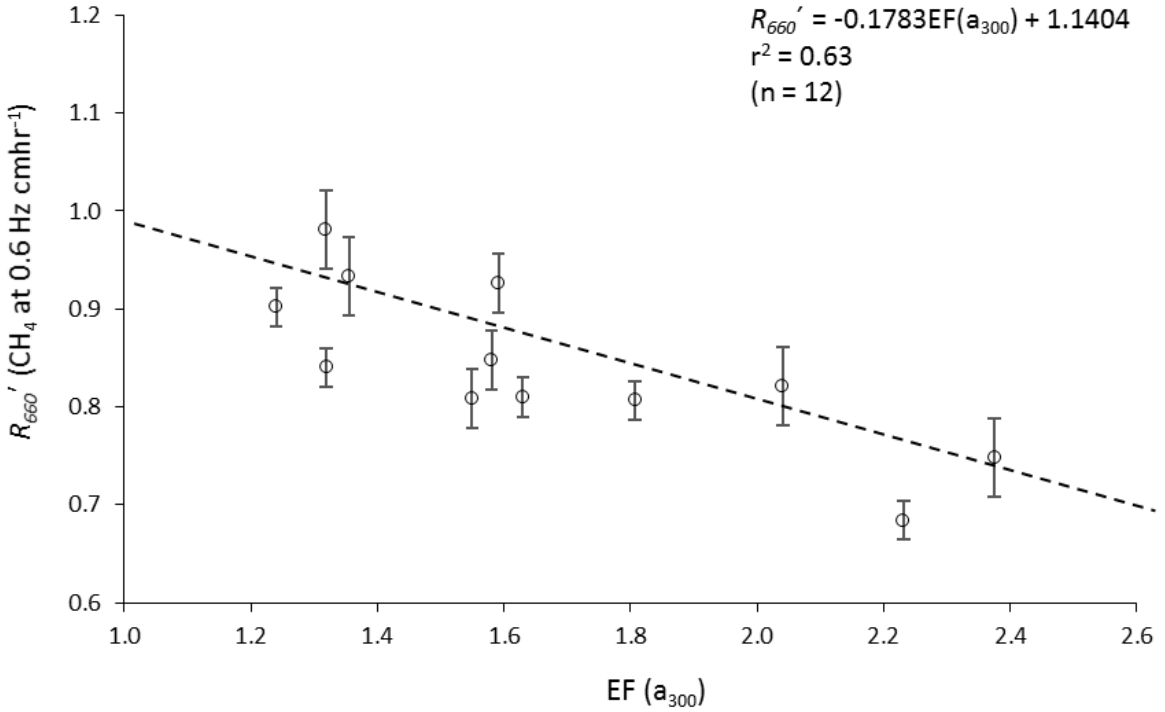

Figure 5.3. CH_4 R_{660}' against CDOM EF (a_{300}) during AMT24. The dashed line represents the linear fit described by the equation, with the corresponding value of the correlation coefficient (r^2). The bars display standard deviation of the mean. Sample numbers (n) are also indicated.

An inverse correlation between CH_4 R_{660} and EF (Total $a_{250-450}$) was also observed for the North Sea but it was not statistically significant (r^2 = 0.30, r = -0.53, p = 0.06, n = 13). This might reflect more diverse CDOM sources in the North Sea due to a strong terrestrial CDOM component that is not seen in the Atlantic Ocean.

While CDOM absorbance is a "bulk" measure of CDOM, the 250:365 nm CDOM absorption ratio (E_2:E_3) indicates relative changes in low molecular weight (LMW) compared to high molecular weight (HMW) organic matter (see section 2.5.6). CDOM (E_2:E_3) decreases with increasing molecular weight due to increasing light absorption (Peuravuori and Pihlaja, 1997). Therefore E_2:E_3 and S_R (see section 2.5.6) both can reveal optical characteristics of DOM relating to composition that might have impacts on k_w suppression.

A statistically weak correlation was found between CH_4 R_{660}' and CDOM (E_2:E_3) in both the SML and in SSW [(CH_4 R_{660}' against SML CDOM (E_2:E_3); r^2 = 0.10, p = 0.30, n = 13) (CH_4 R_{660}' against SSW CDOM (E_2:E_3); r^2 = 0.04, p = 0.52, n = 12)]. However, there was a much stronger positive correlation between CH_4 R_{660}' and EF (E_2:E_3) = (SML E_2:E_3 / corresponding SSW E_2:E_3) (Pearson correlation coefficient; r = 0.83, p = 0.003, n = 10) (Figure 5.4).

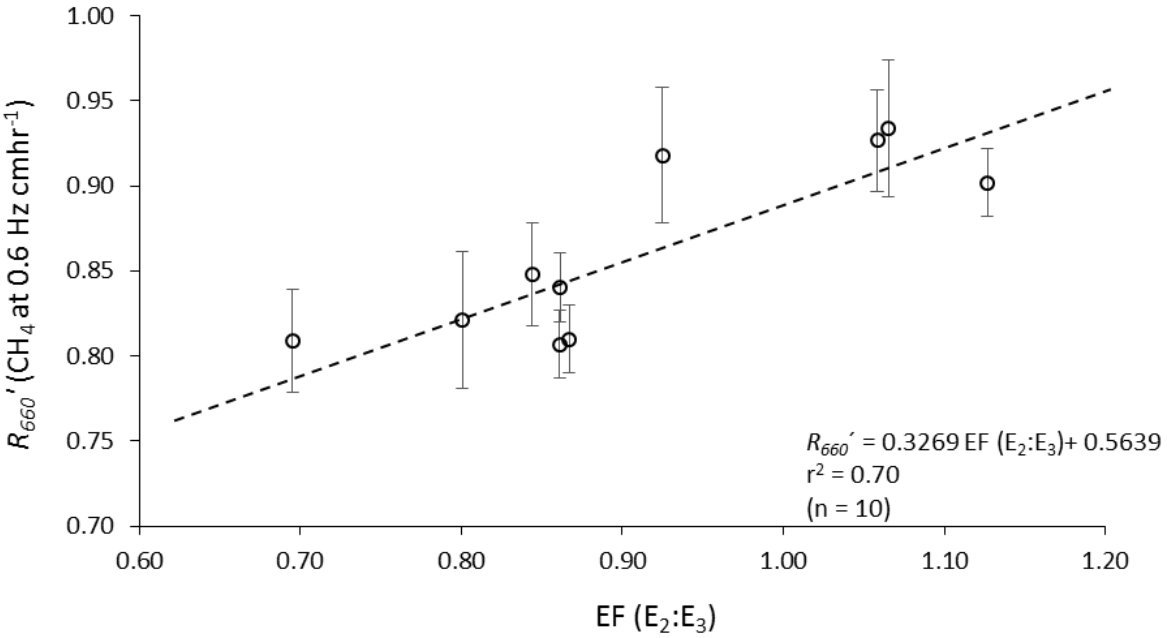

Figure 5.4. CH_4 R_{660}' against EF (E_2:E_3) (i.e. SML E_2:E_3 compared to the corresponding SSW E_2:E_3) on AMT24. The dashed line represents the linear fit described by the equation, with the corresponding value of the correlation coefficient (r^2). Sample numbers (n) are also indicated.

The linear regression model can then be used to predict CH_4 R_{660}' using the enrichment factor of CDOM (E_2: E_3) as a proxy with 70% accuracy (i.e. $r^2 = 0.70$, Figure 5.4).

In agreement, a positive relationship was found for the samples from the North Sea, although the correlation was not statistically significant (Pearson correlation coefficient (r) = 0.46, r^2 = 0.21, p = 0.111, n = 13), presumably due to a wider CDOM compositional range in the North Sea resulting from the greater influence of terrestrial input than in the Atlantic Ocean.

5.2.3 *R660′- chlorophyll association*

A significant correlation (Pearson correlation coefficient, r = 0.85, *p*-value = 0.003, n = 7) was observed between CH_4 R_{660}' and chlorophyll-a on AMT24 (Figure 5.5).

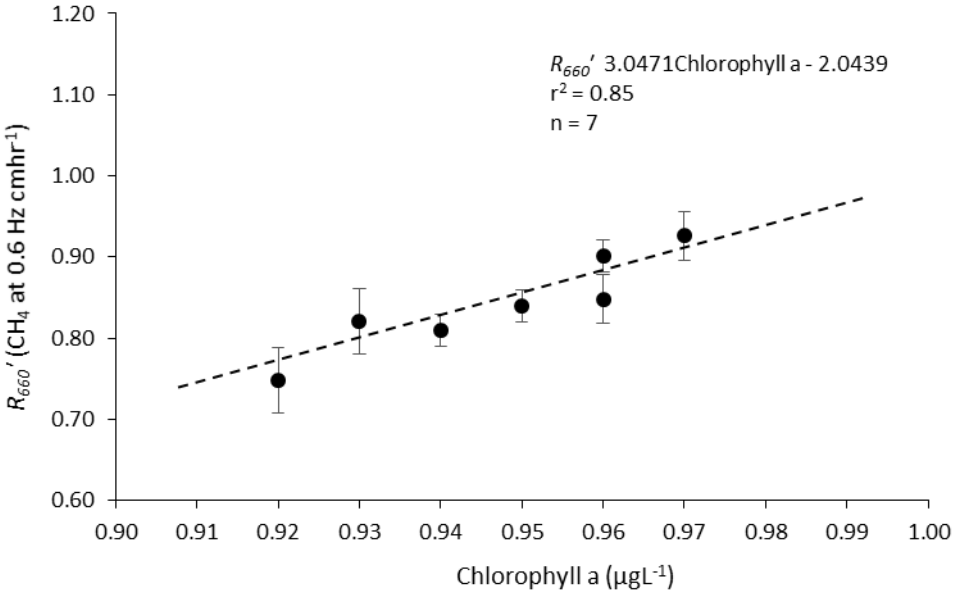

Figure 5.5. CH_4 R_{660}' against chlorophyll a (µgL^{-1}) on AMT24. The dashed line represents the linear fit described by the equation, with the corresponding value of the correlation coefficient (r^2). Sample numbers (n) are also indicated.

Previous results for surface water samples collected on a transect from the East Coast of the USA to Bermuda showed a similar correlation of k_w (determined in a laboratory wind-wave tank) with chlorophyll and also with DOC, although the samples were stored for a considerable time prior to the k_w estimates (Frew, 1997).

In contrast, Pereira *et al*. (2016) recently found no significant relationships between CH_4 R_{660} and chlorophyll-a for North Sea samples and Nightingale *et al*. (2000) found no such correlation during a deliberate iron enrichment experiment that resulted in an algal bloom in the Pacific Ocean. During the Pacific bloom, chlorophyll increased tenfold but there was no reduction in k_w. It was therefore suggested that a simple relationship between k_w and chlorophyll does not exist (Nightingale *et al.*, 2000). Goldman *et al*. (1988) also found no clear relationships between chlorophyll-a and oxygen exchange in the presence of natural surfactants.

5.3 Summary

The value of k_w for CH_4 was suppressed to maximum of 25% in the presence of natural surfactants during gas exchange tank experiments using samples from the AMT24 transect.

The difference between k_w suppression in the presence of surfactants in the North Sea and the Atlantic Ocean might be associated with differences in the compositions of the surfactant pools in these two regions. While a larger terrestrial component is likely in the North Sea, a predominance of biologically-produced surfactants is most likely in the Atlantic. However, the possibility that differences in surfactant composition as well as SA are also important in controlling the gas transfer velocity (Pereira *et al.*, 2016) remains to be investigated.

Surfactants should be accounted for when evaluating rates of air-sea gas exchange. Although as shown in chapter 4, SA does not vary much across large areas of the Atlantic Ocean, either latitudinally or longitudinally, localised maxima could be important. For example, the SA maximum around 40°N in NADR coincides with instrumented shipping routes used to determine CO_2 uptake in the Integrated Carbon Observation System (ICOS). Ignoring the large SA maximum around 40°N may mean that CO_2 uptake rates in this large CO_2 sink region, which are based on conventional gas exchange models that ignore surfactants, might be overestimated.

The results from this and previous chapters suggest that surfactants should be a core measurement for air-sea gas exchange studies. Remote-sensing methods for determining surfactants are not sufficient because they only detect visible slicks and not the soluble surfactants that are so important to air-sea gas exchange (see section 1.2.1).

Chapter 6. General Discussion

6.1 CDOM in the Atlantic Ocean

Characterization of CDOM as a subset of DOM, may help to better understand the details of DOM photochemical properties, including the photochemical characteristics of surfactants. This would help in more clearly identifying the sources and origins of surfactants present in different biogeochemical provinces of the ocean.

CDOM absorption coefficients are proxies of CDOM absorbances whereas CDOM spectral slopes contain information on CDOM composition and DOM molecular weight (Carder *et al.*, 1989; Twardowski *et al.*, 2004; Helms *et al.*, 2008). CDOM sources and modifications including autochthonous production, terrestrial deposition and river outflow (Siegel *et al.*, 2002; Astoreca *et al.*, 2009; Hansell and Carlson, 2014), CDOM photodegradation and microbial uptake are identified by CDOM spectral slopes (Twardowski and Donaghay, 2002; Sulzberger and Durisch-Kaiser, 2009).

During the current study, it was revealed that CDOM absorption coefficients and corresponding spectral slopes display province dependant patterns, particularly in the SML of the Atlantic Ocean (see section 3.5). In agreement, Kitidis *et al*. (2006) found that CDOM was more variable regionally, with distinct depth distributions, than seasonally during AMT transects between 1999 and 2000.

6.1.1 *CDOM enrichment in SML of the Atlantic Ocean*

The results from the current study are in agreement with previous research (see section 3.5.2), clearly indicating that CDOM consistently accumulates in the SML. SML enrichment could be a consequence of faster CDOM accumulation than removal processes, such as photodegradation. Previous laboratory irradiation experiments revealed that photodegradation is a slow process, with time scales of up to weeks (Kitidis *et al.*, 2006).

An alternative suggestion is that CDOM accumulation in the SML is facilitated by efficient upward transport of materials via turbulence and bubble scavenging through sub-surface waters

of the ocean. This is supported by strong positive relationships between SML CDOM (a_{300}) and SSW CDOM (a_{300}) found during this study, in agreement with previous work (see section 3.5.2). This also implies that organic material accumulating in the SML is predominantly supplied from the underlying waters (Zhang and Yang, 2013).

UV-resistant phytoplankton exudates, mycosporine-like amino acids (MAA) were detected in the SML during the current study in agreement with Tilstone *et al*. (2010). The samples containing MAA in this study were mostly located between 25°N and 15°N in NATR on both transects and were exclusive to the SML (see section 3.5.5).

The presence of MAA in SML samples from off the Iberian Peninsula with the maxima during phytoplankton bloom was interpreted to indicate phytoplankton MAA production as a defensive mechanism against photobleaching (Tilstone *et al.*, 2010).

In the present work the high latitudes of the Northern Hemisphere (i.e. ECSW and NADR) were characterized by SML CDOM absorbance maxima, suggestive of terrestrial inputs in continental shelf waters (see section 3.2) in agreement with Kowalczuk *et al*. (2013) and Hansell and Carlson (2014). CDOM absorbance minima on the other hand occurred in the oligotrophic NAST on both transects (see section 3.5.1). It is suggested from the current study that these low SML CDOM oceanic waters can be attributed to reduced CDOM availability in the underlying waters due to low regional productivity (see section 3.2). Also, deepened mixed layer, high stratification and high photodegradation of CDOM in these clear waters exposed to high solar radiation would very likely increase CDOM removal rates (Siegel and Michaels, 1996; Nelson *et al.*, 1998; Kitidis *et al.*, 2006).

The small but discernible SML CDOM absorbance maxima observed in the tropical-equatorial region during this study (see section 3.5.1) might be attributed to upwelling of CDOM-enriched deep waters.

6.1.2 *Depth profile of CDOM in the Atlantic Ocean*

The agreement between the forms of the CDOM profiles found on AMT24 and AMT25 with those from other studies (see section 3.5.4) shows that CDOM consistently decreases between the SML maxima and the sub surface waters at all stations.

Similar to the SML, high CDOM absorbances were found in ECSW and NADR where the locations of these maxima were associated with chlorophyll maxima (see section 3.2), indicating the contribution of autochthonous CDOM components. CDOM absorbance minima in the oligotrophic regions of NAST (in depth shallower than ~ 50 m) and SATL might imply that CDOM depletion occurs faster than CDOM formation in these less productive regions. There are two pathways for CDOM removal in the oligotrophic gyres of the Atlantic Ocean; CDOM expose to high UV radiation in these clear optic waters with light penetration as deep as 80 m and higher temperature enforced water stratification and entrapment of CDOM in the photic layer. This physical mechanism facilitates higher exposure of CDOM to photochemical degradation (Kitidis *et al.*, 2006; Nelson *et al.*, 2007; Smyth, 2011).

The regional/latitudinal CDOM (a_{300}) maxima found in the northern tropical region (see section 3.5.4) coincided with a DCM depth of ~65 m (see section 3.2) during this study are suggestive of upwelled deep CDOM-rich waters and in-situ biological production of CDOM. Kitidis *et al*. (2006) also suggested that remineralization of sinking particles in deep waters or CDOM scavenging to the top layers by migrating zooplankton might result in high CDOM in the area.

The slight increases in CDOM absorbance at high latitudes of the Southern Hemisphere (i.e. the south of 30°S) mostly observed on AMT24 in the current study might be indicative of local CDOM production (see section 3.5). In agreement, Kitidis *et al*. (2006) observed high CDOM absorbance at high latitudes (i.e. north of 40°N and south of 30°S in the Atlantic Ocean), suggestive of in-situ biological production of CDOM in these less stratified regions.

CDOM absorbance throughout the water column (i.e. ≤ 100 m) was more homogeneously distributed in the Southern Hemisphere compared to the Northern Hemisphere during the current study (see section 3.5.4) in agreement with Kitidis *et al*. (2006), suggestive of wind-induced turbulence resulting in well-mixed waters.

6.1.3 *Optical properties of CDOM in the Atlantic Ocean*

CDOM has two pools in the Atlantic Ocean including; recently fresh produced CDOM mainly via biological production associated with high absorption coefficient and low spectral slope against old ‘background’ CDOM with lower absorption coefficient and higher spectral slope

values (Stedmon and Markager, 2001; Kitidis *et al.*, 2006; Hansell and Carlson, 2014) and are joined where the water masses mix in the ocean.

$S_{275-295}$ showed a significant inverse correlation with CDOM absorbance during the current study (see section 3.5.4). Higher $S_{275-295}$ in underlying waters was found compared to the SML, in agreement with Kowalczuk *et al*. (2013), Zhang and Yang (2013) and Galgani and Engel (2016).

The high latitudes of the Northern Hemisphere (i.e. ECSW and NADR) were characterised by CDOM absorbance maxima and $S_{275-295}$ minima compared to the oligotrophic gyres of the Atlantic Ocean with low CDOM absorbance and high $S_{275-295}$ during the current study. In agreement, Kitidis *et al*. (2006) characterized the oligotrophic subtropical gyres by the lowest CDOM (a_{300}) and the highest $S_{275-295}$ between the surface waters and 250 m depth comapred to upwelling regions in the Atlantic Ocean.

Kitidis *et al*. (2006) suggested that in the regions with $S_{275-295}$ maxima (i.e. the oligotrophic regions of the Atlantic Northern and the Southern gyre), CDOM sources are provided from the centre of the gyres (physical transportation) and display 'old' CDOM with high exposure to photodegradation through its history. In contrast, in the regions with $S_{275-295}$ minima (i.e. the higher latitudes of the Northern and Southern Hemisphere) fresh phytoplankton-derived CDOM within the mixed layer may be considered as the main source of CDOM, in concurrence with the current study.

Also, $S_{275-295}$ was assumed to be greater than $S_{350-400}$ in biologically-derived marine CDOM, in contrast to terrestrially derived or more photodegraded CDOM with $S_{350-400}$ greater than $S_{275-295}$ (Helms *et al.*, 2008; Yamashita and Tanoue, 2009). So, based on this assumption, it is suggested that marine sources of CDOM with $S_{275-295} > S_{350-400}$ were the dominant CDOM component in the Atlantic Ocean provinces during the current study (see section 3.5).

Helms *et al*. (2008) showed that S_R is a more relevant indicator of photochemically-derived transformations in the molecular weight of CDOM than spectral slope values. Higher $S_{275-295}$ than $S_{350-400}$ means higher absorption towards shorter wavelengths represent lower molecular weight organic matters compared to long-chain higher molecular weight organics with higher absorption towards the longer wavelengths.

While lower S_R is indicative of higher molecular weight of (dark) microbial transformed CDOM dominant in the terrestrial regions, high S_R indicates lower molecular weight CDOM, suggestive of photodegraded oceanic CDOM (Helms *et al.*, 2008; Kowalczuk *et al.*, 2013). However, CDOM transformation rate by microbial activities is slower than degradation by photochemical activity (Moran *et al.*, 2000; Vähätalo and Wetzel, 2004). Hence, in marine waters, S_R values presumably increase rapidly by photodegradation and decrease more slowly by microbial activity (Helms *et al.*, 2008).

S_R maxima observed in the oligotrophic regions of the NAST and the SATL in the current study might be indicative of lower molecular weight organic matter and/or photodegraded CDOM, in agreement with previous research (Peuravuori and Pihlaja, 1997; Helms *et al.*, 2008). S_R minima were found in the SML around the European continental shelf (i.e. ECSW) on both transects in the present work, suggestive of dominant higher molecular weight humic material of terrestrial origin.

6.1.4 *CDOM composition in the Atlantic Ocean*

CDOM compositions are diverse in the open oceans. For example, the enrichment of amino acids and protein-like components in the surface layers of the oceans with a decrease to the deeper waters, suggestive of local production of phytoplankton-induced DOM in the surface waters were reported (Jørgensen *et al.*, 2011; Stedmon and Álvarez-Salgado, 2011; Kowalczuk *et al.*, 2013).

Galgani and Engel (2016) found protein-like components enriched in the SML in the upwelling region off the coast of Peru, suggestive of microbial production via a photoprotection mechanism or bacterial degradation products. Also, the microbial and photochemical degradation was suggested to be the major sink of CDOM components, controlling surface CDOM dynamics in the region (Galgani and Engel, 2016).

Humic-like components on the other hand showed a significant enhancement in the underlying waters of the Atlantic and the Pacific Ocean (Jørgensen *et al.*, 2011). Overall, the dynamics of humic-type compounds in the oceans are maintained through enrichment via terrestrial inputs or local microbial production in deep waters and removal by photodegradation mainly in the top layers of the oligotrophic regions (Jørgensen *et al.*, 2011; Romera-Castillo *et al.*, 2011;

Kowalczuk *et al.*, 2013). Also, in conditions of low primary productivity, heterotrophic bacteria utilise humic substances as a source of carbon and facilitate CDOM removal (Sundh and Bell, 1992).

In the Atlantic Ocean, CDOM maxima within the mixed layer in the ECSW suggestive of in-situ production of protein-like components, the terrestrial input of mostly humic-type materials and also microbial remineralization of DOM were reported (McKnight *et al.*, 2001; Stedmon *et al.*, 2003; Romera-Castillo *et al.*, 2011; Kowalczuk *et al.*, 2013). The humic-type components was also reported in the oligotrophic gyres and the tropical regions (Nelson *et al.*, 2007; Swan *et al.*, 2009; Nelson *et al.*, 2010) and also in the subsurface waters between 20 m and 50 m in the equatorial upwelling region of the Atlantic Ocean (Kowalczuk *et al.*, 2013). This suggests that CDOM produced by microbial activity in the deeper waters is circulated to the surface layers in the gyres and upwelling regions.

Kowalczuk *et al*. (2013) reported high in-situ production of protein-like components in the Atlantic Southern Hemisphere (i.e. south of 7°S) compared to the Northern Hemisphere (i.e. 15 times higher) along with lower humic-like components (based on fluorescence spectroscopy; see section 1.1.3.2). In contrast, in the Northern Hemisphere, humic-like components are dominant in the mixed layer and just below the base of the mixed layer (Kowalczuk *et al.*, 2013).

6.1.5 *CDOM and Chlorophyll-a*

CDOM-chlorophyll-a association was found to be province-dependant during the current study. Relatively weak correlations between CDOM and chlorophyll-a were found in the water masses from the high latitudes, with the possibility of a non-phytoplankton produced CDOM contribution of terresterial origin (see section 3.5.7). In agreement, Del Castillo and Coble (2000) found no relationship between phytoplankton abundance and CDOM distribution on the West Florida shelf, suggestive of terrestrial CDOM inputs.

However, in agreement with other oceanic regions (DeGrandpre *et al.*, 1996; Nelson *et al.*, 1998) along AMT transects crossing different biogeochemical provinces from the eutrophic continental shelf to the oligotrophic gyres and the upwelling regions, a weak relationship between CDOM and chlorophyll-a is not surprising due to the various CDOM sources and the

complexity of CDOM dynamics. Variables such as nutrient availability, solar irradiation, carbon-nitrogen (C:N) ratio, phytoplankton species and their growth stage and the microbial transformation of CDOM might all influence the distribution of biologically-derived DOM (Søndergaard *et al.*, 2000; Ward and Bronk, 2001; Nelson and Siegel, 2013).

Kitidis *et al*. (2006) also suggested that chlorophyll-a is not a good proxy for CDOM estimation because of temporal decoupling of CDOM and chlorophyll-a in the oceans due to other CDOM production pathways rather than direct phytoplankton exudates.

Seasonally and spatially variable relationship between CDOM absorbance and chlorophyll-a in the Atlantic Bight raised the conclusion that CDOM and chlorophyll-a should be decoupled due to the time delay between the phytoplankton bloom and enhancement of induced-CDOM levels (DeGrandpre *et al.*, 1996).

CDOM enhancement during the summer while phytoplankton biomass was at its lowest in the Sargasso Sea (Nelson *et al.*, 1998), suggests that CDOM is also produced as a degradation product of phytoplankton via zooplankton grazing and/or mostly bacterial degradation (Bricaud *et al.*, 1981; Nelson *et al.*, 1998).

6.1.6 *CDOM association with physical parameters*

During the current study CDOM absorbance in the SML and underlying waters showed an inverse correlation with salinity and temperature in the Atlantic Ocean (see section 3.5.8).

$S_{275\text{-}295}$ on the other hand, increased at higher salinity and temperature both in the SML and throughout the water column (see section 3.5.8).

However, it should be pointed that the range of wavelengths on which CDOM spectral slope values are calculated is important as these might show different behaviours towards salinity and temperature (Carder *et al.*, 1989). For example, Kitidis *et al*. (2006) found that CDOM spectral slope decreases with higher salinity if the slope is calculated above 350 nm whereas CDOM increase with salinity for the spectral slope calculated below 350 nm.

6.2 Surfactant distribution in the Atlantic Ocean

6.2.1 *Surfactant distribution in the SML of the Atlantic Ocean*

SA measurements in the Atlantic Ocean between 50°N and 50°S (Sabbaghzadeh *et al.*, 2017) constitute the first direct measurement of surfactants in the open ocean along a vast latitudinal gradient. The data allow a test of an earlier prediction of SA distributions in the marine environment that was derived from the global maps of primary productivity and wind speed (Wurl *et al.*, 2011b).

SA was enriched in the SML compared to the corresponding SSW at almost all sampling locations during the current study. The strong positive correlation between SML SA and SSW SA clearly implies a continual renewal of SML SA from SSW, as previously discussed (Hardy, 1982; Frew *et al.*, 2006; Cunliffe *et al.*, 2013; Zhang and Yang, 2013; Pereira *et al.*, 2016).

A distinct latitudinal distribution of surfactant was found for both the SML and the SSW of the Atlantic Ocean during the current study. The SA maxima around 40°N in NADR in both the SML and the SSW (see section 4.2.1) is suggestive of terrestrially-derived surfactant deposition in the region. Two small SA maxima that were exclusive to the SML in the northern sub-tropical and tropical regions on AMT24 (see section 4.2.1) might be attributed to enhanced bubble scavenging of surfactants under the somewhat more turbulent conditions experienced during AMT24. In other words, at high turbulence more bubbles are generated with breaking waves, bringing more surfactants to the surface via bubble scavenging. An alternative explanation is that these maxima reflect more intense and/or more frequent local precipitation on AMT24 (lower salinity in the region on AMT24 compared to AMT25, see section 4.2.1) or possibly enhanced net biological production of surface active material.

Elevated SML surfactants following rainfall have previously been confirmed to enhance particulate organic matter in the SML (Wurl *et al.*, 2011b). Aiken *et al*. (2000) also reported a decrease in salinity (~ 35.0) from the sea surface to a depth of 100 m in the tropical and equatorial regions caused by high precipitation. This water mass with distinct temperatures and salinity patterns was identified as Equatorial Surface Water (ESW) during their study using the same basic AMT transect (Aiken *et al.*, 2000).

While a previous rainfall event is plausible, no precipitation was experienced during sampling. An alternative or complementary explanation is the effect of equatorial upwelling, as indicated by low surface salinity on AMT24 relative to deeper waters. The nutrient distribution also showed a change around this region, possibly indicative of nutrient-enriched upwelled waters (see section 3.3).

Another small SA maximum at ~ 50°S (FKLD) observed during AMT24 may indicate high local productivity, or terrestrially-derived surfactants, or an aggregate of both. Evidence for this feature during AMT25 was either absent or comparatively limited (see section 4.2.1). Primary productivity data are unavailable for this sampling location but chlorophyll-a concentration was slightly higher in this region (1.00 µg L^{-1}) than in adjacent waters (~ 0.6 µg L^{-1}), although chlorophyll-a might not be a good proxy for surfactant estimation (Pereira *et al.*, 2016). So, the precise origin of this SA maxima thus remains unknown.

Average SA in the SML and the SSW was statistically higher in the Northern Hemisphere compared to the Southern Hemisphere on both transects (see section 4.2.1). Moreover, SA represents conservative behaviour in the SML in a range of biogeochemical provinces of the Atlantic Southern Hemisphere (i.e. WTRA, SATL and SSTC) indicating no major production (enhancement) or removal (depletion) of surfactants along both transects.

Although a conservative nature of surfactant was also observed in SSW over the full extent of both transects, an exception was found around NADR on AMT25. The similar increase in SA in both the SML and SSW in this region might be attributed to high deposition of terrestrial-derived surfactants on AMT25.

6.2.2 *Surfactant depth profiles in the Atlantic Ocean*

The depth profile of surfactants in the Atlantic Ocean revealed that an earlier view of the SML as a “layer of sudden change” (Zhang *et al.*, 2003) is valid for surfactants and some associated variables in the Atlantic Ocean.

Surfactants and the associated CDOM depth profiles showed similar behaviour within the water column, decreasing sharply from the SML to sub-surface waters and then staying quite constant to 100 m depth. However, SA in the upper 100 m around 40°N on AMT25 was significantly

higher than on AMT24 (see section 4.2.3). The plausible explanation is higher terrestrial deposition around the continental shelf during AMT25.

The main conclusion to draw from the depth distributions of SA and CDOM in the current study is that either surfactants are a major DOM component in the Atlantic Ocean or that similar processes control the distributions of SA and the remainder of DOM. From the data presented in this thesis it is not possible to determine which of these two possibilities is the most likely. Further studies examining the composition of the surfactant and wider DOM pools may better answer this question.

The SA distributions determined in the current study challenge those previously estimated for ocean basins derived from satellite images. For example, Tsai and Liu (2003) suggested vast regions of the Atlantic Ocean between 30°N and 30°S including the Northern and Southern Atlantic oligotrophic gyres to be free of surfactant, based on low satellite-derived primary productivity. The major regions of the global oceans covered by surfactant were suggested to be the subarctic Pacific and the Atlantic Oceans in boreal summer and autumn (i.e. between March and September), the eastern equatorial and subtropical Pacific, Atlantic coastal waters off America and Africa and in the upwelling regions during austral spring and summer (i.e. between July and December). Significant surfactant coverage in the Indian Ocean was assumed only from July to October, and in the Southern ocean commencing in July and reaching a maximum in December and January (Tsai and Liu, 2003; Wurl *et al.*, 2011b).

Wurl *et al*. (2011) further suggested that surfactant only covers the most productive regions of the oceans such as the coastal, upwelling and polar area while large regions of the oceans are surfactants free, based on primary productivity thresholds of oligotrophic and eutrophic waters and wind speed data.

SA within the water column did not show any significant changes around the DCM in the present work. SA however was always higher above the base of the mixed layer compared to deeper waters during the current study, consistent with a greater abundance of phytoplankton metabolism products in the mixed layer than in deep waters (Zubkov *et al.*, 2000b), and/or lower biogeochemical removal of SA in the mixed layer and SA compositional differences.

Protein-like components showed a distinct depth distribution pattern with higher values in the mixed layer, whereas marine humic-type components were concentrated below the base of the mixed layer along previous AMT transects (Kowalczuk *et al.*, 2013).

Ćosović *et al*. (1985) also showed that the composition of DOM varies with depth. While soluble and insoluble hydrophobic surfactants are mostly present in surface layers, the concentration of more hydrophilic refractive substances increased through the water column to a maximum of 400 m depth in the Mediterranean (Ćosović *et al.*, 1985).

Later research also showed that the SML is enriched in lipids from different compounds such as fatty acids, sterols and carotenoids, whereas the sub-surface waters revealed a depletion of these low soluble hydrophobic surfactants in the southern California Bight and the U.S. Middle Atlantic Bight (Frew *et al.*, 2006).

6.2.3 *Enrichment factors (EFs) of surfactants in the Atlantic Ocean*

Accumulation or depletion patterns of any compounds including organic and inorganic matter in the SML relative to the corresponding sub-surface waters is determined by quantifying enrichment factors (EFs) (see section 2.5.5).

The SML was enriched with surfactants (EF > 1) at almost all sampling locations during the current study (see section 4.2.2). The SML enrichment of surfactants could be attributed to the Gibbs surface adsorption process, i.e. high surface tension in the SML promotes adsorption and stabilisation of organic matter and its accumulation in the SML as a consequence (Zhang and Yang, 2013).

Maximal SA EFs were observed at the same locations as SA maxima over the full extent of the transects (see section 4.2.2); around the continental shelves both on the northern and southern end of transects (i.e. ECSW and FKLD), suggestive of some terrestrial discharge in the regions and around the equatorial region, attributable to equatorial upwelling on both transects.

The most plausible explanation for the consistent observations of low EFs associated with high SA in the subsurface waters during the current study is that for any given wind speed, bubble scavenging is proportionally greater in low SA waters than in high SA waters. This is because there is a finite limit to the amount of surfactant that can be supplied by any individual bubble

to the SML. Consequently, SML enrichment is limited by the total number/surface area of bubbles and so in SSW of comparatively low SA a proportionately larger fraction of the available surfactant pool is available for bubble scavenging (leading to high EF) than in SSW of comparatively high SA (leading to low EF). An inverse relationship between EF and SSW SA is therefore inevitable.

6.2.4 *Association of SA with physical and biological indicators in the Atlantic Ocean*

Evidently, there was no trend between surfactant distributions in both the SML and the subsurface waters and the physical properties of seawater including salinity and temperature (see section 4.2.8). Diverse physical mechanisms operate at the sea surface including surface turbulence, breaking waves, accumulation of organics via bubble scavenging and slicks formation resulting in a complex environment that might preclude any simple correlation between SA and physical parameters.

In the current study the similar behaviour of SML and sub-surface samples versus physical parameters might indicate a similar composition of surfactants in both the SML and in corresponding sub-surface waters. This is consistent with the assumption that sub-surface waters are the major source of surfactant to the SML (Salter, 2010).

Overall, a positive relationship was found between chlorophyll-a and SA during this study but the correlation was not statistically significant (see section 4.2.5). These findings are perhaps not surprising given that surfactant production is likely variable among individual phytoplankton species and possible additional contributions from non-chlorophyll containing microorganisms such as bacteria or zooplankton (Kujawinski *et al.*, 2002).

It was also proposed that a time delay between phytoplankton reproduction (i.e. chlorophyll-a increase) and phytoplankton organic matter excretion (i.e. surfactant production) might result in no observable correlation between SA and chlorophyll-a (Gašparović *et al.*, 2011).

Even so, previous work (Wurl *et al.*, 2011a; Pereira *et al.*, 2016) suggested that chlorophyll-a might not be a good proxy for primary productivity as it only accounts for about 50% of total pigment in most marine ecosystems (Barlow *et al.*, 2002), the remainder being contributed principally by other phytoplankton pigments including chlorophyll b and c and carotenoids

(Kirk, 1994). So, total primary productivity associated with SA was also investigated in the current study but no strong correlation was found in the oceanic samples (see section 4.2.5).

In agreement with Wurl and Holmes (2008) the most likely explanation for the discrepancy is that at ocean basin scales as in the current study, with diverse biogeochemical regimes, multiple possible sources of surfactant will be large and include temporal components as well as additional effects from physical parameters. The data from the current study then challenge the use of primary productivity solely as a proxy for surfactant activity distributions.

To conclude, any simple correlation between surfactant distributions and biological indicators such as chlorophyll-a and primary productivity might be hidden by physical variables. For exmple, wind-induceed turbulence, advection and convection partially control the enrichment and depletion of organic matter in the SML (Carlson, 1983; Wurl *et al.*, 2009; Carlson, 2013).

It was concluded from the current study that CDOM may not be used to predict surfactant extent (see section 4.2.7). This might not be unexpected given that SA is often or exclusively only a minor DOM component (see section 1.1.3) and that CDOM behaviour reflected those of some other, dominant, non-surfactant components.

Frew *et al*. (2002) also showed temporal variability in SA/CDOM ratios in the Middle Atlantic Bight, with higher ratios during spring than in late summer and autumn coinciding with a phytoplankton bloom.

6.2.4.1 Association of SA with wind speed in the Atlantic Ocean

The constant enrichment of surfactants in the SML at all recorded wind speeds (up to 13 m s^{-1}) in the current study (see section 4.2.4) was in contrast with Wurl *et al*. (2011) who predicted that at high latitudes in the Atlantic Ocean (i.e. north of 30°N and south of 30°S), organic matter enrichment (including surfactants) would be precluded at the wind speeds greater than 12 m s^{-1}.

We should now be confident that high EFs at such high wind speeds should not be surprising because the SML reforms rapidly within seconds following physical disruption (Dragcevic and Pravdic, 1981; Cunliffe *et al.*, 2013). Organic matter dispersed by breaking waves reabsorbs to the surfaces of air bubbles generated by the same breaking waves (Hunter, 1977; Stefan and Szeri, 1999; Liss *et al.*, 2005; Wurl *et al.*, 2011b) and is transported back to the surface via

bubble scavenging or is ejected to the atmosphere via bubble bursting at the atmosphere-ocean interface.

The results from the current study thus strongly support the notion of a self-sustaining SML, and there is no reason to exclude the operation of the above mechanism at high wind speeds in the high latitudes of the Atlantic Ocean.

Moreover, upward transport facilitated by bubbles may be selective as organic matter with surface active properties (i.e. surfactants) might have a higher potential to be scavenged to the surface compared to the less surface-active organics (Liss, 1975; Stefan and Szeri, 1999).

In contrast, Wurl *et al*. (2009) argued that at high wind speeds bubbles carrying organic matter might penetrate into deeper waters releasing the material into deep waters and take a longer time to return to the upper layers resulting in a temporary depletion in the SML.

With an observed high level of agreement in SA distributions between AMT24 and AMT25, it would appear that there is a dynamic equilibrium operating in oceanic systems. While SML disruption frequently occurs at high latitudes, this is compensated by an enhanced bubble-mediated flux of organic compounds to the ocean's surface, and hence SML enrichments are maintained. This outcome may indicate that SA enrichment of the SML might be decoupled from ambient wind speed in the open oceans.

Additionally, in the presence of fewer surfactants present in SSW, a larger proportion of these compounds absorb to the surface of rising bubbles leading to high EFs, whereas with high concentrations of surfactants in SSW, less surfactant is scavenged due to possibly not enough surface bubbles being available, leading to lower EFs.

The current study also supports previous conclusions regarding the stability of the SML under high wind speeds during both laboratory and field experiments. For example, Broecker *et al.* (1978) reported that an artificial surface film is persistent and resistant to tear up to wind speeds of 13 m s^{-1} in a linear wind-wave tunnel.

However, a simple correlation between surfactant enrichments and wind speed in oceanic waters might be masked by other variables including surface vorticity, wave velocity, surface turbulence, biological indicators and surfactant composition. An alternative possibility from the current study as suggested by Wurl *et al*. (2011) is that surfactants include both dissolved and

particulate fractions, the latter perhaps having a better correlation with wind speed than the dissolved fraction.

6.3 Atmosphere-ocean gas exchange

6.3.1 *Surfactant control of atmosphere-ocean gas exchange*

Surfactant control of the atmosphere-ocean exchange of climate active gases has come to prominence in recent years as climate change issues have received more attention. However, the absence of information on the extent and distribution of surfactants on the global scale has become one of the major obstacles to understanding their importance (Tsai and Liu, 2003).

Surfactant control of gas exchange (through dynamic and static mechanisms) is estimated to be considerable (see section 1.2.1). So, an important role for surfactants in air-sea gas exchange is inevitable. Importantly, the work presented in this thesis shows that previous estimates of gas exchange between the atmosphere and the oceans might be overestimated because the presence of surfactants has not been accounted for, and this is especially relevant to high wind regimes where it was previously thought that surfactants were not enriched in the SML, something that the work in this thesis has shown to be incorrect.

Surfactant suppression of k_w by up to 50% may be typical (Frew, 1997; Bock *et al.*, 1999; Salter *et al.*, 2011) (see Chapter 1). While strong spatiotemporal gradients in surfactants within the SML, and hence in k_w, have been reported for some coastal waters (Frew *et al.*, 1990; Schneider-Zapp *et al.*, 2014; Pereira *et al.*, 2016), prior to the current study surfactant distributions at the ocean basin scale were based only on estimates derived from proxies (Wurl *et al.*, 2011b).

Quantification of the impact of surfactants on gas exchange rates was facilitated using a custom-built experimental tank during the current study. This enabled turbulence to be controlled so that the only relevant variable in the experiments was SA (see section 2.6). The extrapolation of the results derived from the laboratory experiments to larger scales representative of the open ocean might be justifiable but requires additional experiments.

The maximum of ~ 25% in k_w suppression of the Atlantic oceanic samples during the current study was lower than observed for identical tank experiments using coastal North Sea samples that had a maximum of 51% suppression (Pereira *et al.*, 2016).

It should be pointed that these analyses made no consideration of the possible effect of surfactant compositional differences between the two regions (i.e. the North Sea and the Atlantic Ocean). Therefore, from the current study, it is suggested that in addition to SA, differences in surfactant composition indicated by variability in CDOM parameters might affect k_w suppression.

It was suggested previously that the seasonal and spatial variability of water column productivity in the Baltic Sea may drive changes to the thickness and composition of surface films resulting in variability in the suppression of gas transfer (Schmidt and Schneider, 2011).

6.3.2 *Gas exchange and CDOM association*

An inverse linear relationship between CH_4 R_{660}' and CDOM absorbance was found during the current study (see section 5.2.2). However, the correlation was not statistically significant. This was in agreement with the recent conclusion of Pereira *et al*. (2016) who proposed that using remotely sensed CDOM as a proxy for the k_w estimation is not feasible.

From the current study, it is suggested that as the concentration of organic matter in the SML and corresponding sub-surface waters are tightly bound (i.e. sub-surface waters are a source of organic compounds to the SML, see section 4.2.2) and that a better approach might be to use enrichment factors as a proxy rather than absolute values of organic matter concentration (CDOM absorbance) in either the SML or the sub-surface waters (see section 5.2.2).

Furthermore, increasing CDOM (E_2: E_3) is indicative of a greater proportion of lower molecular weight organic matter (Peuravuori and Pihlaja, 1997). That CDOM (E_2: E_3) is enhanced in the SML relative to the corresponding sub-surface waters, implies that organic matter of a lower molecular weight is more abundant in the SML than the sub-surface waters and hence suggestive of it being more important in retarding gas transfer in the SML.

Chapter 7. Conclusion and future work

The current study has provided novel data on the distribution of surfactants and CDOM in SML and throughout the water column (≤ 100 m) of the Atlantic Ocean. The results of this study challenge the suggestion of Wurl *et al*. (2011) that oceanic regions with a monthly average wind speed above 10 m s^{-1} are free of SML and its components (Wurl *et al.*, 2011b).

The present study unequivocally shows that the SML enrichment in surfactants persists at wind speeds higher than the average global oceanic wind speed. This research has contributed evidence that the SML is a self-sustaining environment with respect to organic matter distribution.

The direct measurement of SA in the current study revealed a clear picture of surfactant distribution in the Atlantic Ocean that is an advance on the proposed distribution of Wurl *et al*. (2011) based on proxies including primary productivity and wind speeds.

A generally higher SA was observed in the Atlantic Northern hemisphere compared to the Southern hemisphere, with an SA maximum around 40^{o}N associated with in-situ production or terrestrial discharge. Also, an increase on SA in the Equatorial region suggests SA inputs to the SML via equatorial upwelling.

Further investigation by determining CDOM optical properties revealed more details of the different sources, molecular weights and composition of organic matter dominant in the Atlantic biogeochemical provinces.

In-situ regional production of low molecular weight protein-like components is suggested for most Atlantic provinces. However, there was a possibility of high molecular weight humic materials with a terrestrial origin near the continental shelves during the current study. Also, CDOM exposed to high degradation (i.e. ‘old’ CDOM) might be transported from the centre of the oligotrophic gyres to the surface layers.

Although this thesis presents a considerable dataset on SA and CDOM in the Atlantic Ocean provinces, there remain important concerns that should be considered in future work;

Temporal sampling within the study area

Improvement to the spatiotemporal resolution of SA sampling would help to better determine surfactant coverage in the Atlantic Ocean. If they occur, seasonal gradients in SA would be particularly important in the Atlantic Northern Hemisphere which is a large sink for CO_2.

Air-sea CO_2 exchange rates might are likely to be greatly overestimated if surfactants present in the SML are neglected. Previously observed large seasonal variability in pCO_2 in the North Atlantic was attributed to variabilities in temperature, biological activity, mixing and water currents. However, surfactant control on k_w also needs to be taken into account (Takahashi *et al.*, 2009).

This will require the routine measurement of SA. It is anticipated that future seasonal measurements of the type described in this thesis, will move us to eventually better parameterization of the surfactants control on k_w.

Data resolution in the water column could be improved by collecting more samples below the base of the mixed layer, although this is impossible within the constraints of AMT sampling and also by currently time-consuming sample analysis.

Investigation into surfactants composition

Concerning the various sources of surfactant in the marine environment (see section 1.1.3), a better understanding of surfactant composition will probably be necessary for a better understanding of the variability in surfactant control of air-sea gas exchange, both spatially and temporally.

References

Agogué, H., Casamayor, E.O., Joux, F., Obernosterer, I., Dupuy, C., Lantoine, F., Catala, P., Weinbauer, M.G., Reinthaler, T. and Herndl, G.J. (2004) 'Comparison of samplers for the biological characterization of the sea surface microlayer', *Limnology and Oceanography: methods*, 2, pp. 213-225.

Aiken, G.R., McKnight, D.M., Wershaw, R.L. and MacCarthy, P. (1985) 'An introduction to humic substances in soil, sediment, and water', *Geochemistry, Isolation and Characterization, Wiley: 1-9.*

Aiken, J., Rees, N., Hooker, S., Holligan, P., Bale, A., Robins, D., Moore, G., Harris, R. and Pilgrim, D. (2000) 'The Atlantic Meridional Transect: overview and synthesis of data', *Progress in Oceanography*, 45(3), pp. 257-312.

Alldredge, A.L. and Gotschalk, C. (1988) 'In situ settling behavior of marine snow', *Limnology and Oceanography*, 33(3), pp. 339-351.

Alldredge, A.L., Passow, U. and Logan, B.E. (1993) 'The abundance and significance of a class of large, transparent organic particles in the ocean', *Deep Sea Research Part I: Oceanographic Research Papers*, 40(6), pp. 1131-1140.

Archer, C.L. and Jacobson, M.Z. (2005) 'Evaluation of global wind power', *Journal of Geophysical Research: Atmospheres (1984–2012)*, 110(D12).

Asher, W.E. (1997) 'The sea-surface microlayer and its effect on global air-sea gas transfer', *The sea surface and global change*, pp. 251-286.

Asher, W.E. (2009) 'The effects of experimental uncertainty in parameterizing air-sea gas exchange using tracer experiment data', *Atmospheric Chemistry and Physics*, 9(1), pp. 131-139.

Asher, W.E. and Pankow, J.F. (1986) 'The interaction of mechanically generated turbulence and interfacial films with a liquid phase controlled gaslliquid transport process', *Tellus B: Chemical and Physical Meteorology*, 38(5), pp. 305-318.

Astoreca, R., Rousseau, V. and Lancelot, C. (2009) 'Coloured dissolved organic matter (CDOM) in Southern North Sea waters: Optical characterization and possible origin', *Estuarine, Coastal and Shelf Science*, 85(4), pp. 633-640.

Azam, F. and Long, R.A. (2001) 'Oceanography: Sea snow microcosms', *Nature*, 414(6863), pp. 495-498.

Azetsu-Scott, K. and Passow, U. (2004) 'Ascending marine particles: Significance of transparent exopolymer particles (TEP) in the upper ocean', *Limnology and Oceanography*, 49(3), pp. 741-748.

Baker, A. (2001) 'Fluorescence excitation− emission matrix characterization of some sewage-impacted rivers', *Environmental science & technology*, 35(5), pp. 948-953.

Baker, A. and Spencer, R.G.M. (2004) 'Characterization of dissolved organic matter from source to sea using fluorescence and absorbance spectroscopy', *Science of the Total Environment*, 333(1), pp. 217-232.

Barbier, M., Joly, D., Saliot, A. and Tourres, D. (1973) *Deep Sea Research and Oceanographic Abstracts*. Elsevier.

Barger, W.R. (1991) *A review of experimental observations and remaining questions concerning formation, persistence and disappearance of sea slicks*. NAVAL RESEARCH LAB WASHINGTON DC.

Barger, W.R. and Means, J.C. (1985) 'Clues to the structure of marine organic material from the study of physical properties of surface films', *Marine and Estuarine Geochemistry, Lewis Publishers, Chelsea Michigan. 1985. p 47-67, 6 fig, 6 tab, 25 ref.*, pp. 47-67.

Barker, D.R. and Zeitlin, H. (1972) 'Metal-ion concentrations in sea-surface microlayer and size-separated atmospheric aerosol samples in Hawaii', *Journal of Geophysical Research*, 77(27), pp. 5076-5086.

Barlow, R.G., Aiken, J., Holligan, P.M., Cummings, D.G., Maritorena, S. and Hooker, S. (2002) 'Phytoplankton pigment and absorption characteristics along meridional transects in the Atlantic Ocean', *Deep Sea Research Part I: Oceanographic Research Papers*, 49(4), pp. 637-660.

Benner, R. (2002) 'Chemical composition and reactivity', *Biogeochemistry of marine dissolved organic matter*, 3, pp. 56-90.

Benner, R. and Pakulski, J.D. (1992) 'Bulk chemical characteristics of dissolved organic matter in the ocean', *Science*, 255(5051), p. 1561.

Berger, W.H. and Herguera, J.C. (1992) 'Reading the sedimentary record of the ocean's productivity', in *Primary productivity and biogeochemical cycles in the sea*. Springer, pp. 455-486.

Berman, T. and Holenberg, M. (2005) 'Don't fall foul of biofilm through high TEP levels', *Filtration & separation*, 42(4), pp. 30-32.

Berman, T. and Passow, U. (2007) 'Transparent Exopolymer Particles (TEP): an overlooked factor in the process of biofilm formation in aquatic environments', *Nature, preceedings*.

Bezdek, H.F. and Carlucci, A.F. (1972) 'Surface concentration of marine bacteria', *Limnology and Oceanography*, 17(4), pp. 566-569.

Blough, N.V. and Del Vecchio, R. (2002) 'Chromophoric DOM in the Coastal Environment-Chapter 10', in in Hansell, D.A.a.C., C.A. (ed.) (ed.) *Biogeochemistry of Marine Dissolved Organic Matter*. Academic Press, pp. 509-546.

Bock, E.J., Hara, T., Frew, N.M. and McGillis, W.R. (1999) 'Relationship between air-sea gas transfer and short wind waves', *Journal of Geophysical Research: Oceans*, 104(C11), pp. 25821-25831.

Boss, E., Pegau, W.S., Zaneveld, J.R.V. and Barnard, A.H. (2001) 'Spatial and temporal variability of absorption by dissolved material at a continental shelf', *Journal of Geophysical Research: Oceans*, 106(C5), pp. 9499-9507.

Bricaud, A., Morel, A. and Prieur, L. (1981) 'Absorption by dissolved organic matter of the sea (yellow substance) in the UV and visible domains', *Limnology and oceanography*, 26(1), pp. 43-53.

Brockmann, U.H., Huhnerfuss, H., Kattner, G., Broecker, H.C. and Hentzschel, G. (1982) 'Artificial surface films in the sea area near Sylt', *Limnology and oceanography*, 27(6), pp. 1050-1058.

Broecker, H.C. (1978) 'The influence of wind on CO_2 exchange in a wind-wave tunnel, including the effect of monolayers', *J. mar. Res.*, 36(4), pp. 595-610.

Broecker, H.C., Petermann, J. and Siems, W. (1978) 'Influence of wind on CO2-exchange in a wind-wave tunnel, including effects of monolayers', *Journal of Marine Research*, 36(4), pp. 595-610.

Brown, M. (1977) 'Transmission spectroscopy examinations of natural waters: C. Ultraviolet spectral characteristics of the transition from terrestrial humus to marine yellow substance', *Estuarine and Coastal Marine Science*, 5(3), pp. 309-317.

Campbell, L. and Vaulot, D. (1993) 'Photosynthetic picoplankton community structure in the subtropical North Pacific Ocean near Hawaii (station ALOHA)', *Deep Sea Research Part I: Oceanographic Research Papers*, 40(10), pp. 2043-2060.

Carder, K.L., Steward, R.G., Harvey, G.R. and Ortner, P.B. (1989) 'Marine humic and fulvic acids: Their effects on remote sensing of ocean chlorophyll', *Limnology and oceanography*, 34(1), pp. 68-81.

Carlson, C.A. (2002) 'Production and removal processes', *Biogeochemistry of marine dissolved organic matter*, pp. 91-151.

Carlson, C.A., Ducklow, H.W. and Sleeter, T.D. (1996) 'Stocks and dynamics of bacterioplankton in the northwestern Sargasso Sea', *Deep Sea Research Part II: Topical Studies in Oceanography*, 43(2-3), pp. 491-515.

Carlson, D.J. (1982) 'A field evaluation of plate and screen microlayer sampling techniques', *Marine Chemistry*, 11(3), pp. 189-208.

Carlson, D.J. (1983) 'Dissolved organic materials in surface microlayers: Temporal and spatial variability and relation to sea state', *Limnology and Oceanography*, 28(3), pp. 415-431.

Carlson, D.J. (2013) 'The early diagenesis of organic matter: reaction at the air-sea interface', *Organic Geochemistry MH Engel, SA Macko*, pp. 255-268.

Carpenter, L.J. and Nightingale, P.D. (2015) 'Chemistry and release of gases from the surface ocean', *Chemical reviews*, 115(10), pp. 4015-4034.

Chen, W., Westerhoff, P., Leenheer, J.A. and Booksh, K. (2003) 'Fluorescence excitation− emission matrix regional integration to quantify spectra for dissolved organic matter', *Environmental science & technology*, 37(24), pp. 5701-5710.

Cincinelli, A., Stortini, A.M., Perugini, M., Checchini, L. and Lepri, L. (2001) 'Organic pollutants in sea-surface microlayer and aerosol in the coastal environment of Leghorn-(Tyrrhenian Sea)', *Marine Chemistry*, 76(1), pp. 77-98.

Coble, P.G. (1996) 'Characterization of marine and terrestrial DOM in seawater using excitation-emission matrix spectroscopy', *Marine chemistry*, 51(4), pp. 325-346.

Coble, P.G. (2007) 'Marine optical biogeochemistry: the chemistry of ocean color', *Chemical reviews*, 107(2), pp. 402-418.

Coble, P.G., Green, S.A., Blough, N.V. and Gagosian, R.B. (1990) 'Characterization of dissolved organic matter in the Black Sea by fluorescence spectroscopy', *Nature*, 348(6300), pp. 432-435.

Collignon, A., Hecq, J.-H., Glagani, F., Voisin, P., Collard, F. and Goffart, A. (2012) 'Neustonic microplastic and zooplankton in the North Western Mediterranean Sea', *Marine pollution bulletin*, 64(4), pp. 861-864.

Corzo, A., Morillo, J.A. and Rodríguez, S. (2000) 'Production of transparent exopolymer particles (TEP) in cultures of Chaetoceros calcitrans under nitrogen limitation', *Aquatic Microbial Ecology*, 23(1), pp. 63-72.

Ćosović, B. (2005) 'Surface-Active Properties of the Sea Surface Microlayer and Consequences for Pollution in the Mediterranean Sea', in in Saliot, A.e. (ed.) *The Mediterranean Sea*. Springer, pp. 269-296.

Ćosović, B. and Vojvodić, V. (1982) 'The application of ac polarography to the determination of surface-active substances in seawater1', *Limnology and Oceanography*, 27(2), pp. 361-369.

Ćosović, B. and Vojvodić, V. (1998) 'Voltammetric analysis of surface active substances in natural seawater', *Electroanalysis*, 10(6), pp. 429-434.

Ćosović, B., Zutic, V., Kozarac, Z., Vojvodic, V. and Novakovic, T. (1979) 'Investigation of surfactants in North Adriatic in the period of 1974 to 1978. Evaluation of natural variations and pollution effects', *Rapports et Proces-Verbaux des Reunions-Commission Internationale pour l'Exploration Scientifique de la Mer Mediterranee (CIESM)*.

Ćosović, B., Ẑutić, V., Vojvodić, V. and Pleše, T. (1985) 'Determination of surfactant activity and anionic detergents in seawater and sea surface microlayer in the Mediterranean', *Marine chemistry*, 17(2), pp. 127-139.

Croot, P.L., Passow, U., Assmy, P., Jansen, S. and Strass, V.H. (2007) 'Surface active substances in the upper water column during a Southern Ocean Iron Fertilization Experiment (EIFEX)', *Geophysical research letters*, 34(3).

Cullen, J.J., MacIntyre, H.L. and Carlson, D.J. (1989) 'Distributions and photosynthesis of phototrophs in sea-surface films', *Marine Ecology Progress Series*, pp. 271-278.

Cunliffe, M., Engel, A., Frka, S., Gašparović, B., Guitart, C., Murrell, J.C., Salter, M., Stolle, C., Upstill-Goddard, R. and Wurl, O. (2013) 'Sea surface microlayers: A unified physicochemical and biological perspective of the air–ocean interface', *Progress in Oceanography*, 109, pp. 104-116.

Cunliffe, M., Harrison, E., Salter, M., Schaefer, H., Upstill-Goddard, R.C. and Murrell, J.C. (2009a) 'Comparison and validation of sampling strategies for the molecular microbial analysis of surface microlayers', *Aquatic Microbial Ecology*, 57(1), pp. 69-77.

Cunliffe, M. and Murrell, J.C. (2009) 'The sea-surface microlayer is a gelatinous biofilm', *The ISME journal*, 3(9), p. 1001.

Cunliffe, M. and Murrell, J.C. (2010) 'Eukarya 18S rRNA gene diversity in the sea surface microlayer: implications for the structure of the neustonic microbial loop', *The ISME journal*, 4(3), pp. 455-458.

Cunliffe, M., Salter, M., Mann, P.J., Whiteley, A.S., Upstill-Goddard, R.C. and Murrell, J.C. (2009b) 'Dissolved organic carbon and bacterial populations in the gelatinous surface microlayer of a Norwegian fjord mesocosm', *FEMS microbiology letters*, 299(2), pp. 248-254.

Cunliffe, M., Upstill-Goddard, R.C. and Murrell, J.C. (2011) 'Microbiology of aquatic surface microlayers', *FEMS microbiology reviews*, 35(2), pp. 233-246.

Cunliffe, M. and Wurl, O. (2014) *Guide to best practices to study the ocean's surface*. Marine Biological Association of the United Kingdom.

Cuscov, M. and Muller, F.L.L. (2015) 'Differentiating humic and algal surface active substances in coastal waters by their pH-dependent adsorption behaviour', *Marine Chemistry*, 174, pp. 35-45.

da Silveira, I.C.A., Miranda, L.B. and Brown, W.S. (1994) 'On the origins of the North Brazil Current', *Journal of Geophysical Research: Oceans*, 99(C11), pp. 22501-22512.

Davies, J.T. (1966) *Proceedings of the Royal Society of London A: Mathematical, Physical and Engineering Sciences*. The Royal Society.

de Boyer Montégut, C., Madec, G., Fischer, A.S., Lazar, A. and Iudicone, D. (2004) 'Mixed layer depth over the global ocean: An examination of profile data and a profile-based climatology', *Journal of Geophysical Research: Oceans*, 109(C12).

De Haan, H. and De Boer, T. (1987) 'Applicability of light absorbance and fluorescence as measures of concentration and molecular size of dissolved organic carbon in humic Lake Tjeukemeer', *Water Research*, 21(6), pp. 731-734.

DeGrandpre, M.D., Vodacek, A., Nelson, R.K., Bruce, E.J. and Blough, N.V. (1996) 'Seasonal seawater optical properties of the US Middle Atlantic Bight', *Journal of Geophysical Research: Oceans*, 101(C10), pp. 22727-22736.

Del Castillo, C.E. and Coble, P.G. (2000) 'Seasonal variability of the colored dissolved organic matter during the 1994–95 NE and SW monsoons in the Arabian Sea', *Deep Sea Research Part II: Topical Studies in Oceanography*, 47(7), pp. 1563-1579.

Del Vecchio, R. and Blough, N.V. (2004) 'Spatial and seasonal distribution of chromophoric dissolved organic matter and dissolved organic carbon in the Middle Atlantic Bight', *Marine Chemistry*, 89(1), pp. 169-187.

Dragcevic, D. and Pravdic, V. (1981) 'Properties of the seawater-air interface. 2. Rates of surface film formation under steady state conditions1', *Limnology and Oceanography*, 26(3), pp. 492-499.

Duinker, J.C. and Boon, J.P. (1986) 'PCB congeners in the marine environment-a review', in *Organic micropollutants in the aquatic environment*. Springer, pp. 187-205.

Elasri, M.O. and Miller, R.V. (1999) 'Study of the response of a biofilm bacterial community to UV radiation', *Applied and Environmental Microbiology*, 65(5), pp. 2025-2031.

Emery, W.J. and Meincke, J. (1986) 'Global water masses-summary and review', *Oceanologica acta*, 9(4), pp. 383-391.

Engel, A. (2004) 'Distribution of transparent exopolymer particles (TEP) in the northeast Atlantic Ocean and their potential significance for aggregation processes', *Deep Sea Research Part I: Oceanographic Research Papers*, 51(1), pp. 83-92.

Engel, A., Goldthwait, S., Passow, U. and Alldredge, A. (2002) 'Temporal decoupling of carbon and nitrogen dynamics in a mesocosm diatom bloom', *Limnology and Oceanography*, 47(3), pp. 753-761.

Fedoseev, A. (1970) 'Geostrophic circulation of surface waters on the shelf of north-west Africa', *Rapp PV Reun Cons Int Explor Mer*, 159, pp. 165-175.

Ferrari, G.M., Dowell, M.D., Grossi, S. and Targa, C. (1996) 'Relationship between the optical properties of chromophoric dissolved organic matter and total concentration of dissolved organic carbon in the southern Baltic Sea region', *Marine Chemistry*, 55(3-4), pp. 299-316.

Fogg, G.E. (1966) 'The extracellular products of algae', *Oceanogr. Mar. Biol. Annu. Rev*, 4(19), p. 212.

Franklin, M.P., McDonald, I.R., Bourne, D.G., Owens, N.J.P., Upstill-Goddard, R.C. and Murrell, J.C. (2005) 'Bacterial diversity in the bacterioneuston (sea surface microlayer): the bacterioneuston through the looking glass', *Environmental Microbiology*, 7(5), pp. 723-736.

Frew, N.M. (1997) 'The role of organic films in air-sea gas exchange, The Sea Surface and Global Change PS Liss, RA Duce, 121–171', in Liss, P.S.a.D., R.A. (ed.) *The Sea Surface and Global Change*. Cambridge Univ. Press, New York.

Frew, N.M. (2005) 'The role of organic films in air-sea gas exchange', *The Sea Surface and Global Change, edited by PS. Liss, and RA. Duce*, pp. 121-163.

Frew, N.M., Bock, E.J., Schimpf, U., Hara, T., Haußecker, H., Edson, J.B., McGillis, W.R., Nelson, R.K., McKenna, S.P. and Uz, B.M. (2004) 'Air-sea gas transfer: Its dependence on wind stress, small-scale roughness, and surface films', *Journal of Geophysical Research: Oceans (1978–2012)*, 109(C8), pp. 1-23.

Frew, N.M., Goldman, J.C., Dennett, M.R. and Johnson, A.S. (1990) 'Impact of phytoplankton-generated surfactants on air-sea gas exchange', *Journal of Geophysical Research: Oceans*, 95(C3), pp. 3337-3352.

Frew, N.M. and Nelson, R.K. (1992) 'Scaling of marine microlayer film surface pressure-area isotherms using chemical attributes', *Journal of Geophysical Research: Oceans*, 97(C4), pp. 5291-5300.

Frew, N.M., Nelson, R.K. and Johnson, C.G. (2006) 'Sea slicks: variability in chemical composition and surface elasticity', in *Marine Surface Films*. Springer, pp. 45-56.

Frew, N.M., Nelson, R.K., McGillis, W.R., Edson, J.B., Bock, E.J. and Hara, T. (2002) 'Spatial variations in surface microlayer surfactants and their role in modulating air-sea exchange', *Gas Transfer at Water Surfaces*, pp. 153-159.

Frka, S., Dautović, J., Kozarac, Z., Ćosović, B., Hoffer, A. and Kiss, G. (2012) 'Surface-active substances in atmospheric aerosol: an electrochemical approach', *Tellus B*, 64, pp. 1-13.

Frka, S., Kozarac, Z. and Ćosović, B. (2009) 'Characterization and seasonal variations of surface active substances in the natural sea surface micro-layers of the coastal Middle Adriatic stations', *Estuarine, coastal and shelf science*, 85(4), pp. 555-564.

Gade, M., Hühnerfuss, H. and Korenowski, G. (2006) *Marine surface films*. Springer.

Galgani, L. and Engel, A. (2016) 'Changes in optical characteristics of surface microlayers hint to photochemically and microbially mediated DOM turnover in the upwelling region off the coast of Peru', *Biogeosciences*, 13(8), pp. 2453-2473.

Gao, Q., Leck, C., Rauschenberg, C. and Matrai, P.A. (2012) 'On the chemical dynamics of extracellular polysaccharides in the high Arctic surface microlayer', *Ocean Science*, 8(4), pp. 401-418.

Gardener, D. (1977) 'Nutrients as tracer of water mass structure in the coastal upwelling of Northwest Africa', in Angel, M. (ed.) *Voyage of discovery*. Pergamon Press, Oxford and NY, pp. 305-326.

Garrett, W.D. (1965) 'Collection of slick-forming materials from the sea surface', *Limnology and Oceanography*, 10(4), pp. 602-605.

Gašparović, B. (2012) 'Decreased production of surface-active organic substances as a consequence of the oligotrophication in the northern Adriatic Sea', *Estuarine, coastal and shelf science*, 115, pp. 33-39.

Gašparović, B. and Ćosović, B. (1994) 'Electrochemical estimation of the dominant type of surface active substances in seawater samples using o-nitrophenol as a probe', *Marine chemistry*, 46(1-2), pp. 179-188.

Gašparović, B. and Ćosović, B. (2001) 'Distribution of surface active substances in the northern Adriatic Sea', *Marine chemistry*, 75(4).

Gašparović, B., Djakovac, T., Tepić, N. and Degobbis, D. (2011) 'Relationships between surface-active organic substances, chlorophyll a and nutrients in the northern Adriatic Sea', *Continental Shelf Research*, 31(10), pp. 1149-1160.

Gašparović, B., Kozarac, Z., Saliot, A., Ćosović, B. and Möbius, D. (1998) 'Physicochemical Characterization of Natural andex-SituReconstructed Sea-Surface Microlayers', *Journal of colloid and interface science*, 208(1), pp. 191-202.

Gašparović, B., Plavšić, M., Ćosović, B. and Saliot, A. (2007) 'Organic matter characterization in the sea surface microlayers in the subarctic Norwegian fjords region', *Marine Chemistry*, 105(1), pp. 1-14.

Gašparović, B., Vojvodić, V. and Ćosović, B. (1997) 'Characterization of organic matter in fractionated seawater samples using o-nitrophenol as an electrochemical probe', *Analytica chimica acta*, 338(3), pp. 179-190.

Giam, C.S., Chan, H.S., Neff, G.S. and Atlas, E.L. (1978) 'Phthalate ester plasticizers: a new class of marine pollutant', *Science*, 199(4327), pp. 419-421.

Gladyshev, M.I. (2002) *Biophysics of the surface microlayer of aquatic ecosystems*. UK: IWA Publishing.

Goering, J.J. and Menzel, D.W. (1965) 'The nutrient chemistry of the sea surface', *Deep Sea Research and Oceanographic Abstracts*, 12, pp. 839-843.

Gogou, A. and Repeta, D.J. (2010) 'Particulate-dissolved transformations as a sink for semi-labile dissolved organic matter: Chemical characterization of high molecular weight dissolved and surface-active organic matter in seawater and in diatom cultures', *Marine Chemistry*, 121(1), pp. 215-223.

Goldman, J.C., Dennett, M.R. and Frew, N.M. (1988) 'Surfactant effects on air-sea gas exchange under turbulent conditions', *Deep Sea Research Part A. Oceanographic Research Papers*, 35(12), pp. 1953-1970.

Goutx, M. and Saliot, A. (1980) 'Relationship between dissolved and particulate fatty acids and hydrocarbons, chlorophyll a and zooplankton biomass in Villefranche Bay, Mediterranean Sea', *Marine Chemistry*, 8(4), pp. 299-318.

Grasshoff, K., Kremling, K. and Ehrhardt, M. (2009) *Methods of seawater analysis*. John Wiley & Sons.

Green, S.A. (1992) *Applications of fluorescence spectroscopy to environmental chemistry*. USA: Woods Hole Oceanographic Institution MA.

Green, S.A. and Blough, N.V. (1994) 'Optical absorption and fluorescence properties of chromophoric dissolved organic matter in natural waters', *Limnology and Oceanography*, 39(8), pp. 1903-1916.

Guitart, C., Garcia-Flor, N., Bayona, J.M. and Albaigés, J. (2007) 'Occurrence and fate of polycyclic aromatic hydrocarbons in the coastal surface microlayer', *Marine Pollution Bulletin*, 54(2), pp. 186-194.

Guitart, C., García-Flor, N., Dachs, J., Bayona, J.M. and Albaigés, J. (2004) 'Evaluation of sampling devices for the determination of polycyclic aromatic hydrocarbons in surface microlayer coastal waters', *Marine pollution bulletin*, 48(9), pp. 961-968.

Guo, X., Yin, Y., Tan, Z., Zhang, Z., Chen, Y. and Liu, J. (2016) 'Significant Enrichment of Engineered Nanoparticles in Water Surface Microlayer', Environmental Science & Technology Letters, 3(10), pp. 381-385.

Hamilton, B., Dean, C., Kurata, N., Vella, K., Soloviev, A., Tartar, A., Shivji, M., Perrie, W. and Lehner, S. (2014) *Proceedings of the 2014 IEEE International Geoscience & Remote Sensing Symposium and 35th Canadian Symposium on Remote Sensing*. IEEE Xplore.

Hamilton, E.I. and Clifton, R.J. (1979) 'Techniques for sampling the air-sea interface for estuarine and coastal waters', *Limnology and Oceanography*, 24(1), pp. 188-193.

Hansell, D.A. (2013) 'Recalcitrant dissolved organic carbon fractions', *Annual Review of Marine Science*, 5, pp. 421-445.

Hansell, D.A. and Carlson, C.A. (2014) *Biogeochemistry of marine dissolved organic matter*. Academic Press.

Hardy, J.T. (1971) *Ecology of phytoneuston in a temperate marine lagoon*. University of Washington.

Hardy, J.T. (1973) 'Phytoneuston ecology of a temperate marine lagoon', *Limnol. Oceanogr*, 18(4), pp. 525-533.

Hardy, J.T. (1982) 'The sea surface microlayer: Biology, chemistry and anthropogenic enrichment', *Progress in Oceanography*, 11(4), pp. 307-328.

Hardy, J.T., Crecelius, E.A., Antrim, L.D., Kiesser, S.L., Broadhurst, V.L., Boehm, P.D., Steinhauer, W.G. and Coogan, T.H. (1990) 'Aquatic surface microlayer contamination in Chesapeake Bay', *Marine Chemistry*, 28(4), pp. 333-351.

Harvey, G.R., Boran, D.A., Chesal, L.A. and Tokar, J.M. (1983) 'The structure of marine fulvic and humic acids', *Marine Chemistry*, 12(2-3), pp. 119-132.

Harvey, G.W. and Burzell, L.A. (1972) 'A simple microlayer method for small samples', *Limnology and Oceanography*, 17(1), pp. 156-157.

Hatcher, R.F. and Parker, B.C. (1974) 'Laboratory comparisons of four surface microlayer samplers', *Limnology and Oceanography*, 19(1), pp. 162-165.

Haug, A. and Myklestad, S. (1976) 'Polysaccharides of marine diatoms with special reference to Chaetoceros species', *Marine Biology*, 34(3), pp. 217-222.

Heinonen, K.B., Ward, J.E. and Holohan, B.A. (2007) 'Production of transparent exopolymer particles (TEP) by benthic suspension feeders in coastal systems', *Journal of Experimental Marine Biology and Ecology*, 341(2), pp. 184-195.

Helms, J.R., Stubbins, A., Ritchie, J.D., Minor, E.C., Kieber, D.J. and Mopper, K. (2008) 'Absorption spectral slopes and slope ratios as indicators of molecular weight, source, and photobleaching of chromophoric dissolved organic matter', *Limnology and Oceanography*, 53(3), pp. 955-969.

Heywood, J.L., Zubkov, M.V., Tarran, G.A., Fuchs, B.M. and Holligan, P.M. (2006) 'Prokaryoplankton standing stocks in oligotrophic gyre and equatorial provinces of the Atlantic Ocean: evaluation of inter-annual variability', *Deep Sea Research Part II: Topical Studies in Oceanography*, 53(14), pp. 1530-1547.

Hisatsuka, K.i., Nakahara, T., Sano, N. and Yamada, K. (1971) 'Formation of rhamnolipid by Pseudomonas aeruginosa and its function in hydrocarbon fermentation', *Agricultural and Biological Chemistry*, 35(5), pp. 686-692.

Hooker, S.B., Rees, N.W. and Aiken, J. (2000) 'An objective methodology for identifying oceanic provinces', *Progress in Oceanography*, 45(3), pp. 313-338.

Hudson, N., Baker, A. and Reynolds, D. (2007) 'Fluorescence analysis of dissolved organic matter in natural, waste and polluted waters—a review', *River Research and Applications*, 23(6), pp. 631-649.

Hühnerfuss, H. (2006) 'Basic physicochemical principles of monomolecular sea slicks and crude oil spills', in *Marine Surface Films*. Springer, pp. 21-35.

Hunter, K.A. (1975) 'Chemistry of the sea surface microlayer', in Liss, P.a.D., R. (ed.) *Chemical oceanography*. UK: Cambridge University Press, pp. 287-319.

Hunter, K.A. (1997) 'Chemistry of the sea-surface microlayer', *The sea surface and global change*, pp. 287-319.

Hunter, K.A. and Liss, P.S. (1981) 'Organic sea surface films', *Elsevier Oceanography Series*, 31, pp. 259-298.

Jähne, B., Heinz, G. and Dietrich, W. (1987a) 'Measurement of the diffusion coefficients of sparingly soluble gases in water', *Journal of Geophysical Research: Oceans*, 92(C10), pp. 10767-10776.

Jähne, B., Münnich, K.O., Bösinger, R., Dutzi, A., Huber, W. and Libner, P. (1987b) 'On the parameters influencing air-water gas exchange', *Journal of Geophysical Research: Oceans*, 92(C2), pp. 1937-1949.

Jiao, N., Herndl, G.J., Hansell, D.A., Benner, R., Kattner, G., Wilhelm, S.W., Kirchman, D.L., Weinbauer, M.G., Luo, T. and Chen, F. (2010) 'Microbial production of recalcitrant dissolved organic matter: long-term carbon storage in the global ocean', *Nature reviews. Microbiology*, 8(8), p. 593.

Johannessen, S.C., Miller, W.L. and Cullen, J.J. (2003) 'Calculation of UV attenuation and colored dissolved organic matter absorption spectra from measurements of ocean color', *Journal of Geophysical Research: Oceans*, 108(C9).

Jørgensen, L., Stedmon, C.A., Kragh, T., Markager, S., Middelboe, M. and Søndergaard, M. (2011) 'Global trends in the fluorescence characteristics and distribution of marine dissolved organic matter', *Marine Chemistry*, 126(1), pp. 139-148.

Joux, F., Agogué, H., Obernosterer, I., Dupuy, C., Reinthaler, T., Herndl, G.J. and Lebaron, P. (2006) 'Microbial community structure in the sea surface microlayer at two contrasting coastal sites in the northwestern Mediterranean Sea', *Aquatic Microbial Ecology*, 42(1), pp. 91-104.

Kirk, J.T.O. (1994) *Light and photosynthesis in aquatic ecosystems*. 2nd edn. UK: Cambridge university press.

Kitidis, V., Stubbins, A.P., Uher, G., Goddard, R.C.U., Law, C.S. and Woodward, E.M.S. (2006) 'Variability of chromophoric organic matter in surface waters of the Atlantic Ocean', *Deep Sea Research Part II: Topical Studies in Oceanography*, 53(14), pp. 1666-1684.

Kjelleberg, S. and Håkansson, N. (1976) 'Distribution of lipolytic, proteolytic, and amylolytic marine bacteria between the lipid film and the subsurface water', *Marine Biology*, 39(1), pp. 103-109.

Kolattukudy, P.E. (1976) 'Chemistry and biochemistry of natural waxes Elsevier', *Amsterdam (459pp.)*.

Komada, T., Schofield, O.M.E. and Reimers, C.E. (2002) 'Fluorescence characteristics of organic matter released from coastal sediments during resuspension', *Marine Chemistry*, 79(2), pp. 81-97.

Korshin, G.V., Li, C.-W. and Benjamin, M.M. (1997) 'Monitoring the properties of natural organic matter through UV spectroscopy: a consistent theory', *Water Research*, 31(7), pp. 1787-1795.

Kowalczuk, P. (1999) 'Seasonal variability of yellow substance absorption in the surface layer of the Baltic Sea', *Journal of Geophysical Research: Oceans*, 104(C12), pp. 30047-30058.

Kowalczuk, P., Tilstone, G.H., Zabłocka, M., Röttgers, R. and Thomas, R. (2013) 'Composition of dissolved organic matter along an Atlantic Meridional Transect from fluorescence spectroscopy and Parallel Factor Analysis', *Marine Chemistry*, 157, pp. 170-184.

Krauss, W., Käse, R.H. and Hinrichsen, H.H. (1990) 'The branching of the Gulf Stream southeast of the Grand Banks', *Journal of Geophysical Research: Oceans*, 95(C8), pp. 13089-13103.

Kujawinski, E.B., Farrington, J.W. and Moffett, J.W. (2002) 'Evidence for grazing-mediated production of dissolved surface-active material by marine protists', *Marine chemistry*, 77(2), pp. 133-142.

Kurata, N., Vella, K., Hamilton, B., Shivji, M., Soloviev, A., Matt, S., Tartar, A. and Perrie, W. (2016) 'Surfactant-associated bacteria in the near-surface layer of the ocean', *Scientific reports*, 6, pp. 1-8.

Kuznetsova, M. and Lee, C. (2001) 'Enhanced extracellular enzymatic peptide hydrolysis in the sea-surface microlayer', *Marine Chemistry*, 73(3), pp. 319-332.

Kuznetsova, M., Lee, C., Aller, J. and Frew, N. (2004) 'Enrichment of amino acids in the sea surface microlayer at coastal and open ocean sites in the North Atlantic Ocean', *Limnology and oceanography*, 49(5), pp. 1605-1619.

Lakowicz, J.R. (1999) 'Introduction to fluorescence', in Lakowicz, J.R. (ed.) *Principles of fluorescence spectroscopy*. 2nd edn. Springer, pp. 1-23.

Lang, S. and Wullbrandt, D. (1999) 'Rhamnose lipids–biosynthesis, microbial production and application potential', *Applied Microbiology and Biotechnology*, 51(1), pp. 22-32.

Le Quéré, C. and Saltzman, E.S. (2013) *Surface Ocean: Lower Atmosphere Processes*. John Wiley & Sons.

Ledwell, J.J. (1984) 'The variation of the gas transfer coefficient with molecular diffusity', in Brutsaert, W.a.J., G.H. (ed.) *Gas transfer at water surfaces*. Springer, pp. 293-302.

Leenheer, J.A. and Croué, J.-P. (2003) 'Peer reviewed: characterizing aquatic dissolved organic matter'. ACS Publications.

Ling, S.C. and Alldredge, A.L. (2003) 'Does the marine copepod Calanus pacificus consume transparent exopolymer particles (TEP)?', *Journal of plankton research*, 25(5), pp. 507-515.

Liss, P.S. (1975) 'Chemistry of the sea surface microlayer', *Chemical oceanography*, 2, pp. 193-243.

Liss, P.S. (1983) *Gas transfer: experiments and geochemical implications*. Springer.

Liss, P.S., Liss, P.S. and Duce, R.A. (2005) 'The sea surface and global change', in *The sea surface and global change* Cambridge University Press, pp. 121-172.

Liss, P.S. and Martinelli, F.N. (1978) 'The effect of oil films on the transfer of oxygen and water vapour across an air-water interface', *Thalassia Jugoslavica*, 14(1/2), pp. 215-220.

Liss, P.S. and Slater, P.G. (1974) 'Flux of gases across the air-sea interface', *Nature*, 247(5438), pp. 181-184.

Loiselle, S., Vione, D., Minero, C., Maurino, V., Tognazzi, A., Dattilo, A.M., Rossi, C. and Bracchini, L. (2012) 'Chemical and optical phototransformation of dissolved organic matter', *Water research*, 46(10), pp. 3197-3207.

Lombardini, P.P., Fiscella, B., Trivero, P., Cappa, C. and Garrett, W.D. (1989) 'Modulation of the spectra of short gravity waves by sea surface films: slick detection and characterization with a microwave probe', *Journal of Atmospheric and Oceanic Technology*, 6(6), pp. 882-890.

Longhurst, A. (1995) 'Seasonal cycles of pelagic production and consumption', *Progress in oceanography*, 36(2), pp. 77-167.

Longhurst, A., Sathyendranath, S., Platt, T. and Caverhill, C. (1995) 'An estimate of global primary production in the ocean from satellite radiometer data', *Journal of plankton Research*, 17(6), pp. 1245-1271.

Longhurst, A.R. (2010) *Ecological geography of the sea*. 2nd edn. Academic Press.

MacIntyre, F. (1974) 'The top millimeter of the ocean', *Scientific American*, 230(5), pp. 62-77.

Mann, P. (2010) '*Ammonium photoproduction and CDOM biogeochemistry in marine systems*', University of Newcastle upon Tyne.

Mari, X. and Kiørboe, T. (1996) 'Abundance, size distribution and bacterial colonization of transparent exopolymeric particles (TEP) during spring in the Kattegat', *Journal of Plankton Research*, 18(6), pp. 969-986.

Marumo, R., Taga, N. and Nakai, T. (1971) 'Neustonic bacteria and phytoplankton in surface microlayers of the equatorial waters', *Bull. Plankton Soc. Japan*, 18, pp. 36-41.

Matrai, P.A., Tranvik, L., Leck, C. and Knulst, J.C. (2008) 'Are high Arctic surface microlayers a potential source of aerosol organic precursors?', *Marine Chemistry*, 108(1), pp. 109-122.

Matsumoto, G. (1981) 'Comparative study on organic constituents in polluted and unpolluted inland aquatic environments—II: Features of fatty acids for polluted and unpolluted waters', *Water Research*, 15(7), pp. 779-787.

Mazurek, Z.A., Pogorzelski, J.S. and Boniewicz-Szmyt, K. (2008) 'Evolution of natural sea surface film structure as a tool for organic matter dynamics tracing', *Journal of Marine Systems*, 74, pp. S52-S64.

McKee, M.P., Ward, J.E., MacDonald, B.A. and Holohan, B.A. (2005) 'Production of transparent exopolymer particles (TEP) by the eastern oyster Crassostrea virginica', *Marine Ecology Progress Series*, 288, pp. 141-149.

McKenna, S.P. and McGillis, W.R. (2004) 'The role of free-surface turbulence and surfactants in air–water gas transfer', *International Journal of Heat and Mass Transfer*, 47(3), pp. 539-553.

McKnight, D.M., Boyer, E.W., Westerhoff, P.K., Doran, P.T., Kulbe, T. and Andersen, D.T. (2001) 'Spectrofluorometric characterization of dissolved organic matter for indication of precursor organic material and aromaticity', *Limnology and Oceanography*, 46(1), pp. 38-48.

McNeil, C. and D'Asaro, E. (2007) 'Parameterization of air-sea gas fluxes at extreme wind speeds', *Journal of Marine Systems*, 66(1), pp. 110-121.

Metzger, I. and Dobbins, W.E. (1967) 'Role of fluid properties in gas transfer', *Environmental science & technology*, 1(1), pp. 57-65.

Meyers-Schulte, K.J. and Hedges, J.I. (1986) 'Molecular evidence for a terrestrial component of organic matter dissolved in ocean water', *Nature*, 321(6065), pp. 61-63.

Michaels, A.F. and Knap, A.H. (1996) 'Overview of the US JGOFS Bermuda Atlantic Time-series Study and the Hydrostation S program', *Deep Sea Research Part II: Topical Studies in Oceanography*, 43(2), pp. 157-198.

Miller, R.L., Belz, M., Del Castillo, C. and Trzaska, R. (2002) 'Determining CDOM absorption spectra in diverse coastal environments using a multiple pathlength, liquid core waveguide system', *Continental Shelf Research*, 22(9), pp. 1301-1310.

Mittelstaedt, E. (1991) 'The ocean boundary along the northwest African coast: circulation and oceanographic properties at the sea surface', *Progress in Oceanography*, 26(4), pp. 307-355.

Momzikoff, A., Brinis, A., Dallot, S., Gondry, G., Saliot, A. and Lebaron, P. (2004) 'Field study of the chemical characterization of the upper ocean surface using various samplers', *Limnol. Oceanogr.: Methods*, 2, pp. 374-386.

Mopper, K. (1989) 'Photochemical source of biological substrates in sea water: Implications for carbon cycling', *Nature*, 341, p. 19.

Mopper, K., Feng, Z., Bentjen, S.B. and Chen, R.F. (1996) 'Effects of cross-flow filtration on the absorption and fluorescence properties of seawater', *Marine Chemistry*, 55(1), pp. 53-74.

Mopper, K., Ramana, K.S. and Drapeau, D.T. (1995) 'The role of surface-active carbohydrates in the flocculation of a diatom bloom in a mesocosm', *Deep Sea Research Part II: Topical Studies in Oceanography*, 42(1), pp. 47-73.

Mopper, K. and Schultz, C.A. (1993) 'Fluorescence as a possible tool for studying the nature and water column distribution of DOC components', *Marine Chemistry*, 41(1-3), pp. 229-238.

Moran, M.A., Sheldon, W.M. and Zepp, R.G. (2000) 'Carbon loss and optical property changes during long-term photochemical and biological degradation of estuarine dissolved organic matter', *Limnology and Oceanography*, 45(6), pp. 1254-1264.

Murray, H.E., Ray, L.E. and Giam, C.S. (1981a) 'Analysis of marine sediment, water and biota for selected organic pollutants', *Chemosphere*, 10(11-12), pp. 1327-1334.

Murray, H.E., Ray, L.E. and Giam, C.S. (1981b) 'Phthalic acid esters, total DDTs, and polychlorinated biphenyls in marine samples from Galveston Bay, Texas', *Bulletin of environmental contamination and toxicology*, 26(1), pp. 769-774.

Myklestad, S. (1974) 'Production of carbohydrates by marine planktonic diatoms. I. Comparison of nine different species in culture', *Journal of Experimental Marine Biology and Ecology*, 15(3), pp. 261-274.

Nagata, T. (2000) 'Production mechanisms of dissolved organic matter', *Microbial ecology of the oceans*, pp. 121-152.

Naumann, E. (1917) 'Uber das neuston des Süsswassers', *Biol. Centralblatt*, 37, pp. 98-106.

Nelson, J.R. and Guarda, S. (1995) 'Particulate and dissolved spectral absorption on the continental shelf of the southeastern United States', *Journal of Geophysical Research: Oceans*, 100(C5), pp. 8715-8732.

Nelson, N.B., Carlson, C.A. and Steinberg, D.K. (2004) 'Production of chromophoric dissolved organic matter by Sargasso Sea microbes', *Marine Chemistry*, 89(1), pp. 273-287.

Nelson, N.B. and Siegel, D.A. (2002) 'Chromophoric DOM in the open ocean', in Hansell, D.A.a.C., C.A. (ed.) *Biogeochemistry of marine dissolved organic matter*. pp. 547-578.

Nelson, N.B. and Siegel, D.A. (2013) 'The global distribution and dynamics of chromophoric dissolved organic matter', *Annual Review of Marine Science*, 5, pp. 447-476.

Nelson, N.B., Siegel, D.A., Carlson, C.A., Swan, C., Smethie, W.M. and Khatiwala, S. (2007) 'Hydrography of chromophoric dissolved organic matter in the North Atlantic', *Deep Sea Research Part I: Oceanographic Research Papers*, 54(5), pp. 710-731.

Nelson, N.B., Siegel, D.A., Carlson, C.A. and Swan, C.M. (2010) 'Tracing global biogeochemical cycles and meridional overturning circulation using chromophoric dissolved organic matter', *Geophysical Research Letters*, 37(3).

Nelson, N.B., Siegel, D.A. and Michaels, A.F. (1998) 'Seasonal dynamics of colored dissolved material in the Sargasso Sea', *Deep Sea Research Part I: Oceanographic Research Papers*, 45(6), pp. 931-957.

Nightingale, P.D. (2009) 'Air-sea gas exchange', in *Surface ocean-lower atmosphere processes*. American Geophysical Union, pp. 69-97.

Nightingale, P.D., Liss, P.S. and Schlosser, P. (2000) 'Measurements of air-sea gas transfer during an open ocean algal bloom', *Geophysical Research Letters*, 27(14), pp. 2117-2120.

Nissenbaum, A. (1974) 'The organic geochemistry of marine and terrestrial humic substances: implications of carbon and hydrogen isotope studies', *Advances in Organic Geochemistry: Amsterdam (Elsevier)*, pp. 39-52.

Norkrans, B. (1980) 'Surface microlayers in aquatic environments', in *Advances in microbial ecology*. Springer, pp. 51-85.

Olson, R.J., Chisholm, S.W., Zettler, E.R., Altabet, M.A. and Dusenberry, J.A. (1990) 'Spatial and temporal distributions of prochlorophyte picoplankton in the North Atlantic Ocean', *Deep Sea Research Part A. Oceanographic Research Papers*, 37(6), pp. 1033-1051.

Olson, R.J., Chisholm, S.W., Zettler, E.R. and Armbrust, E.V. (1988) 'Analysis of Synechococcus pigment types in the sea using single and dual beam flow cytometry', *Deep Sea Research Part A. Oceanographic Research Papers*, 35(3), pp. 425-440.

Omori, Y., Hama, T., Ishii, M. and Saito, S. (2010) 'Relationship between the seasonal change in fluorescent dissolved organic matter and mixed layer depth in the subtropical western North Pacific', *Journal of Geophysical Research: Oceans*, 115(C6), pp. 1-12.

Ortega-Retuerta, E., Passow, U., Duarte, C.M. and Reche, I. (2009) 'Effects of ultraviolet B radiation on (not so) transparent exopolymer particles', *Biogeosciences*, 6(12), pp. 3071-3080.

Parlanti, E., Wörz, K., Geoffroy, L. and Lamotte, M. (2000) 'Dissolved organic matter fluorescence spectroscopy as a tool to estimate biological activity in a coastal zone submitted to anthropogenic inputs', *Organic Geochemistry*, 31(12), pp. 1765-1781.

Parrish, C.C. (1988) 'Dissolved and particulate marine lipid classes: a review', *Marine Chemistry*, 23(1-2), pp. 17-40.

Parrish, C.C., Thompson, R.J. and Deibel, D. (2005) 'Lipid classes and fatty acids in plankton and settling matter during the spring bloom in a cold ocean coastal environment', *Marine Ecology Progress Series*, 286, pp. 57-69.

Passow, U. (2002a) 'Production of transparent exopolymer particles (TEP) by phyto-and bacterioplankton', *Marine Ecology Progress Series*, 236, pp. 1-12.

Passow, U. (2002b) 'Transparent exopolymer particles (TEP) in aquatic environments', *Progress in oceanography*, 55(3), pp. 287-333.

Passow, U. and Alldredge, A.L. (1999) 'Do transparent exopolymer particles (TEP) inhibit grazing by the euphausiid Euphausia pacifica?', *Journal of Plankton Research*, 21(11), pp. 2203-2217.

Passow, U., Shipe, R.F., Murray, A., Pak, D.K., Brzezinski, M.A. and Alldredge, A.L. (2001) 'The origin of transparent exopolymer particles (TEP) and their role in the sedimentation of particulate matter', *Continental Shelf Research*, 21(4), pp. 327-346.

Patel-Sorrentino, N., Mounier, S. and Benaim, J.Y. (2002) 'Excitation-emission fluorescence matrix to study pH influence on organic matter fluorescence in the Amazon basin rivers', *Water Research*, 36(10), pp. 2571-2581.

Penezić, A., Gašparović, B., Burić, Z. and Frka, S. (2010) 'Distribution of marine lipid classes in salty Rogoznica Lake (Croatia)', *Estuarine, coastal and shelf science*, 86(4), pp. 625-636.

Pereira, R., Schneider-Zapp, K. and Upstill-Goddard, R.C. (2016) 'Surfactant control of gas transfer velocity along an offshore coastal transect: results from a laboratory gas exchange tank', *Biogeosciences*, 13(13), p. 3981.

Peterson, R.G. and Stramma, L. (1991) 'Upper-level circulation in the South Atlantic Ocean', *Progress in oceanography*, 26(1), pp. 1-73.

Peuravuori, J. and Pihlaja, K. (1997) 'Molecular size distribution and spectroscopic properties of aquatic humic substances', *Analytica Chimica Acta*, 337(2), pp. 133-149.

Plavšić, M. and Ćosović, B. (2000) 'Adsorption properties of different polysaccharides on mercury in sodium chloride solutions', *Electroanalysis*, 12(12), pp. 895-900.

Pollard, J.M., Shi, A.J. and Göklen, K.E. (2006) 'Solubility and partitioning behavior of surfactants and additives used in bioprocesses', *Journal of Chemical & Engineering Data*, 51(1), pp. 230-236.

Reinthaler, T., Sintes, E. and Herndl, G.J. (2008) 'Dissolved organic matter and bacterial production and respiration in the sea-surface microlayer of the open Atlantic and the western Mediterranean Sea', *Limnology and Oceanography*, 53(1), p. 122.

Reverdin, G., Niiler, P.P. and Valdimarsson, H. (2003) 'North Atlantic ocean surface currents', *Journal of Geophysical Research: Oceans*, 108(C1).

Reygondeau, G., Longhurst, A., Martinez, E., Beaugrand, G., Antoine, D. and Maury, O. (2013) 'Dynamic biogeochemical provinces in the global ocean', *Global Biogeochemical Cycles*, 27(4), pp. 1046-1058.

Richardson, P.L. and Reverdin, G. (1987) 'Seasonal cycle of velocity in the Atlantic North Equatorial Countercurrent as measured by surface drifters, current meters, and ship drifts', *Journal of Geophysical Research: Oceans*, 92(C4), pp. 3691-3708.

Robinson, C., Holligan, P., Jickells, T. and Lavender, S. (2009) 'The Atlantic Meridional Transect Programme (1995–2012)', *Deep Sea Research II*, 56, pp. 895-898.

Robinson, C., Poulton, A.J., Holligan, P.M., Baker, A.R., Forster, G., Gist, N., Jickells, T.D., Malin, G., Upstill-Goddard, R. and Williams, R.G. (2006) 'The Atlantic Meridional Transect (AMT) programme: a contextual view 1995–2005', *Deep Sea Research Part II: Topical Studies in Oceanography*, 53(14), pp. 1485-1515.

Romano, J.-C. (1996) 'Sea-surface slick occurrence in the open sea (Mediterranean, Red Sea, Indian Ocean) in relation to wind speed', *Deep Sea Research Part I: Oceanographic Research Papers*, 43(4), pp. 411-423.

Romera-Castillo, C., Sarmento, H., Álvarez-Salgado, X.A., Gasol, J.M. and Marrasé, C. (2011) 'Net production and consumption of fluorescent colored dissolved organic matter by natural bacterial assemblages growing on marine phytoplankton exudates', *Applied and environmental microbiology*, 77(21), pp. 7490-7498.

Rosenberg, E., Zuckerberg, A., Rubinovitz, C. and Gutnick, D.L. (1979) 'Emulsifier of Arthrobacter RAG-1: isolation and emulsifying properties', *Applied and Environmental Microbiology*, 37(3), pp. 402-408.

Russell, L.M., Hawkins, L.N., Frossard, A.A., Quinn, P.K. and Bates, T.S. (2010) 'Carbohydrate-like composition of submicron atmospheric particles and their production from ocean bubble bursting', *Proceedings of the National Academy of Sciences*, 107(15), pp. 6652-6657.

Sabbaghzadeh, B., Upstill-Goddard, R.C., Beale, R., Pereira, R. and Nightingale, P.D. (2017) 'The Atlantic Ocean surface microlayer from 50° N to 50° S is ubiquitously enriched in surfactants at wind speeds up to 13 m s− 1', *Geophysical Research Letters*, 44(6), pp. 2852-2858.

Sakugawa, H. and Handa, N. (1985a) 'Chemical studies on dissolved carbohydrates in the water samples collected from the North Pacific and Bering Sea', *Oceanologica acta*, 8(2), pp. 185-196.

Sakugawa, H. and Handa, N. (1985b) 'Isolation and chemical characterization of dissolved and particulate polysaccharides in Mikawa Bay', *Geochimica et Cosmochimica Acta*, 49(5), pp. 1185-1193.

Saliot, A. (1981) 'Natural Hydrocarbons in Sea Water Alain Saliot', *Elsevier Oceanography Series*, 31, pp. 327-374.

Salter, M.E. (2010) *A Role for Natural Surfactants in Air-sea Gas Exchange?* University of Newcastle upon Tyne.

Salter, M.E., Upstill-Goddard, R.C., Nightingale, P.D., Archer, S.D., Blomquist, B., Ho, D.T., Huebert, B., Schlosser, P. and Yang, M. (2011) 'Impact of an artificial surfactant release on air-sea gas fluxes during Deep Ocean Gas Exchange Experiment II', *Journal of Geophysical Research: Oceans*, 116(C11).

Saylor, J.R. (2003) 'The fate of soluble and insoluble surfactant monolayers subjected to drop impacts', *Experiments in Fluids*, 34(5), pp. 540-547.

Schmidt, R. and Schneider, B. (2011) 'The effect of surface films on the air-sea gas exchange in the Baltic Sea', *Marine Chemistry*, 126(1), pp. 56-62.

Schneider-Zapp, K., Salter, M.E. and Upstill-Goddard, R.C. (2014) 'An automated gas exchange tank for determining gas transfer velocities in natural seawater samples', *Ocean Science*, 10(4), p. 587.

Sherr, E. and Sherr, B. (1988) 'Role of microbes in pelagic food webs: a revised concept', *Limnology and Oceanography*, 33(5), pp. 1225-1227.

Sieburth, J.M. (1979) 'Sea microbes: a survey of the habitats, field and laboratory methods, morphology, nutrition, taxonomy, and ecology of marine bacteria, fungi, microalgae, and protozoa', in Sieburth, J. (ed.) *Sea microbes*. New York: Oxford University Press, p. 491.

Sieburth, J.M. (1983) 'Microbiological and organic-chemical processes in the surface and mixed layers', in Liss, P.S.a.S., W.G.N. (ed.) *Air-sea exchange of gases and particles*. Springer, pp. 121-172.

Sieburth, J.M. and Conover, J.T. (1965) 'Slicks associated with Trichodesmium blooms in the Sargasso Sea', *Nature*, 205(4973), pp. 830-831.

Sieburth, J.M., Willis, P.-J., Johnson, K.M., Burney, C.M., Lavoie, D.M., Hinga, K.R., Caron, D.A., French, F.W., Johnson, P.W. and Davis, P.G. (1976) 'Dissolved organic matter and heterotrophic microneuston in the surface microlayers of the North Atlantic', *Science*, 194(4272), pp. 1415-1418.

Siegel, D.A., Maritorena, S., Nelson, N.B. and Behrenfeld, M.J. (2005a) 'Independence and interdependencies among global ocean color properties: Reassessing the bio-optical assumption', *Journal of Geophysical Research: Oceans*, 110(C7).

Siegel, D.A., Maritorena, S., Nelson, N.B., Behrenfeld, M.J. and McClain, C.R. (2005b) 'Colored dissolved organic matter and its influence on the satellite-based characterization of the ocean biosphere', *Geophysical Research Letters*, 32(20).

Siegel, D.A., Maritorena, S., Nelson, N.B., Hansell, D.A. and Lorenzi-Kayser, M. (2002) 'Global distribution and dynamics of colored dissolved and detrital organic materials', *Journal of Geophysical Research: Oceans*, 107(C12).

Siegel, D.A. and Michaels, A.F. (1996) 'Quantification of non-algal light attenuation in the Sargasso Sea: Implications for biogeochemistry and remote sensing', *Deep Sea Research Part II: Topical Studies in Oceanography*, 43(2), pp. 321-345.

Siegel, D.A., Michaels, A.F., Sorensen, J.C., O'Brien, M.C. and Hammer, M.A. (1995) 'Seasonal variability of light availability and utilization in the Sargasso Sea', *Journal of Geophysical Research: Oceans*, 100(C5), pp. 8695-8713.

Smith, R.C., Prezelin, B.B., Baker, K.S.e.a., Bidigare, R.R., Boucher, N.P., Coley, T., Karentz, D., MacIntyre, S., Matlick, H.A. and Menzies, D. (1992) 'Ozone depletion: ultraviolet radiation and phytoplankton biology in Antarctic waters', *Science*, 255(5047), pp. 952-959.

Smyth, T.J. (2011) 'Penetration of UV irradiance into the global ocean', *Journal of Geophysical Research: Oceans*, 116(C11).

Søndergaard, M., Borch, N.H. and Riemann, B. (2000) 'Dynamics of biodegradable DOC produced by freshwater plankton communities', *Aquatic Microbial Ecology*, 23(1), pp. 73-83.

Springer, T.G. and Pigford, R.L. (1970) 'Influence of surface turbulence and surfactants on gas transport through liquid interfaces', *Industrial & Engineering Chemistry Fundamentals*, 9(3), pp. 458-465.

Stedmon, C.A. and Álvarez-Salgado, X.A. (2011) 'Shedding light on a black box: UV-visible spectroscopic characterization of marine dissolved organic matter', *Jiao, N. and Azam, F., Senders*, pp. 62-63.

Stedmon, C.A. and Markager, S. (2001) 'The optics of chromophoric dissolved organic matter (CDOM) in the Greenland Sea: An algorithm for differentiation between marine and terrestrially derived organic matter', *Limnology and Oceanography*, 46(8), pp. 2087-2093.

Stedmon, C.A. and Markager, S. (2005) 'Tracing the production and degradation of autochthonous fractions of dissolved organic matter by fluorescence analysis', *Limnology and Oceanography*, 50(5), pp. 1415-1426.

Stedmon, C.A., Markager, S. and Bro, R. (2003) 'Tracing dissolved organic matter in aquatic environments using a new approach to fluorescence spectroscopy', *Marine Chemistry*, 82(3), pp. 239-254.

Stedmon, C.A., Markager, S. and Kaas, H. (2000) 'Optical properties and signatures of chromophoric dissolved organic matter (CDOM) in Danish coastal waters', *Estuarine, Coastal and Shelf Science*, 51(2), pp. 267-278.

Stefan, R.L. and Szeri, A.J. (1999) 'Surfactant scavenging and surface deposition by rising bubbles', *Journal of colloid and interface science*, 212(1), pp. 1-13.

Stubbins, A., Spencer, R.G.M., Chen, H., Hatcher, P.G., Mopper, K., Hernes, P.J., Mwamba, V.L., Mangangu, A.M., Wabakanghanzi, J.N. and Six, J. (2010) 'Illuminated darkness: molecular signatures of Congo River dissolved organic matter and its photochemical alteration as revealed by ultrahigh precision mass spectrometry', *Limnology and Oceanography*, 55(4), pp. 1467-1477.

Stubbins, A., Uher, G., Law, C.S., Mopper, K., Robinson, C. and Upstill-Goddard, R.C. (2006) 'Open-ocean carbon monoxide photoproduction', *Deep Sea Research Part II: Topical Studies in Oceanography*, 53(14), pp. 1695-1705.

Sulzberger, B. and Durisch-Kaiser, E. (2009) 'Chemical characterization of dissolved organic matter (DOM): A prerequisite for understanding UV-induced changes of DOM absorption properties and bioavailability', *Aquatic Sciences-Research Across Boundaries*, 71(2), pp. 104-126.

Sundh, I. and Bell, R.T. (1992) 'Extracellular dissolved organic carbon released from phytoplankton as a source of carbon for heterotrophic bacteria in lakes of different humic content', *Hydrobiologia*, 229(1), pp. 93-106.

Sverdrup, H.U., Johnson, M.W. and Fleming, R.H. (1942) *The Oceans: Their physics, chemistry, and general biology*. Prentice-Hall New York.

Swan, C.M., Siegel, D.A., Nelson, N.B., Carlson, C.A. and Nasir, E. (2009) 'Biogeochemical and hydrographic controls on chromophoric dissolved organic matter distribution in the Pacific Ocean', *Deep Sea Research Part I: Oceanographic Research Papers*, 56(12), pp. 2175-2192.

Takahashi, T., Sutherland, S.C., Wanninkhof, R., Sweeney, C., Feely, R.A., Chipman, D.W., Hales, B., Friederich, G., Chavez, F. and Sabine, C. (2009) 'Climatological mean and decadal change in surface ocean pCO 2, and net sea–air CO 2 flux over the global oceans', *Deep Sea Research Part II: Topical Studies in Oceanography*, 56(8), pp. 554-577.

Tan, C.-Y. and Huang, Y.-X. (2015) 'Dependence of refractive index on concentration and temperature in electrolyte solution, polar solution, nonpolar solution, and protein solution', *Journal of Chemical & Engineering Data*, 60(10), pp. 2827-2833.

Tarran, G.A., Heywood, J.L. and Zubkov, M.V. (2006) 'Latitudinal changes in the standing stocks of nano-and picoeukaryotic phytoplankton in the Atlantic Ocean', *Deep Sea Research Part II: Topical Studies in Oceanography*, 53(14), pp. 1516-1529.

Teira, E., Mouriño, B., Marañón, E., Pérez, V., Pazó, M.J., Serret, P., de Armas, D., Escanez, J., Woodward, E.M.S. and Fernández, E. (2005) 'Variability of chlorophyll and primary production in the Eastern North Atlantic Subtropical Gyre: potential factors affecting phytoplankton activity', *Deep Sea Research Part I: Oceanographic Research Papers*, 52(4), pp. 569-588.

Thurman, E.M. (1985) 'Aquatic humic substances', in *Organic geochemistry of natural waters*. Springer, pp. 273-361.

Tilstone, G.H., Vicente, V.M., Widdicombe, C. and Llewellyn, C. (2010) 'High concentrations of mycosporine-like amino acids and colored dissolved organic matter in the sea surface microlayer off the Iberian Peninsula', *Limnology and Oceanography*, 55(5), pp. 1835-1850.

Tsai, W.-T. and Yue, D.K.P. (1995) 'Effects of soluble and insoluble surfactant on laminar interactions of vortical flows with a free surface', *Journal of Fluid Mechanics*, 289, pp. 315-349.

Tsai, W.T. (1996) 'Impact of a surfactant on a turbulent shear layer under the air-sea interface', *Journal of Geophysical Research: Oceans*, 101(C12), pp. 28557-28568.

Tsai, W.t. and Liu, K.K. (2003) 'An assessment of the effect of sea surface surfactant on global atmosphere-ocean CO2 flux', *Journal of Geophysical Research: Oceans (1978–2012)*, 108(C4), pp. 24-1-24-16.

Tseng, R.S., Viechnicki, J.T., Skop, R.A. and Brown, J.W. (1992) 'Sea-to-air transfer of surface-active organic compounds by bursting bubbles', *Journal of Geophysical Research: Oceans*, 97(C4), pp. 5201-5206.

Turner, A. and Rawling, M.C. (2000) 'The behaviour of di-(2-ethylhexyl) phthalate in estuaries', *Marine Chemistry*, 68(3), pp. 203-217.

Twardowski, M.S., Boss, E., Sullivan, J.M. and Donaghay, P.L. (2004) 'Modeling the spectral shape of absorption by chromophoric dissolved organic matter', *Marine Chemistry*, 89(1), pp. 69-88.

Twardowski, M.S. and Donaghay, P.L. (2002) 'Photobleaching of aquatic dissolved materials: Absorption removal, spectral alteration, and their interrelationship', *Journal of Geophysical Research: Oceans*, 107(C8), pp. 6-1-6-10.

Upstill-Goddard, R.C. (2006) 'Air–sea gas exchange in the coastal zone', *Estuarine, Coastal and Shelf Science*, 70(3), pp. 388-404.

Vähätalo, A.V. and Wetzel, R.G. (2004) 'Photochemical and microbial decomposition of chromophoric dissolved organic matter during long (months–years) exposures', *Marine Chemistry*, 89(1), pp. 313-326.

Vaulot, D., Marie, D., Olson, R.J. and Chisholm, S.W. (1995) 'Growth of Prochlorococcus, a photosynthetic prokaryote, in the equatorial Pacific Ocean', *SCIENCE-NEW YORK THEN WASHINGTON-*, pp. 1480-1480.

Verdugo, P., Alldredge, A.L., Azam, F., Kirchman, D.L., Passow, U. and Santschi, P.H. (2004) 'The oceanic gel phase: a bridge in the DOM–POM continuum', *Marine Chemistry*, 92(1), pp. 67-85.

Vodacek, A., Blough, N.V., DeGrandpre, M.D. and Nelson, R.K. (1997) 'Seasonal variation of CDOM and DOC in the Middle Atlantic Bight: Terrestrial inputs and photooxidation', *Limnology and Oceanography*, 42(4), pp. 674-686.

Vojvodić, V., Ćosović, B. and Mirić, V. (1994) 'Fractionation of surface active substances on the XAD-8 resin Part I. Mixtures of model substances', *Analytica chimica acta*, 295(1-2), pp. 73-83.

Wandschneider, K. (1979) 'Vertical distribution of phytoplankton during investigations of a natural surface film', *Marine biology*, 52(2), pp. 105-111.

Wanninkhof, R., Asher, W., Weppernig, R., Chen, H., Schlosser, P., Langdon, C. and Sambrotto, R. (1993) 'Gas transfer experiment on Georges Bank using two volatile deliberate tracers', *Journal of Geophysical Research: Oceans*, 98(C11), pp. 20237-20248.

Wanninkhof, R., Hitchcock, G., Wiseman, W.J., Vargo, G., Ortner, P.B., Asher, W., Ho, D.T., Schlosser, P., Dickson, M.L. and Masserini, R. (1997) 'Gas exchange, dispersion, and biological productivity on the west Florida shelf: Results from a Lagrangian tracer study', *Geophysical Research Letters*, 24(14), pp. 1767-1770.

Ward, B.B. and Bronk, D.A. (2001) 'Net nitrogen uptake and DON release in surface waters: importance of trophic interactions implied from size fractionation experiments', *Marine Ecology Progress Series*, 219, pp. 11-24.

Wei-Chun, C., Orellana, M.V. and Verdugo, P. (1998) 'Spontaneous assembly of marine dissolved organic matter into polymer gels', *Nature*, 391(6667), p. 568.

Williams, P.M. (1967) 'Sea surface chemistry: organic carbon and organic and inorganic nitrogen and phosphorus in surface films and subsurface waters', *Deep Sea Research and Oceanographic Abstracts*, 14, pp. 791IN19797-796IN20800.

Williams, P.M. (1986) *ONR Workshop Proceedings-Role of Surfactant Films on the Interfacial Properties of the Sea Surface. Report C-11–86 Office of Naval Research. Arlington, California*.

Williams, P.M., Carlucci, A.F., Henrichs, S.M., Van Vleet, E.S., Horrigan, S.G., Reid, F.M.H. and Robertson, K.J. (1986) 'Chemical and microbiological studies of sea-surface films in the southern Gulf of California and off the west coast of Baja California', *Marine Chemistry*, 19(1), pp. 17-98.

Wilson, W.D., Johns, E. and Molinari, R.L. (1994) 'Upper layer circulation in the western tropical North Atlantic Ocean during August 1989', *Journal of Geophysical Research: Oceans (1978–2012)*, 99(C11), pp. 22513-22523.

Woolf, D.K. (1997) 'Bubbles and their role in gas exchange', in Liss, P.S.a.D., R.A. (ed.) *The sea surface and global change*. pp. 173-205.

Wright, W.R. and Worthington, L.V. (1970) *The water masses of the North Atlantic Ocean: a volumetric census of temperature and salinity*. American Geographic Society.

Wurl, O. and Holmes, M. (2008) 'The gelatinous nature of the sea-surface microlayer', *Marine Chemistry*, 110(1), pp. 89-97.

Wurl, O., Miller, L., Röttgers, R. and Vagle, S. (2009) 'The distribution and fate of surface-active substances in the sea-surface microlayer and water column', *Marine Chemistry*, 115(1), pp. 1-9.

Wurl, O., Miller, L. and Vagle, S. (2011a) 'Production and fate of transparent exopolymer particles in the ocean', *Journal of Geophysical Research: Oceans*, 116(C7).

Wurl, O. and Obbard, J.P. (2004) 'A review of pollutants in the sea-surface microlayer (SML): a unique habitat for marine organisms', *Marine pollution bulletin*, 48(11), pp. 1016-1030.

Wurl, O., Wurl, E., Miller, L., Johnson, K. and Vagle, S. (2011b) 'Formation and global distribution of sea-surface microlayers', *Biogeosciences*, 8(1), pp. 121-135.

Yamashita, Y. and Tanoue, E. (2009) 'Basin scale distribution of chromophoric dissolved organic matter in the Pacific Ocean', *Limnology and Oceanography*, 54(2), pp. 598-609.

Yang, G.-P., Jing, W.-W., Li, L., Kang, Z.-Q. and Song, G.-S. (2006) 'Distribution of dimethylsulfide and dimethylsulfoniopropionate in the surface microlayer and subsurface water of the Yellow Sea, China during spring', *Journal of Marine Systems*, 62(1), pp. 22-34.

Yang, G.-P., Levasseur, M., Michaud, S., Merzouk, A., Lizotte, M. and Scarratt, M. (2009) 'Distribution of dimethylsulfide and dimethylsulfoniopropionate and its relation with phytoneuston in the surface microlayer of the western North Atlantic during summer', *Biogeochemistry*, 94(3), pp. 243-254.

Yang, G.-P., Tsunogai, S. and Watanabe, S. (2005) 'Biogeochemistry of dimethylsulfoniopropionate (DMSP) in the surface microlayer and subsurface seawater of Funka Bay, Japan', *Journal of oceanography*, 61(1), pp. 69-78.

Yang, G.-P., Watanabe, S. and Tsunogai, S. (2001) 'Distribution and cycling of dimethylsulfide in surface microlayer and subsurface seawater', *Marine Chemistry*, 76(3), pp. 137-153.

Zappa, C.J., McGillis, W.R., Raymond, P.A., Edson, J.B., Hintsa, E.J., Zemmelink, H.J., Dacey, J.W.H. and Ho, D.T. (2007) 'Environmental turbulent mixing controls on air-water gas exchange in marine and aquatic systems', *Geophysical Research Letters*, 34(10), pp. 1-6.

Zepp, R.G., Erickson Iii, D.J., Paul, N.D. and Sulzberger, B. (2011) 'Effects of solar UV radiation and climate change on biogeochemical cycling: interactions and feedbacks', *Photochemical & Photobiological Sciences*, 10(2), pp. 261-279.

Zhang, J. and Yang, G. (2013) 'Chemical properties of colored dissolved organic matter in the sea-surface microlayer and subsurface water of Jiaozhou Bay, China in autumn and winter', *Acta Oceanologica Sinica*, 32(6), pp. 26-39.

Zhang, Z., Liu, L., Liu, C. and Cai, W. (2003) 'Studies on the sea surface microlayer: II. The layer of sudden change of physical and chemical properties', *Journal of Colloid and Interface Science*, 264(1), pp. 148-159.

Zubkov, M.V., Sleigh, M.A., Burkill, P.H. and Leakey, R.J.G. (2000a) 'Bacterial growth and grazing loss in contrasting areas of North and South Atlantic', *Journal of Plankton Research*, 22(4), pp. 685-711.

Zubkov, M.V., Sleigh, M.A., Burkill, P.H. and Leakey, R.J.G. (2000b) 'Picoplankton community structure on the Atlantic Meridional Transect: a comparison between seasons', *Progress in oceanography*, 45(3), pp. 369-386.

Zubkov, M.V., Sleigh, M.A., Tarran, G.A., Burkill, P.H. and Leakey, R.J.G. (1998) 'Picoplanktonic community structure on an Atlantic transect from 50 N to 50 S', *Deep Sea Research Part I: Oceanographic Research Papers*, 45(8), pp. 1339-1355.

Zutic, V., Cosovic, B., Marcenko, E., Bihari, N. and Krsinic, F. (1979) 'Surfactant production by marine phytoplankton. Field observations and laboratory culture experiments', *Rapports et Proces-Verbaux des Reunions-Commission Internationale pour l'Exploration Scientifique de la Mer Mediterranee (CIESM)*.

Žutić, V., Ćosović, B., Marčenko, E., Bihari, N. and Kršinić, F. (1981) 'Surfactant production by marine phytoplankton', *Marine Chemistry*, 10(6), pp. 505-520.

Zvonaric, V. and Zutic, V.B. (1979) 'Cruises of RV" Vila Velebita" in the Kvarner region of the Adriatic sea', *VI. Electrochemical determination of dissolved surfactants. Thalassia Jugoslavia*, 15, pp. 113-121.

Appendices

Appendix 1.

Table A.1. Descriptive statistics of temperature (°C), salinity and U_{10n} (ms^{-1}) in biogeochemical provinces for 100m depth in the Atlantic Ocean. The provinces are including European Continental Shelf water (ECSW), North Atlantic Drift Region (NADR), North Atlantic Subtropical Region (NAST), North Atlantic Tropical Region (NATR), Western and Eastern Tropical Atlantic (W/E TRA), South Atlantic Gyral (SATL), South Sub Tropical Convergence (SSTC) and Falkland Islands (FKLD)

	Temperature (°C)		Salinity		U_{10n} (ms^{-1})	
Provinces	**AMT24**	**AMT25**	**AMT24**	**AMT25**	**AMT24**	**AMT25**
ECSW						
n	71	58	-	-	1	-
Ave.	14.34	14.85	-	-	5.48	-
SD.	0.66	0.47	-	-	-	-
Min.	13.84	14.36	-	-	-	-
Max.	15.65	15.48	-	-	-	-
NADR						
n	691	393	691	491	7	4
Ave.	15.7	15.34	35.63	35.62	3.59	3.08
SD.	2.8	2.01	0.06	0.07	1.90	0.80
Min.	12.27	12.08	35.5	35.50	0.65	2.16
Max.	20.44	18.22	35.77	35.73	6.3	3.87
NAST						
n	1088	1612	1088	1612	11	16
Ave.	20.21	20.95	36.47	36.4	6.13	3.69
SD.	3.9	3.6	0.56	0.43	1.55	1.89
Min.	13.11	13.53	35.75	35.71	3.71	0.29
Max.	26.71	27.04	37.59	37.4	8.8	7.25
NATR						
n	887	1264	887	1264	8	10
Ave.	23.28	22.94	36.69	36.64	8.6	3.15
SD.	3.74	4.12	0.50	0.60	1.61	1.67
Min.	13.72	13.72	35.51	35.30	6.7	1.01
Max.	28.3	29.27	37.44	37.64	11.88	6.64
W/E (TRA)						
n	796	775	796	775	8	5
Ave.	24.07	22.92	35.88	35.74	5.28	3.26
SD.	4.45	4.54	0.29	0.26	2.18	1.06
Min.	13.22	14.64	34.55	35.10	2.43	1.52
Max.	28.90	28.85	36.39	36.27	9.81	4.21

Table A.1. (continued) Descriptive statistics of temperature (°C), salinity and U_{10n} (ms^{-1}) in biogeochemical provinces for 100m depth in the Atlantic Ocean. The provinces are including European Continental Shelf water (ECSW), North Atlantic Drift Region (NADR), North Atlantic Subtropical Region (NAST), North Atlantic Tropical Region (NATR), Western and Eastern Tropical Atlantic (W/E TRA), South Atlantic Gyral (SATL), South Sub Tropical Convergence (SSTC) and Falkland Islands (FKLD)

	Temperature (°C)		Salinity		U_{10n} (ms^{-1})	
Provinces	**AMT24**	**AMT25**	**AMT24**	**AMT25**	**AMT24**	**AMT25**
SATL						
n	2460	2312	2460	2216	23	11
Ave.	19.90	20.11	36.21	36.25	7.64	3.78
SD.	4.63	3.77	0.74	0.64	2.71	1.28
Min.	11.61	10.23	34.83	34.6	2.52	1.89
Max.	26.14	24.62	37.17	37.14	12.94	6.38
SSTC						
n	589	287	589	192	6	1
Ave.	10.10	9.80	34.61	34.52	9.95	2.44
SD.	1.20	0.72	0.18	0.04	1.39	-
Min.	8.36	8.66	34.44	34.46	7.96	-
Max.	11.66	11.14	34.98	34.58	11.76	-
FKLD						
n	288	189	288	535	2	1
Ave.	5.97	4.65	34.21	34.91	8.91	6.84
SD.	2.00	0.26	0.19	0.76	2.98	-
Min.	3.36	4.07	34.02	34.08	6.81	-
Max.	8.81	5.13	34.49	36.06	11.01	-

Appendix 2.

AGU PUBLICATIONS

Geophysical Research Letters

RESEARCH LETTER
10.1002/2017GL072988

The Atlantic Ocean surface microlayer from 50°N to 50°S is ubiquitously enriched in surfactants at wind speeds up to 13 m s^{-1}

B. Sabbaghzadeh[1], R. C. Upstill-Goddard[1], R. Beale[2], R. Pereira[3], and P. D. Nightingale[2]

[1]School of Marine Science and Technology, Newcastle University, Newcastle upon Tyne, UK, [2]Plymouth Marine Laboratory, Prospect Place, Plymouth, UK, [3]Lyell Centre, Heriot-Watt University, Edinburgh, UK

Key Points:
- First measurements of surfactant activity (SA) in the sea surface microlayer (SML) and in subsurface waters at the ocean basin scale
- The Atlantic Ocean SML is ubiquitously enriched in SA relative to underlying water between 50°N and 50°S and up to wind speeds ~13 m s^{-1}
- The high-latitude ocean contribution to air-sea gas exchange globally may be lower than previously assumed and should be reexamined

Supporting Information:
- Supporting Information S1

Correspondence to:
B. Sabbaghzadeh and R. C. Upstill-Goddard,
b.sabbaghzadeh@ncl.ac.uk;
rob.goddard@ncl.ac.uk

Citation:
Sabbaghzadeh, B., R. C. Upstill-Goddard, R. Beale, R. Pereira, and P. D. Nightingale (2017), The Atlantic Ocean surface microlayer from 50°N to 50°S is ubiquitously enriched in surfactants at wind speeds up to 13 m s^{-1}, *Geophys. Res. Lett.*, *44*, 2852–2858, doi:10.1002/2017GL072988.

Received 7 FEB 2017
Accepted 13 MAR 2017
Accepted article online 20 MAR 2017
Published online 31 MAR 2017

Abstract We report the first measurements of surfactant activity (SA) in the sea surface microlayer (SML) and in subsurface waters (SSW) at the ocean basin scale, for two Atlantic Meridional Transect from cruises 50°N to 50°S during 2014 and 2015. Northern Hemisphere (NH) SA was significantly higher than Southern Hemisphere (SH) SA in the SML and in the SSW. SA enrichment factors (EF = SA_{SML}/SA_{SSW}) were also higher in the NH, for wind speeds up to ~13 m s^{-1}, questioning a prior assertion that Atlantic Ocean wind speeds >12 m s^{-1} poleward of 30°N and 30°S would preclude high EFs and showing the SML to be self-sustaining with respect to SA. Our results imply that surfactants exert a control on air-sea CO_2 exchange across the whole North Atlantic CO_2 sink region and that the contribution made by high wind, high latitude oceans to air-sea gas exchange globally should be reexamined.

1. Introduction

The physics and biogeochemistry of the sea surface microlayer (SML) afford it a unique role in global element cycling and in the production and removal of climate active gases [*Upstill-Goddard et al.*, 2003; *Cunliffe et al.*, 2013; *Carpenter and Nightingale*, 2015]. Open ocean surfactants include polysaccharides, lipids and proteins [*Allan et al.*, 1972; *Myklestad*, 1974; *Sakugawa and Handa*, 1985], transparent exopolymer particles [*Wurl and Holmes*, 2008], and chromophoric dissolved organic matter [*Tilstone et al.*, 2010]. They are mainly biologically derived, from phytoplankton [*Žutić et al.*, 1981], via zooplankton grazing [*Kujawinski et al.*, 2002] and from bacteria [*Kurata et al.*, 2016], with additional small components of terrestrial [*Frew et al.*, 2002] origin and from the in situ photochemical reworking of preexisting organics [*Tilstone et al.*, 2010]. Surfactants accumulate in the SML through bubble scavenging from subsurface water (SSW) [*Tseng et al.*, 1992], generating marine boundary layer aerosols [*Leck and Bigg*, 1999; *Ovadnevaite et al.*, 2011] and lowering the air-sea gas transfer velocity (k_w) of CO_2 and other climate-active gases [*Nightingale*, 2009]. Surfactant suppression of k_w by up to 50% may be typical [*Bock et al.*, 1999; *Frew*, 2005; *Salter et al.*, 2011]. While strong spatiotemporal gradients in SML surfactant, and hence in k_w, have been reported for some coastal waters [*Frew et al.*, 1990; *Schneider-Zapp et al.*, 2014; *Pereira et al.*, 2016], surfactant distributions at the ocean basin scale are currently estimates derived from proxies [*Wurl et al.*, 2011]. Here we present the first comprehensive measurements of total surfactant activity (SA) in the SML and SSW across large spatial scales and up to high wind speeds, from two Atlantic Meridional Transect (AMT) cruises between 50°N and 50°S: AMT 24 (2014) and AMT 25 (2015).

2. Study Site and Sampling

The annual AMT cruises target distinct "biogeographical ocean provinces", as defined by the regulation of phytoplankton distributions by hydrographic properties [*Longhurst*, 1995; *Reygondeau et al.*, 2013], between ~50°N and ~50°S. AMT 24 (21 September to 6 November 2014) and AMT 25 (11 September to 4 November 2015) both ran from Immingham (UK), to Punta Arenas (Chile) and Port Stanley (Falkland Islands), respectively (Figure 1).

The SML was sampled twice daily, during predawn and solar noon hydrocasts when the ship (RRS *James Clark Ross*: JCR) was on-station. Although collecting SML samples from a moving ship or from its stern disrupts SML integrity [*Wurl and Soloviev*, 2014], the SML can be successfully sampled from the bow of a large vessel while on-station. We achieved this by aligning JCR head to wind to minimize ship-derived contamination. Doing this, we found that even under high-wind conditions surface water was continually advected toward the

AGU Geophysical Research Letters 10.1002/2017GL072988

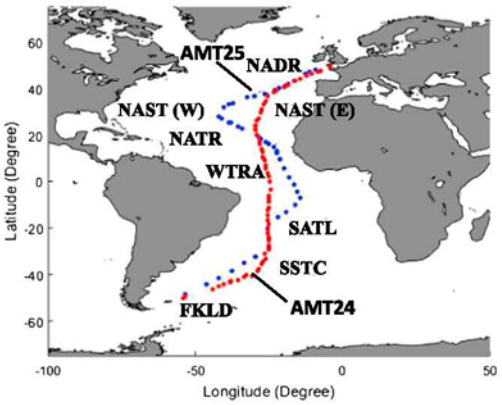

Figure 1. Sampling locations on AMT 24 (red circles, $n = 66$) and AMT 25 (blue circles, $n = 47$) and corresponding biogeographical provinces [*Reygondeau et al.*, 2013]. NADR, North Atlantic Drift Region; NAST (E), North-East Atlantic Subtropical gyre; NAST (W), North-West Atlantic Subtropical gyre; NATR, North Atlantic Tropical gyre; WTRA, Western Tropical Atlantic; SATL, South Atlantic Subtropical gyre; SSTC, South Subtropical Convergence; FKLD, Southwest Atlantic Continental shelf.

bow and the protrusion of the fore-deck ~3 m ahead of the waterline ensured that sampling was always well away from JCR's hull. With such conditions satisfied we previously sampled the SML for surfactants from the bow of a large research vessel [*Salter et al.*, 2011], and in another study *Kurata et al.* [2016] similarly sampled SML bacteria. Observing these protocols we collected SML samples by using a Garrett Screen [*Garrett*, 1965] (mesh: 16, wire diameter: 0.36 mm, and effective surface area: 2025 cm^2), as in our previous work [*Salter et al.*, 2011].

Deployment and recovery of the Garrett Screen followed standard procedures described in *Gašparović et al.* [2014], which also discusses appropriate procedures for cleaning and for optimizing sampling efficiency. Each deployment typically collected 15–16 cm^3 of the SML, and each sample comprised water from three repeat deployments (40–50 cm^3) to provide a sufficient volume for analysis. SSW samples were collected simultaneously via a hull-mounted "nontoxic" seawater inlet at 7 m.

3. Analytical Methods

Samples were left unfiltered to retain particulate surfactants [*Ćosović and Vojvodić*, 1987; *Wurl et al.*, 2011; *Pereira et al.*, 2016] and stored in clean, high-density polyethylene bottles prerinsed with analytical grade water (18.2 ohm Milli-Q, Millipore System Inc., USA) followed by excess sample. SA was measured immediately in triplicate by phase sensitive AC voltammetry (797VA Computrace, Metrohm, Switzerland) using a hanging mercury drop electrode [*Ćosović and Vojvodić*, 1987]. Calibration was against a nonionic soluble surfactant (Triton T-X-100 (Sigma-Aldrich, UK); data reported in mg L^{-1} T-X-100 equivalents) in a 0.55 mol L^{-1} NaCl matrix. Samples were adjusted to the same ionic strength as the standards by adding of 3 mol L^{-1} NaCl solution typically up to a maximum of 50 μL. Analytical precision was always better than ±10% and was frequently better than ±4%. Wind speeds from the ship's anemometer were corrected to U_{10n}, the value at 10 m height and neutral stability, as in *Nightingale et al.* [2000]. Total chlorophyll (Chl *a–c*) and total pigments were measured according to *Zapata et al.* [2000], and total primary productivity and size-fractioned phytoplankton productivity were determined according to *Serret et al.* [2001]; these data are currently available for AMT 24 only.

4. Results

Latitudinal SA distributions on AMT 24 and AMT 25 were rather similar (Figure 2), both in the SML and in the SSW. Given that the two transects differed by up to 13° of longitude between ~40°N and 20°S, AMT25 proceeding further into the North Atlantic Gyre between 20°N and 40°N and somewhat more easterly between the equator and 20°S (Figure 1), it appears that longitudinal SA gradients are comparatively small across a substantial part of the Atlantic Ocean and that surfactant distributions remain relatively constant between consecutive years. The most notable features of the data, common to both transects and in both the SML and the SSW, were distinct SA maxima centered on ~40°N, in North Atlantic Drift Region (NADR) (AMT 24, SML 1.00 ± 0.28 mg L^{-1} T-X-100, SSW 0.36 ± 0.15 mg L^{-1} T-X-100; AMT 25, SML 1.76 ± 0.1 mg L^{-1} T-X-100, SSW 0.58 ± 0.16 mg L^{-1} T-X-100; Figure 2). On AMT 24 there were also two small SA maxima that were

AGU Geophysical Research Letters 10.1002/2017GL072988

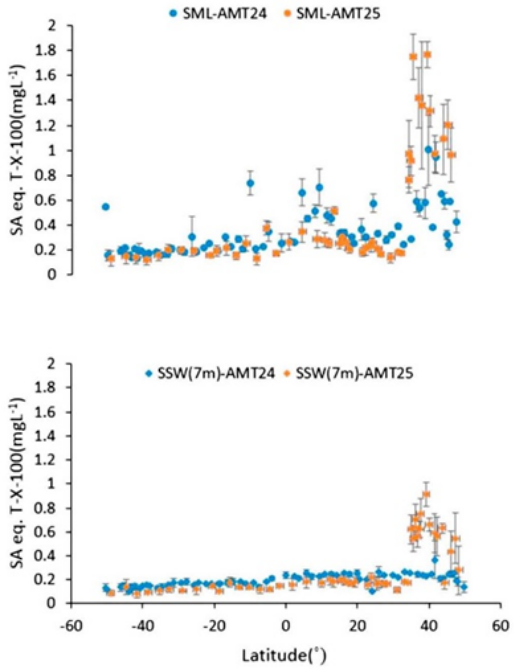

Figure 2. Surfactant activity (SA) during AMT 24 and AMT 25 in the Atlantic Ocean. Latitudinal distribution of SA (top) in the SML and (bottom) in the SSW (7 m depth). The error bars represent the standard deviation of the mean for each sample.

exclusive to the SML, between ~36°N and ~26°N (North-East/West Atlantic Subtropical gyre (NAST)) and at ~10°N (Western Tropical Atlantic (WTRA)).

During AMT 24 the ranges in U_{10} between 36°N and 26°N and between 12°N and 9°N ($6.69 \pm 1.33\ m\ s^{-1}$; $3.91 \pm 0.71\ m\ s^{-1}$) were somewhat higher than on AMT25 ($4.77 \pm 1.14\ m\ s^{-1}$; $1.26 \pm 0.35\ m\ s^{-1}$), consistent with the possibility that these SML maxima are a consequence of enhanced bubble scavenging under the somewhat more turbulent conditions experienced during AMT 24. An alternative explanation is that these maxima reflect more intense and/or more frequent local precipitation on AMT 24 than during AMT 25. Elevated SML surfactant following rainfall has been ascribed to an enhanced rate of delivery of particulate organics to the SML [*Wurl et al.*, 2011], but in the absence of precipitation data for either cruise we are unable to substantiate or otherwise, this possibility.

Additional high SA at ~50°S (Southwest Atlantic Continental shelf (FKLD)) ($0.54 \pm 0.01\ mg\ L^{-1}$ T-X-100, $n = 3$) during AMT 24 may indicate high local productivity, terrestrially derived surfactants on the Falklands shelf, or an aggregate of both. During AMT 25 this feature was much less evident (Figure 2). While indices of terrestrially derived surfactant are detectable offshore in other regions [*Cuscov and Muller*, 2015; *Pereira et al.*, 2016], they were not measured here and primary productivity, total chlorophyll, and total pigments are unavailable for 50°S. We additionally did not detect any measurable difference in salinity that might indicate a freshwater input signal at this location. The precise origin of this SA maximum thus remains unknown.

These important details of the SA distributions aside, on both transects SA was significantly higher overall (*t* test, $p < 0.05$) in the Northern Hemisphere than in the Southern Hemisphere, both in the SML and in the SSW (Table S1 in the supporting information). Excluding the SA maxima, there were small but discernible trends of progressively decreasing SA from north to south on both transects, both in the SML and in the SSW (Figure 2). SA was enriched in the SML (enrichment factor, $EF = SA_{SML}/SA_{SSW}$) at 64 of 66 and 45 of 47 locations ($EF > 1$) during AMT 24 and AMT 25, respectively (maximum EF = 4.5; Figure 3 and Table S1); the remaining four EF values being equal to unity within the analytical error (Table S1). Evidently, the SML is typically enriched in SA at all values of U_{10n} up to the highest recorded ($12.9\ m\ s^{-1}$; Figure 4). In agreement with this observation *Wurl et al.* [2011] consistently found $EF > 1$ in 44 oceanic samples (>20 km from land) from the North Pacific (mean 2.7 ± 1.3; range = 1.1–5.6). On this evidence surfactant enrichment of the SML could be a ubiquitous feature of the open ocean. In contrast, of 18 SML samples collected during seasonal transects up to 20 km from the North Sea coast, two had $EF < 1$ and values overall (mean EF 1.2 ± 0.3; range = 0.8–1.5) were comparatively low [*Pereira et al.*, 2016]. *Wurl et al.* [2011] also found EFs < 1, in 21% of low wind speed (0–2 m s $^{-1}$) and in 9% of moderate wind speed (2–5 m s $^{-1}$) samples from coastal and offshore sites

AGU Geophysical Research Letters 10.1002/2017GL072988

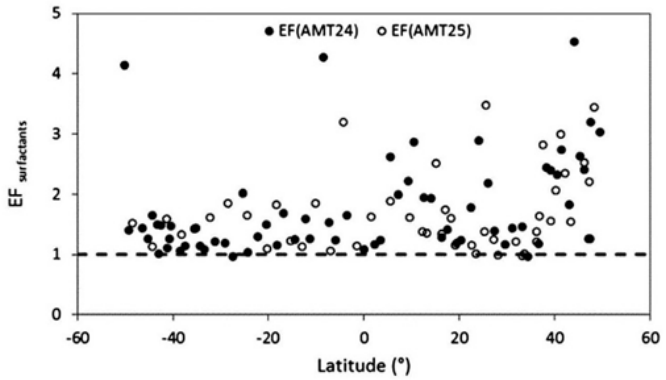

Figure 3. Latitudinal distribution of SA enrichment factors (EFs) in the SML.

(<20 km from land) in the North Pacific Ocean, Beaufort and Labrador Seas, and Baffin Bay. The persistent, high EFs during AMT 24 and AMT 25 are mirrored in high surface enrichments in dissolved organic carbon and amino acids in the subtropical Atlantic and western Mediterranean Sea at wind speeds approaching 10 m s^{-1} [*Reinthaler et al.*, 2008]. Mean EFs for the complete data set and for the Northern and Southern Hemispheres individually were statistically identical for both transects (*t* test, $p > 0.05$; Table S1). As observed for SA, mean Northern Hemisphere EF was higher than mean Southern Hemisphere EF, although the difference was only significant during AMT 24 (*t* test, $p < 0.05$) (Table S1). For both transects high EFs were mostly observed when SSW SA was <0.4 mg L^{-1} T-X-100. For SSW SA > 0.4 mg L^{-1} T-X-100, EF was always <2.6 (Figure 4).

We found no clear relationships between SA in the SML and either total chlorophyll or total pigments, for either the whole data set or on an individual province basis (Figure S1 in the supporting information), and we similarly found no relationships with either total or size-fractionated primary production (Figure S2). Although this is consistent with our finding no clear relationship between SA and chlorophyll *a* in the coastal North Sea [*Pereira et al.*, 2016], it contrasts with earlier work showing mean SA in the SML to increase linearly with "trophic state," as defined by using estimates of primary production, which implies at least a broad relationship between SML SA and primary production [*Wurl et al.*, 2011].

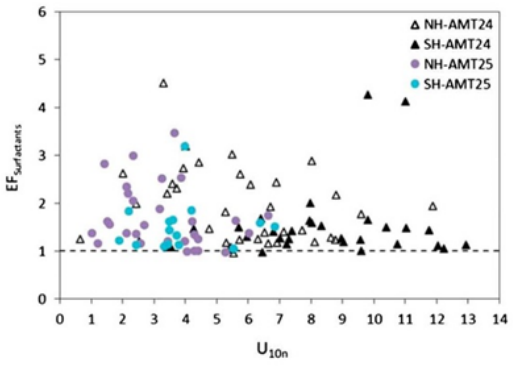

Figure 4. EF versus U_{10n} in the Northern Hemisphere (NH) and the Southern Hemisphere (SH). The dashed line represents EF = 1.

5. Discussion

The SA values we observed in the SML between 50°N and 50°S in the Atlantic Ocean (Figure 3) constitute the first direct test of an earlier prediction of SA distributions at the ocean basin scale derived from global maps of primary productivity and wind speed [*Wurl et al.*, 2011]. These authors reported SA values of 0.49 ± 0.4 mg L^{-1} T-X-100 in the SML (range: 0.1–1.57 mg L^{-1} T-X-100) for several oligotrophic regions including the North Pacific, the subtropical North Pacific, and the Arctic. Our ranges in SA and EF (Table S1) were within those given by *Wurl et al.* [2011], but our

AGU Geophysical Research Letters 10.1002/2017GL072988

failure to observe any relationships between SA and either total chlorophyll (Figure S1), total primary production (Figure S2), or size-fractionated primary production (Figure S2) must challenge the validity of using either estimates of total primary production or indices thereof in a predictive capacity for SA. Even so, we do not find this surprising given the variability in surfactant production rates among individual species of phytoplankton [*Žutić et al.*, 1981], by bacteria [*Kurata et al.*, 2016], and following phytoplankton grazing by zooplankton [*Kujawinski et al.*, 2002]. While an additional possibility is that any relationships between surfactant and indices of primary productivity could be masked, at least in part, by the bacterial degradation of surfactant, the evidence for surfactant degradation by bacteria is rather limited, being restricted to coastal locations [*Nguyen and Sigoillot*, 1990; *Sigoillot and Nguyen*, 1996].

At ocean basin scales with diverse biogeochemical regimes, variability in the pathways of bacterial surfactant production will likely be maximal, involving temporal signals and additional effects from advection and mixing. Even so, our observations suggest a rather small interannual variability in Atlantic Ocean surfactant distributions, with major latitudinal contrasts being maintained (Figure 2).

Wurl et al. [2011] also predicted that high EFs for SA, and presumably for some other SML components, poleward of both 30°N and 30°S in the Atlantic Ocean, would be precluded by high ambient wind speeds ($>12\ m\ s^{-1}$). On the contrary, our data clearly show high EFs (up to ~4.5) both north of 30°N and south of 30°S (Figure 4) and up to the maximum wind speed we observed ($U_{10n} = 12.9\ m\ s^{-1}$; Figure 4). We contend that high EFs at such wind speeds should not be unexpected because it has long been known that the SML reforms rapidly following physical disruption [*Dragcevic and Pravdic*, 1981], something we later confirmed experimentally with respect to SA [*Cunliffe et al.*, 2013]. It is now well established that rapid SML recovery occurs because SML organics dispersed by breaking waves readily reabsorb to the surfaces of rising bubbles generated by the same breaking waves [*Stefan and Szeri*, 1999; *Woolf*, 2005], to be released back to the SML and or ejected to air via bubble bursting at the air-sea interface. Consequently, our data strongly support the notion of an essentially self-sustaining SML and we have no reason to suspect that this mechanism would cease to operate either at or beyond the maximum wind speeds we observed. The high level of agreement in SA distributions in the SML between AMT 24 and AMT 25 therefore likely indicates a dynamic equilibrium, whereby increased SML disruption at higher sea states is at least largely compensated by concomitantly increased bubble fluxes that act to continuously restore surfactant material to the SML. In other words, the greater is the SML disruption, the greater is the bubble flux acting to restore the status quo.

An important outcome of our reasoning is that SA enrichment of the SML should be essentially decoupled from ambient wind speed, a conclusion that was also reached by *Wurl et al.* [2011] for dissolved surfactant and by *Carlson* [1983] for surface dissolved organic carbon. Indeed, SA EFs are evidently more closely correlated with SSW SA. Our consistent observation of low EF coincident with high SSW SA (EF always <2.6 for SSW SA values $>0.4\ mg\ L^{-1}$ T-X-100 is also supported by *Wurl et al.* [2011], who reported EF values <2.7 for SSW SA values $>0.6\ mg\ L^{-1}$ T-X-100 in waters ranging from nearshore to oceanic. We believe the most plausible explanation for these observations is that for any given wind speed, bubble scavenging is proportionally greater in low SA waters than in high SA waters. This is a result of there being a finite limit to the amount of surfactant that can be supplied by any individual bubble to the SML. Consequently, SML enrichment is limited by the total number/surface area of bubbles and so in SSW of comparatively low SA a proportionately larger fraction of the available surfactant pool is available for bubble scavenging (leading to high EF) than in SSW of comparatively high SA (leading to low EF). An inverse relationship between EF and SSW SA is therefore inevitable.

6. Implications and Conclusions

A better understanding of the spatial and temporal variabilities of SML surfactants [*Frew*, 2005; *Schneider-Zapp et al.*, 2014; *Pereira et al.*, 2016] will be critical to improving future estimates of air-sea gas exchange rates. Ultimately, such understanding will enhance our ability to predict the variability in regional- to global-scale trace gas fluxes and feedback. For CO_2 the lack of direct measurements of SA, both in the SML and in the SSW, constitutes a large proportion of the current uncertainty surrounding the inherent spatiotemporal variability of k_w. Even correcting for such errors in k_w as may arise from methodological differences [*Asher*, 2009], this uncertainty is much larger than the spatiotemporal uncertainty in surface ΔpCO_2 [*Takahashi et al.*, 2009]. Two aspects of our SA data from AMT are especially relevant. First, the elevated SA

AGU Geophysical Research Letters 10.1002/2017GL072988

values we observed in the NADR between 38°N and 48°N strongly imply that surfactant control of the air-sea exchange of CO_2 may be important over at least a substantial fraction of the North Atlantic, an ocean region that not only is a major CO_2 sink [*Watson et al.*, 1995; *Takahashi et al.*, 2009], but which shows a high variability in respect of its CO_2 uptake rate on subdecadal time scales that remains incompletely understood [*Schuster and Watson*, 2007; *Schuster et al.*, 2009; *Watson et al.*, 2009]. Second, our observations strongly imply that high-wind, high-latitude oceans may make a smaller contribution to air-sea gas exchange globally than is currently perceived. High SA in the SML at high latitudes suggests that air-sea trace gas fluxes might be lower than predicted from wind speed parameterizations alone, a conclusion that is supported by our earlier work in which a deliberate surfactant release in the North Atlantic resulted in up to 55% reduction in k_w relative to adjacent waters that were surfactant unamended, at a mean wind speed of 11 m s^{-1} [*Salter et al.*, 2011]. For coastal North Sea waters we also found evidence for strong k_w control, due not only to variability in SA but evidently also reflecting variability in the chemical composition of the surfactant pool that still remains largely unresolved [*Pereira et al.*, 2016].

To conclude, there is a clear need for continued measurements of SA in the SML and SSW at ocean basin scales, at contrasting times of year and over the full range of environmental wind speeds. Moreover, the mechanisms of surfactant production and consumption and the chemical composition of the surfactant pool need to be much better characterized in order to further advance our understanding of one of the most important environmental controls of k_w, and ultimately of the global budgets of a suite of climate-active gases.

Acknowledgments

AMT director Andy Rees (PML) enabled our participation in JCR cruises 303 and 304. We thank Denise Cummings and Ruth Airs (PML) for chlorophyll and pigment data, Gavin Tilstone (PML) for primary productivity data, the British Oceanographic Data Centre (BODC) for calibrated ancillary data, and Jon Barnes (Newcastle) for assisting with cruise mobilization. This work was supported by the UK Natural Environment Research Council (NERC: grant NE/K00252X/1 to R.C.U.G.) and is a component of RAGNARoCC (Radiatively active gases from the North Atlantic Region and Climate Change), which contributes to NERC's Greenhouse Gas Emissions and Feedbacks program (http://www.nerc.ac.uk/research/funded/programmes/greenhouse/). AMT contributes to the international IMBER initiative and is supported by NERC National Capability funding to PML and the National Oceanography Centre, Southampton. This is AMT contribution number 295. Data used in this study are available from the authors on request.

References

Allan, G. G., J. Lewin, and P. G. Johnson (1972), Marine polymers. IV. Diatom polysaccharides (excretion production of phytoplankton), *Bot. Mar.*, *15*, 102–108.

Asher, W. E. (2009), The effects of experimental uncertainty in parameterizing air-sea gas exchange using tracer experiment data, *Atmos. Chem. Phys.*, *9*, 131–139.

Bock, E. J., T. Hara, N. M. Frew, and W. R. McGillis (1999), Relationship between air-sea gas transfer and short wind waves, *J. Geophys. Res.*, *104*(C11), 25,821–25,831, doi:10.1029/1999JC900200.

Carlson, D. J. (1983), Dissolved organic materials in surface microlayers: Temporal and spatial variability and relation to sea state, *Limnol. Oceanogr.*, *28*, 415–431.

Carpenter, L. J., and P. D. Nightingale (2015), Chemistry and release of gases from the surface ocean, *Chem. Rev.*, *115*, 4015–4034.

Ćosović, B., and V. Vojvodić (1987), Direct determination of surface active substances in natural waters, *Mar. Chem.*, *22*(1987), 363–373.

Cunliffe, M., A. Engel, S. Frka, B. Gašparović, C. Guitart, J. C. Murrell, M. Salter, C. Stolle, R. C. Upstill-Goddard, and O. Wurl (2013), Sea surface microlayers: A unified physicochemical and biological perspective of the air–ocean interface, *Prog. Oceanogr.*, *109*, 104–116.

Cuscov, M., and F. L. L. Muller (2015), Differentiating humic and algal surface active substances in coastal waters by their pH-dependent adsorption behaviour, *Mar. Chem.*, *174*, 35–45.

Dragcevic, D., and V. Pravdic (1981), Properties of the seawater-air interface. 2. Rates of surface film formation under steady state conditions, *Limnol. Oceanogr.*, *26*, 492–499.

Frew, N. M. (2005), The role of organic films in air-sea gas exchange, in *The Sea Surface and Global Change*, edited by P. S. Liss and R. A. Duce, pp. 121–171, Cambridge Univ. Press, U. K.

Frew, N. M., J. C. Goldman, M. R. Dennett, and A. S. Johnson (1990), Impact of phytoplankton-generated surfactants on air-sea gas exchange, *J. Geophys. Res.*, *95*, 3337–3352, doi:10.1029/JC095iC03p03337.

Frew, N. M., R. K. Nelson, W. R. McGillis, J. B. Edson, E. J. Bock, and T. Hara (2002), Spatial variations in surface microlayer surfactants and their role in modulating air-sea exchange, in *Gas Transfer at Water Surfaces*, *Geophys. Monogr. Ser.*, vol. 127, edited by M. A. Donelan et al., pp. 153–159, AGU, Washington D. C.

Garrett, W. D. (1965), Collection of slick-forming materials from the sea surface, *Limnol. Oceanogr.*, *10*, 602–605.

Gašparović, B., K. Laß, S. Frka, A. Reunamo, G.-P. Yang, and R. Upstill-Goddard (2014), Sampling technique: Screen sampler, in *Guide to Best Practices to Study the Ocean's Surface*, edited by M. Cunliffe and O. Wurl, pp. 19–31, Marine Biological Association, Plymouth, U. K.

Kujawinski, E. B., J. W. Farrington, and J. W. Moffett (2002), Evidence for grazing-mediated production of dissolved surface-active material by marine protists, *Mar. Chem.*, *77*, 133–142.

Kurata, N., K. Vella, B. Hamilton, M. Shivji, A. Soloviev, S. Matt, A. Tartar, and W. Perrie (2016), Surfactant-associated bacteria in the near-surface layer of the ocean, *Nat. Sci. Rep.*, 19123, doi:10.1038/srep19123.

Leck, C., and E. K. Bigg (1999), Aerosol production over remote marine areas—A new route, *Geophys. Res. Lett.*, *26*, 3577–3580, doi:10.1029/1999GL010807.

Longhurst, A. (1995), Seasonal cycles of pelagic production and consumption, *Prog. Oceanogr.*, *36*, 77–167.

Myklestad, S. (1974), Production of carbohydrates by marine planktonic diatoms. I. Comparison of nine different species in culture (marine phytoplankton exudation products), *J. Exp. Mar. Biol. Ecol.*, *15*, 261–274.

Nguyen, M.-H., and J.-C. Sigoillot (1990), Isolation and characterization of surfactant degrading bacteria in a marine environment, *FEMS Microbiol. Lett.*, *73*, 50–67.

Nightingale, P. D. (2009), Air-sea gas exchange, in *Surface Ocean-lower Atmosphere Processes*, *Geophys. Monogr. Ser.*, vol. 187, edited by C. LeQuéré and E. S. Saltzman, pp. 67–97, AGU, Washington, D. C.

Nightingale, P. D., G. Malin, C. S. Law, A. J. Watson, P. S. Liss, M. I. Liddicoat, J. Boutin, and R. C. Upstill-Goddard (2000), In situ evaluation of air-sea gas exchange parameterizations using novel conservative and volatile tracers, *Global Biogeochem. Cycles*, *14*, 373–388, doi:10.1029/1999GB900091.

AGU Geophysical Research Letters 10.1002/2017GL072988

Ovadnevaite, J., C. O'Dowd, M. Dall'Osto, D. Ceburnis, D. R. Worsnop, and H. Berresheim (2011), Detecting high contributions of primary organic matter to marine aerosol: A case study, *Geophys. Res. Lett.*, *38*, L02807, doi:10.1029/2010GL046083.

Pereira, R., K. Schneider-Zapp, and R. C. Upstill-Goddard (2016), Surfactant control of gas transfer velocity along an offshore coastal transect: Results from a laboratory gas exchange tank, *Biogeosciences*, *13*, 3981–3989.

Reinthaler, T., E. Sintes, and G. J. Herndl (2008), Dissolved organic matter and bacterial production and respiration in the sea-surface microlayer of the open Atlantic and the western Mediterranean Sea, *Limnol. Oceanogr.*, *53*, 122–136.

Reygondeau, G., A. Longhurst, E. Martinez, G. Beaugrand, D. Antoine, and O. Maury (2013), Dynamic biogeochemical provinces in the global ocean, *Global Biogeochem. Cycles*, *27*, 1046–1058, doi:10.1002/gbc.20089.

Sakugawa, H., and N. Handa (1985), Isolation and chemical characterization of dissolved and particulate polysaccharides in Mikawa Bay (marine phytoplankton exudation with surface active properties during phytoplankton blooms), *Geochim. Cosmochim. Acta*, *49*, 1185–1193.

Salter, M. E., R. C. Upstill-Goddard, P. D. Nightingale, S. D. Archer, B. Blomquist, D. T. Ho, B. Huebert, P. Schlosser, and M. Yang (2011), Impact of an artificial surfactant release on air-sea gas fluxes during Deep Ocean Gas Exchange Experiment II, *J. Geophys. Res.*, *116*, C11016, doi:10.1029/2011JC007023.

Schneider-Zapp, K., M. E. Salter, and R. C. Upstill-Goddard (2014), An automated gas exchange tank for determining gas transfer velocities in natural seawater samples, *Ocean Sci.*, *10*, 587–600.

Schuster, U., and A. J. Watson (2007), A variable and decreasing sink for atmospheric CO_2 in the North Atlantic, *J. Geophys. Res.*, *112*, C11006, doi:10.1029/2006JC003941.

Schuster, U., A. J. Watson, N. Bates, A. Corbière, M. Gonzalez-Davila, N. Metzl, D. Pierrot, and M. Santana-Casiano (2009), Trends in North Atlantic sea surface pCO_2 from 1990 to 2006, *Deep Sea Res., Part II*, *56*, 620–629.

Serret, P., R. Robinson, E. Fernández, E. Teira, and G. Tilstone (2001), Latitudinal variation of the balance between plankton photosynthesis and respiration in the eastern Atlantic Ocean, *Limnol. Oceanogr.*, *46*, 1642–1652.

Sigoillot, J.-C., and M.-H. Nguyen (1996), Isolation from coastal seawater and characterization of bacterial strains involved in non-ionic surfactant degradation, *Biodegradation*, *7*, 369–375.

Stefan, R. L., and A. J. Szeri (1999), Surfactant scavenging and surface deposition by rising bubbles, *J. Colloid Interface Sci.*, *212*, 1–13.

Takahashi, T., S. C. Sutherland, R. Wanninkhof, C. Sweeney, R. A. Feely, D. W. Chipman, B. Hales, G. Friederich, F. Chavez, and C. Sabine (2009), Climatological mean and decadal change in surface ocean pCO_2, and net sea–air CO_2 flux over the global oceans, *Deep Sea Res. II: Top. Stud. Oceanogr.*, *56*, 554–577.

Tilstone, G. H., R. L. Airs, V. Martínez-Vicent, C. Widdicombe, and C. Llewellyn (2010), High concentrations of mycosporine-like amino acids and colored dissolved organic matter in the sea surface microlayer off the Iberian Peninsula, *Limnol. Oceanogr.*, *55*, 1835–1850.

Tseng, R.-S., J. T. Viechnicki, R. A. Skop, and J. W. Brown (1992), Sea-to-air transfer of surface-active organic compounds by bursting bubbles, *J. Geophys. Res.*, *97*, 5201–5206, doi:10.1029/91JC00954.

Upstill-Goddard, R. C., T. Frost, G. Henry, M. Franklin, J. C. Murrell, and N. J. P. Owens (2003), Bacterioneuston control of air-water methane exchange determined with a laboratory gas exchange tank, *Global. Biogeochem. Cycles*, *17*(4), 1108, doi:10.1029/2003GB002043.

Watson, A. J., P. D. Nightingale, and D. J. Cooper (1995), Modelling atmosphere-ocean CO_2 transfer, *Phil. Trans. R. Soc. B*, *348*, 125–132.

Watson, A. J., et al. (2009), Tracking the variable North Atlantic Sink for atmospheric CO_2, *Science*, *326*, 1391–1393.

Woolf, D. K. (2005), Bubbles and their role gas exchange, in *The Sea Surface and Global Change*, edited by P. S. Liss and R. A. Duce, pp. 173–205, Cambridge Univ. Press, U. K.

Wurl, O., and M. Holmes (2008), The gelatinous nature of the sea-surface microlayer, *Mar. Chem.*, *110*, 89–97.

Wurl, O., and A. Soloviev (2014), Selection of sampling sites and suitable sampling platforms, in *Guide to Best Practices to Study the Ocean's Surface*, edited by M. Cunliffe and O. Wurl, pp. 16–18, Marine Biological Association, Plymouth, U. K.

Wurl, O., E. Wurl, L. Miller, K. Johnson, and S. Vagle (2011), Formation and global distribution of sea-surface microlayers, *Biogeosciences*, *8*, 121–135.

Zapata, M., F. Rodriguez, and J. L. Garrido (2000), Separation of chlorophylls and carotenoids from marine phytoplankton: A new HPLC method using a reversed phase C_8 column and pyridine-containing mobile phases, *Mar. Ecol. Prog. Ser.*, *195*, 29–45.

Žutić, V., B. Ćosović, E. Marčenko, N. Bihari, and F. Kršinić (1981), Surfactant production by marine phytoplankton, *Mar. Chem.*, *10*, 505–520.

Appendix.3

Table A2. CTD information for AMT24 and AMT25

Cruise_Station	yyyymmdd [GT]	Latitude[°+veN]	Longitude[°+veE]	Bot_depth[m]	Firing_Seq	MLD(m)	DCM(m)	O_2Max.(m)
AMT24S001	25/09/2014 09:59	49.83	-4.76	1.5	23	15	17	15
AMT24S001	25/09/2014 09:59	49.83	-4.76	10.2	22			
AMT24S001	25/09/2014 09:59	49.83	-4.76	20.7	19			
AMT24S001	25/09/2014 09:59	49.83	-4.76	61.6	4			
AMT24S001	25/09/2014 09:59	49.83	-4.76	71.5	1			
AMT24S002	26/09/2014 03:17	47.87	-7.94	1.2	23 x			
AMT24S002	26/09/2014 03:17	47.87	-7.94	3.9	22			
AMT24S002	26/09/2014 03:17	47.87	-7.94	6.5	21			
AMT24S002	26/09/2014 03:17	47.87	-7.94	12.2	19			
AMT24S002	26/09/2014 03:17	47.87	-7.94	18.5	17			
AMT24S002	26/09/2014 03:17	47.87	-7.94	21.6	16		✓	
AMT24S002	26/09/2014 03:17	47.87	-7.94	28.4	11	✓		
AMT24S002	26/09/2014 03:17	47.87	-7.94	38.5	9		✓	
AMT24S002	26/09/2014 03:17	47.87	-7.94	49.3	8			
AMT24S002	26/09/2014 03:17	47.87	-7.94	74.9	6			
AMT24S002	26/09/2014 03:17	47.87	-7.94	99.8	5			
AMT24S002	26/09/2014 03:17	47.87	-7.94	200.9	4			
AMT24S002	26/09/2014 03:17	47.87	-7.94	302.4	3			
AMT24S002	26/09/2014 03:17	47.87	-7.94	403.2	1			
AMT24S003	26/09/2014 10:09	47.19	-8.82	2	23		x	
AMT24S003	26/09/2014 10:09	47.19	-8.82	5.5	22			
AMT24S003	26/09/2014 10:09	47.19	-8.82	9.4	21			
AMT24S003	26/09/2014 10:09	47.19	-8.82	16.4	19			
AMT24S003	26/09/2014 10:09	47.19	-8.82	20.4	18			
AMT24S003	26/09/2014 10:09	47.19	-8.82	28.2	15			
AMT24S003	26/09/2014 10:09	47.19	-8.82	30.3	13	✓		
AMT24S003	26/09/2014 10:09	47.19	-8.82	38.2	10			
AMT24S003	26/09/2014 10:09	47.19	-8.82	50.2	9	✓		
AMT24S003	26/09/2014 10:09	47.19	-8.82	65.7	7			
AMT24S003	26/09/2014 10:09	47.19	-8.82	98.2	6			
AMT24S003	26/09/2014 10:09	47.19	-8.82	209.5	4			
AMT24S003	26/09/2014 10:09	47.19	-8.82	309.9	3			
AMT24S003	26/09/2014 10:09	47.19	-8.82	411.3	2			
AMT24S003	26/09/2014 10:09	47.19	-8.82	512.4	1			

Table A2. (continued) CTD information for AMT24 and AMT25

Cruise_Station	yyyymmdd [GT]	Latitude[°+veN]	Longitude[°+veE]	Bot_depth[m]	Firing_Seq	MLD(m)	DCM(m)	O_2Max.(m)
AMT24S004	27/09/2014 12:06	47.57	-8.50	1.7	23	10		42
AMT24S004	27/09/2014 12:06	47.57	-8.50	4.5	22			
AMT24S004	27/09/2014 12:06	47.57	-8.50	9.1	21			
AMT24S004	27/09/2014 12:06	47.57	-8.50	15.9	19			
AMT24S004	27/09/2014 12:06	47.57	-8.50	28.2	15			
AMT24S004	27/09/2014 12:06	47.57	-8.50	44.1	11		✓	
AMT24S004	27/09/2014 12:06	47.57	-8.50	49.6	8			
AMT24S004	27/09/2014 12:06	47.57	-8.50	65.5	6			
AMT24S005	28/09/2014 04:27	46.39	-10.98	1.3	24	20		
AMT24S005	28/09/2014 04:27	46.39	-10.98	5.5	21			
AMT24S005	28/09/2014 04:27	46.39	-10.98	7.5	20			
AMT24S005	28/09/2014 04:27	46.39	-10.98	13.7	19			
AMT24S005	28/09/2014 04:27	46.39	-10.98	23.3	16			
AMT24S005	28/09/2014 04:27	46.39	-10.98	34.4	14		✓	✓
AMT24S005	28/09/2014 04:27	46.39	-10.98	41.7	10			
AMT24S005	28/09/2014 04:27	46.39	-10.98	54.4	9			
AMT24S005	28/09/2014 04:27	46.39	-10.98	506.6	3			
AMT24S005	28/09/2014 04:27	46.39	-10.98	505.8	2			
AMT24S006	28/09/2014 13:02	45.50	-12.49	1.9	23	30		
AMT24S006	28/09/2014 13:02	45.50	-12.49	4.9	22			
AMT24S006	28/09/2014 13:02	45.50	-12.49	9.8	21			
AMT24S006	28/09/2014 13:02	45.50	-12.49	18	19			
AMT24S006	28/09/2014 13:02	45.50	-12.49	32.8	15			
AMT24S006	28/09/2014 13:02	45.50	-12.49	50.5	11		✓	✓
AMT24S006	28/09/2014 13:02	45.50	-12.49	58.2	8			
AMT24S006	28/09/2014 13:02	45.50	-12.49	76.3	7			
AMT24S006	28/09/2014 13:02	45.50	-12.49	504.6	1			
AMT24S007	29/09/2014 04:11	44.09	-14.92	1.5	22	39		60
AMT24S007	29/09/2014 04:11	44.09	-14.92	4.7	20			
AMT24S007	29/09/2014 04:11	44.09	-14.92	9.9	19			
AMT24S007	29/09/2014 04:11	44.09	-14.92	18	18			
AMT24S007	29/09/2014 04:11	44.09	-14.92	31.9	15			
AMT24S007	29/09/2014 04:11	44.09	-14.92	57.2	13			
AMT24S007	29/09/2014 04:11	44.09	-14.92	67.2	12		✓	
AMT24S007	29/09/2014 04:11	44.09	-14.92	75.7	8			
AMT24S007	29/09/2014 04:11	44.09	-14.92	504.4	2			

Table A2. (continued) CTD information for AMT24 and AMT25

Cruise_Station	yyyymmdd [GT]	Latitude[°+veN]	Longitude[°+veE]	Bot_depth[m]	Firing_Seq	MLD(m)	DCM(m)	O_2Max.(m)
AMT24S008	29/09/2014 13:05	43.17	-16.43	2.7	23	20	x	
AMT24S008	29/09/2014 13:05	43.17	-16.43	5.4	22			
AMT24S008	29/09/2014 13:05	43.17	-16.43	12.5	21			
AMT24S008	29/09/2014 13:05	43.17	-16.43	22.5	17			
AMT24S008	29/09/2014 13:05	43.17	-16.43	38.5	16			
AMT24S008	29/09/2014 13:05	43.17	-16.43	64.5	11		✓	
AMT24S008	29/09/2014 13:05	43.17	-16.43	67.8	8			
AMT24S008	29/09/2014 13:05	43.17	-16.43	88.8	7			
AMT24S008	29/09/2014 13:05	43.17	-16.43	505.2	1			
AMT24S009	30/09/2014 04:01	41.77	-18.76	1.4	24	20		
AMT24S009	30/09/2014 04:01	41.77	-18.76	8.6	20			
AMT24S009	30/09/2014 04:01	41.77	-18.76	15.5	19			
AMT24S009	30/09/2014 04:01	41.77	-18.76	26.2	16			
AMT24S009	30/09/2014 04:01	41.77	-18.76	30.4	15			✓
AMT24S009	30/09/2014 04:01	41.77	-18.76	35.6	13		✓	
AMT24S009	30/09/2014 04:01	41.77	-18.76	46.3	9			
AMT24S009	30/09/2014 04:01	41.77	-18.76	60.7	8			
AMT24S009	30/09/2014 04:01	41.77	-18.76	505.4	2			
AMT24S010	30/09/2014 13:02	40.84	-20.21	1.9	23	20	x	
AMT24S010	30/09/2014 13:02	40.84	-20.21	4.9	22			
AMT24S010	30/09/2014 13:02	40.84	-20.21	8.9	21			
AMT24S010	30/09/2014 13:02	40.84	-20.21	15.9	20			
AMT24S010	30/09/2014 13:02	40.84	-20.21	28.7	16			
AMT24S010	30/09/2014 13:02	40.84	-20.21	40	11		✓	
AMT24S010	30/09/2014 13:02	40.84	-20.21	51.4	8			
AMT24S010	30/09/2014 13:02	40.84	-20.21	66.2	7			
AMT24S010	30/09/2014 13:02	40.84	-20.21	505.6	1			
AMT24S011	01/10/2014 04:02	39.40	-22.46	1.8	24	35		
AMT24S011	01/10/2014 04:02	39.40	-22.46	9.9	20			
AMT24S011	01/10/2014 04:02	39.40	-22.46	19	19			
AMT24S011	01/10/2014 04:02	39.40	-22.46	33.6	16			
AMT24S011	01/10/2014 04:02	39.40	-22.46	47.8	14			✓
AMT24S011	01/10/2014 04:02	39.40	-22.46	58.1	13			
AMT24S011	01/10/2014 04:02	39.40	-22.46	63.4	12		✓	
AMT24S011	01/10/2014 04:02	39.40	-22.46	75.5	8			
AMT24S011	01/10/2014 04:02	39.40	-22.46	504.5	2			

Table A2. (continued) CTD information for AMT24 and AMT25

Cruise_Station	yyyymmdd [GT]	Latitude[°+veN]	Longitude[°+veE]	Bot_depth[m]	Firing_Seq	MLD(m)	DCM(m)	O_2Max.(m)
AMT24S012	01/10/2014 13:02	38.50	-23.89	2	23	40		55
AMT24S012	01/10/2014 13:02	38.50	-23.89	5.4	22			
AMT24S012	01/10/2014 13:02	38.50	-23.89	9.1	21			
AMT24S012	01/10/2014 13:02	38.50	-23.89	16.1	20			
AMT24S012	01/10/2014 13:02	38.50	-23.89	28.1	16			
AMT24S012	01/10/2014 13:02	38.50	-23.89	49.4	14			
AMT24S012	01/10/2014 13:02	38.50	-23.89	60	10		✓	
AMT24S012	01/10/2014 13:02	38.50	-23.89	505	1			
AMT24S013	02/10/2014 13:02	36.95	-25.91	1.9	23	20		75
AMT24S013	02/10/2014 13:02	36.95	-25.91	5	22			
AMT24S013	02/10/2014 13:02	36.95	-25.91	11.3	21			
AMT24S013	02/10/2014 13:02	36.95	-25.91	20.2	18			
AMT24S013	02/10/2014 13:02	36.95	-25.91	36.3	16			
AMT24S013	02/10/2014 13:02	36.95	-25.91	64.3	14			
AMT24S013	02/10/2014 13:02	36.95	-25.91	78.4	10		✓	
AMT24S013	02/10/2014 13:02	36.95	-25.91	83.3	7			
AMT24S013	02/10/2014 13:02	36.95	-25.91	504.9	1			
AMT24S014	03/10/2014 04:02	34.74	-26.61	2.2	24	40		60
AMT24S014	03/10/2014 04:02	34.74	-26.61	5.3	21			
AMT24S014	03/10/2014 04:02	34.74	-26.61	11	20			
AMT24S014	03/10/2014 04:02	34.74	-26.61	20.3	17			
AMT24S014	03/10/2014 04:02	34.74	-26.61	36.3	16			
AMT24S014	03/10/2014 04:02	34.74	-26.61	60.8	14			
AMT24S014	03/10/2014 04:02	34.74	-26.61	75.4	12		✓	
AMT24S014	03/10/2014 04:02	34.74	-26.61	126.7	7			
AMT24S014	03/10/2014 04:02	34.74	-26.61	504.4	2			
AMT24S015	03/10/2014 13:02	33.35	-27.08	1.5	23	40		68
AMT24S015	03/10/2014 13:02	33.35	-27.08	4.6	22			
AMT24S015	03/10/2014 13:02	33.35	-27.08	14.4	21			
AMT24S015	03/10/2014 13:02	33.35	-27.08	26.4	17			
AMT24S015	03/10/2014 13:02	33.35	-27.08	45.1	16			
AMT24S015	03/10/2014 13:02	33.35	-27.08	80.6	13			
AMT24S015	03/10/2014 13:02	33.35	-27.08	100.8	10		✓	
AMT24S015	03/10/2014 13:02	33.35	-27.08	105.7	7			
AMT24S015	03/10/2014 13:02	33.35	-27.08	504.4	1			

Table A2. (continued) CTD information for AMT24 and AMT25

Cruise_Station	yyyymmdd [GT]	Latitude[°+veN]	Longitude[°+veE]	Bot_depth[m]	Firing_Seq	MLD(m)	DCM(m)	O_2Max.(m)
AMT24S016	04/10/2014 04:02	31.30	-27.70	2.1	24	40		60
AMT24S016	04/10/2014 04:02	31.30	-27.70	14.3	20			
AMT24S016	04/10/2014 04:02	31.30	-27.70	60.5	15			
AMT24S016	04/10/2014 04:02	31.30	-27.70	100.7	12		✓	
AMT24S016	04/10/2014 04:02	31.30	-27.70	504.3	2			
AMT24S017	04/10/2014 13:03	29.90	-28.17	16.1	21	40		75
AMT24S017	04/10/2014 13:03	29.90	-28.17	52	16			
AMT24S017	04/10/2014 13:03	29.90	-28.17	115.5	10		✓	
AMT24S017	04/10/2014 13:03	29.90	-28.17	504	1			
AMT24S018	05/10/2014 05:05	27.50	-28.86	1.9	24	40		
AMT24S018	05/10/2014 05:05	27.50	-28.86	18	20			
AMT24S018	05/10/2014 05:05	27.50	-28.86	75.7	15		✓	
AMT24S018	05/10/2014 05:05	27.50	-28.86	135.5	11		✓	
AMT24S018	05/10/2014 05:05	27.50	-28.86	504.2	2			
AMT24S019	05/10/2014 14:03	26.11	-29.31	2	23			
AMT24S019	05/10/2014 14:03	26.11	-29.31	2.1	24	35		65
AMT24S019	05/10/2014 14:03	26.11	-29.31	16.1	21			
AMT24S019	05/10/2014 14:03	26.11	-29.31	29	17			
AMT24S019	05/10/2014 14:03	26.11	-29.31	92.6	13			
AMT24S019	05/10/2014 14:03	26.11	-29.31	120.6	9		✓	
AMT24S019	05/10/2014 14:03	26.11	-29.31	504.5	1			
AMT24S020	06/10/2014 05:06	24.06	-29.88	2.1	24	35		
AMT24S020	06/10/2014 05:06	24.06	-29.88	4.6	21			
AMT24S020	06/10/2014 05:06	24.06	-29.88	12.9	20			
AMT24S020	06/10/2014 05:06	24.06	-29.88	25.5	17			
AMT24S020	06/10/2014 05:06	24.06	-29.88	43.1	16			
AMT24S020	06/10/2014 05:06	24.06	-29.88	62	14		✓	
AMT24S020	06/10/2014 05:06	24.06	-29.88	100.7	11		✓	
AMT24S020	06/10/2014 05:06	24.06	-29.88	504	2			
AMT24S021	06/10/2014 14:01	22.66	-29.87	2.7	23	40	✓	
AMT24S021	06/10/2014 14:01	22.66	-29.87	13.3	21			
AMT24S021	06/10/2014 14:01	22.66	-29.87	43.3	16			
AMT24S021	06/10/2014 14:01	22.66	-29.87	100.7	9		✓	
AMT24S021	06/10/2014 14:01	22.66	-29.87	503.6	1			

Table A2. (continued) CTD information for AMT24 and AMT25

Cruise_Station	yyyymmdd [GT]	Latitude[°+veN]	Longitude[°+veE]	Bot_depth[m]	Firing_Seq	MLD(m)	DCM(m)	O_2Max.(m)
AMT24S022	07/10/2014 05:06	20.45	-29.25	2.7	24	30		
AMT24S022	07/10/2014 05:06	20.45	-29.25	5.5	21			
AMT24S022	07/10/2014 05:06	20.45	-29.25	14.6	20			
AMT24S022	07/10/2014 05:06	20.45	-29.25	26.2	17			
AMT24S022	07/10/2014 05:06	20.45	-29.25	45.9	16			
AMT24S022	07/10/2014 05:06	20.45	-29.25	61.5	14			✓
AMT24S022	07/10/2014 05:06	20.45	-29.25	80.7	13			
AMT24S022	07/10/2014 05:06	20.45	-29.25	95.5	12		✓	
AMT24S022	07/10/2014 05:06	20.45	-29.25	105.5	8			
AMT24S022	07/10/2014 05:06	20.45	-29.25	504	2			
AMT24S024	07/10/2014 14:06	19.86	-29.14	2.7	23	50		75
AMT24S024	07/10/2014 14:06	19.86	-29.14	13	21			
AMT24S024	07/10/2014 14:06	19.86	-29.14	40.9	16			
AMT24S024	07/10/2014 14:06	19.86	-29.14	91	10		✓	
AMT24S024	07/10/2014 14:06	19.86	-29.14	504.8	1			
AMT24S025	08/10/2014 05:10	17.83	-28.68	2.2	24	44		
AMT24S025	08/10/2014 05:10	17.83	-28.68	10.1	20			
AMT24S025	08/10/2014 05:10	17.83	-28.68	50.8	14			✓
AMT24S025	08/10/2014 05:10	17.83	-28.68	67.7	12		✓	
AMT24S025	08/10/2014 05:10	17.83	-28.68	504.1	2			
AMT24S026	08/10/2014 14:00	16.44	-28.40	2.4	23			60
AMT24S026	08/10/2014 14:00	16.44	-28.40	13.3	21			
AMT24S026	08/10/2014 14:00	16.44	-28.40	41.1	16	✓		
AMT24S026	08/10/2014 14:00	16.44	-28.40	79.9	10		✓	
AMT24S026	08/10/2014 14:00	16.44	-28.40	503.6	1			
AMT24S027	09/10/2014 05:10	14.22	-27.91	2.2	23	25		
AMT24S027	09/10/2014 05:10	14.22	-27.91	9.8	20			
AMT24S027	09/10/2014 05:10	14.22	-27.91	29.5	15			✓
AMT24S027	09/10/2014 05:10	14.22	-27.91	52	10		✓	
AMT24S027	09/10/2014 05:10	14.22	-27.91	503.6	2			

Table A2. (continued) CTD information for AMT24 and AMT25

Cruise_Station	yyyymmdd [GT]	Latitude[°+veN]	Longitude[°+veE]	Bot_depth[m]	Firing_Seq	MLD(m)	DCM(m)	O_2Max.(m)
AMT24S028	09/10/2014 14:03	12.84	-27.65	2	23	25		30
AMT24S028	09/10/2014 14:03	12.84	-27.65	9.2	21			
AMT24S028	09/10/2014 14:03	12.84	-27.65	26.9	16			
AMT24S028	09/10/2014 14:03	12.84	-27.65	39.8	11		✓	
AMT24S028	09/10/2014 14:03	12.84	-27.65	504.1	1			
AMT24S029	10/10/2014 05:16	10.76	-27.20	1.9	24	20		
AMT24S029	10/10/2014 05:16	10.76	-27.20	9.8	20			
AMT24S029	10/10/2014 05:16	10.76	-27.20	25.6	16		✓	
AMT24S029	10/10/2014 05:16	10.76	-27.20	47.4	13		✓	
AMT24S029	10/10/2014 05:16	10.76	-27.20	503.1	2			
AMT24S030	10/10/2014 14:03	9.37	-26.92	1.4	23	30		25
AMT24S030	10/10/2014 14:03	9.37	-26.92	7.8	21			
AMT24S030	10/10/2014 14:03	9.37	-26.92	23.5	16			
AMT24S030	10/10/2014 14:03	9.37	-26.92	45.1	10		✓	
AMT24S030	10/10/2014 14:03	9.37	-26.92	503.3	1			
AMT24S031	11/10/2014 05:08	7.28	-26.51	2.1	23	30		
AMT24S031	11/10/2014 05:08	7.28	-26.51	10.1	20			
AMT24S031	11/10/2014 05:08	7.28	-26.51	50.6	14		✓	
AMT24S031	11/10/2014 05:08	7.28	-26.51	68.7	10		✓	
AMT24S031	11/10/2014 05:08	7.28	-26.51	503.4	2			
AMT24S032	11/10/2014 14:03	5.90	-26.20	1.9	23	35		
AMT24S032	11/10/2014 14:03	5.90	-26.20	11.5	21			
AMT24S032	11/10/2014 14:03	5.90	-26.20	48.4	15			
AMT24S032	11/10/2014 14:03	5.90	-26.20	74.6	9		✓	
AMT24S032	11/10/2014 14:03	5.90	-26.20	503.3	1			

Table A2. (continued) CTD information for AMT24 and AMT25

Cruise_Station	yyyymmdd [GT]	Latitude[°+veN]	Longitude[°+veE]	Bot_depth[m]	Firing_Seq	MLD(m)	DCM(m)	O_2Max.(m)
AMT24S033	12/10/2014 05:06	3.78	-25.77	2.4	24	50		
AMT24S033	12/10/2014 05:06	3.78	-25.77	11.6	20			
AMT24S033	12/10/2014 05:06	3.78	-25.77	69.3	13			✓
AMT24S033	12/10/2014 05:06	3.78	-25.77	74.9	11		✓	
AMT24S033	12/10/2014 05:06	3.78	-25.77	502	1			
AMT24S034	12/10/2014 14:03	2.38	-25.49	1.6	23	78		25
AMT24S034	12/10/2014 14:03	2.38	-25.49	12.6	21			
AMT24S034	12/10/2014 14:03	2.38	-25.49	20	18			
AMT24S034	12/10/2014 14:03	2.38	-25.49	66.5	10		✓	
AMT24S034	12/10/2014 14:03	2.38	-25.49	503.3	1			
AMT24S035	13/10/2014 05:33	0.00	-25.00	1.7	22			30
AMT24S035	13/10/2014 05:33	0.00	-25.00	2	24			
AMT24S035	13/10/2014 05:33	0.00	-25.00	8.4	19			
AMT24S035	13/10/2014 05:33	0.00	-25.00	50.6	11	✓	✓	
AMT24S035	13/10/2014 05:33	0.00	-25.00	503.6	2			
AMT24S036	14/10/2014 05:06	-3.90	-25.00	2.1	22	73		20
AMT24S036	14/10/2014 05:06	-3.90	-25.00	10.6	19			
AMT24S036	14/10/2014 05:06	-3.90	-25.00	35	15			
AMT24S036	14/10/2014 05:06	-3.90	-25.00	72.7	11		✓	
AMT24S036	14/10/2014 05:06	-3.90	-25.00	503.8	2			
AMT24S037	14/10/2014 14:04	-5.32	-25.03	2.4	23	80		50
AMT24S037	14/10/2014 14:04	-5.32	-25.03	11.1	21			
AMT24S037	14/10/2014 14:04	-5.32	-25.03	34.4	17			
AMT24S037	14/10/2014 14:04	-5.32	-25.03	70.7	10		✓	
AMT24S037	14/10/2014 14:04	-5.32	-25.03	504.2	1			
AMT24S038	15/10/2014 05:03	-7.48	-25.01	1.9	22	40		✓
AMT24S038	15/10/2014 05:03	-7.48	-25.01	12.6	19			
AMT24S038	15/10/2014 05:03	-7.48	-25.01	41.4	15			
AMT24S038	15/10/2014 05:03	-7.48	-25.01	92.7	11		✓	
AMT24S038	15/10/2014 05:03	-7.48	-25.01	503.8	2			

Table A2. (continued) CTD information for AMT24 and AMT25

Cruise_Station	yyyymmdd [GT]	Latitude[°+veN]	Longitude[°+veE]	Bot_depth[m]	Firing_Seq	MLD(m)	DCM(m)	O_2Max.(m)
AMT24S039	15/10/2014 14:03	-8.91	-25.04	12.8	21	90		108
AMT24S039	15/10/2014 14:03	-8.91	-25.04	41.6	17			
AMT24S039	15/10/2014 14:03	-8.91	-25.04	82.1	10		✓	
AMT24S039	15/10/2014 14:03	-8.91	-25.04	503.4	1			
AMT24S040	16/10/2014 05:05	-11.05	-25.02	2.1	22	100		120
AMT24S040	16/10/2014 05:05	-11.05	-25.02	17.3	19			
AMT24S040	16/10/2014 05:05	-11.05	-25.02	56.3	15			
AMT24S040	16/10/2014 05:05	-11.05	-25.02	125	11		✓	
AMT24S040	16/10/2014 05:05	-11.05	-25.02	503.9	2			
AMT24S041	16/10/2014 14:01	-12.49	-25.07	2.1	23	60		100
AMT24S041	16/10/2014 14:01	-12.49	-25.07	15.3	21			
AMT24S041	16/10/2014 14:01	-12.49	-25.07	47.1	17			
AMT24S041	16/10/2014 14:01	-12.49	-25.07	122.8	8		✓	
AMT24S041	16/10/2014 14:01	-12.49	-25.07	503.3	1			
AMT24S042	17/10/2014 05:03	-14.67	-25.05	2.3	22	140		150
AMT24S042	17/10/2014 05:03	-14.67	-25.05	17.1	19			
AMT24S042	17/10/2014 05:03	-14.67	-25.05	56.4	15			
AMT24S042	17/10/2014 05:03	-14.67	-25.05	125.6	11		✓	
AMT24S042	17/10/2014 05:03	-14.67	-25.05	503.9	2			
AMT24S043	17/10/2014 14:02	-16.13	-25.08	2.3	23	100	x	
AMT24S043	17/10/2014 14:02	-16.13	-25.08	23.1	18			
AMT24S043	17/10/2014 14:02	-16.13	-25.08	73.5	15			
AMT24S043	17/10/2014 14:02	-16.13	-25.08	166.4	8		✓	
AMT24S043	17/10/2014 14:02	-16.13	-25.08	503.8	1			
AMT24S044	18/10/2014 05:06	-18.32	-25.06	2.3	22	100	✓	
AMT24S044	18/10/2014 05:06	-18.32	-25.06	21.3	17			
AMT24S044	18/10/2014 05:06	-18.32	-25.06	160.8	11		✓	
AMT24S044	18/10/2014 05:06	-18.32	-25.06	504.8	1			

Table A2. (continued) CTD information for AMT24 and AMT25

Cruise_Station	yyyymmdd [GT]	Latitude[°+veN]	Longitude[°+veE]	Bot_depth[m]	Firing_Seq	MLD(m)	DCM(m)	O_2Max.(m)
AMT24S045	18/10/2014 14:04	-18.55	-25.07	1.9	20	180		
AMT24S045	18/10/2014 14:04	-18.55	-25.07	24.9	16			
AMT24S045	18/10/2014 14:04	-18.55	-25.07	77.8	14			
AMT24S045	18/10/2014 14:04	-18.55	-25.07	176.5	7		✓	
AMT24S045	18/10/2014 14:04	-18.55	-25.07	503.3	1			
AMT24S047	20/10/2014 05:04	-20.86	-25.05	2.1	22	160		165
AMT24S047	20/10/2014 05:04	-20.86	-25.05	20.3	19			
AMT24S047	20/10/2014 05:04	-20.86	-25.05	60.3	15			
AMT24S047	20/10/2014 05:04	-20.86	-25.05	140.7	12		✓	
AMT24S047	20/10/2014 05:04	-20.86	-25.05	503.9	1			
AMT24S047	20/10/2014 05:04	-20.86	-25.05	503.9	2			
AMT24S048	20/10/2014 14:03	-22.32	-25.06	2.6	23	180	x	
AMT24S048	20/10/2014 14:03	-22.32	-25.06	20.1	21			
AMT24S048	20/10/2014 14:03	-22.32	-25.06	70.2	17			
AMT24S048	20/10/2014 14:03	-22.32	-25.06	155.8	11		✓	
AMT24S048	20/10/2014 14:03	-22.32	-25.06	503.9	1			
AMT24S049	21/10/2014 05:03	-24.43	-25.04	1.7	24	100		25
AMT24S049	21/10/2014 05:03	-24.43	-25.04	19.9	17			
AMT24S049	21/10/2014 05:03	-24.43	-25.04	65.3	15			
AMT24S049	21/10/2014 05:03	-24.43	-25.04	150.9	11		✓	
AMT24S049	21/10/2014 05:03	-24.43	-25.04	504	2			
AMT24S050	21/10/2014 14:01	-25.59	-25.04	2.5	23	175		50
AMT24S050	21/10/2014 14:01	-25.59	-25.04	18	21			
AMT24S050	21/10/2014 14:01	-25.59	-25.04	58.8	17			
AMT24S050	21/10/2014 14:01	-25.59	-25.04	135.5	11		✓	
AMT24S050	21/10/2014 14:01	-25.59	-25.04	503.6	1			
AMT24S051	22/10/2014 05:06	-27.75	-25.03	2.4	22	25	x	
AMT24S051	22/10/2014 05:06	-27.75	-25.03	4.7	20			
AMT24S051	22/10/2014 05:06	-27.75	-25.03	16.8	19			
AMT24S051	22/10/2014 05:06	-27.75	-25.03	53.9	15			
AMT24S051	22/10/2014 05:06	-27.75	-25.03	125.1	11		✓	
AMT24S051	22/10/2014 05:06	-27.75	-25.03	503.7	2			

Table A2. (continued) CTD information for AMT24 and AMT25

Cruise_Station	yyyymmdd [GT]	Latitude[°+veN]	Longitude[°+veE]	Bot_depth[m]	Firing_Seq	MLD(m)	DCM(m)	O_2Max.(m)
AMT24S052	22/10/2014 14:02	-29.15	-25.28	3	23	150		50
AMT24S052	22/10/2014 14:02	-29.15	-25.28	17.2	21			
AMT24S052	22/10/2014 14:02	-29.15	-25.28	56.2	16			
AMT24S052	22/10/2014 14:02	-29.15	-25.28	126.2	11		✓	
AMT24S052	22/10/2014 14:02	-29.15	-25.28	504.3	1			
AMT24S053	23/10/2014 06:04	-31.36	-26.10	2.4	23	28		50
AMT24S053	23/10/2014 06:04	-31.36	-26.10	12.5	19			
AMT24S053	23/10/2014 06:04	-31.36	-26.10	42.4	15			
AMT24S053	23/10/2014 06:04	-31.36	-26.10	100.8	11		✓	
AMT24S053	23/10/2014 06:04	-31.36	-26.10	504.3	2			
AMT24S054	23/10/2014 15:00	-32.72	-26.63	2.1	23	50		60
AMT24S054	23/10/2014 15:00	-32.72	-26.63	11.8	21			
AMT24S054	23/10/2014 15:00	-32.72	-26.63	40	16			
AMT24S054	23/10/2014 15:00	-32.72	-26.63	87.3	10		✓	
AMT24S054	23/10/2014 15:00	-32.72	-26.63	504	1			
AMT24S055	24/10/2014 06:02	-34.69	-27.43	2.5	22	50		70
AMT24S055	24/10/2014 06:02	-34.69	-27.43	12.3	19			
AMT24S055	24/10/2014 06:02	-34.69	-27.43	38.9	15			
AMT24S055	24/10/2014 06:02	-34.69	-27.43	70.8	12		✓	
AMT24S055	24/10/2014 06:02	-34.69	-27.43	505.6	2			
AMT24S056	24/10/2014 15:02	-35.80	-27.87	2.1	23	65		50
AMT24S056	24/10/2014 15:02	-35.80	-27.87	8.9	21			
AMT24S056	24/10/2014 15:02	-35.80	-27.87	27.5	16			
AMT24S056	24/10/2014 15:02	-35.80	-27.87	44.7	12		✓	
AMT24S056	24/10/2014 15:02	-35.80	-27.87	504.8	1			
AMT24S057	25/10/2014 06:08	-37.89	-28.77	2.8	24	150	x	
AMT24S057	25/10/2014 06:08	-37.89	-28.77	4.1	20			
AMT24S057	25/10/2014 06:08	-37.89	-28.77	19.9	18			
AMT24S057	25/10/2014 06:08	-37.89	-28.77	39.4	13		✓	
AMT24S057	25/10/2014 06:08	-37.89	-28.77	503.4	2			

Table A2. (continued) CTD information for AMT24 and AMT25

Cruise_Station	yyyymmdd [GT]	Latitude[°+veN]	Longitude[°+veE]	Bot_depth[m]	Firing_Seq	MLD(m)	DCM(m)	O_2Max.(m)
AMT24S058	25/10/2014 15:07	-38.96	-29.17	2.5	23	150		38
AMT24S058	25/10/2014 15:07	-38.96	-29.17	9.1	21			
AMT24S058	25/10/2014 15:07	-38.96	-29.17	28.1	17			
AMT24S058	25/10/2014 15:07	-38.96	-29.17	50	11		✓	
AMT24S058	25/10/2014 15:07	-38.96	-29.17	503.4	1			
AMT24S059	26/10/2014 06:18	-40.10	-30.90	2.6	24	125		mixed
AMT24S059	26/10/2014 06:18	-40.10	-30.90	9.9	20			
AMT24S059	26/10/2014 06:18	-40.10	-30.90	30.1	16			
AMT24S059	26/10/2014 06:18	-40.10	-30.90	49.9	14		✓	
AMT24S059	26/10/2014 06:18	-40.10	-30.90	503.6	2			
AMT24S060	26/10/2014 15:06	-40.69	-32.10	2.7	23	110		mixed
AMT24S060	26/10/2014 15:06	-40.69	-32.10	7.9	21			
AMT24S060	26/10/2014 15:06	-40.69	-32.10	24.6	17			
AMT24S060	26/10/2014 15:06	-40.69	-32.10	40.4	13		✓	
AMT24S060	26/10/2014 15:06	-40.69	-32.10	503.4	1			
AMT24S061	27/10/2014 06:05	-41.47	-33.88	1.9	22			
AMT24S061	27/10/2014 06:05	-41.47	-33.88	10.1	19			
AMT24S061	27/10/2014 06:05	-41.47	-33.88	29.9	15			
AMT24S061	27/10/2014 06:05	-41.47	-33.88	50	12	✓	✓	✓
AMT24S061	27/10/2014 06:05	-41.47	-33.88	504.3	2			
AMT24S062	27/10/2014 15:30	-42.08	-35.10	5	23	90		
AMT24S062	27/10/2014 15:30	-42.08	-35.10	10	21			
AMT24S062	27/10/2014 15:30	-42.08	-35.10	17.9	20			
AMT24S062	27/10/2014 15:30	-42.08	-35.10	40.7	13		✓	✓
AMT24S062	27/10/2014 15:30	-42.08	-35.10	504	1			

Table A2. (continued) CTD information for AMT24 and AMT25

Cruise_Station	yyyymmdd [GT]	Latitude[°+veN]	Longitude[°+veE]	Bot_depth[m]	Firing_Seq	MLD(m)	DCM(m)	O_2Max.(m)
AMT24S063	28/10/2014 06:26	-43.00	-37.14	2.1	22	135		30
AMT24S063	28/10/2014 06:26	-43.00	-37.14	7.9	19			
AMT24S063	28/10/2014 06:26	-43.00	-37.14	25.3	15			
AMT24S063	28/10/2014 06:26	-43.00	-37.14	50.1	12		✓	
AMT24S063	28/10/2014 06:26	-43.00	-37.14	504.3	2			
AMT24S064	28/10/2014 15:05	-43.59	-38.39	1.5	23	100		x
AMT24S064	28/10/2014 15:05	-43.59	-38.39	8.5	21			
AMT24S064	28/10/2014 15:05	-43.59	-38.39	27.6	17			
AMT24S064	28/10/2014 15:05	-43.59	-38.39	42.3	13		✓	
AMT24S064	28/10/2014 15:05	-43.59	-38.39	504.6	1			
AMT24S065	29/10/2014 06:05	-44.63	-40.73	1.9	22	60		25
AMT24S065	29/10/2014 06:05	-44.63	-40.73	9.5	19			
AMT24S065	29/10/2014 06:05	-44.63	-40.73	27.9	15			
AMT24S065	29/10/2014 06:05	-44.63	-40.73	44.6	12		✓	
AMT24S065	29/10/2014 06:05	-44.63	-40.73	503.9	2			
AMT24S066	29/10/2014 15:05	-45.29	-42.20	2.3	23	26		x
AMT24S066	29/10/2014 15:05	-45.29	-42.20	8	21			
AMT24S066	29/10/2014 15:05	-45.29	-42.20	26.3	17			
AMT24S066	29/10/2014 15:05	-45.29	-42.20	45.9	13		✓	
AMT24S066	29/10/2014 15:05	-45.29	-42.20	504.6	1			
AMT24S067	30/10/2014 06:02	-46.07	-44.21	2	24	30		30
AMT24S067	30/10/2014 06:02	-46.07	-44.21	36.9	14		✓	
AMT24S067	30/10/2014 06:02	-46.07	-44.21	504	2			
AMT24S069	01/11/2014 07:07	-49.58	-53.07	2.8	24	40		75
AMT24S069	01/11/2014 07:07	-49.58	-53.07	9.9	20			
AMT24S069	01/11/2014 07:07	-49.58	-53.07	30.2	17			
AMT24S069	01/11/2014 07:07	-49.58	-53.07	80.5	12		✓	
AMT24S069	01/11/2014 07:07	-49.58	-53.07	505.7	1			
AMT24S070	01/11/2014 16:04	-50.26	-54.53	3	22	50		x
AMT24S070	01/11/2014 16:04	-50.26	-54.53	35.7	13		✓	
AMT24S070	01/11/2014 16:04	-50.26	-54.53	504.2	1			

Table A.2. (continued) CTD information for AMT24 nd AMT25

Cruise_Station	yyyymmdd [GT]	Latitude[°veN]	Longitude[°+veE]	Bot_depth[m]	Firing_Seq	MLD(m)	DCM(m)	O2Max.(m)
AMT25_S002	19/09/2015 04:09	48.4093	-9.1979	3.6	22		37	
AMT25_S002	19/09/2015 04:09	48.4093	-9.1979	6.7	18			
AMT25_S002	19/09/2015 04:09	48.4093	-9.1979	15.5	16			
AMT25_S002	19/09/2015 04:09	48.4093	-9.1979	23.6	15	x		
AMT25_S002	19/09/2015 04:09	48.4093	-9.1979	39.4	11			
AMT25_S002	19/09/2015 04:09	48.4093	-9.1979	51.5	7			
AMT25_S002	19/09/2015 04:09	48.4093	-9.1979	142.9	1			
AMT25_S003	19/09/2015 13:03	47.5095	-11.0623	2.7	22		25	
AMT25_S003	19/09/2015 13:03	47.5095	-11.0623	5.8	21			
AMT25_S003	19/09/2015 13:03	47.5095	-11.0623	20.7	18			
AMT25_S003	19/09/2015 13:03	47.5095	-11.0623	25.3	15		x	
AMT25_S003	19/09/2015 13:03	47.5095	-11.0623	34.7	14	x		
AMT25_S003	19/09/2015 13:03	47.5095	-11.0623	81.4	9			
AMT25_S003	19/09/2015 13:03	47.5095	-11.0623	505.3	1			
AMT25_S004	20/09/2015 04:04	46.2764	-12.9354	2.9	23		20	
AMT25_S004	20/09/2015 04:04	46.2764	-12.9354	13.8	18			
AMT25_S004	20/09/2015 04:04	46.2764	-12.9354	21.1	14		x	
AMT25_S004	20/09/2015 04:04	46.2764	-12.9354	23.5	13	x		
AMT25_S004	20/09/2015 04:04	46.2764	-12.9354	51.3	8			
AMT25_S004	20/09/2015 04:04	46.2764	-12.9354	504.3	1			
AMT25_S006	21/09/2015 04:10	44.455	-15.6897	2.8	22		35	
AMT25_S006	21/09/2015 04:10	44.455	-15.6897	13.1	19			
AMT25_S006	21/09/2015 04:10	44.455	-15.6897	14.3	18	x		
AMT25_S006	21/09/2015 04:10	44.455	-15.6897	36	13		x	
AMT25_S006	21/09/2015 04:10	44.455	-15.6897	50.5	10			
AMT25_S006	21/09/2015 04:10	44.455	-15.6897	502.4	1			
AMT25_S007	21/09/2015 13:06	43.7119	-16.7791	3.6	22		70	120
AMT25_S007	21/09/2015 13:06	43.7119	-16.7791	19.1	19			
AMT25_S007	21/09/2015 13:06	43.7119	-16.7791	32.9	18	x		
AMT25_S007	21/09/2015 13:06	43.7119	-16.7791	70.9	12		x	
AMT25_S007	21/09/2015 13:06	43.7119	-16.7791	504.7	1			

Table A.2. (continued) CTD information for AMT24 nd AMT25

Cruise_Station	yyyymmdd [GT]	Latitude[°veN]	Longitude[°+veE]	Bot_depth[m]	Firing_Seq	MLD(m)	DCM(m)	O2Max.(m)
AMT25_S008	22/09/2015 04:01	42.3078	-18.8061	2.7	22		70	70
AMT25_S008	22/09/2015 04:01	42.3078	-18.8061	20.7	19			
AMT25_S008	22/09/2015 04:01	42.3078	-18.8061	35.7	18 x			
AMT25_S008	22/09/2015 04:01	42.3078	-18.8061	70.9	12	x		
AMT25_S008	22/09/2015 04:01	42.3078	-18.8061	504.1	1			
AMT25_S009	22/09/2015 13:00	41.5246	-19.8713	2.4	24		50	45
AMT25_S009	22/09/2015 13:00	41.5246	-19.8713	26.2	18 x			
AMT25_S009	22/09/2015 13:00	41.5246	-19.8713	50.6	14	x		
AMT25_S009	22/09/2015 13:00	41.5246	-19.8713	504.4	1			
AMT25_S010	23/09/2015 04:05	40.0436	-21.9261	2.5	22		70	60
AMT25_S010	23/09/2015 04:05	40.0436	-21.9261	33.2	18 x			
AMT25_S010	23/09/2015 04:05	40.0436	-21.9261	70.7	12	x		
AMT25_S010	23/09/2015 04:05	40.0436	-21.9261	504.1	1			
AMT25_S011	23/09/2015 12:59	39.2032	-23.0456	2.2	24		65	50
AMT25_S011	23/09/2015 12:59	39.2032	-23.0456	25.4	18 x			
AMT25_S011	23/09/2015 12:59	39.2032	-23.0456	65.6	12	x		
AMT25_S011	23/09/2015 12:59	39.2032	-23.0456	503.8	1			
AMT25_S012	24/09/2015 04:02	37.6887	-25.0589	2.9	22	40	80	55
AMT25_S012	24/09/2015 04:02	37.6887	-25.0589	23.2	19			
AMT25_S012	24/09/2015 04:02	37.6887	-25.0589	40	18 x			
AMT25_S012	24/09/2015 04:02	37.6887	-25.0589	81.3	12	x		
AMT25_S012	24/09/2015 04:02	37.6887	-25.0589	504.4	1			
AMT25_S013	24/09/2015 13:04	37.5058	-26.6566	2.5	22	20	55	50
AMT25_S013	24/09/2015 13:04	37.5058	-26.6566	5	21			
AMT25_S013	24/09/2015 13:04	37.5058	-26.6566	25.3	18 x			
AMT25_S013	24/09/2015 13:04	37.5058	-26.6566	55.3	12	x		
AMT25_S013	24/09/2015 13:04	37.5058	-26.6566	503.6	1			

Table A.2. (continued) CTD information for AMT24 nd AMT25

Cruise_Station	yyyymmdd [GT]	Latitude[°veN]	Longitude[°+veE]	Bot_depth[m]	Firing_Seq	MLD(m)	DCM(m)	O2Max.(m)
AMT25_S014	25/09/2015 04:01	36.8376	-29.9555	2.8	23	30	90	58
AMT25_S014	25/09/2015 04:01	36.8376	-29.9555	5.4	21			
AMT25_S014	25/09/2015 04:01	36.8376	-29.9555	30.8	18 x			
AMT25_S014	25/09/2015 04:01	36.8376	-29.9555	90.3	14		x	
AMT25_S014	25/09/2015 04:01	36.8376	-29.9555	504.1	1			
AMT25_S015	25/09/2015 18:42	36.2466	-32.761	2	24			2000
AMT25_S015	25/09/2015 18:42	36.2466	-32.761	51	23			
AMT25_S015	25/09/2015 18:42	36.2466	-32.761	101.1	20		x	
AMT25_S015	25/09/2015 18:42	36.2466	-32.761	201.8	19			
AMT25_S015	25/09/2015 18:42	36.2466	-32.761	505.9	12			
AMT25_S016	27/09/2015 06:00	36.2286	-32.7719	2.8	22		80	2200
AMT25_S016	27/09/2015 06:00	36.2286	-32.7719	5.4	21			
AMT25_S016	27/09/2015 06:00	36.2286	-32.7719	52.9	18 x			
AMT25_S016	27/09/2015 06:00	36.2286	-32.7719	80.6	15		x	
AMT25_S016	27/09/2015 06:00	36.2286	-32.7719	404.6	7			
AMT25_S017	28/09/2015 04:05	35.6113	-34.1666	7.4	23		130	2000
AMT25_S017	28/09/2015 04:05	35.6113	-34.1666	27.8	20			
AMT25_S017	28/09/2015 04:05	35.6113	-34.1666	45.6	19 x			
AMT25_S017	28/09/2015 04:05	35.6113	-34.1666	80.3	17			
AMT25_S017	28/09/2015 04:05	35.6113	-34.1666	132.4	12		x	
AMT25_S017	28/09/2015 04:05	35.6113	-34.1666	504.3	7			
AMT25_S018	28/09/2015 13:06	35.0636	-35.4433	5.5	22	40	110	60
AMT25_S018	28/09/2015 13:06	35.0636	-35.4433	15.2	20			
AMT25_S018	28/09/2015 13:06	35.0636	-35.4433	25.4	19			
AMT25_S018	28/09/2015 13:06	35.0636	-35.4433	111.1	12		x	
AMT25_S018	28/09/2015 13:06	35.0636	-35.4433	503.5	1			

Table A.2. (continued) CTD information for AMT24 nd AMT25

Cruise_Station	yyyymmdd [GT]	Latitude[°veN]	Longitude[°+veE]	Bot_depth[m]	Firing_Seq	MLD(m)	DCM(m)	O2Max.(m)
AMT25_S019	29/09/2015 04:04	33.9988	-37.575	6.9	23	33	120	67
AMT25_S019	29/09/2015 04:04	33.9988	-37.575	32.8	19 x			
AMT25_S019	29/09/2015 04:04	33.9988	-37.575	73.4	17			
AMT25_S019	29/09/2015 04:04	33.9988	-37.575	123.4	13	x		
AMT25_S019	29/09/2015 04:04	33.9988	-37.575	505.3	6			
AMT25_S020	29/09/2015 12:59	33.2215	-38.9216	4.7	24	50	102	70
AMT25_S020	29/09/2015 12:59	33.2215	-38.9216	47.6	19 x			
AMT25_S020	29/09/2015 12:59	33.2215	-38.9216	103.3	15	x		
AMT25_S020	29/09/2015 12:59	33.2215	-38.9216	505	1			
AMT25_S021	30/09/2015 04:02	31.151	-40.9179	4.3	23	60	115	90
AMT25_S021	30/09/2015 04:02	31.151	-40.9179	17.3	21			
AMT25_S021	30/09/2015 04:02	31.151	-40.9179	117.5	15	x		
AMT25_S021	30/09/2015 04:02	31.151	-40.9179	504.3	6			
AMT25_S023	01/10/2015 04:03	28.2558	-42.3096	5.1	23	40	136	60
AMT25_S023	01/10/2015 04:03	28.2558	-42.3096	32.9	20			
AMT25_S023	01/10/2015 04:03	28.2558	-42.3096	139.6	15	x		
AMT25_S023	01/10/2015 04:03	28.2558	-42.3096	505.6	7			
AMT25_S024	01/10/2015 12:56	27.4746	-41.1108	3.3	24			
AMT25_S024	01/10/2015 12:56	27.4746	-41.1108	25.3	19 x		135	60
AMT25_S024	01/10/2015 12:56	27.4746	-41.1108	74.7	16			
AMT25_S024	01/10/2015 12:56	27.4746	-41.1108	136.2	12	x		
AMT25_S024	01/10/2015 12:56	27.4746	-41.1108	503.4	1			
AMT25_S025	02/10/2015 04:02	25.9342	-38.827	2	23			
AMT25_S025	02/10/2015 04:02	25.9342	-38.827	40.7	18 x		135	50
AMT25_S025	02/10/2015 04:02	25.9342	-38.827	100.6	15			
AMT25_S025	02/10/2015 04:02	25.9342	-38.827	135.7	12	x		
AMT25_S025	02/10/2015 04:02	25.9342	-38.827	503.1	1			
AMT25_S026	02/10/2015 10:24	25.4532	-38.0744	2.6	22	30		48
AMT25_S026	02/10/2015 10:24	25.4532	-38.0744	13.5	20			
AMT25_S026	02/10/2015 10:24	25.4532	-38.0744	48.5	15			
AMT25_S026	02/10/2015 10:24	25.4532	-38.0744	117.8	10	x		
AMT25_S026	02/10/2015 10:24	25.4532	-38.0744	404	4			

Table A.2. (continued) CTD information for AMT24 nd AMT25

Cruise_Station	yyyymmdd [GT]	Latitude[°veN]	Longitude[°+veE]	Bot_depth[m]	Firing_Seq	MLD(m)	DCM(m)	O2Max.(m)
AMT25_S027	03/10/2015 04:10	23.8985	-35.7556	2.6	22	33	120	65
AMT25_S027	03/10/2015 04:10	23.8985	-35.7556	15.2	20			
AMT25_S027	03/10/2015 04:10	23.8985	-35.7556	61.4	15			
AMT25_S027	03/10/2015 04:10	23.8985	-35.7556	121.4	9		x	
AMT25_S027	03/10/2015 04:10	23.8985	-35.7556	504.2	1			
AMT25_S028	03/10/2015 13:05	22.9866	-34.3891	2.6	22	43	105	80
AMT25_S028	03/10/2015 13:05	22.9866	-34.3891	13.7	20			
AMT25_S028	03/10/2015 13:05	22.9866	-34.3891	43.7	16	x		
AMT25_S028	03/10/2015 13:05	22.9866	-34.3891	105.8	7		x	
AMT25_S028	03/10/2015 13:05	22.9866	-34.3891	503.5	1			
AMT25_S031	05/10/2015 04:05	19.2677	-28.995	2.5	23	36	78	60
AMT25_S031	05/10/2015 04:05	19.2677	-28.995	10.8	20			
AMT25_S031	05/10/2015 04:05	19.2677	-28.995	30.2	16			
AMT25_S031	05/10/2015 04:05	19.2677	-28.995	78.7	8		x	
AMT25_S031	05/10/2015 04:05	19.2677	-28.995	503.9	1			
AMT25_S032	05/10/2015 13:00	18.4807	-28.028	2.8	22	35	72	62
AMT25_S032	05/10/2015 13:00	18.4807	-28.028	11.1	19			
AMT25_S032	05/10/2015 13:00	18.4807	-28.028	62.3	11			
AMT25_S032	05/10/2015 13:00	18.4807	-28.028	72	8		x	
AMT25_S032	05/10/2015 13:00	18.4807	-28.028	504	1			
AMT25_S033	06/10/2015 03:58	17.1778	-26.4558	2.6	22	30	65	55
AMT25_S033	06/10/2015 03:58	17.1778	-26.4558	10.8	20			
AMT25_S033	06/10/2015 03:58	17.1778	-26.4558	50.7	13			
AMT25_S033	06/10/2015 03:58	17.1778	-26.4558	66	9		x	
AMT25_S033	06/10/2015 03:58	17.1778	-26.4558	504	1			
AMT25_S034	06/10/2015 12:58	16.4329	-25.5498	3.6	23	37	60	46
AMT25_S034	06/10/2015 12:58	16.4329	-25.5498	8.3	20			
AMT25_S034	06/10/2015 12:58	16.4329	-25.5498	23.8	15			
AMT25_S034	06/10/2015 12:58	16.4329	-25.5498	60.4	7		x	
AMT25_S034	06/10/2015 12:58	16.4329	-25.5498	503.4	1			

Table A.2. (continued) CTD information for AMT24 nd AMT25

Cruise_Station	yyyymmdd [GT]	Latitude[°veN]	Longitude[°+veE]	Bot_depth[m]	Firing_Seq	MLD(m)	DCM(m)	O2Max.(m)
AMT25_S035	07/10/2015 03:57	15.0956	-23.9468	2.4	23	15	42	25
AMT25_S035	07/10/2015 03:57	15.0956	-23.9468	8.6	20			
AMT25_S035	07/10/2015 03:57	15.0956	-23.9468	42.7	10		x	
AMT25_S035	07/10/2015 03:57	15.0956	-23.9468	504.6	1			
AMT25_S036	08/10/2015 04:10	13.3793	-22.905	2.5	23	15	47	23
AMT25_S036	08/10/2015 04:10	13.3793	-22.905	7.6	20			
AMT25_S036	08/10/2015 04:10	13.3793	-22.905	23.3	15			
AMT25_S036	08/10/2015 04:10	13.3793	-22.905	47	10		x	
AMT25_S036	08/10/2015 04:10	13.3793	-22.905	503.6	1			
AMT25_S037	08/10/2015 13:00	12.369	-22.5323	1.8	23	17	50	22
AMT25_S037	08/10/2015 13:00	12.369	-22.5323	8	20			
AMT25_S037	08/10/2015 13:00	12.369	-22.5323	22.1	16			
AMT25_S037	08/10/2015 13:00	12.369	-22.5323	50.2	9		x	
AMT25_S037	08/10/2015 13:00	12.369	-22.5323	504.2	1			
AMT25_S038	09/10/2015 03:58	9.9953	-21.6016	2.3	23	15	70	45
AMT25_S038	09/10/2015 03:58	9.9953	-21.6016	11.5	20			
AMT25_S038	09/10/2015 03:58	9.9953	-21.6016	35	16			
AMT25_S038	09/10/2015 03:58	9.9953	-21.6016	70.6	9		x	
AMT25_S038	09/10/2015 03:58	9.9953	-21.6016	503.5	1			
AMT25_S040	10/10/2015 04:00	5.8774	-20.0271	3	23	38	64	43
AMT25_S040	10/10/2015 04:00	5.8774	-20.0271	10.7	20			
AMT25_S040	10/10/2015 04:00	5.8774	-20.0271	33.8	16			
AMT25_S040	10/10/2015 04:00	5.8774	-20.0271	65	11		x	
AMT25_S040	10/10/2015 04:00	5.8774	-20.0271	503.8	1			
AMT25_S042	11/10/2015 03:59	1.9329	-18.4323	3.1	23	68	85	60
AMT25_S042	11/10/2015 03:59	1.9329	-18.4323	10.8	20			
AMT25_S042	11/10/2015 03:59	1.9329	-18.4323	21.3	18			
AMT25_S042	11/10/2015 03:59	1.9329	-18.4323	86.5	8		x	
AMT25_S042	11/10/2015 03:59	1.9329	-18.4323	504.1	1			

Table A.2. (continued) CTD information for AMT24 nd AMT25

Cruise_Station	yyyymmdd [GT]	Latitude[°veN]	Longitude[°+veE]	Bot_depth[m]	Firing_Seq	MLD(m)	DCM(m)	O2Max.(m)
AMT25_S044	12/10/2015 04:30	-1.6801	-16.977	3.4	22	65		45
AMT25_S044	12/10/2015 04:30	-1.6801	-16.977	10.5	20			
AMT25_S044	12/10/2015 04:30	-1.6801	-16.977	17.1	18			
AMT25_S044	12/10/2015 04:30	-1.6801	-16.977	46	13			
AMT25_S044	12/10/2015 04:30	-1.6801	-16.977	61.2	11	x		
AMT25_S044	12/10/2015 04:30	-1.6801	-16.977	503.9	1			
AMT25_S045	13/10/2015 03:58	-4.4238	-15.8679	2.9	23	62	73	65
AMT25_S045	13/10/2015 03:58	-4.4238	-15.8679	8.8	20			
AMT25_S045	13/10/2015 03:58	-4.4238	-15.8679	26.6	15			
AMT25_S045	13/10/2015 03:58	-4.4238	-15.8679	62.5	8	x		
AMT25_S045	13/10/2015 03:58	-4.4238	-15.8679	504.5	1			
AMT25_S047	14/10/2015 04:00	-7.1099	-14.7596	3.4	23	29	65	44
AMT25_S047	14/10/2015 04:00	-7.1099	-14.7596	11.3	19			
AMT25_S047	14/10/2015 04:00	-7.1099	-14.7596	34.1	16			
AMT25_S047	14/10/2015 04:00	-7.1099	-14.7596	41	15			
AMT25_S047	14/10/2015 04:00	-7.1099	-14.7596	66.5	11	x		
AMT25_S047	14/10/2015 04:00	-7.1099	-14.7596	504.2	1			
AMT25_S055	19/10/2015 03:59	-10.1135	-16.5745	2.9	23	74	95	78
AMT25_S055	19/10/2015 03:59	-10.1135	-16.5745	10.8	20			
AMT25_S055	19/10/2015 03:59	-10.1135	-16.5745	34.5	16			
AMT25_S055	19/10/2015 03:59	-10.1135	-16.5745	96.1	9	x		
AMT25_S055	19/10/2015 03:59	-10.1135	-16.5745	503.8	1			
AMT25_S057	20/10/2015 04:57	-13.0002	-19.4722	2.7	23	102	124	88
AMT25_S057	20/10/2015 04:57	-13.0002	-19.4722	15.5	20			
AMT25_S057	20/10/2015 04:57	-13.0002	-19.4722	47.3	16			
AMT25_S057	20/10/2015 04:57	-13.0002	-19.4722	88.5	13			
AMT25_S057	20/10/2015 04:57	-13.0002	-19.4722	124.9	9	x		
AMT25_S057	20/10/2015 04:57	-13.0002	-19.4722	504.6	1			
AMT25_S059	21/10/2015 04:57	-15.691	-22.1881	3.6	23	62	156	100
AMT25_S059	21/10/2015 04:57	-15.691	-22.1881	17.1	20			
AMT25_S059	21/10/2015 04:57	-15.691	-22.1881	53.2	16			
AMT25_S059	21/10/2015 04:57	-15.691	-22.1881	101.8	13			
AMT25_S059	21/10/2015 04:57	-15.691	-22.1881	157.8	9	x		
AMT25_S059	21/10/2015 04:57	-15.691	-22.1881	504.4	1			

Table A.2. (continued) CTD information for AMT24 nd AMT25

Cruise_Station	yyyymmdd [GT]	Latitude[°veN]	Longitude[°+veE]	Bot_depth[m]	Firing_Seq	MLD(m)	DCM(m)	O2Max.(m)
AMT25_S061	22/10/2015 04:54	-18.502	-25.0019	2.3	23	80	160	100
AMT25_S061	22/10/2015 04:54	-18.502	-25.0019	23.6	19			
AMT25_S061	22/10/2015 04:54	-18.502	-25.0019	73.8	16			
AMT25_S061	22/10/2015 04:54	-18.502	-25.0019	100.8	15			
AMT25_S061	22/10/2015 04:54	-18.502	-25.0019	161.1	12	x		
AMT25_S061	22/10/2015 04:54	-18.502	-25.0019	504.3	1			
AMT25_S062	23/10/2015 04:57	-20.5417	-25.0686	2.8	23	150	165	50
AMT25_S062	23/10/2015 04:57	-20.5417	-25.0686	21	19			
AMT25_S062	23/10/2015 04:57	-20.5417	-25.0686	50.6	16		x	
AMT25_S062	23/10/2015 04:57	-20.5417	-25.0686	76.4	15			
AMT25_S062	23/10/2015 04:57	-20.5417	-25.0686	165.9	10	x		
AMT25_S062	23/10/2015 04:57	-20.5417	-25.0686	502.7	1			
AMT25_S064	24/10/2015 04:56	-24.9083	-25.0736	3.6	23			
AMT25_S064	24/10/2015 04:56	-24.9083	-25.0736	24.4	19	50	158	60
AMT25_S064	24/10/2015 04:56	-24.9083	-25.0736	61.5	16		x	
AMT25_S064	24/10/2015 04:56	-24.9083	-25.0736	74.5	15			
AMT25_S064	24/10/2015 04:56	-24.9083	-25.0736	160	11	x		
AMT25_S064	24/10/2015 04:56	-24.9083	-25.0736	504.6	1			
AMT25_S066	25/10/2015 05:12	-28.7968	-25.4593	6.9	23	38	135	105
AMT25_S066	25/10/2015 05:12	-28.7968	-25.4593	21.8	20			
AMT25_S066	25/10/2015 05:12	-28.7968	-25.4593	66.8	17			
AMT25_S066	25/10/2015 05:12	-28.7968	-25.4593	107.1	15			
AMT25_S066	25/10/2015 05:12	-28.7968	-25.4593	137.2	11	x		
AMT25_S066	25/10/2015 05:12	-28.7968	-25.4593	505.1	1			
AMT25_S070	27/10/2015 05:08	-32.39	-29.8533	6.4	23	85	110	100
AMT25_S070	27/10/2015 05:08	-32.39	-29.8533	16	20			
AMT25_S070	27/10/2015 05:08	-32.39	-29.8533	51	16			
AMT25_S070	27/10/2015 05:08	-32.39	-29.8533	101.6	12		x	
AMT25_S070	27/10/2015 05:08	-32.39	-29.8533	111.4	11	x		
AMT25_S070	27/10/2015 05:08	-32.39	-29.8533	504.5	1			

Table A.2. (continued) CTD information for AMT24 nd AMT25

Cruise_Station	yyyymmdd [GT]	Latitude[°veN]	Longitude[°+veE]	Bot_depth[m]	Firing_Seq	MLD(m)	DCM(m)	O2Max.(m)
AMT25_S072	28/10/2015 06:02	-35.3339	-33.646	2.7	23	140	65	30
AMT25_S072	28/10/2015 06:02	-35.3339	-33.646	9	20			
AMT25_S072	28/10/2015 06:02	-35.3339	-33.646	26.7	16			
AMT25_S072	28/10/2015 06:02	-35.3339	-33.646	30.9	15		x	
AMT25_S072	28/10/2015 06:02	-35.3339	-33.646	65.8	10	x		
AMT25_S072	28/10/2015 06:02	-35.3339	-33.646	504.4	1			
AMT25_S074	29/10/2015 05:57	-38.4792	-37.7521	3.5	23	15	40 -	
AMT25_S074	29/10/2015 05:57	-38.4792	-37.7521	10.9	20			
AMT25_S074	29/10/2015 05:57	-38.4792	-37.7521	21.7	17		x	
AMT25_S074	29/10/2015 05:57	-38.4792	-37.7521	41.4	15	x		
AMT25_S074	29/10/2015 05:57	-38.4792	-37.7521	504.2	1			
AMT25_S076	30/10/2015 06:03	-41.6779	-42.2299	3.2	23	40	50 -	
AMT25_S076	30/10/2015 06:03	-41.6779	-42.2299	10	20			
AMT25_S076	30/10/2015 06:03	-41.6779	-42.2299	29.7	16			
AMT25_S076	30/10/2015 06:03	-41.6779	-42.2299	51.7	13	x		
AMT25_S076	30/10/2015 06:03	-41.6779	-42.2299	505.1	1			
AMT25_S078	31/10/2015 06:00	-44.5917	-46.3548	2.9	23	22	35	40
AMT25_S078	31/10/2015 06:00	-44.5917	-46.3548	10.4	20			
AMT25_S078	31/10/2015 06:00	-44.5917	-46.3548	31	16			
AMT25_S078	31/10/2015 06:00	-44.5917	-46.3548	36.2	14	x		
AMT25_S078	31/10/2015 06:00	-44.5917	-46.3548	503.4	1			
AMT25_S080	02/11/2015 07:08	-48.8725	-53.107	7.1	23	60	60 -	
AMT25_S080	02/11/2015 07:08	-48.8725	-53.107	12.7	21			
AMT25_S080	02/11/2015 07:08	-48.8725	-53.107	32.6	17			
AMT25_S080	02/11/2015 07:08	-48.8725	-53.107	62.4	13	x		
AMT25_S080	02/11/2015 07:08	-48.8725	-53.107	505.9	1			